

**Glycosaminoglycans and Collagen Fibril Organization in  
Corneal Tissue**

A Thesis Submitted to the Cardiff University for the Degree of  
Doctorate of Philosophy

School of Optometry and Vision Sciences

2011

**Leona T. Y. Ho**

UMI Number: U585492

All rights reserved

INFORMATION TO ALL USERS

The quality of this reproduction is dependent upon the quality of the copy submitted.

In the unlikely event that the author did not send a complete manuscript and there are missing pages, these will be noted. Also, if material had to be removed, a note will indicate the deletion.



UMI U585492

Published by ProQuest LLC 2013. Copyright in the Dissertation held by the Author.  
Microform Edition © ProQuest LLC.

All rights reserved. This work is protected against  
unauthorized copying under Title 17, United States Code.



ProQuest LLC  
789 East Eisenhower Parkway  
P.O. Box 1346  
Ann Arbor, MI 48106-1346

---

## Declaration

This work has not previously been accepted in substance for any degree and is not concurrently submitted in candidature for any degree.

Signed .....  ..... (candidate)      Date ... 7/7/2011 .....

### STATEMENT 1

This thesis is being submitted in partial fulfillment of the requirements for the degree of PhD.

Signed .....  ..... (candidate)      Date ..... 7/7/2011 .....

### STATEMENT 2

This thesis is the result of my own independent work/investigation, except where otherwise stated. Other sources are acknowledged by explicit references.

Signed .....  ..... (candidate)      Date ..... 7/7/2011 .....

### STATEMENT 3

I hereby give consent for my thesis, if accepted, to be available for photocopying and for inter-library loan, and for the title and summary to be made available to outside organizations.

Signed .....  ..... (candidate)      Date ..... 7/7/2011 .....

---

## Abstract

**Introduction:** The cornea is the clear window at the front of the eye. Its transparency is due to the special arrangement of collagen fibrils, which constitute most of the cornea. The precise regulation of the size and spacing of the fibrils is attributed to the interactions between proteoglycans and collagen fibrils. Proteoglycans consist of glycosaminoglycan chains attached to a protein core and in the cornea there are two main types of chain: keratan sulphate and chondroitin/dermatan sulphate. Much evidence has shown that these proteoglycans play different vital roles in the corneal extracellular matrix in order to maintain the architecture of the cornea.

**Hypothesis:** The hypothesis of this research is that changes in the sulphation patterns of the glycosaminoglycans are directly related to changes in ultrastructure, and hence transparency of the cornea.

**Aims:** The aims of this research were to investigate glycosaminoglycan sulphation patterns and collagen fibril ultrastructure from central to peripheral regions of the cornea, and to gain a greater understanding in the effects of keratan sulphate and its reliance on oxygen supply.

**Methods:** The bovine corneal extracellular matrix composition and collagen fibril parameters (fibril diameter and interfibrillar spacing) were biochemically and biophysically evaluated. This involved taking measurements of corneal thickness and hydration, as well as the amount of hydroxyproline and sulphated glycosaminoglycan. Immunolocalization of proteoglycan protein cores (lumican and keratocan) and specific glycosaminoglycans, particularly their sulphation distribution were studied using specific antibodies. Sulphation patterns of keratan sulphate were also quantified using specific antibodies. Transmission electron microscopy coupled with synchrotron small angle x-ray fibre diffraction was also employed to gain a greater understanding of the corneas' collagen fibril architecture and its interaction with glycosaminoglycans across the depths of the cornea.

---

**Results:** The bovine cornea is thicker in the outer peripheral regions of the cornea and accordingly an increased amount of hydroxyproline is found at this region of the tissue. Keratan sulphate is predominantly found in the bovine cornea and is particularly heavily sulphated across the cornea. The degree of sulphation of keratan sulphate decreases at the outer peripheral regions of the cornea, which, interestingly, is where a transition of collagen fibrils occurs in that fibrils become less uniformly arranged, changes in fibril diameter are seen, and interfibrillar spacing values alter. Depth-profiled synchrotron microbeam analyses show that at different radial positions, from the corneal centre outwards, fibril diameter is greater superficially than in deep stromal regions. This does not include Bowman's layer which is below the spatial resolution of the analysis. The mid-depth stroma has higher interfibrillar spacing than is seen in posterior regions of the stroma, where fibril spacing appeared more compact. Previous work has pointed to a link between glycosaminoglycan content and oxygen availability. Work presented here indicates that in rabbit corneas, after 24 hr in 2% atmospheric O<sub>2</sub>, the glycosaminoglycan sulphation pattern changes significantly, with a significant increase of the high sulphated epitope of keratan sulphate.

**Conclusion:** My data reveal that collagen fibrils in the central regions of the cornea are more closely packed and uniform in diameter than those in the outer peripheral cornea, and this may have potential implications for the transparency of the tissue. Stromal architecture is likely governed by sulphated proteoglycans, and changes in the types and sulphation patterns of corneal glycosaminoglycans from the corneal centre to periphery might be linked to differences in collagen ultrastructure. Moreover, the findings of differences in collagen fibril ultrastructure with depth through the cornea are possibly linked to biochemical alterations in proteoglycans. Finally, it is hypothesised that detrimental conditions, such as hypoxia after contact lens wear, might have an effect on the type and sulphation status of glycosaminoglycan synthesized and *in vitro* evidence for this is presented and discussed.

---

## Acknowledgements

It is a pleasure to thank the many people who made this thesis possible.

Foremost, I would like to express my sincere gratitude to my supervisors Professors Keith Meek and Andrew Quantock for their continuous support of my PhD study and research, for their patience, motivation, enthusiasm, and immense knowledge.

My sincere thanks also go to Professors Bruce Caterson, Vic Duance, Drs Rob Young and Hidetoshi Tanioka for their guidance and support throughout my studies. As well as this I would like to thank Andrew once again and JSPS who gave me the opportunity for me to study in Japan.

I would like to give a special thank you to Professor Noriko Koizumi for being such a brilliant host supervisor during my time in Japan and has truly inspired me to further research.

I would also like to thank my friends for being such kindred spirits who have been consistently supportive and helpful as I progressed through my studies. Lastly, and by no means least, I would like to thank my family (especially my brother, Michael and my sister, Jenny) for their constant love and encouragement.

Without all these help this project may not have been possible. I am truly blessed with all of you.

---

# Contents

<b>Declaration</b> .....	<b>I</b>
<b>Abstract</b> .....	<b>II</b>
<b>Acknowledgements</b> .....	<b>IV</b>
<b>1</b> .....	<b>10</b>
1.1. <i>The anatomy and physiology of the eye</i> .....	11
1.2. <i>The structure and composition of the corneal stroma</i> .....	12
1.3. <i>Stromal collagen</i> .....	14
1.3.1. Structure and function of ocular collagens.....	16
1.3.2. Biosynthesis of collagen.....	17
1.3.3. Fibril forming collagen.....	19
1.3.3.1. Type I collagen.....	19
1.3.3.2. Type V collagen.....	20
1.3.4. Filamentous collagen.....	21
1.3.4.1. Type VI collagen.....	21
1.3.5. Other ocular collagens.....	22
1.3.6. Organization of collagen fibrils in the corneal stroma.....	23
1.4. <i>Extracellular matrix components - Proteoglycans</i> .....	25
1.4.1. Glycosaminoglycans (GAGs).....	27
1.4.1.1. Keratan sulphate (KS).....	28
1.4.1.2. Importance of KS.....	31
1.4.1.3. Dermatan sulphate (DS).....	32
1.4.2. Proteoglycan core protein - Lumican.....	34
1.4.3. Proteoglycan core protein - Keratocan.....	35
1.4.4. Proteoglycan core protein - Mimecan.....	36
1.4.5. Proteoglycan core protein - Decorin.....	37
1.5. <i>Collagen and PG associations</i> .....	38
1.6. <i>Collagen and Proteoglycan interactions</i> .....	39
1.7. <i>Transparency</i> .....	43
1.8. <i>Summary and objectives</i> .....	45
<b>2</b> .....	<b>48</b>
2.1. <i>Corneal preparation</i> .....	48
2.1.1. Papain digest.....	49
2.1.1.1. Papain protocol.....	50
2.1.2. Pepsin digestion.....	50
2.1.2.1. Guanidine extraction and pepsin digestion protocol.....	50
2.2. <i>Determining matrix content</i> .....	51
2.2.1. Hydroxyproline assay.....	51
2.2.1.1. Hydroxyproline assay protocol.....	51
2.2.2. Dimethylmethylene blue (DMMB) assay.....	52

2.2.2.1.	DMMB assay protocol .....	52
2.2.2.2.	Hydroxyproline and sulphate GAG quantification.....	53
2.3.	<i>KS quantifications using antibodies</i> .....	53
2.3.1.	Antibodies (Ab).....	53
2.3.1.1.	Antibody isotypes.....	54
2.3.1.2.	Monoclonal antibodies versus polyclonal antibodies .....	55
2.3.2.	Antibodies and pre-enzyme treatments used in this study .....	56
2.3.3.	Immunohistochemical microscopy .....	58
2.3.3.1.	IHC protocol.....	58
2.3.4.	Enzyme-linked immunosorbent assay (ELISA).....	60
2.3.4.1.	ELISA protocol .....	60
2.3.4.2.	ELISA - Determining antibody concentration .....	62
2.3.4.3.	Keratan sulphate quantification.....	62
2.4.	<i>Transmission electron microscopy (TEM)</i> .....	63
2.4.1.	General preparation for TEM analysis.....	63
2.4.1.1.	Positive and negative staining of collagen .....	64
2.4.1.2.	Cupromeronic blue staining for GAG chains .....	66
2.5.	<i>X-ray diffraction of collagen</i> .....	67
2.5.1.	X-ray diffraction preparation.....	69
2.5.2.	Small angle X-ray scattering data collection .....	69
2.5.2.1.	Small angle x-ray scattering data analysis.....	71
2.5.2.2.	Calculation of the intensity distribution from the equatorial scatter component:....	72
2.5.2.3.	Step 1 - Removal of background scatter (B) caused by other tissue components....	73
2.5.2.4.	Step 2 – Removal of fibril transform (F2) .....	74
2.5.2.5.	Step 3 - Calculating the interfibrillar Bragg spacing (IFBS) of corneal collagen.....	75
2.5.2.6.	Step 4 – Calculating fibril diameter .....	77
<b>3.</b>	.....	<b>79</b>
3.1	<i>Introduction</i> .....	79
3.2	<i>Methods</i> .....	80
3.2.1	Corneal thickness measurements .....	80
3.2.2	Sample preparation for biochemical studies .....	80
3.2.2.1	Papain digestion .....	81
3.2.3	Hydroxyproline assay .....	81
3.2.4	DMMB assay.....	81
3.2.5	Immunohistochemistry .....	81
3.2.6	KS quantification .....	82
3.3	<i>Results – Biochemical studies</i> .....	82
3.4	<i>Results – Immunohistochemical analysis</i> .....	85
3.5	<i>Results – KS quantifications</i> .....	93
3.6	<i>Discussion</i> .....	94
<b>4.</b>	.....	<b>102</b>
4.1	<i>Introduction</i> .....	102
4.2	<i>Methods</i> .....	105

4.2.1	Small angle x-ray diffraction.....	105
4.2.2	Electron microscopy.....	106
4.3	<i>Results</i> .....	106
4.3.1	Collagen fibril measurements - TEM analysis.....	106
4.3.2	X-ray diffraction analysis: Collagen fibril measurements across the cornea as a function of position	111
4.3.3	X-ray diffraction analysis: Depth profile studies on collagen fibrils.....	113
4.3.4	TEM analysis – PGs stained with cupromeronic blue.....	116
4.4	<i>Discussion</i> .....	118
<b>5.</b>		<b>124</b>
5.1	<i>Introduction</i> .....	124
5.5.1	Low O <sub>2</sub> and its biochemical affects.....	125
5.5.2	Low O <sub>2</sub> and its affects on collagen.....	126
5.5.3	Low O <sub>2</sub> and its affects on GAGs.....	127
5.6	<i>Aims</i> .....	129
5.7	<i>Methods</i> .....	129
5.7.1	Sample preparation.....	130
5.7.2	Papain digestion.....	131
5.7.3	Hydroxyproline and DMMB assay.....	131
5.7.4	KS quantification.....	131
5.7.5	Immunohistochemistry.....	131
5.8	<i>Results</i> .....	132
5.8.1	Corneal hydration.....	132
5.8.2	Results: Sulphated GAG pattern.....	134
5.8.3	Results: Immunolocalization of KS patterns and its core proteins.....	136
	Immunolocalization on oversulphated N-acetyl lactosamine disaccharides of KS.....	137
	Immunolocalization on lesser sulphated N-acetyl lacosamine disaccharides of KS.....	138
	Immunolocalization of KS neopeptides (N-acetyl-glucosamine-6-sulphate) at the non-reducing terminal of KS (BKS-1 antibody).....	139
	Immunolocalization of KSPG: lumican.....	140
	Immunolocalization of KSPG: keratocan.....	141
	Negative control.....	142
5.8.4	KS quantification.....	142
5.8.5	The effects of hydroxyproline content in low oxygen levels.....	143
5.9	<i>Discussion</i> .....	144
<b>6.</b>		<b>150</b>
6.1.	<i>GAGs and collagen fibril organization across the cornea</i> .....	150
6.2.	<i>GAGs and collagen fibril organization across the depths of the cornea</i> .....	153
6.3.	<i>The effects of the cornea in low O<sub>2</sub></i> .....	154
6.4.	<i>Summary and future work</i> .....	155
	<b>Website references</b> .....	<b>174</b>

---

<b>Appendix 1 .....</b>	<b>175</b>
<b>Appendix 2 .....</b>	<b>180</b>

---

## List of figure

Figure 1.1 The anatomy of the eye .....	10
Figure 1.2 A diagram showing the different surface zones in the human cornea (anterior corneal surface).....	12
Figure 1.3 The structure of the cornea and its constituent layers .....	12
Figure 1.4 Fibril forming collagen synthesis .....	18
Figure 1.5 A model of type I/V heterotypic fibril .....	20
Figure 1.6 A schematic diagram of type VI collagen .....	22
Figure 1.7 Axial packing arrangements of collagen molecules in a fibril (A), as derived from analysis of the negative (B) and positive (C) staining patterns .....	23
Figure 1.8 The chemical composition of proteoglycans and its different glycosaminoglycan chains attached .....	27
Figure 1.9 A simplified diagram of corneal keratan sulphate (KSI) structure .....	29
Figure 1.10 The structural differences between corneal KS (KSI) and cartilage KS (KSII) .....	30
Figure 1.11 A simplified diagram of chondroitin sulphate (CS) and dermatan sulphate (DS) structure... ..	33
Figure 1.12 A three-dimension model of keratocan .....	35
Figure 1.13 Crystal structure of the dimeric protein core of decorin, the archetypal small leucine-rich repeat proteoglycan.....	37
Figure 1.14 Mapping of binding sites of PGs along the collagen fibril .....	39
Figure 1.15 A schematic diagram of Müller <i>et al.</i> (2004) proposed model on the organization of the collagen fibrils and proteoglycans.....	40
Figure 1.16 A proposed model of collagen interactions seen in corneal stroma.....	41
Figure 1.17 Electron micrographs of deep-etched, ultra rapidly-frozen human (glutaraldehyde-fixed) (A) and rabbit (non chemically-fixed) (B) corneal stroma.....	42
Figure 1.18 CS/DS and KS interaction between collagen fibrils .....	43
Figure 2.1 A diagram showing the different corneal surface regions in the bovine cornea (anterior corneal surface).....	48
Figure 2.2 A simplified diagram showing how the corneal tissue (bovine) was prepared for the biochemical experiments .....	49
Figure 2.3 Chemical process of papain and pepsin digestion .....	49
Figure 2.4 The structure of a typical antibody (IgG) and the different antibody isotypes .....	54
Figure 2.5 A simple diagram illustrating the cleavage sites of the enzymes used in experiments .....	57
Figure 2.6 A simple diagram showing how competitive ELISAs work .....	60
Figure 2.7 Determining 5D4 and 1B4 antibody concentration used for quantifying the unknown amounts of KS content in the bovine corneal extracts .....	62
Figure 2.8 An example of a 5D4 standard curve calculation from optical density.....	63
Figure 2.9 A schematic diagram showing how an array of fibrils held vertically in an x-ray beam gives rise to meridional reflections in a direction parallel to the fibril axes equatorial reflections in a direction perpendicular to the fibril axes .....	67
Figure 2.10 A simplistic diagram showing how the corneas were prepared for x-ray analysis .....	70
Figure 2.11 Small angle x-ray scattering pattern from a mid central region of a bovine cornea.....	72
Figure 2.12 Linear background generation (LOGBK) against radial position (LOGR) .....	73
Figure 2.13 The fibril transform (BESSEL) fitted to the profile of the scattering intensity (collagen) multiplied by radial position (RI_BACK) .....	74
Figure 2.14 Diagram showing the scattering of a sample (rat tail tendon or bovine cornea) .....	75
Figure 2.15 Small angle x-ray intensity profile pattern of a rat tail tendon .....	77
Figure 3.1 Summary plan of experiments .....	80

---

Figure 3.2 Measurements of thickness, hydration, hydroxyproline and sulphated GAG content across the bovine cornea as a function of position.....	84
Figure 3.3 Immunolocalization of type I collagen (green) and nuclear stained cells (blue), using anti-type I collagen and DAPI, respectively .....	86
Figure 3.4 Immunolocalization of over-sulphated KS (green) and nuclear stained cells (blue), using 5D4 antibody and DAPI, respectively .....	87
Figure 3.5 Immunolocalization of lesser-sulphated KS (green) and nuclear stained cells (blue), using 1B4 antibody and DAPI, respectively .....	88
Figure 3.6 Immunolocalization of neopeptide at the non-reducing terminal ends of KS (green) and nuclear stained cells (blue), using BKS-1 antibody and DAPI, respectively.....	89
Figure 3.7 Immunolocalization of chondroitin-6-sulphate (green) and nuclear stained cells (blue), using 3B3 antibody and DAPI, respectively .....	90
Figure 3.8 Immunolocalization of chondroitin-4-sulphate (green) and nuclear stained cells (blue), using 2B6 antibody and DAPI, respectively .....	91
Figure 3.9 Immunolocalization of chondroitin-0-sulphate and nuclear stained cells, using 1B5 antibody and DAPI, respectively.....	92
Figure 3.10 Negative controls for immunolocalization of specific GAG types .....	93
Figure 3.11 KS GAG sulphation content across the bovine cornea.....	94
Figure 4.1 Light transmission as a function of position in human (n=8) (A) and bovine (n=8) (B) corneal stroma at 550nm.....	102
Figure 4.2 Electron micrographs of collagen fibrils along the central vertical axis from human central cornea to sclera.....	103
Figure 4.3 Average collagen fibril diameter and mean centre-to-centre collagen fibril Bragg spacing in the left (solid triangles) and right (open circles) human eye-bank corneas.....	104
Figure 4.4 A summary of plan .....	105
Figure 4.5 Transmission electron micrographs across the bovine cornea (anterior stroma) .....	108
Figure 4.6 Transmission electron micrographs across the bovine cornea (mid stroma) .....	109
Figure 4.7. Transmission electron micrographs across the bovine cornea (posterior stroma) .....	110
Figure 4.8 The mean fibril diameter measurements from transmission electron micrographs at different depths across the bovine cornea .....	111
Figure 4.9 Collagen fibril diameter (left) and IFBS (right) measurements across the bovine cornea .....	112
Figure 4.10 Collagen fibril diameter (left) and IFBS (right) measurements across and through the depth of the bovine cornea .....	114
Figure 4.11 Data from experiments 1-3: collagen fibril diameters as a function of tissue depth in bovine cornea .....	115
Figure 4.12 Data from experiments 1-3: collagen IFBS as a function of tissue depth in bovine cornea. ....	116
Figure 4.13 Transmission electron micrographs from define regions of the bovine cornea, stained with cuperomeric blue .....	117
Figure 5.1 Embden-Meyerhof pathway (EMP) – glucose degradation .....	125
Figure 5.2 Biochemical effects during contact lens wear.....	126
Figure 5.3 Diagram of the O <sub>2</sub> -dependent pathway with NAD at the centre, leading to the synthesis of KS or CS .....	128
Figure 5.4 A summary of experiments that was employed .....	130
Figure 5.5 Hydration differences between normal and hypoxic organ cultured corneas from centre to sclera .....	133
Figure 5.6 Total sulphated GAG differences between normal and hypoxic organ cultured corneas from centre to sclera .....	135
Figure 5.7 Immunolocalization of over-sulphated KS disaccharides (green), probed with 5D4 antibody and DAPI for cells (nucleus) (blue) .....	137

---

---

Figure 5.8 Immunolocalization of lesser-sulphated KS disaccharides (green), probed with 1B4 antibody and DAPI for cells (nucleus) (blue) .....	138
Figure 5.9 Immunolocalization of neoepitopes at the non-reducing terminal ends of KS (green), probed with BKS-1 antibody and DAPI for cells (nucleus) (blue) .....	139
Figure 5.10 Immunolocalization of lumican (green), probed with Lum-1 antibody and DAPI for cells (nucleus) (blue) .....	140
Figure 5.11 Immunolocalization of keratocan (green), probed with Ker-1 antibody and DAPI for cells (nucleus) (blue) .....	141
Figure 5.12 Negative controls for immunolocalization of the different sulphation patterns of KS GAGs and its core proteins .....	142
Figure 5.13 Sulphation patterns of keratan sulphate in normal and hypoxic (2% O <sub>2</sub> level) organ cultured corneas at the central region .....	143
Figure 5.14 The hydroxyproline content in normal and hypoxic atmospheric conditions over a time course.....	144

## List of tables

Table 1.1 A summary table of the different layers of the cornea .....	13
Table 1.2 The collagen family: ocular distribution found in vertebrate corneas .....	16
Table 1.3 Different types of proteoglycans .....	34
Table 2.1 A table showing the specificities of antibodies used during the project.....	56
Table 2.2 Preparation of enzymes used for IHC.....	59
Table 3.1 A summary of the antibodies used for this experiment.....	81
Table 4.1 Details of the x-ray parameters for the different tissue preparations .....	105
Table 5.1 Antibody dilutions used.....	132

---

## List of abbreviations

Ag	Antigen
BSA	Bovine serum albumin
CS	Chondroitin sulphate
DS	Dermatan sulphate
DMMB	Dimethylmethylene blue
ELISA	Enzyme-linked immunosorbent assay
EM	Electron microscopy
ECM	Extracellular matrix
FACIT	Fibril-associated collagens with interrupted triple helices
GAG	Glycosaminoglycan
HS	Heparin sulphate
Ig	Immunoglobulin
IHC	Immunohistochemistry
KS	Keratan sulphate
LRR	Leu-rich repeats
mAb	Monoclonal antibody
PBS	Phosphate-buffered saline
PMMA	Polymethylmethacrylate
PG	Proteoglycan
RGP	Rigid gas permeable
RER	Rough endoplasmic reticulum
SLRPs	Small leucine-rich family of proteins
SDS-PAGE	Sodium dodecyl sulphate polyacrylamide gel electrophoreses
TEM	Transmission electron microscopy
TSA	Tris saline azide
w/v	Weight/volume
v/v	Volume/volume

## Chapter 1: Introduction

# 1.

This thesis is concerned with the nature of glycosaminoglycan chains on proteoglycans and their possible roles in the corneal stroma. In this chapter a brief description of the cornea and its relationship to the other ocular tissues will be presented. This will then be followed by a detailed description of the structure of the corneal stroma, which will outline the structure and function of collagen and the importance of proteoglycan interactions.

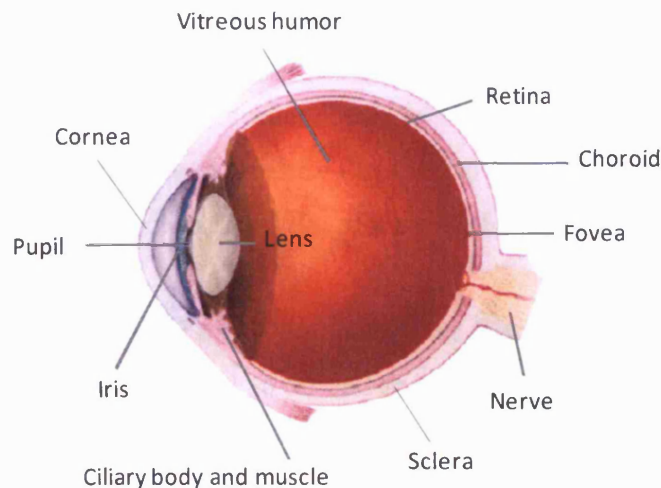


**Figure 1.1** The anatomy of the eye (<http://www.eyecare-for-you.com/anatomy-of-the-eye.php>, 2009).

The adult human eye is approximately 2.5 cm in diameter (Forrester et al., 2002). At the posterior end of the eye, approximately 85% is covered by the sclera, a white, dense, opaque protective coat that is not directly involved in the visual process (Figure 1.1). The cornea covers the remaining portion (anterior) of the eye, which is a uniquely transparent tissue with a high refractive power (Berman, 1991). Its posterior surface is bathed by the aqueous humor and is secreted by the ciliary epithelium.

When an object is observed, light passes through both the cornea and the lens (a transparent tissue), both of whose functions are to focus light rays onto the retina (Forrester et al., 2002). The light rays then pass through the vitreous, a transparent, viscous gel, which occupies approximately 90% of the total volume of the eye. Once the light rays are focused onto the retina, they are absorbed by the photoreceptors

(specialized cells located on the retina) and converted into electrical impulses, which are then transmitted through the optic nerve to the brain, and translated to a visual image (Berman, 1991).

### **1.1. The anatomy and physiology of the eye**

The cornea and the sclera together form the outer covering of the eye and can withstand both internal and external forces to maintain the shape of the eyeball and to protect the contents from mechanical injury (Maurice, 1957; Komai and Ushiki, 1991). Unlike other connective tissues, including sclera, the cornea is transparent. Anything that alters the underlying structure of the cornea, such as external damage or swelling resulting from the intraocular pressure exerted by fluid in the eye, can affect the mechanical and optical properties and affect the function of the eye (Huang and Meek, 1999).

The cornea is a dome-shaped tissue that covers the iris, pupil and the anterior chamber. It has a refractive index greater than air and is responsible for a large part of the optical power of the eye. Typically the cornea accounts for 2/3 of the focussing of the eye; the lens produces the remaining optical power (Forrester et al., 2002). The adult human cornea is approximately 11 mm in diameter (vertically), 0.52 mm thick at its central portion, increasing slightly at the outer-peripheral-limbal region (0.67 mm) (also known as corneoscleral junction; the region where the cornea meets the sclera) (Forrester et al., 2002).

The central third of the cornea is also referred to as the optical zone (Waring, 1989) and provides the majority of the cornea's refractive function. The near-spherical optical zone forms the foveal image (central vision) through the pupil and is often known as the prepupillary cornea (Boote et al., 2003). The remaining peripheral part of the cornea is less curved and serves mainly as a refractive surface for peripheral vision (Figure 1.2).

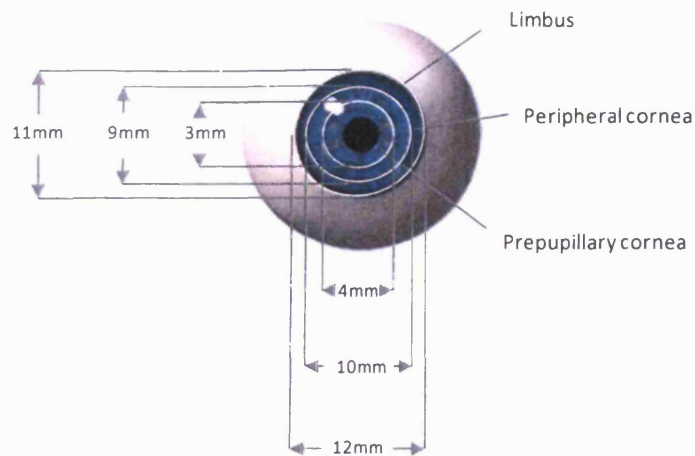


**Figure 1.2** A diagram showing the different surface zones in the human cornea (anterior corneal surface). Diagram adapted from (Boote et al., 2003; [http://www.nlm.nih.gov/medlineplus/ency/presentations/100206\\_2.htm](http://www.nlm.nih.gov/medlineplus/ency/presentations/100206_2.htm), 2010).

## 1.2. The structure and composition of the corneal stroma

The cornea comprises 5 layers: epithelium, Bowman's, stroma, Descemet's membrane and the endothelium (Figure 1.3) and the structure and function is summarized in Table 1.1.

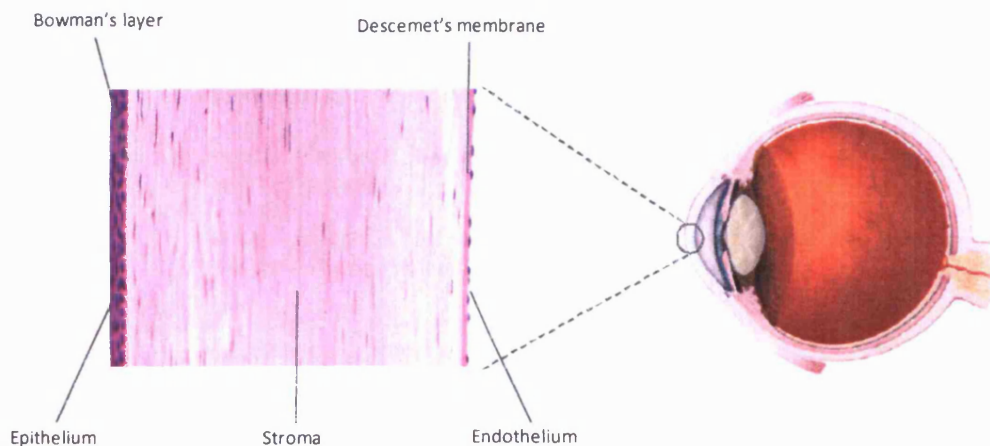


**Figure 1.3** The structure of the cornea and its constituent layers. Diagram adapted from ([http://www.images.missionforvisionusa.org/anatomy/2005\\_10\\_01\\_archive.html](http://www.images.missionforvisionusa.org/anatomy/2005_10_01_archive.html), 2005; <http://www.eyecare-for-you.com/anatomy-of-the-eye.php>, 2009).

Composition layer	Structure	Role
<b>Epithelium</b>	5-6 cell layers that cover the surface of the cornea	Block the passage of foreign material (e.g. dust, water and bacteria) into the eye
	50-60µm thick in man	Provide a smooth surface to absorb oxygen and cell nutrients from tears and then distribute these nutrients to the rest of the cornea
	Filled with tiny nerve endings that make the cornea extremely sensitive to pain when rubbed or scratched	Serves as a foundation on which the epithelial cells organize and anchor themselves by a basement membrane complex to a Bowman's membrane  The attachment of the epithelial cells to the basement membrane is thought to be mediated by hemidesmosomes through anchoring filaments and adhesive glycoprotein's (e.g. laminin and fibronectin)  (Berman, 1991; Forrester et al., 2002)
<b>Bowman's</b>	8-12µm thick in adult human	The role of Bowman's layer remains unclear, but it has been hypothesised to act to maintain corneal structural integrity or as a barrier against viral penetration  (Komai and Ushiki, 1991, Wilson and Hong, 2000)
	Transparent sheet of tissue  Consists of fine, randomly arranged protein fibres (collagen; type I, III, V and VII – anchoring filaments aiding network of filaments adding epithelial adhesion)	
<b>Stroma</b>	Main layer of the cornea	The transparency of the cornea is closely associated with the regular spacing of the collagen fibres (interfibrillar distance), which in turn is regulated by glycosaminoglycans and proteoglycans forming bridges between the collagen fibrils  (Müller, Pels and Vrensen, 1995; Forrester et al., 2002)
	Primarily composed of collagen fibres orientated parallel to the corneal surface  Between the collagen fibres, lay keratocyte cells and are connected by gap junctions to their neighbouring cells and are arranged in a corkscrew pattern	
<b>Descemet's membrane and endothelium</b>	Contains fibronectin, type IV, collagen and laminin	These particular cells are essential in maintaining the homeostasis of fluid and ions (e.g. Na <sup>+</sup> and Cl <sup>-</sup> ) within the stroma and aqueous humor, which are crucial to the corneal dehydration and transparency  (Berman, 1991, Beuerman and Pedroza, 1996)
	Type VIII collagen is also present, which forms a hexagonal lattice  Thin layer comprising of glycoprotein's (e.g. fibronectin and laminin), collagen and endothelial cells (4-6µm)	

**Table 1.1 A summary table of the different layers of the cornea.**

From the forgoing description of the 5 distinct layers of the cornea, the corneal stroma is the main layer (~500 µm thick, ~90% of the thickness of the cornea) and its ground

substance mainly consists of water (~78%), but its main structural components include collagen fibrils (~12-15% wet wt of tissue) and proteoglycans (~1-3% wet wt of tissue) (Baum, Maurice and McCarey, 1984; Berman, 1991). Other components found in the stroma include glycoproteins, soluble proteins, lipids and keratocytes (Berman, 1991).

The cornea is avascular, but nerve axons and their associated Schwann cells are occasionally observed in the anterior and mid stroma (Jalbert and Stapleton, 2005). The stroma consists numerous bundles or lamellae (over 200 lamellae in man), of collagen fibres. In the stroma, the lamella traverses a complete arc of the cornea and in each lamella the collagen fibres are parallel and equidistant from each other. Transparency of the cornea depends particularly on the degree of spatial order of its collagen fibrils which are narrow in diameter and closely packed in a regular manner (Maurice, 1957). The lamellae are denser, narrower (0.5-30  $\mu\text{m}$ ), thinner (0.2-1.2  $\mu\text{m}$ ) (Komai and Ushiki, 1991) and more intertwined (McTigue, 1967) in the anterior third of the stroma, compared to the posterior two thirds, where lamellae are wider (100-200  $\mu\text{m}$ ) (Komai and Ushiki, 1991), more parallel, orthogonally aligned (Meek and Quantock, 2001) and can be up to 4  $\mu\text{m}$  thick (McTigue, 1967; Komai and Ushiki, 1991). The collagen fibrils themselves are weak scatterers, as their fibril diameters are less than the wavelength of light, and fibril refractive index is close to that of the ground substance (Goodfellow, Elliott and Woolgar, 1978). The stromal keratocytes are irregularly found between neighbouring lamellae and are designed to scatter minimal light.

### **1.3. Stromal collagen**

Collagen is the most abundant protein in connective tissues. The maintenance of structural strength of most connective tissues is controlled by collagen molecules, which form the fibrillar elements found in the extracellular space of such tissues. Currently, there are 28 different collagen types identified, which are encoded by at least 40 different genes (Prockop and Kivirikko, 1995; Fitzgerald and Bateman, 2001; Boot-Handford et al., 2003; Gordon and Hahn, 2010) and exhibit characteristic tissue-specific patterns of expression. Several of these collagens have been found in the eye (Table 1.2). All collagens possess one or more triple helical domains. These domains are made of three polypeptide  $\alpha$  chains wrapped around each other into a right-handed

triple helix so that the final structure is a “rope-like rod” (Prockop and Kivirikko, 1995). This characteristic in collagen gives rise to a common feature in all collagen types, where glycine is on every third amino acid generating a repeating (Gly X-Y)<sub>n</sub> pattern, where X is often alanine or proline, and Y, hydroxyproline. Collagens are also rich in lysine and some in hydroxylysine residues, which participate in intramolecular and intermolecular cross-linking. In addition collagens have non-triple-helical regions, which are present at the ends of the molecule, but may additionally be interspersed, between triple- helical regions. Based on their structure and function, collagens have been classified into different groups:

- Fibril-forming collagens (e.g. types I, II, III, V, XI collagen)
- Fibril-associated (fibril-associated collagen with interrupted triple helices, FACIT) collagens (e.g. types IX, XII, XIV, XVI, XIX collagen)
- Collagens that form structures unrelated to fibril
- Short chain collagens (e.g. types VIII, X collagen)
- Basement membrane collagen (e.g. type IV collagen)
- Anchoring fibrils (e.g. type VII collagen)
- Microfibrillar (e.g. type VI collagen)
- Other collagens (e.g. types XIII, XV, XVII, XVIII, XX, XXI, XXII, XXIII, XXIV, XXV, XXVI, XXVII, XXVIII collagen)

Collagen type	Corneal sites					Notes
	Ep	B	S	D	En	
I		x	x			- Structural fibres
II	x <sup>a</sup>		x <sup>a</sup>			- Structural fibres
III			x			- Limits fibril diameter and repairs fibres
IV	x	x				- Network and scaffolding forming collagen
V			x			- Limits fibril diameter and cell shape
VI			x			- Beaded filament forming collagen for adhesion
VII		x				- Anchors fibrils for adhesion
VIII				x		- Forms scaffolds
IX	x <sup>a</sup>					- Co-distributes with type II collagen and regulates fibril diameter
XII	x	x	x		x	- Adhesion
XIII			x			- Found two thirds of the stroma and consists of a transmembrane domain
XIV		x <sup>a</sup>	x <sup>a</sup>			- Regulates fibrillogenesis and matrix assembly
XVII	x <sup>a</sup>		x <sup>a</sup>			- Known as the bullous pemphigoid antigen 2/BP180; localised to epithelia; an epithelial adhesion molecule; ectodomain cleaved by ADAM proteinases
XVIII	x	x				- Associated with basement membranes; endostatin is proteolytically released from the C-terminus of collagen XVIII; important for retinal vasculogenesis

**Table 1.2 The collagen family: ocular distribution found in vertebrate corneas.** Table modified from (Michelacci, 2003). EP = epithelium, B = Bowman's layer, S = stroma, D = Descemet's membrane and EN = endothelium. x<sup>a</sup> = found during chick embryonic development.

### 1.3.1. Structure and function of ocular collagens

The characteristics of different extracellular matrices (ECMs), whether it is in cartilage or in cornea for example, are determined by the synthesis, assembly, deposition of collagen molecules and their organization into unique macromolecular structures. Fibrillar collagen molecules are organized into fibrils, that are organized into tissue-specific macroaggregates such as regular layers (cornea and bone), cables (tendons and ligaments), or irregular layers (dermis, sclera). At each level of this hierarchy the collagen fibrils have tissue specific characteristics, i.e. fibril diameter, packing and organization. As previously mentioned, the corneal stroma has small, uniform diameter fibrils that are regularly packed and organized into orthogonal layers (lamella). These characteristics permit this tissue to be strong and transparent. In contrast, the Bowman's

layer has very small diameter fibrils with irregular packing, organized as a fibrillar weave at the interface between the epithelial basement membrane and the corneal stroma.

The corneal stroma itself mainly consists of type I collagen (75%) and low proportions of type V (8%) and type VI collagen (17%) (Kern, Menasche and Robert, 1991). Type II collagen is found during corneal development (Gelse, Poschl and Aigner, 2003; Michelacci, 2003) while type III collagen is found during wound healing, inflammation and several pathological conditions (Nakamura, 2003).

### ***1.3.2. Biosynthesis of collagen***

Like all proteins, collagen biosynthesis is a multi-step process that starts with the transcription and translation of the individual collagen gene. The type of collagen to be formed is characterized by the presence of a large number of co- and post-translational modifications, many of them being unique to collagens or collagen-like proteins (Prockop and Kivirikko, 1995). The fibril-forming collagens (also referred as striated collagen) are synthesized as procollagens (where each of the 3 polypeptide chains has a globular domain at the N- and C-termini) on the ribosomes located on the rough endoplasmic reticulum (RER) in cells and is illustrated in Figure 1.4. Briefly, the procollagen molecule is secreted into the ECM where specific proteases at the cell surface remove the N- and C-terminal non-helical, globular ends. The resulting collagen molecules can then associate in a staggered array to form collagen fibrils of various lengths and diameters. Lysyl oxidase then converts the amino groups on some of the lysine residues in the collagen polypeptide chain to aldehydes that react with amino groups on lysines in other chains to form covalent crosslinks.

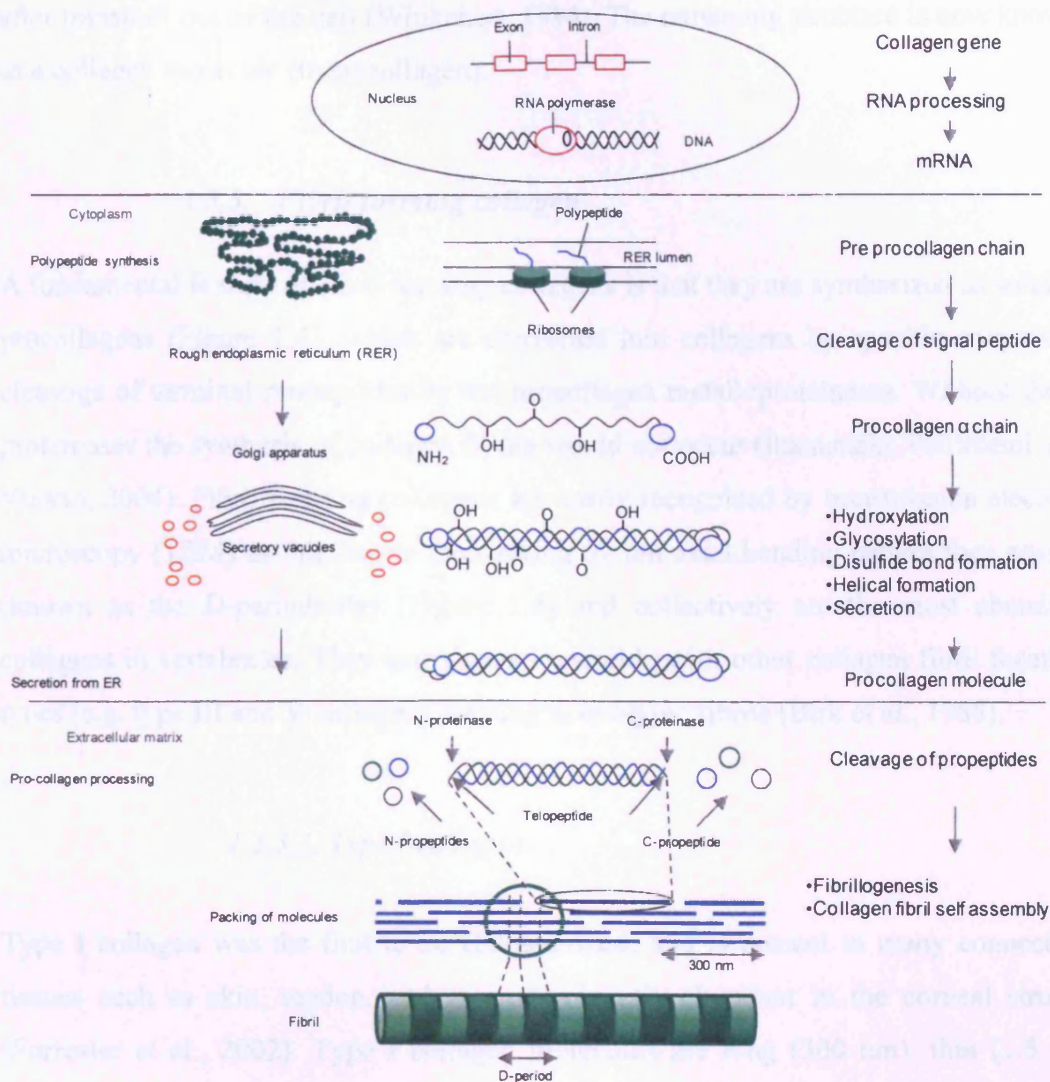


**Figure 1.4 Fibril forming collagen synthesis.** The collagen precursor chains are co-translationally translocated into the endoplasmic reticulum (ER) lumen, where specific post-translational modifications occur. Three collagen  $\alpha$ -chains associate specifically via their C-terminal domains (Khoshnoodi et al., 2006) to form heterotrimers or homotrimers. The helical collagens are trafficked via the Golgi network to the plasma membrane, and secreted into the extracellular space. The fibril-forming collagens are secreted as precursor forms, called procollagens, with N- and C-terminal non-collagenous domains. These domains are removed by the action of specific proteases, and the collagens are assembled into dense fibrils with a characteristic D-periodicity. The fibril is stabilized by covalent lysine- and hydroxylysine-derived crosslinks. Diagram adapted from (Kadler et al., 1996).

The type of collagen to be formed is partially determined by the kinds of post-translational modifications that occur to the triple helix as well as the degree to which the chains are hydroxylated. In the fibril forming collagens (types I, II, III, V), and similarly in some other types, large portions of the non-helical N- and C-terminal peptides (extension peptides) are removed by the catalytic action of peptidase enzymes

after transport out of the cell (Whikehart, 1994). The remaining structure is now known as a collagen molecule (tropocollagen).

### 1.3.3. Fibril forming collagen

A fundamental feature of fibril forming collagens is that they are synthesized as soluble procollagens (Figure 1.4), which are converted into collagens by specific enzymatic cleavage of terminal propeptides by the procollagen metalloproteinases. Without these proteinases the synthesis of collagen fibrils would not occur (Ihanamäki, Pelliniemi and Vuorio, 2004). Fibril forming collagens are easily recognized by transmission electron microscopy (TEM) as this due to the striking 67 nm axial banding pattern they possess (known as the *D*-periodicity) (Figure 1.4) and collectively are the most abundant collagens in vertebrates. They can also co-assemble with other collagen fibril forming types (e.g. type III and V collagen) creating heterotypic fibrils (Birk et al., 1988).

#### 1.3.3.1. Type I collagen

Type I collagen was the first to be characterized, and is present in many connective tissues such as skin, tendon, and is predominantly abundant in the corneal stroma (Forrester et al., 2002). Type I collagen molecules are long (300 nm), thin (1.5 nm diameter) proteins that consists of three coiled subunits, designated as  $[\alpha 1(I)]_2 [\alpha 2(I)]$  (Whikehart, 1994). Each chain contains 1050 amino acids wound around each other in a right-handed triple helix structure. They form the *D*-periodic striated fibrils in the extracellular space, giving the tissue their:

- Mechanical strength
- Biomechanical scaffold for cell attachment (e.g. platelets and fibroblasts)
- Anchorage of macromolecules (e.g. integrins, fibonectin, fibromodulin and decorin) (Hulmes and Miller, 1981).

In addition, type I collagen molecules are (*in vivo*) normally incorporated with other collagen molecules such as type III collagen (in skin and reticular fibres) (Fleischmajer et al., 1990) or type V collagen (in bone, tendons and corneal stroma) (Niyibizi and Eyre, 1989a; Michelacci, 2003).

### 1.3.3.2. Type V collagen

Type V collagen is a minor fibrillar collagen present in tissues where type I collagen co-assemble as heterotypic fibrils (Figure 1.5). This heterotypic collagen molecule can form very small diameter fibrils, where the NH<sub>2</sub> of type V collagen epitopes are exposed, and triple helical epitopes are masked by the fibril structure (Birk, 2001). The most common isoform of type V collagen found in the cornea is [ $\alpha$ 1(V)<sub>2</sub>  $\alpha$ 2(V)] (Birk, Fitch and Linsenmayer, 1986; Birk et al., 1988; Birk et al., 1990). However, other isoforms;  $\alpha$ (V)<sub>3</sub> homotrimer and [ $\alpha$ 1(V)  $\alpha$ 2(V)  $\alpha$ 3(V)] have been reported (Sage and Bornstein, 1979; Madri, Foellmer and Furthmayr, 1982; Niyibizi, Fietzek and van der Rest, 1984). Type V collagen  $\alpha$  chains also form heterotypic molecules with type XI collagen  $\alpha$  chains (Niyibizi and Eyre, 1989b; Mayne et al., 1993), however, the distribution functional roles of these isoforms remains unclear.

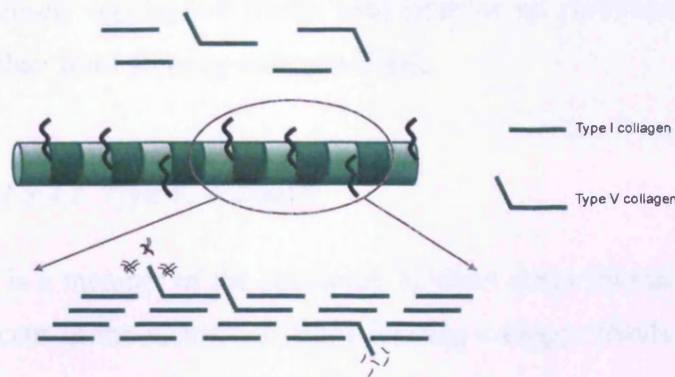


**Figure 1.5 A model of type I/V heterotypic fibril.** Type I and V collagens co-assemble to form a striated fibril. This co-assembly requires that the NH<sub>2</sub>-terminal domain of type V collagen project through the gap region and be exposed on the fibril surface. The triple helical portion of the type V molecule is packed with the type I molecules so that it is internalized. The NH<sub>2</sub>-terminal domains on the fibril surface increase as assembly proceeds and either alone and/or in conjunction with other macromolecules alters the properties of the fibril surface (Birk, 2001).

In the cornea, the tightly packed and highly organized fibrils are composed of types I and V collagens, and contain the largest relative amount of type V collagen (Tseng, Smuckler and Stern, 1982). The presence of type V collagen is one of the factors influencing fibril diameter, which has been proposed to contribute to corneal transparency (Birk et al., 1990). *In vitro* studies (Birk et al., 1990) have demonstrated that when small amounts (2-5%) of type I collagen are added, numerous striated fibrils are formed. Type I collagen alone formed fibrils with a broad range of diameters. In the

presence of increasing amounts of type V collagen the mean diameter progressively decreased. Furthermore, when the NH<sub>2</sub>-terminal domain of type V collagen was removed, a high concentration was needed to produce a measurable decrease in fibril diameter. It was suggested that the NH<sub>2</sub> domain of the type V collagen is responsible for the regulatory effects of this collagen on fibril diameter. Corneal abnormalities, including flattened corneas and micro corneas, due to abnormal fibrillogenesis have been reported to result from type V collagen gene mutations both in mice (Andrikopoulos et al., 1995) and in human (Nicholls et al., 1996; Giunta and Steinmann, 2000).

#### ***1.3.4. Filamentous collagen***

Filamentous collagens can be subdivided into pericellular and matrix collagens. They sometimes form loosely aggregated fibrils with little or no periodicity but they are frequently thinner than fibril forming collagen fibrils.

##### *1.3.4.1. Type VI collagen*

Type VI collagen, is a member of the subfamily of short chain filamentous collagens. These collagens occur in the vicinity of fibril forming collagen fibrils, but are absent from the fibrils themselves, and are located to a fine filamentous network associated with the striated fibril bundles (Figure 1.6) (Abedin, Ayad and Weiss, 1982; von der Mark et al., 1984). Type VI collagen is a rod-like molecule whose triple helical portion is approximately 105 nm long (von der Mark et al., 1984; Kadler et al., 2007). Each of the three different chains of the type VI collagen protein contains a short triple-helical domain, and of large N- and C-terminal globular domains (Prockop and Kivirikko, 1995) making up more than half of the molecular weight of the collagen molecule (Bishop, 1996). Collagen type VI exploits disulphide bonds to form anti-parallel coiled dimers, and these are assembled both linearly (to form beaded filaments) and laterally (to form open networks) via their globular terminal domains (Knupp and Squire, 20012005).

In skin, type VI filaments are highly concentrated around endothelia basement membranes and form a loose sheath around the blood vessels, as well as nerves and fat cells. A study by Burgeson (1988) has suggested that the loose sheath of type VI collagen filaments serves to separate blood vessels, nerves, and fat cells from bundles of striated fibrils which make up tissue compartments; this also provides free movement between striated fibril bundles and cellular elements (Burgeson, 1988).

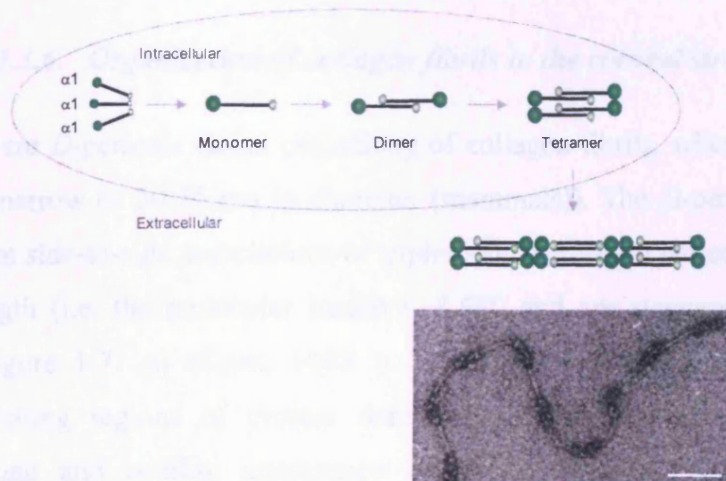


**Figure 1.6 A schematic diagram of type VI collagen.** The individual collagen helices are not secreted as monomers but assemble intracellularly into antiparallel overlapping dimers (two triple-helical collagen VI molecules), which then align to form tetramers (four triple-helical collagen VI molecules) (Kadler et al., 2007). Collagen VI is secreted as tetrameric structures of four collagen VI molecules that aggregate end-to-end to form long thin periodically beaded microfibrils. Scale bar 100 nm.

In cartilage and in the eye small amounts of type VI collagen microfibrils are found and these are thought to serve a function in stabilizing different fibrillar structures (Marshall, Konstas and Lee, 1993; Thomas, Ayad and Grant, 1994; Bishop, 1996). In the vitreous, type VI collagen microfibrils have been suggested to contribute to the gel structure by linking together the heterotypic collagen fibrils or by linking the heterotypic fibrils to the hyaluronan network (Bishop, 1996; Bishop, 2000).

### 1.3.5. Other ocular collagens

New collagen types are continuously being discovered and some of these are found within the corneal stroma, whilst others have been found within the cornea itself. For example collagen type XII is found within the corneal stroma. It is distributed

periodically along collagen fibrils (periodicity of 150-200 nm) (Wessel et al., 1997) and is thought to stabilize the collagen fibril arrangement by bridging the fibrils (Keene et al., 1991) through the interactions of proteoglycans (Koch et al., 1995). In addition it is also thought that collagen type XII may play an important role in the morphogenesis of corneal scar tissue and healing (Zhan, Burrows and Cintron, 1995; El-Shabrawi, Kublin and Cintron, 1998).

### 1.3.6. Organization of collagen fibrils in the corneal stroma

Corneal fibrils are  $D$ -periodic (axial periodicity of collagen fibrils, where  $D \approx 65$  nm) and uniformly narrow ( $\approx 30$ -35 nm in diameter (mammals)). The  $D$ -periodicity of the fibril arises from side-to-side associations of triple-helical collagen molecules that are  $\approx 300$  nm in length (i.e. the molecular length =  $4.4D$ ) and are staggered by an axial distance  $D$  (Figure 1.7. A) (Scott, 1988 ). The staggering of collagen molecules produces alternating regions of protein density in the fibril, which explains the characteristic gap and overlap appearance of fibrils negatively contrasted from transmission electron microscopy (TEM) (Figure 1.7 B).

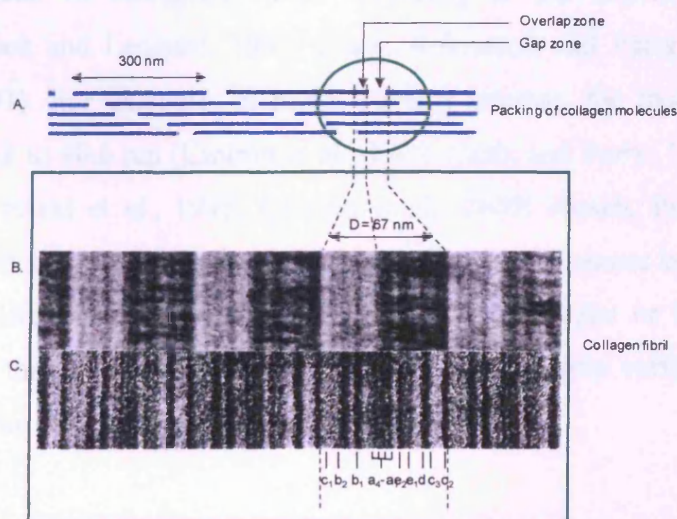


**Figure 1.7 Axial packing arrangements of collagen molecules in a fibril (A), as derived from analysis of the negative (B) and positive (C) staining patterns. (B)** Collagen fibril negatively stained with sodium phosphotungstic acid (1%, pH 7). The fibril is from reconstituted from acetic acid soluble calf-skin collagen. The repeating broad dark and light zones are produced by preferential stain penetration into gap regions. (C) Fibrils positively stained with phosphotungstic acid (1%, pH 3.4) and the uranyl acetate (1%, pH 4.2). The darkly staining transverse bands are the result of uptake of electron-dense heavy metal ions from the staining solutions onto charged residue side groups of collagen (Kadler et al., 1996).

Between corneal collagen molecules and collagen fibril exist another level of organization, the microfibrils. The microfibrils have a lateral spacing of approximately 4 nm and a tilt of 15° to the fibril axis (Holmes et al., 2001 ). This tilting may lead to the reduced axial periodicity in the cornea compared with tendon tissue (Meek and Boote, 2004).

Examination in the electron microscope, using positive staining, discloses the distribution of charged amino acid residues. In the case of collagen, each *D*-period displays five staining zones labelled *a* to *e* (Figure 1.7 C). These zones are further subdivided at a higher resolution, leading to 12 so-called positive staining bands, *a*1 to *e*2 (Hodge and Schmitt, 1960). The bands are often used to describe the axial position along a collagen fibril; *a*1 and *a*2 are in the gap zone, *a*3 is at the gap/overlap junction, *a*4, *b*1, *b*2 and *c*1 are in the overlap zone, *c*2 is at the gap/overlap junction and *c*3, *d* and *e*2 are in the gap zone (Chapman, 1974; Meek, Chapman and Hardcastle, 1979).

The diameter of collagen fibril is highly uniform, and has been measured by both microscopically and diffraction techniques. Electron microscopy studies have showed that the diameter of collagens varies according to the experimental preparation employed (Meek and Leonard, 1993; Craig, Robertson and Parry, 1996; Meek and Fullwood, 2001). For example, in rabbit corneal stromas, the mean fibril diameters range from 17.8 to 40.6 nm (Cintron et al., 1978; Craig and Parry, 1981; Yamabayashi et al., 1991; Freund et al., 1995; Cannon et al., 2000; Hirsch, Prenant and Renard, 2001). This variation alternatively could be due to the differences between rabbits (i.e. inter-sample differences that might be related to age, gender or breed), or regional differences in the actual fibril dimensions (i.e. intra-sample variations between the anterior to posterior aspects of the corneal stroma).

Early electron microscopy studies on human cornea have showed that the interfibrillar spacing of collagen fibrils decreased with age and the fibril diameter remained constant (Kanai and Kaufman, 1973). However, using x-ray diffraction, a number of studies have shown that the diameter of human corneal collagen is approximately 31 nm and increases to approximately 34 nm with age (Meek and Leonard, 1993; Daxer et al., 1998). The spatial arrangement of the collagen fibrils in the cornea is thought to be of

major importance for the tissue's transparency (Maurice, 1957). Such difference in results may have been due to the preparations of the experiment (discussed later in Chapter 2).

3-D reconstruction from micrographs taken over a range of tilt angles, Sandler (1974) revealed that corneal collagen fibrils are not entirely parallel within the lamella. Some are relatively straight, others are oblique, and others appear to wave (Sandler, 1974). These results were also indicated in x-ray diffraction analysis (Goodfellow et al., 1978), where collagen fibrils did not pack in a lattice formation within the corneal stroma, but instead a short-range order occurs (Sayers et al., 1982). However this short-range order is thought to be sufficient to allow corneal transparency (Farrell and McCally, 2000). Within each lamella the collagen fibrils run in the same direction, and are parallel to the corneal surface, however, the fibril direction in adjacent lamellae varies (Komai and Ushiki, 1991). Wide angle X-ray diffraction experiments on human corneas indicated two preferred orientations for the lamellae and their component fibrils in the plane of the cornea at its centre that are 90° apart: a temporal-nasal and a superior-inferior orientation (throughout the width of the cornea) (Meek et al., 1987; Boote et al., 2005). This may be linked to the eye muscles and the biomechanical stability (Boote et al., 2005; Meek and Boote, 2009). At the limbus region, in the human cornea, collagen fibril orientation becomes circumferential (Newton and Meek, 1998; Meek and Boote, 2004).

#### **1.4. Extracellular matrix components - Proteoglycans**

Proteoglycans (PGs) are glycoprotein which consists of a core protein with one or more covalently attached glycosaminoglycan (GAG) chain attached to the core protein. They have since also been grouped into families based homologous sequences of amino acids in their core protein that confer a particular activity and now they are named and grouped according to the type of GAG chain attached to the core protein. Most PGs fit into one of 3 categories:

- Intercalate into plasma membranes
- Bind to hyaluronan
- Modulate collagen fibril formation

Hyaluronan is a GAG but it is not attached to a core protein and is usually found in synovial fluid, vitreous humor, and in the ECM of loose connective tissues.

PGs are found in all connective tissues, extracellular matrices and on the surface of many cells. These functions are often due to the interaction of proteins with the glycosaminoglycan (GAG) chains, which can have variable affinity, and specificity, dependant on charge interactions (Kjellen and Lindahl, 1991).

PG core proteins range in size from 20-450 kDa and regions of the core protein often show homology to motifs contained in globular type proteins. In cornea, there are four PGs in the adult corneal stromal ECM; decorin (Li et al., 1992), lumican (Blochberger et al., 1992; Kao et al., 2006), keratocan (Corpuz et al., 1996; Chakravarti, 2006) and mimecan (Funderburgh et al., 1997). The GAG side chains are repeating disaccharides with sulphate esters and can be as large as 70 kDa. In many species, the predominant corneal GAG side chains include; chondroitin sulphate/dermatan sulphate (CS/DS), keratan sulphate (KS) and small amounts of heparan sulphate (HS) (Hassell, Kimura and Hascall, 1986). Each GAG is a polymer of a disaccharide, in KS *N*-acetylglucosamine (GlcNAc) and galactose (Gal) and in DS *N*-acetylgalactosamine (GalNAc) and glucuronic/ iduronic acid (GlcA/IdoA). GAG carbohydrates are sulphated to various degrees (Figure 1.8).

The core protein is synthesized in the RER and the GAG side chains are added to the core protein in the Golgi body. The PGs are then secreted into the ECM. Corneal PGs, like most other PGs, interact strongly with other components in the ECM and can only be quantitatively extracted and in an intact by denaturing solvents (Rada, Cornuet and Hassell, 1993).

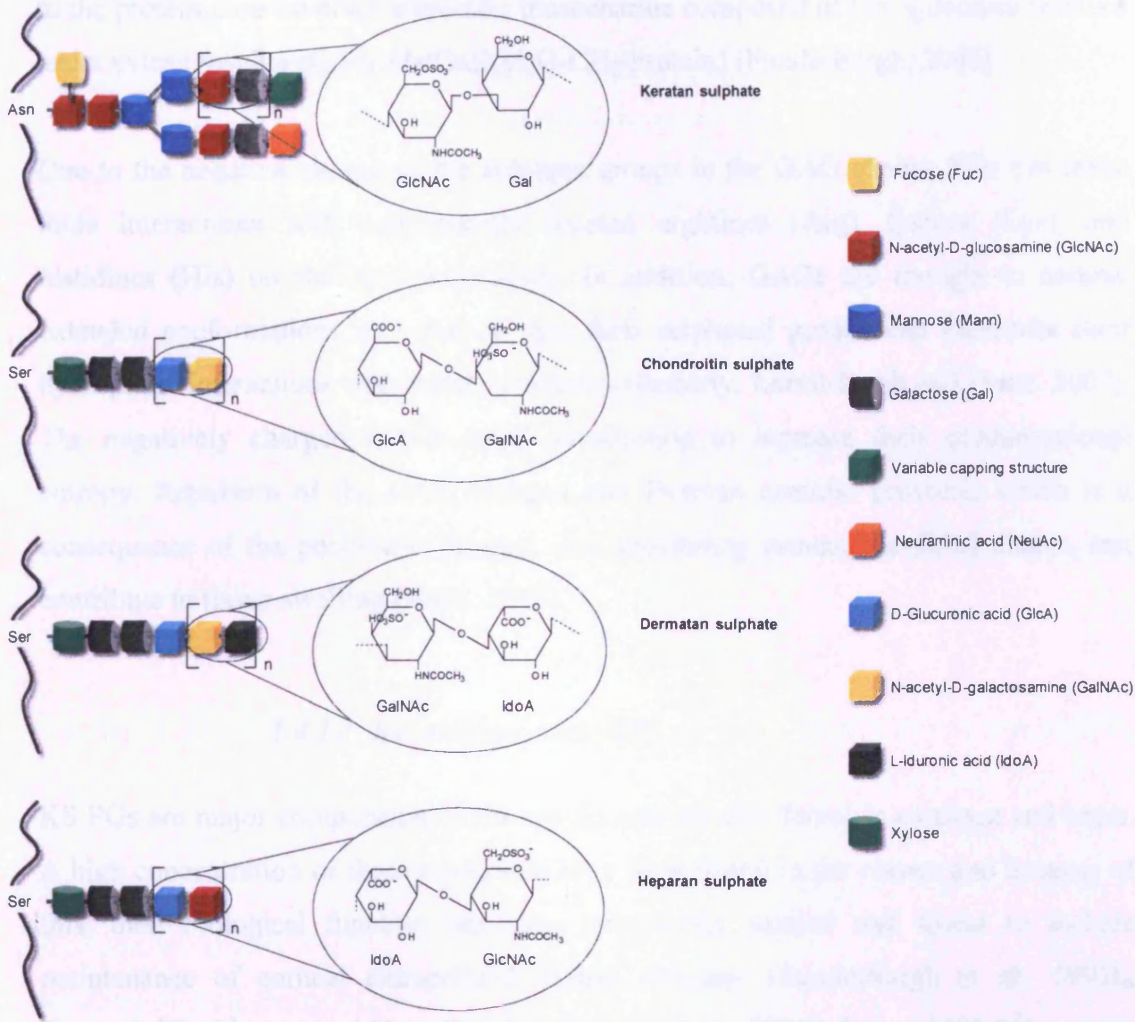


Figure 1.8 The chemical composition of proteoglycans and its different glycosaminoglycan chains attached.

### 1.4.1. Glycosaminoglycans (GAGs)

Structurally, GAGs are unbranched chains of repeating disaccharide units where one of the monosaccharides is an amino sugar, and one or both monosaccharides contain a sulphate or carboxylate group (Kjellen and Lindahl, 1991; Gandhi and Mancera, 2008). Corneal PGs belong to the small leucine-rich protein (SLRP) family and their polysaccharide chains typically consist of repeating disaccharide motifs, with alternative residues of hexosamine and uronic acid (either *D*-GlcA or *L*-IdoA) or sugar (either GlcNAc or GalNAc) and are often sulphated. At physiological conditions, the sulphate and uronic groups are charged and it is this that provides the GAG chains with a very high negative charge density (Gandhi and Mancera, 2008). The linkage of GAGs

to the protein core involves a specific trisaccharide composed of two galactose residues and a xylose residue (GAG-GalGalXyl-O-CH<sub>2</sub>-protein) (Funderburgh, 2000).

Due to the negative charge of the sulphate groups in the GAG chains, PGs can make ionic interactions with conveniently located arginines (Arg), lysines (Lys), and histidines (His) on the surface proteins. In addition, GAGs are thought to assume extended conformations in water so that their sulphated groups can maximize their hydrophilic interactions with water molecules (Imberty, Lortat-Jacob and Perez, 2007). The negatively charged GAGs swell in solution to increase their conformational entropy. Repulsion of the GAG charges and Donnan osmotic pressure, which is a consequence of the positively charged ions gravitating around the GAG chains, can contribute to tissue swelling (Scott, 2003).

#### 1.4.1.1. Keratan sulphate (KS)

KS PGs are major components of the cornea and are also found in cartilage and brain. A high concentration of these molecules have been found in the cornea and because of this, their biological function has been extensively studied and found to include maintenance of corneal extracellular matrix structure (Funderburgh et al., 1991b; Cornuet, Blochberger and Hassell, 1994; Connon et al., 2004). Corneal KS PGs consist of PG core proteins, such as lumican, keratocan, and mimecan, carrying KS GAGs in an *N*-linked manner (Funderburgh, 2002). KS was first identified by Suzuki (1939) in extracts of the cornea (Suzuki, 1939) and has been characterized as linear polymer of lactosamine, 3Gal $\beta$ 1-4GlcNAc $\beta$ 1, sulphated at the C6 of both hexose (*N*-acetylglucosamine (GlcNAc) and galactose (Gal)) moieties (Meyer et al., 1953) (Figure 1.9). Synthesis of KS GAG chains on PGs is processed by glycosyltransferases and sulfotransferases localized in the Golgi body, and matured KS PGs are secreted into the extracellular matrix. Elongation of the carbohydrate backbone of the GAG chain is catalyzed by enzymes of two glycosyltransferases ( $\beta$ 1-3-*N*-acetylglucosaminyltransferase ( $\beta$ 3GnT) and  $\beta$ 1,4-galactosyltransferase ( $\beta$ 4GalT) and sulphation of the chain is catalyzed by two carbohydrate sulfotransferases (Kitayama et al., 2007).

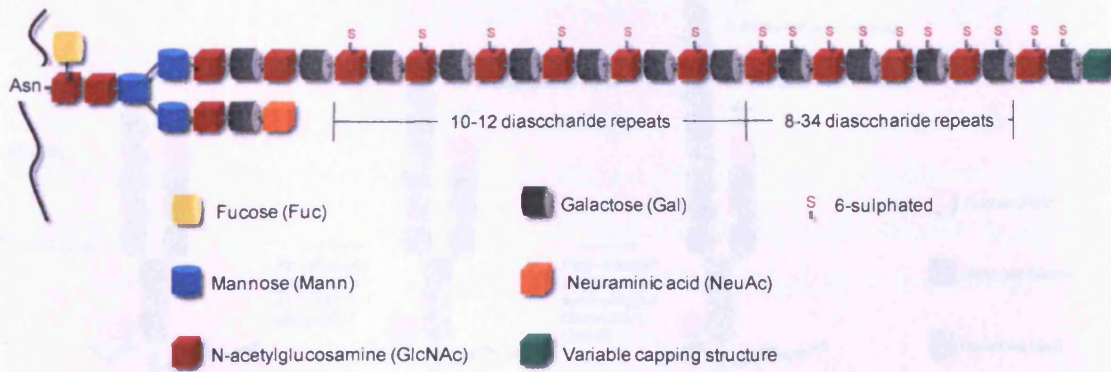


**Figure 1.9 A simplified diagram of corneal keratan sulphate (KSI) structure.** The disaccharide structure of KS can either be mono-, di- or un- sulphated on the repeat disaccharide units. Disulphated structures occur towards the non-reducing terminal, monosulphated disaccharides towards the middle of the structure and unsulphated disaccharides occur towards the linkage region of the chain. Diagram adapted from (Funderburgh, 2000).

Over the decades, KS has been divided into two classes (KSI and KSII) to distinguish KS from cornea (KSI) and that of cartilage (KSII) (Figure 1.10). The corneal KS is N-linked to asparagine (Asn) residues in the core protein, with the KS extending one branch and sialic acid terminating the second branch (Nilsson et al., 1983). Cartilage KS chains are shorter than KS of cornea (5-11 disaccharides) and are highly sulphated, consisting of disulphated monomers interrupted occasionally by single mono-sulphated lactosamine monomers (Nieduszynski et al., 1990). KSII are O-linked to serine (Ser) or threonine (Thr) residues (Funderburgh, 2000).

KS has also been implicated in motility of corneal endothelial cells, a single layer epithelium that lines the posterior surface of the cornea. These cells normally display a mosaic distribution of KS at their apical surface, but after wounding the KS is reduced or absent on migrating cells. KS returns in abundance to the cell surface when the cells cease migration (Davies et al., 1999).

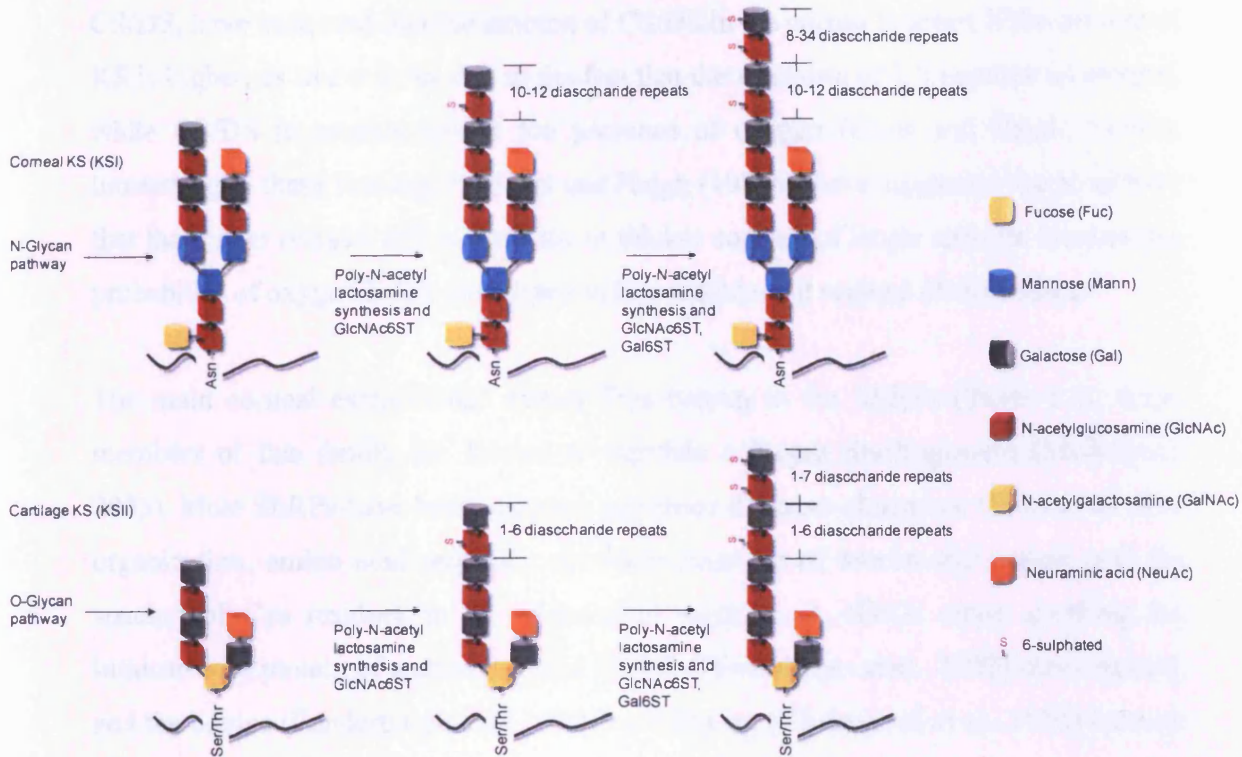


**Figure 1.10** The structural differences between corneal KS (KSI) and cartilage KS (KSII). The major difference between the two KS is based upon the protein linkage: KSI are N-linked to Asp amino acids via N-acetylglucosamine and KSII are O-linked to specific Ser/Thr amino acids via N-acetyl galactosamine. The diagram also illustrates the synthesis of the two KS. GlcNAc6ST = GlcNAc-6-sulfotransferase, Gal6ST = Gal-6-sulfotransferase. Diagram adapted from (Funderburgh, 2000; Brown, Crawford and Esko, 2007).

The degree of sulphation is a major component to GAGs and results from its synthetic pathway. Corneal KS sulphation is neither uniformly nor randomly distributed along the linear GAG chain (Quantock, Young and Akama, 2010). In bovine and human corneal KS, studies have indicated that the carbohydrate chain length has approximately 14 (Plaas et al., 2001; Quantock et al., 2010) to 32 (Tai, Huckerby and Nieduszynski, 1996; Tai et al., 1997) disaccharide repeat units (~4% unsulphated, ~42% monosulphated, and 54% disulphated disaccharides). The sulphation in GAGs is an important and has implications for corneal extracellular matrix structure, for example collagen interfibrillar spacing, mechanical stability between individual fibril, hydration content and tissue transparency.

KS is found to be more abundant in the corneas of animals that have thick corneas, and this predominantly may be due to the high presence of the over-sulphated terminal domain of KS (Scott and Bosworth, 1990). Comparative studies between KS and

CS/DS, have indicated that the amount of CS/DS in the cornea is lower if the amount of KS is higher, as this may be due to the fact that the synthesis of KS requires no oxygen, while CS/DS is synthesized in the presence of oxygen (Scott and Haigh, 1988b). Interestingly, these findings by Scott and Haigh (1988b), have suggested the possibility that the longer oxygen diffusion paths in thicker corneas of larger animals increase the probability of oxygen being consumed before reaching all regions of the cornea.

The main corneal extracellular matrix PGs belong to the SLRPs (Table 1.3). Some members of this family are known to regulate collagen fibrillogenesis (Michelacci, 2003). Most SLRPs have been grouped into three different classes on the basis of gene organization, amino acid sequence similarity, number of leucine-rich repeat, and the spacing of Cys residues in the N-terminal segment. A cDNA clone encoding the lumican core protein of a chick corneal KS PG (Blochberger et al., 1992) was obtained, and the bovine (Funderburgh et al., 1993) and human (Chakravarti et al., 1995) lumican core proteins were cloned later. Two other KS PGs, keratocan and mimecan (or osteoglycin), were cloned from the bovine cornea (Corpuz et al., 1996). Although expressed in other tissues, lumican, keratocan, and mimecan are glycosylated only in the cornea with sulphated KS chains.

#### 1.4.1.2. Importance of KS

Macular corneal dystrophy (MCD) is a common corneal disease, it is an autosomal recessive condition, in which progressive corneal opacification is initiated at an early age. The disease phenotype has been biochemically and genetically linked to defects in KS metabolism by keratocytes (Hassell et al., 1980; Nakazawa et al., 1984) and at least three biochemical subtypes (types I, IA and II) of the disease have been identified. It has been identified that MCD patients have a defective gene, localized at chromosome 16 and has shown to encode the *N*-acetylglucosamine-6-sulfotransferase (c-GlcNAc6ST) (Lui et al., 1998; Akama et al., 2000), the enzyme that initiates sulphation of KS chains on PGs. Cell extracts prepared from MCD type I corneas are unable to sulphate GlcNAc residues on exogenously added oligosaccharide acceptors (Hasegawa et al., 2000), unlike the normal corneal extracts, suggesting that these types of mutations result in the production of non-functional enzymes. MCD is thought to be caused by a metabolic defect in the synthesis of KS, particularly with type I Macular

dystrophy (a subgroup of Macular dystrophy) (Edward et al., 1990). Disruption of KS synthesis exerts major effects on corneal clarity. MCD I corneas produce an immature form of KS with a smaller protein core (Nakazawa et al., 1984) resulting in progressive clouding from reduced interfibrillar spacing and corneal thickness (Quantock et al., 1990).

Although MCD I phenotype is linked to heritable defects in KS synthesis, more C-6-S is found (Klintworth, 1976) and over sulphated CS PGs are reported (Nakazawa et al., 1984; Meek et al., 1989). In addition, it has been reported (Plaas et al., 2001) that MCD type 1, KS chains were significantly reduced to 3-4 disaccharides (~14 disaccharides per chain in normal corneas) and chain sulphations were absent. Chondroitin/dermatan sulphate chain sizes were also significantly reduced to ~15 disaccharides (~40 disaccharides per chain in normal corneas); however, the contents of 4- and 6-sulphated disaccharides were proportionally increased. It was suggested that such changes may imply a modified tissue content of individual PGs and/or an altered efficiency of chain substitution of the core proteins.

#### 1.4.1.3. Dermatan sulphate (DS)

DS is composed of linear polysaccharides, *N*-acetylgalactosamine (GalNAc) or GlcA joined by  $\beta$ 1,4 or 1,3 linkages respectively. The structure of DS and CS are very similar, e.g. DS is defined as a CS by the presence of GalNAc. The presence of IdoA in DS distinguishes it from chondroitin-4-sulphate and chondroitin-6-sulphate (Trowbridge and Gallo, 2002) (Figure 1.11) CS/DS PGs can be structurally diverse, as this could be due to the chains having very low to moderate levels (15-64%) of sulphated disaccharides, and differing marked levels of 4- and 6- sulphate groups (Achur et al., 2004). CS/DS can be significantly long, ~40 disaccharides per chain, and consists of ~64% unsulphated, ~28% 4-sulphated, and ~8% 6-sulphated disaccharides.

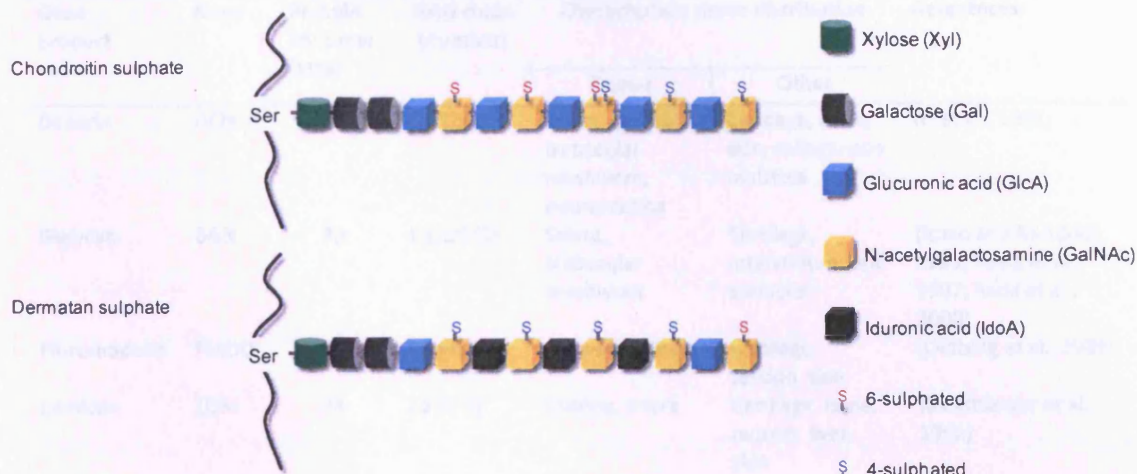


**Figure 1.11** A simplified diagram of chondroitin sulphate (CS) and dermatan sulphate (DS) structure. Diagram modified from (Esko, Kimata and Lindahl, 2008).

PGs which contain DS are covalently attached via an *O*-xylase linkage to serine residues of the core protein. The two most extensively studied DS PGs are the SLRPs; decorin and biglycan. Both decorin and biglycan have a pro-peptide that is highly conserved and may function as recognition signal for xylosyltransferase (the first enzyme involved in the synthesis of GAG chains) (Iozzo, 1997). In addition, both proteins have a common feature which is the presence of 10 leu-rich repeats (LRRs), flanked by Cys-rich regions. These PGs contain an N-terminal domain that is usually substituted with either one (decorin) or two (biglycan) CS/DS side chains (Iozzo, 1999).

## 1.2.2. *Proteoglycan core protein - Laminin*

Laminin was initially described as a normal PGC, it is now known to be expressed in a variety of tissues following injury (Friedenstein et al., 1991a), lung (Dobnikoff et al., 1998), cellular carcinoma (Sawata et al., 1999) and skin (Chakravarti et al., 1998; Chakravarti et al., 1999). Current evidence of normally expressed by smooth muscle cells, however, during the early phase of corneal wound healing it is transiently expressed by the corneal epithelial cells (Li et al., 2000).

Gene product	Gene	Protein core mw (kDa)	GAG chain (number)	Characteristic tissue distribution		References
				Ocular	Other	
<b>Decorin</b>	DCN	36	CS/DS [1]	Sclera, cornea, trabecular meshwork, neural retina	Cartilage, bone, skin, collagenous matrices	(Li et al., 1992)
<b>Biglycan</b>	BGN	38	CS/DS [2]	Sclera, trabecular meshwork	Cartilage, interstitium, cell surfaces	(Iozzo and Murdoch, 1996; Wirtz et al., 1997; Rada et al., 2000)
<b>Fibromodulin</b>	FMOD	42	KS [4]	Cornea, sclera	Cartilage, tendon, skin	(Oldberg et al., 1989)
<b>Lumican</b>	LUM	38	KS [1-3]	Cornea, sclera	Cartilage, bone, muscle, liver, skin	(Blochberger et al., 1992)
<b>Keratocan</b>	KERA	37	KS [3]	Cornea, sclera	Cartilage, skin, ligament	(Corpuz et al., 1996)
<b>Mimecan</b>	OGN	25	KS [1]	Cornea, sclera	Cartilage, skin, blood vessels, brain	(Funderburgh et al., 1997)
<b>Versican</b>	GSPG2	265-370	CS?DS [10-30]	Vitreous humor, trabecular meshwork	Cartilage, skin, blood vessels, brain	(Koga et al., 2005)
<b>Aggrecan</b>	AGC1	220	CS [~100] and KS	Sclera	Cartilage, blood vessels, brain	(Iozzo and Murdoch, 1996)
<b>Neurocan</b>	MNC1	136	CCS [3-7]	Developing neural retina	Brain, cartilage	(Iozzo and Murdoch, 1996)
<b>Syndecan-1</b>	SDC1	45, 53	CS/HS [5]	Trabecular meshwork	Epithelial cells	(Kokenyesi and Bernfield, 1994; Wirtz et al., 1997; Jaakkola and Jalkanen, 1999)
<b>Perlocan</b>	HSPG2	400-467	HS/CS [3-10]	Trabecular meshwork	Basement membranes, cell surfaces, cartilage	(Iozzo and Murdoch, 1996; Wirtz et al., 1997)

**Table 1.3 Different types of proteoglycans.** Note: CS = chondroitin sulphate, DS = dermatan sulphate, KS = keratan sulphate, ILM = internal limiting membrane of the retina.

#### ***1.4.2. Proteoglycan core protein - Lumican***

Lumican was initially described as a corneal PG, it is now known to be expressed in a variety of tissues, including artery (Funderburgh et al., 1991a), lung (Dolhnikoff et al., 1998), articular cartilage (Grover et al., 1995) and skin (Chakravarti et al., 1998; Chakravarti et al., 2000). Corneal lumican is normally expressed by stromal keratocytes, however during the early phase of corneal wound healing it is transiently expressed by the corneal epithelium (Saika et al., 2000).

The core protein of lumican consists of a 338 amino acid residue sequence (37 kDa). Its KS chains are highly sulphated, consists of 2-3 KS attachment sites (Funderburgh et al., 1997) and a single Tyr site adjacent to the acidic residues Glu/Asp, which may be a signal for post-translation addition of further KS chains (Carlson et al., 2003).

Lumican KO mice studies (Chakravarti et al., 1998; Chakravarti et al., 2000) have shown that these mice display skin laxity, fragility (resembling certain types of Ehlers-Danlos syndrome) and mice developing bilateral corneal opacification. These underlying causes are thought to be due to the deregulated growth of collagen fibrils with a significant proportion of abnormally thick collagen fibrils and abnormal architecture in the skin and cornea (posterior region of the stroma). In addition, the lumican core protein itself has been shown to inhibit *in vitro* collagen fibrillogenesis, suggesting this function to be entirely core protein mediated (Rada et al., 1993).

#### 1.4.3. *Proteoglycan core protein - Keratocan*

The keratocan core protein has a molecular weight of 38 kDa and when bound to sulphate chains, it has a molecular weight of 200 kDa (Corpuz et al., 1996). Keratocan is also expressed by keratocytes and is abundant in the cornea and sclera but is also found to a lesser degree in non corneal tissues, such as skin, ligament and cartilage (non-sulphated glycoprotein). It has been proposed that lumican and keratocan may be structurally similar. For example their core protein is composed of Leu-rich motifs which are coiled in a spiral and are stacked in a parallel  $\beta$ -sheet array (Figure 1.12). The location of the first 10 LRR of lumican and keratocan are located in the central part of the spiralled coil which bend into a horseshoe-like structure, whereas the putative  $\beta$ -sheet is found at the top surface of the coiled domain (Dunlevy et al., 2000).



**Figure 1.12** A three-dimensional model of keratocan. The model was based on a theoretical structure of the acid-labile subunit (ALS) of a serum insulin-like growth factor (Lehmann et al., 2001).

Keratocan-null mice have been reported to have normal corneal transparency, however, subtle abnormalities in collagen fibril organization such as increased fibril diameter, thinned stroma, and a smaller cornea-iris angle of the anterior segment (Liu et al., 2003). Similarly, human mutations in the keratocan gene (*KERA*) cause corneal flattening and a consequent decrease in visual acuity (Pellegata et al., 2000).

#### **1.4.4. *Proteoglycan core protein - Mimecan***

Mimecan was initially isolated from bovine bone and later isolated in bovine cornea as a minor KS PG. This corneal KS PG is a 25 kDa and the product of the gene producing osteoglycin. Mimecan carries KS GAG chains in human, chick and bovine cornea, but not in the murine cornea (Funderburgh et al., 1997). Northern blotting analysis has revealed three distinct size classes of mimecan mRNA that vary in abundance depending on the tissue source, the smallest 2.4 kilobase (kb) form is predominant in corneal and scleral tissue. Such heterogeneity can arise as a result of alternative splicing of RNA or an alternate usage of polyadenylation sites (Funderburgh et al., 1997).

Corneal KS PGs lumican or keratocan have a lesser sequence homology to mimecan. However, comparison of structural domains among all three proteins indicates molecular feature conservation, such that each protein contains one or more Tyr residues adjacent to acidic amino acids in the N-terminal region; consensus sites for Tyr sulphation (Funderburgh et al., 1997).

Mice lacking mimecan have displayed no significant changes in the corneal clarity and corneal thickness. However, ultrastructural analysis revealed that the average collagen fibril was thicker than the mimecan-null mice. Collagen fibrils from the cornea of mutant mice showed an average diameter of  $31.84 \pm 0.322$  nm, versus  $22.40 \pm 0.296$  nm in their wild type litter-mates. As a result it was concluded that mimecan may have a role in regulating collagen fibrillogenesis *in vivo* (Tasheva et al., 2002). Furthermore, Beecher and co-workers showed (using x-ray diffraction) no significant changes in centre-to-centre collagen fibrillar spacing, when compared to corneas of wild-type mice. From these results, it was suggested that mimecan may have a lesser role in the control of the architecture in mouse corneal stroma (Beecher et al., 2005).

#### 1.4.5. *Proteoglycan core protein – Decorin*

Decorin belongs to a growing family of SLRPs that mediate fundamental cellular processes, including regulation of the orderly assembly of ECMs, corneal transparency, tensile strength of skin and tendon, viscoelasticity of blood vessels, and tumour cell proliferation (Vogel, Paulsson and Heinegard, 1984; Hedbom and Heinegard, 1993; Kresse, Hausser and Schonherr, 1993; Iozzo, 1998, 1999). The biological functions of decorin include the formation and/or organization of collagen (Scott, 1992c) and modulation of cell adhesion mediated by fibronectin and thrombospondin (Winnemöller et al., 1992). Decorin also modulates the activity of growth factors, such as transforming growth factor- $\beta$ -independent (TGF- $\beta$ ) effects on the cell proliferation and behaviour (Iozzo et al., 1999; Häkkinen et al., 2000).

Mammalian decorin contains a protein core and a single CS/DS GAG chain, attached to a serine residue near the N-terminus and is the best characterized member of the SLRPs, by having a domain of tandem leucine rich repeats, flanked on either side by clusters of conserved Cys residues (Scott et al., 2004). To date, the structure of decorin remains unclear, although, evidence suggests that decorin may be a dimer (Figure 1.13) (Scott et al., 2003; Scott et al., 2004; McEwan et al., 2006) and it dimerizes through the concave surfaces of the leucine-rich repeat domains. However, Goldoni and co-workers suggested that decorin is monomeric and that the dimerization is artifactual (Goldoni et al., 2004).

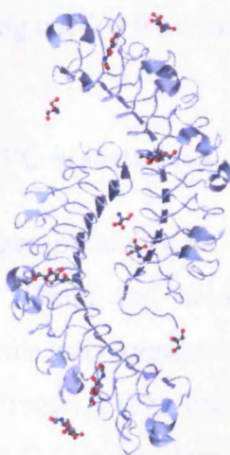


**Figure 1.13** Crystal structure of the dimeric protein core of decorin, the archetypal small leucine-rich repeat proteoglycan (McEwan et al., 2006).

The core proteins and not their GAG side chains, of lumican and decorin have been shown to inhibit collagen fibril formation and reduce collagen fibril diameter using the *in vitro* collagen fibril-forming assays (Rada et al., 1993). Decorin and lumican made as recombinant products have been shown to act on different phases of fibril growth, interact with different regions of the collagen molecule and serve to stabilize the collagen fibril once formed (Sini et al., 1997; Neame et al., 2000). Other studies using chick and mouse tendons have suggested that decorin may delay individual collagen molecule fusion (Vogel et al., 1984; Vogel and Trotter, 1987; Birk, Nurminskaya and Zycband, 1995; Birk et al., 1996).

It has been found that the synthesis of non-glycosylated decorin in avian cornea leads to the disruption in lamellar organization, suggesting that DS PGs are not involved in the regulation of collagen fibril diameter, but are more important to fibril-fibril spacing and lamellar cohesiveness (Nakazawa et al., 1995). Furthermore, in corneal explants from embryonic chicken, an increase synthesis of KS PGs and a decrease synthesis of DS PG was detected, which coincided with the onset of tissue transparency, suggesting a correlation between PG composition and corneal transparency (Nakazawa et al., 1995). In addition, studies (Bredrup et al., 2005; Rodahl et al., 2006) have shown that human congenital stromal corneal dystrophy, where cloudy corneas develop shortly after birth, is associated with a mutation in the gene for decorin. Thus in summary, the coordinated synthesis of different collagen types and core proteins of PGs as well as post-translational modifications of the collagens and PG are required to produce collagen fibrils with the size and spacing needed for corneal stromal transparency.

### **1.5. Collagen and PG associations**

The first evidence of collagen-proteoglycan interaction was by Smith and Frame (1969). Using alkaline lead citrate and uranyl acetate staining, Smith and Frame showed 4 nm diameter filaments interconnecting the collagen fibrils and postulated that these were PGs (Smith and Frame, 1969). Further studies have been carried out since then and specific staining of GAGs has been developed using cationic dyes (alcian blue, cuproinic blue, cupromeronic blue) in a critical electrolyte concentration (CEC) (Scott, 1985). Electron histochemical studies (Scott and Haigh, 1985) have shown that PGs generally associate with collagen fibrils at the *a*, *c*, *d* and *e* bands within the 65nm

*D*-period, and that KS PGs occupy the *a* and *c* bands, with CS/DS PGs at the *d* and *e* bands (Figure 1.14) (Scott and Haigh, 1985; Meek, Elliott and Nave, 1986; Scott and Haigh, 1988a). The histochemical data obtained by Scott (1988) revealed that the GAGs bridge and link adjacent collagen fibrils (Scott, 1988).

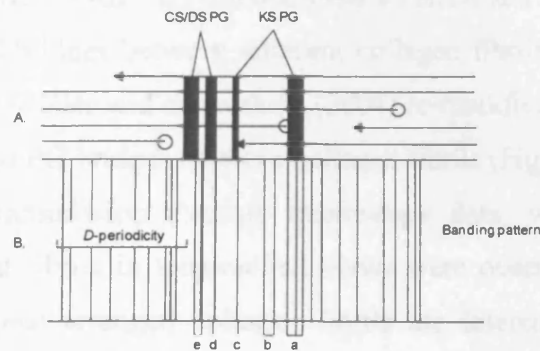


**Figure 1.14 Mapping of binding sites of PGs along the collagen fibril.** The packing of collagen molecules are arranged in a quarter staggered manner (A).  $\rightarrow$  = N terminal;  $\circ$  = C terminal. The *a-e* banding patterns within the *D*-period of collagen type I fibril (B). Cupromeronic blue staining showing PG filaments at the surface of the fibril demonstrated 4 PG binding sites, in the *a*, *c*, *d* and *e* bands (Scott, 1988). In corneas of large animals all 4 are occupied by CS/DS or KS. In small animals (e.g. mouse) there is little or no KS and the *a* and *c* bands carry no PGs.

In addition, Scott and Haigh (1988a) found that different species (mouse, rat and rabbit) have different GAG staining patterns (Scott and Haigh, 1988a). Negligible amounts of KS were detected in mouse, but considerable amounts in rat and rabbit stroma. Mouse corneal stroma PG filaments were located predominantly at the gap zone of the collagen fibrils, mainly at the *d* band, with few at the *a* and *c* bands. However PG filaments from rat and rabbit cornea, were located at the *a* and *c* bands, as well as the *d* and *e* bands. These findings support the proposal that the *a* and *c* bands are specific binding sites for KS PG (Scott and Haigh, 1985). In addition to Scott and Haigh's findings, studies on the cornea and cartilage suggested that KS, rather than CS is produced in  $O_2$ -lack conditions (discussed further in Chapter 5).

### 1.6. Collagen and Proteoglycan interactions

Electron microscope measurements from bovine corneas showed that stained CS/DS PGs are ~70 nm long, whereas KS PGs are ~40 nm long (Scott, 1992a). The protein cores of PGs were thought to attach to collagen fibrils with their GAG chains free to

interact with other components of the extrafibrillar matrix. Given that PGs occupy the ECM, the interactions between PGs and collagen fibril models have been proposed, one of which illustrated that six PGs, attached to the collagen fibrils, are connected to a central collagen fibril with six neighbouring fibrils thus securing a regular spacing of the collagen fibrils (Maurice, 1962). By the late 1960's Farrell and Hart suggested that PG GAG chains formed bridges between adjacent collagen fibrils (Farrell and Hart, 1969). Recent studies by Müller and co-workers (2004) re-modified Farrell and Hart's model which also featured PG bridges between collagen fibrils (Figure 1.15). This new model was based on transmission electron microscopy data, where GAG chains connecting three adjacent fibrils in longitudinal views were observed. The proposed model illustrated hexagonal arranged collagen fibrils are interconnected at regular distances with their next-nearest neighbours by groups of six PGs. These are attached orthogonally to the circumference of the fibrils, forming a ring-like network enwrapping the collagen fibrils at regular distances along their full length; PG complexes do not form bridges between adjacent fibrils but between next nearest neighbouring fibrils, thus accounting for the size of some PG complexes that are seen to be longer than the average interfibrillar spacing (Müller et al., 2004).

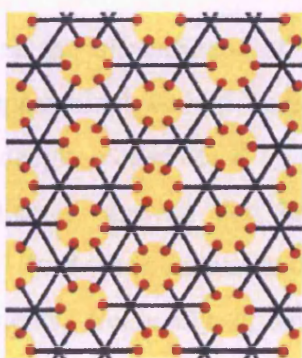


**Figure 1.15** A schematic diagram of Müller *et al.* (2004) proposed model on the organization of the collagen fibrils and proteoglycans. Six core proteins of PGs are attached to the hexagonal arranged collagen fibrils. The GAG of the PGs is connecting to the next nearest neighbour collagen fibrils to form a ring-like structure around each collagen fibril (Müller *et al.*, 2004).

However, other models of PG-collagen interaction have showed that the core protein of PGs lies along the length of the collagen fibril, to which it is non-covalently attached, and that highly charged hydrophilic GAG chains protrude outwards from the fibril to regulate collagen spacing. Scott (1991) proposed that GAGs of neighbouring collagen

fibrils interact with each other to form a duplex, which serves to maintain collagen fibril separation (Scott, 1991a/1992a) (Figure 1.16). In support of this, Rada *et al.* (1993) reported that PGs bind to collagen fibrils with their GAG chains extending into the interfibrillar space (Rada *et al.*, 1993).

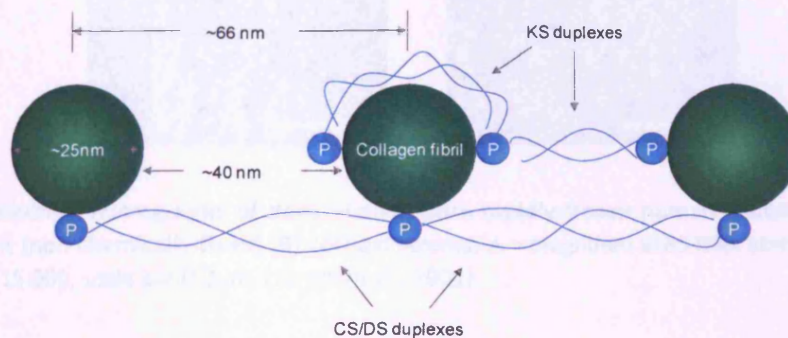


**Figure 1.16 A proposed model of collagen interactions seen in corneal stroma.** P = protein core of PG. It is proposed that observed GAG filaments contain at least 2 glycan chains side-by-side. The small PGs frequently contain 2 glycan chains, which are suggested to lie at  $180^\circ$  to each other, thus giving an image that sometimes extends in a straight line across 3 or more fibrils. The gaps between the centres of fibrils are approximately the same size as a CS/DS GAG chain; compatible with the tangential arrangement is visible in the tissue. KS GAG chains are shorter than those of CS/DS. KS duplexes may circumvent the fibrils, as well as bridge the interfibrillar gaps, since each step along this route is of equal length (Scott, 1992a).

Hirsch and co-workers visualized the ultrastructure of the corneal stroma, using ultra-rapid-freezing (frozen onto a copper block cooled by liquid helium or liquid nitrogen), deep-etching freeze-fracturing (deeply etched for 8-10 min) and rotary replication with platinum-carbon. The data collected showed that both human and rabbit stromal matrices were similar (Figure 1.17). Both in human and rabbit corneal stroma had 8-12 nm interfibrillar bridging filaments, frequently ornamented with globular domains, which they suggested were PGs joining neighbouring collagen fibrils like steps to a ladder (Hirsch *et al.*, 2001).

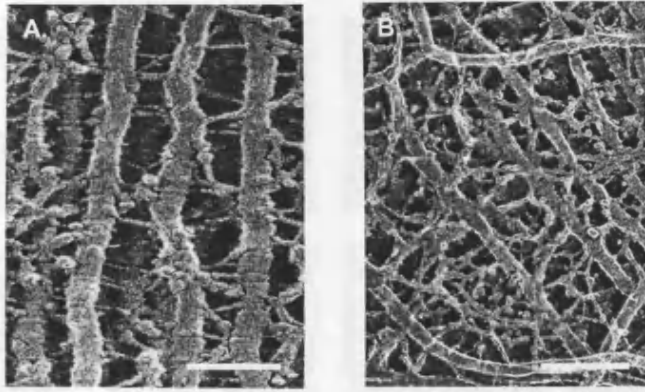


**Figure 1.17** Electron micrographs of deep-etched, ultra rapidly-frozen human (glutaraldehyde-fixed) (A) and rabbit (non chemically-fixed) (B) corneal stroma. A = magnified x185 000, scale bar 0.1 $\mu$ m. B = magnified x115 000, scale bar 0.2 $\mu$ m. (Hirsch et al., 2001).

More recently, studies within the author's lab have used electron tomography of cupromeronic blue-stained cow (Lewis et al., 2010) and mouse (Parfitt et al., 2010) corneal stromas to produce three-dimensional reconstructions, which revealed the interactions between collagen fibrils and stained PG filaments. The reconstruction model indicated that the core proteins of the PGs are attached to the collagen fibrils and that these PGs can interact via their GAG chains with other PGs on nearby fibrils forming anti-parallel multiplexes (Figure 1.18). However, no systematic six-fold arrangement of PGs around collagens are found, there are bridges that connect all adjacent fibrils at different axial positions, with the overall effect that a pseudo-hexagonal arrangement of fibrils are obtained. This arrangement is thought to be sustained by the balance of two opposing forces (repulsive force - osmotic pressure, attractive force – thermal motion) created by the PGs.

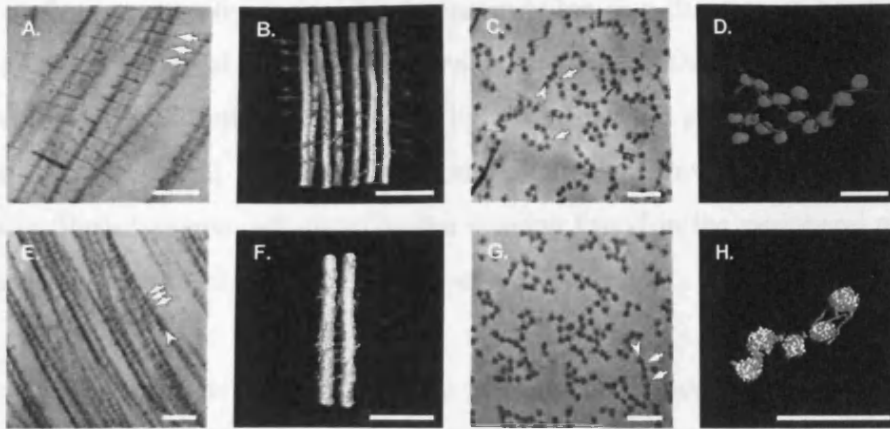


**Figure 1.18 CS/DS and KS interaction between collagen fibrils.** Panel (A) and (C) - Keratanase treatment to remove KS GAG chains, leaving CS/DS chains. Panel (E) and (G) - chondroitinase ABC treatment to remove CS/DS GAG chains, leaving KS chains. Collagen fibrils are indicated by arrowheads and PGs by arrows. Panel (B) and (D) are stereo pairs from longitudinal and transverse 3D reconstructions of keratanase-treated specimens. The collagen fibrils are coloured in blue, the CS/DS chains in red. Long CS/DS chains are seen to interact with a 65nm axial periodicity with several collagen fibrils. Panels (F) and (H) are reconstructions from chondroitinase ABC-treated specimens, with collagen depicted in blue and KS chains in orange. Here, KS chains form axially periodic bridges between collagen fibrils. Scale bars = 100 nm (Lewis et al., 2010).

### 1.7. Transparency

The transparency of the cornea results from the fact that normal cornea does not absorb visible light and light scatter is minimal. Maurice (1957) suggested that the basis of the transparency of the cornea is the uniform diameter and regular spacing of the corneal stroma collagen fibrils, which lie parallel to each other within layers (lamellae), which themselves stack parallel to the surface of the cornea. It was also suggested that the collagen fibrils of the corneal stroma are arranged regularly in a lattice and that scattered light is eliminated by destructive interference so that only forward travelling light can be permitted (Maurice, 1957). However, factors involved in maintaining collagen fibril spacing and size remains unclear. It has been suggested collagen fibril spacing is probably thought to be a function of PG-collagen interaction (Komai and Ushiki, 1991) and that minor collagens (such as type V collagen) may control the molecular aggregation of the collagen fibril diameters, whilst PGs, are thought to prevent fibril growth by fusion (Meek and Leonard, 1993). Reduced corneal transparency occurs with age, due to the three dimensional growth of collagen fibrils in the stroma (Daxer et al., 1998).

Recent studies investigating corneal light transmission as a function of position across in human (Doutch et al., 2008) and bovine (Doutch, 2009) corneal stroma, have indicated that in both human and bovine, light transmission gradually decreased from the central to peripheral regions of the corneal stroma. This may be caused by the changes in fibril diameter and interfibrillar spacing found in the peripheral regions of the cornea (Borcherding et al., 1975; Boote et al., 2003)

Keratocytes have been largely ignored as a potential hindrance to stromal transparency but recent clinical evidence suggests that they may play a major role in the development of corneal haze (Moller-Pedersen, 2004). Keratocytes have a compact cell body with numerous cytoplasmic lamellipodia, this gives them a dendritic-like morphology, and they are interconnected in a three dimensional network by these lamellapodia (Poole, Brookes and Clover, 1993). The compact cell body minimizes the surface area of the keratocyte exposed to light and this may serve to reduce light scattering while their processes provide the cell-cell communications. The corkscrew-like circular arrangement of keratocytes as described by Müller and co-workers, suggested that they may be involved in maximising stromal transparency as this organization creates equal chances for minimization of light scattering over the entire cornea (Müller et al., 1995).

Over the years, developmental studies of the cornea have showed the various events for the onset of transparency. For example chick embryo corneal development studies have suggested that the glycosylation is very important for the corneal transparency process (Cornuet et al., 1994). Lumican with non-sulphated KS side chains was detected as early as day 7 of embryonic development in chicken, but sulphated GAG side chains were detected only on day 15, when transparency started to increase. In embryonic mice, sulphated KS PGs only appeared after the eyes opened (Ying et al., 1997). In addition, during rabbit (Gregory et al., 1988) and chick (Dunlevy et al., 2000) corneal development, studies have shown sulphation alterations or changes in the fine structure of KS chain PG (lumican, keratocan and mimecan). Therefore from these animal studies, it is thought that the structure of GAG chains in KS PGs may be important for the development of corneal transparency, possibly leading to organization of the corneal tissue (Michelacci, 2003).

The level of corneal hydration is an important factor in corneal transparency. Physiologically, corneal hydration is maintained at approximately 78%. During edema, light scattering increases and transparency is reduced due to the disruption of the collagen matrix. The collagen fibrils themselves swell very little and most of the additional water enters the interfibrillar spaces, where the PGs absorb the water and this causes collagen fibril aggregation and disorganization, producing extra scattering and absorption of light and consequently a reduction in corneal transparency (Meek et al., 1991).

### 1.8. Summary and objectives

Structural changes occur at a molecular level in diseased corneas, and these can affect the transparency of the cornea. It is thought that the structural organization of the cornea, in particular the uniform size and the spacing of its constituent collagen fibrils, is a major factor responsible for its transparency. It is already known that PGs play an important role in collagen fibril organization however the exact role still remains unclear. The high degree of collagen organization found in the cornea compared with other connective tissues makes this tissue a unique model for investigating collagen-proteoglycan interactions. Furthermore, light transmission studies across the human and bovine stromal cornea, indicated that light transmission decreases in the peripheral regions of the cornea (Doutch et al., 2008; Doutch, 2009). Studies have suggested that this may be due to the changes in fibril spacing and diameter found in the peripheral regions of the cornea, as revealed in electron microscopic studies (Borcherding et al., 1975) and x-ray studies (Boote et al., 2003). To date, however, limited experimental data have been provided to link corneal biochemistry and stromal fibril ultrastructure as a function of position, i.e. looking at the sulphation patterns of GAG from central to peripheral regions in the bovine cornea, in relation to collagen fibril architecture.

**Hypothesis:** The hypothesis of this research is that changes in the sulphation patterns of GAG's are directly related to changes in ultrastructure, and hence transparency of the cornea.

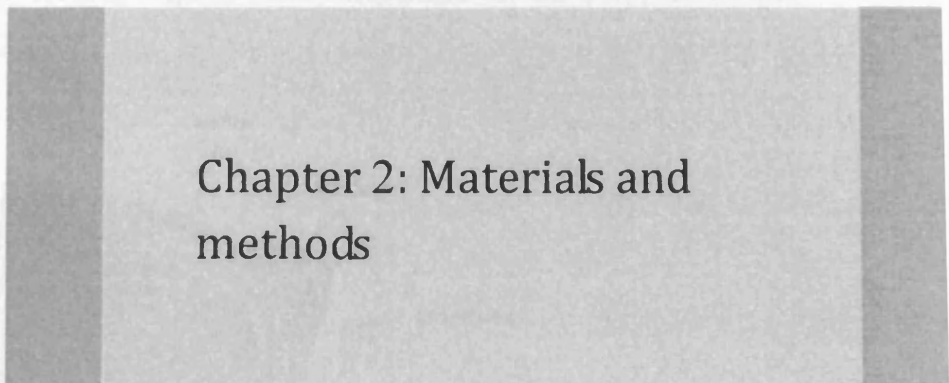
**Aims:** The aims of this research were to investigate:

- The biochemical sulphation patterns of GAG chains across the cornea as a function of position
- The biophysical structure across the cornea as a function of position
- The effects of GAG sulphation in normal and hypoxic conditions

Bovine (in Chapters 3 and 4) and rabbit (in Chapter 5) corneas were used for this project instead of human corneas, as this was because both latter animals were more easily accessible than human corneas. The bovine cornea may be larger anatomically and thicker than in human and rabbit corneas (which are very similar in size), the structural layers of the cornea are very similar, however rabbit corneas, they lack the Bowman's layer, but overall they are similar. Ultrastructurally, the hydroxyproline content are very similar to both animal models, contain large quantities of highly sulphated KS and lesser amounts of CS/DS (Scott and Bosworth, 1990). Therefore overall, making both the latter animal models good analogues to gain a greater understanding on the structure of the cornea, hence would be essential for understanding the function and consequently explaining how the transparency of the cornea is mediated. In the future this may provide new insights for the development of novel therapeutic approaches, optimize refractive surgeries and corneal dystrophies.

## 2.1.1. Synthesis

This particular chapter focuses mainly on the experimental procedures that are followed throughout the project. It includes the overall procedure, the hardware, molecular modelling, and finally the statistical approaches. It starts with the overall procedure (Figure 1.1), which includes the different stages of the project. The hardware section, the next part of the project, is presented for the purpose of this thesis in Figure 1.2.



# Chapter 2: Materials and methods

Figure 2.1.1. Diagram showing the different stages of the project in the thesis. The first stage is the overall procedure, the second is the hardware, the third is the molecular modelling, and the fourth is the statistical approaches.

### 2.1.1. Overall procedure

When all the data are given, the first step is to read the data and to prepare the data for the following steps. The data are read from the files and are stored, which are then used for the next steps. The data are then used for the next steps, which are the molecular modelling and the statistical approaches. The data are then used for the next steps, which are the molecular modelling and the statistical approaches. The data are then used for the next steps, which are the molecular modelling and the statistical approaches.

## 2.

This particular chapter focuses mainly on the experimental procedures employed throughout the project. This consists of corneal preparations, the biochemical, molecular experiments, and finally the biophysical experiments. Because, unlike the human eye (Figure 1.2), no terminology exists for the different regions across the bovine cornea, the bovine corneal regions were categorised for the purposes of this thesis as shown in Figure 2.1.

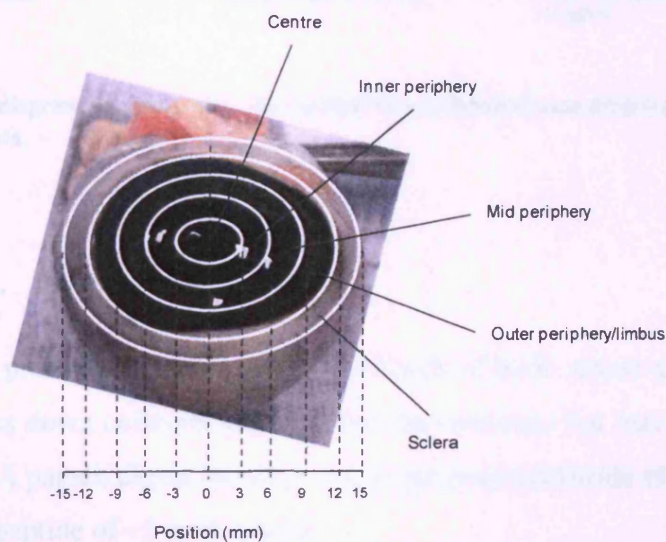


**Figure 2.1** A diagram showing the different corneal surface regions in the bovine cornea (anterior corneal surface). The image of the bovine eye was kindly given by Dr Sally Hayes (Cardiff University).

### 2.1. Corneal preparation

Whole adult bovine eye globes were obtained from a local abattoir and transported on ice to the laboratory. Healthy eyes with clear/transparent corneas were selected, whole and 3 mm x 3 mm pieces of corneal tissue were cut from the centre of the cornea outwards (outer periphery/limbus region (9-12mm)) (Figure 2.2). Prior to excising the corneal stroma, the cellular layers, such as the epithelium and endothelium corneal layers were removed using a scalpel and blotted to remove excess wet weight. Tissues were weighed, freeze dried, weighed again, after which hydrations was calculated using the following formula (Equation 1).

**Equation 1:**  $\text{Hydration} = (\text{wet wt} - \text{dry wt}) / \text{dry wt}$

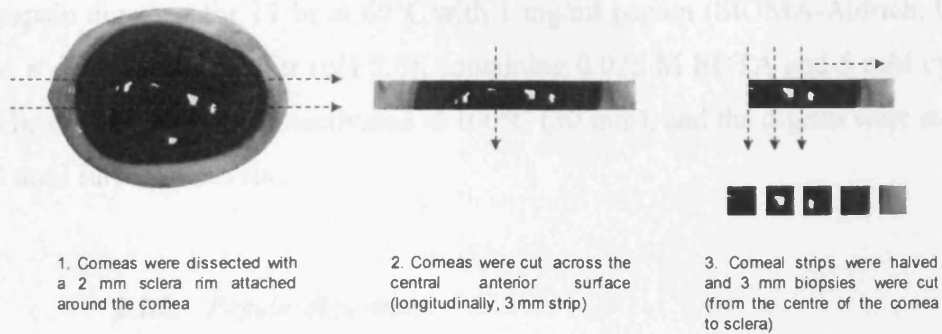


**Figure 2.2** A simplified diagram showing how the corneal tissue (bovine) was prepared for the biochemical experiments.

### 2.1.1. Papain digest

Papain is a cysteine protease that cleaves peptide bonds of basic amino acids; leucine or glycine which breaks down collagen and core protein structures but leaves GAG chains intact (Figure 2.3). A papain digest would yield single polysaccharide chains (i.e. GAG chains) attached to peptide of ~5 amino acids.

Note: this particular enzymatic digestion would not be suitable for analyzing the polypeptide profile of the collagen types. However, the amount of collagen can still be quantified using the hydroxyproline assay, since highly concentrated HCl is used to hydrolyse the protein samples into amino acids, prior to the hydroxyproline assay.

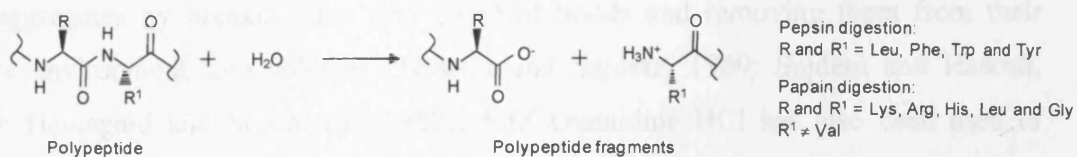


**Figure 2.3** Chemical process of papain and pepsin digestion.

### *2.1.1.1. Papain protocol*

Corneal biopsies (n = 10) at specific regions were papain digested. Briefly, the samples were papain digested for 17 hr at 60°C with 1 mg/ml papain (SIGMA-Aldrich, UK) in 0.05 M sodium acetate buffer (pH 5.6), containing 0.025 M EDTA and 5 mM cysteine HCl. The enzyme was then inactivated at 100°C (30 min), and the digests were stored at -20°C until further analysis.

### *2.1.2. Pepsin digestion*

Pepsin is a member of the aspartyl protease family and is a non-specific endopeptidase, produced in an inactive precursor form (pepsinogen) in the mucosal lining of the stomach of vertebrates. Pepsin has broad substrate specificity. It cleaves proteins preferentially at carboxylic groups of aromatic amino acids (e.g. phenylalanine, tryptophan and tyrosine). It will not cleave at bonds containing valine, alanine or glycine, thus will be ideal for collagen extraction (Figure 2.3).

#### *2.1.2.1. Guanidine extraction and pepsin digestion protocol*

Note: in some studies, a guanidine extraction is initiated prior to the digestion as this is because ECM molecules such as collagen and PGs are closely associated within their tissues in a naturally occurring native state. In order to isolate various collagen fibrils and PGs, they must be dissociated from their surrounding environmental tissue. By doing this, the tissue can be extracted by Guanidine-HCl. In cartilage, the standard PG extraction involves 4 M Guanidine HCl (a chaotropic agent), which acts to dissociate PG aggregates by breaking any non covalent bonds and removing them from their native environment into solution (Hascall and Sajdera, 1969; Sajdera and Hascall, 1969; Heinegard and Sommarin, 1987). 4 M Guanidine HCl has also been used to facilitate the extractions of SLRPs from corneal extracellular matrices (Gregory et al., 1988; Cornuet et al., 1994; Young et al., 2005).

Prior to optimizing the amount of GAG chains, a guanidine extraction was employed followed by a papain digest and in another study a pepsin digestion was also carried out. Briefly, once the corneal stroma was obtained, the tissue was finely chopped and

extracted in 4 M Guanidine HCl in the presence of protease inhibitors (0.05 M sodium acetate, 0.01 M disodium EDTA, 0.1 M 6-amino hexanoic acid, 0.005 M benzamidine HCl and 0.5 mM PMSF [pH 5.8-6.8]), overnight at 4°C, to remove PGs and non-collagenous proteins. Samples were then centrifuged at 14,000 rpm for 30 min at 4°C and the supernatant was collected (this will contain solubilized GAGs and possibly some collagen) and the pellet/residue was subjected to digestion. However the data presented in this project only shows the papain digestion method, as greater amounts of GAG was obtained compared to pepsin digestion.

Although pepsin digestion was not employed for this particular study, as part of preliminary studies, digesting the corneal tissue with pepsin was employed. Briefly, 1 ml of pepsin (0.5 mg/ml in 0.5 M acetic acid) per 50 mg of wet wt tissue was added, incubated overnight at 4°C, with continuous mixing. The supernatant was removed via centrifugation at 13,000 rpm for 30 min at 4°C and the residue was further pepsin digested. Pooled supernatant was then subjected to dialysis and stored at -20°C.

## **2.2. Determining matrix content**

### **2.2.1. Hydroxyproline assay**

A hydroxyproline assay was employed to quantify the amount of collagen extracted from the corneal tissue. The hydroxyproline stabilizes the collagen triple helix by forming hydrogen bonds, and is commonly used to quantify collagen as a control marker specifically to collagenous sequences (Edwards and O'Brien, 1980).

#### **2.2.1.1. Hydroxyproline assay protocol**

Corneal extracts that were papain digested from individual corneas were hydrolyzed by using equal volumes of 11.7N HCl to supernatant at 110°C overnight. Specimens were then lyophilized. Dried hydrolysates were reconstituted in their starting volume of dH<sub>2</sub>O and centrifuged at 7000 rpm (10 min) to remove particulate material. Hydroxyproline residues were assayed against known standards (L-Hydroxyproline, Sigma-Aldrich, UK) and read at 540 nm after 10-20 min incubation at 70°C.

Hydroxyproline residues were assayed in 30  $\mu$ l of sample against known L-hydroxyproline (SIGMA-Aldrich, UK) concentrations (30  $\mu$ l) (0  $\mu$ g/ml, 2  $\mu$ g/ml, 4  $\mu$ g/ml, 6  $\mu$ g/ml, 8  $\mu$ g/ml and 10  $\mu$ g/ml) into triplicate wells on a 96 well plate. 70  $\mu$ l of diluent (67% propan-2-ol) and 50  $\mu$ l of oxidant (0.7 g chloramine T, 10 ml dH<sub>2</sub>O and 50 ml stock buffer (0.42 M sodium acetate trihydrate, 0.13 M sodium citrate dehydrate, 26 mM citric acid and 4% (v/v) propan-2-ol)) was added to the plate wells and placed onto a plate shaker at room temperature for 5 min. 125  $\mu$ l of colour reagent (7.5 g dimethylamino benzaldehyde, 11.25 ml perchloric acid (60%) (or 9.46 ml perchloric acid (70%) and 1.61 ml dH<sub>2</sub>O) and 62.5 ml propan-2-ol) was added to the plate wells, mixed on a plate shaker, incubated at 70°C for 15 min and an absorbance ( $\text{\AA}540$ ) reading was recorded.

### ***2.2.2. Dimethylmethylene blue (DMMB) assay***

The dimethylmethylene blue (DMMB) (also known as 1,9-dimethylmethylene blue) dye-binding technique is widely used for the quantification of sulphated GAG and PGs. This assay is a spectrophotometric assay for PGs based on the metachromasia resulting when DMMB is used to stain sulphated GAGs on PGs. This method can be used as a quantitative assay procedure without prior precipitation of the GAGs (de Jong et al., 1989). Binding of the cation dye with sulphated GAGs results in the formation of a complex with an absorption maximum at  $\text{\AA}525$  (Stone et al., 1994).

#### ***2.2.2.1. DMMB assay protocol***

Briefly, 40  $\mu$ l of sample was assayed against 40  $\mu$ l of chondroitin sulphate C (sodium salt from shark cartilage (SIGMA-Aldrich, UK) as known concentrations (0  $\mu$ g/ml, 10  $\mu$ g/ml, 20  $\mu$ g/ml, 30  $\mu$ g/ml and 40  $\mu$ g/ml), onto a 96 well plate. 200  $\mu$ l of DMMB solution (DMMB stock solution: 32 mg DMMB, 1.5 L dH<sub>2</sub>O, 20 ml ethanol, 59 ml 1M NaOH, 7 ml 98% formic acid) was added to the wells and an absorbance ( $\text{\AA}525$ ) reading was recorded. A standard curve of the known concentrations was plotted and the unknown samples were calculated.

#### 2.2.2.2. Hydroxyproline and sulphate GAG quantification

The hydroxyproline standard curves were generated using known amounts of hydroxyproline and unknown amounts of hydroxyproline from the bovine corneal extracts were deduced. The amount of hydroxyproline was calculated by reading across the absorbance (Y axis) compared to known hydroxyproline  $\mu\text{g/ml}$  (X axis) on the standard curve and then multiplied by the dilution factor and units were expressed in mg per mg dry weight (dry wt).

Note: the total amount of collagen can deduced by the fact that hydroxyproline constitutes 14% of type I collagen, thus the amount of collagen can be extrapolated by multiplying the hydroxyproline content by 7.46 (Woessner, 1961). However in the case of this project, the total amount of hydroxyproline was presented.

The sulphated GAG content in the bovine corneal extracts was also deduced the same way, but using its respective standard curve. The units were expressed in  $\mu\text{g/mg}$  dry wt.

### 2.3. KS quantifications using antibodies

#### 2.3.1. Antibodies (Ab)

Antibodies (Ab) are essentially immunoglobulins (Igs) (glycoproteins), which bind very tightly to their target antigen (Ag). They are produced in vertebrates as a defence against infection. Abs exists as one or more copies of Y-shaped unit, composed of four polypeptide chains (Figure 2.4 A). Note, although different Ig can differ structurally, they all are built from the same basic units.

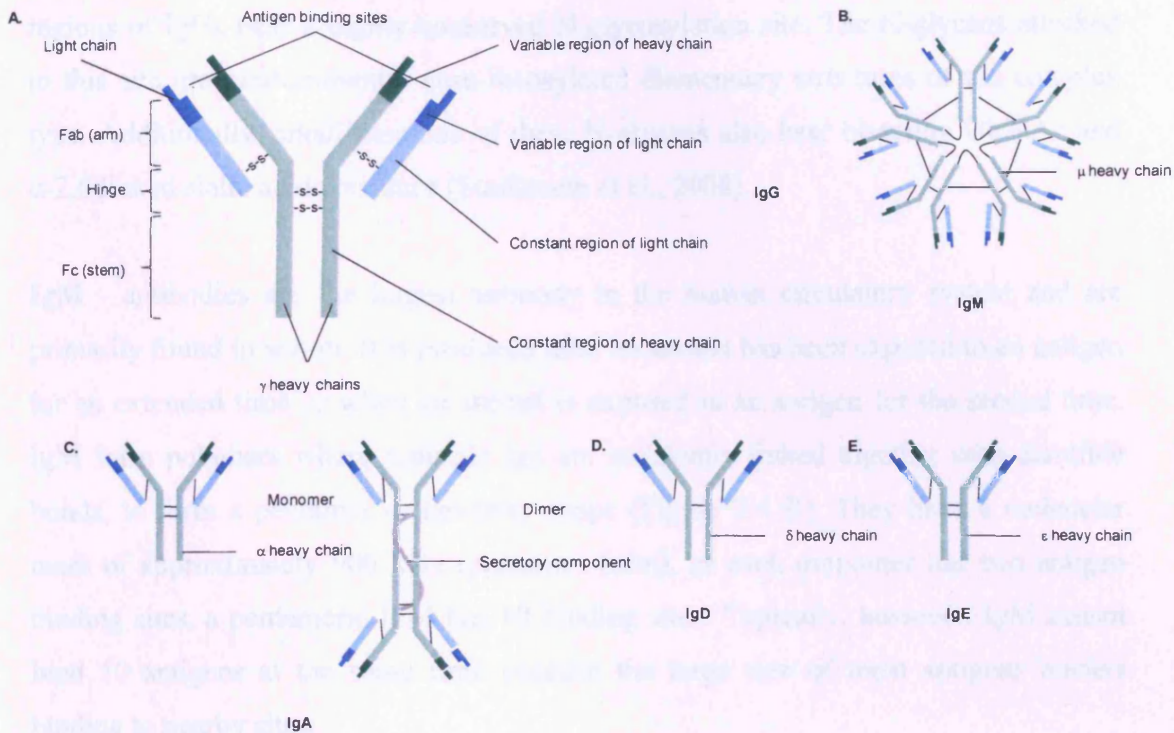


**Figure 2.4** The structure of a typical antibody (IgG) and the different antibody isotypes.

### 2.3.1.1. Antibody isotypes

In mammals, antibodies can be divided into five isotypes or classes: IgG, IgM, IgA, IgD and IgE, based on the number of Y units and the type of heavy chain. Heavy chains of IgG, IgM, IgA, IgD, and IgE, are known as  $\gamma$ ,  $\mu$ ,  $\alpha$ ,  $\delta$ , and  $\epsilon$ , respectively (Figure 2.3). The 2 antibody isotypes of interest for this particular work are IgG and IgM. Ig's can also be classified by the type of light chain that they have. Light chain types are based on differences in the amino acid sequence in the constant region of the light chain:  $\kappa$  and  $\lambda$ .

**IgG** - accounts for approximately 80% of all Ig's in humans, synthesized and secreted by plasma B cells. IgG antibodies are large molecules of about 150 kDa composed of 4 peptide chains. It contains 2 identical heavy chains of about 50 kDa and 2 identical light chains of about 25 kDa, thus tetrameric quaternary structure. The two heavy chains are linked to each other and to a light chain each by disulfide bonds. The resulting tetramer has two identical halves which together form the Y-like shape (Figure 2.4 A). Each end of the fork contains an identical antigen binding site. The Fc

regions of IgGs bear a highly conserved N-glycosylation site. The N-glycans attached to this site are predominantly core-fucosylated diantennary structures of the complex type. Additionally, small amounts of these N-glycans also bear bisecting GlcNAc and  $\alpha$ -2,6 linked sialic acids residues (Stadlmann et al., 2008).

**IgM** - antibodies are the largest antibody in the human circulatory system and are primarily found in serum. It is produced after an animal has been exposed to an antigen for an extended time or when an animal is exposed to an antigen for the second time. IgM form polymers where multiple Igs are covalently linked together with disulfide bonds, to form a pentamer or hexamer shape (Figure 2.4 B). They have a molecular mass of approximately 900 kDa (pentamer form), as each monomer has two antigen binding sites, a pentameric IgM has 10 binding sites. Typically, however, IgM cannot bind 10 antigens at the same time because the large size of most antigens hinders binding to nearby sites.

### *2.3.1.2. Monoclonal antibodies versus polyclonal antibodies*

Monoclonal antibodies are typically made by fusing myeloma cells with the spleen cells from a mouse for example, which has been immunized with the desired antigen. These cells are cultured with cells from a myeloma, a cancer of the plasma cells, to create a hybridoma which will endlessly replicate itself. The replications can be tested to find the cells which are producing the desired antibody or antibodies, these cells can be cloned and used to develop a large store of monoclonal antibodies. This mixture of cells is then diluted and clones are grown from single parent cells on microtitre wells. The antibodies secreted by the different clones are then assayed for their ability to bind to the antigen (with a test such as ELISA or Antigen Microarray Assay) or immune-dot-blot. The most productive and stable clone is then selected for future use. Polyclonal antibodies are antibodies which have been derived from multiple B cells or cell lines, that recognize different epitopes and have different degrees of specificity on the antigen. In contrast, the antibodies in a monoclonal preparation are derived from one clonal type and recognize the same epitope with the same degree of specificity.

### 2.3.2. Antibodies and pre-enzyme treatments used in this study

The antibodies used for this project are summarized in Table 2.1 and in Figure 2.5 (Chondroitinase ABC, Endo- $\beta$ -Galactosidase, Keratanase, and Keratanase II) illustrate where different enzymes digest definitive sites of specific GAG chains.

Antibody	Recognition	Additional notes	References	
KS GAG chain antibodies	5D4	Recognizes the antigenic determinant linear penta-sulphated sequence of N-acetyl-lactosamine disaccharide of KSPGs with both GalNAc and Gal sulphated	A mouse monoclonal antibody (IgG) Raised against KS on the core protein of human articular cartilage PG Have shown to have no response with other GAG such as CS/DS.	(Caterson et al., 1985; Mehmet et al., 1986)
	1B4	Have an affinity for linear tetra-sulphated sequences of N-acetyl-lactosamine disaccharide of KSPGs	A mouse monoclonal antibody (IgG)	(Mehmet et al., 1986)
	BKS-1	Specifically recognizes a Keratanase generated neo-epitope (N-acetyl-glucosamine-6-sulphate [GlcNAc-6-S]) at the non-reducing terminal of corneal and skeletal KS GAG chains	A monoclonal antibody (IgM) Pre-treatments needed prior to usage: Keratanase and/or Keratanase II to reveal neo-epitope	(Young et al., 2007a; Akhtar et al., 2008b)
CS/DS GAG chain antibodies	3B3	Anti chondroitin-6-sulphate Reacts with a non-reducing terminal-sulphated $\delta$ -4,5-unsaturated glucuronic acid residues adjacent to N-acetyl galactosamine-6-sulphate	Raised against pre-treated chondroitinase ABC to generate neoepitope "stub" Pre-treatments needed prior to usage: Chondroitinase ABC	(Caterson et al., 1985; Bartold, 1992; Young et al., 2005)
	2B6	Anti chondroitin-4-sulphate Recognizes $\delta$ -unsaturated disaccharides of C-4-S generated after chondroitinase ABC digestion of PGs containing C-4-S/DS	Raised against pre-treated chondroitinase ABC to generate neoepitope "stub" Pre-treatments needed prior to usage: Chondroitinase ABC	(Caterson et al., 1985; Bartold, 1992; Young et al., 2005)
	1B5	Anti chondroitin-0-sulphate Recognizes $\delta$ -unsaturated disaccharides of unsulphated chondroitin generated after chondroitinase ABC digestion	Raised against pre-treated chondroitinase ABC to generate neoepitope "stub" Pre-treatments needed prior to usage: Chondroitinase ABC	(Caterson et al., 1985; Mehmet et al., 1986; Bartold, 1992; Young et al., 2005)
PG core protein antibodies	LUM-1	Recognizes the core protein of lumican	Pre-treatments needed prior to usage: Endo- $\beta$ -galactosidase, Keratanase, Keratanase II, Chondroitinase ABC	
	KER-1	Recognizes the core protein of keratocan	A monoclonal antibody (IgM) Light chain with specificity for protein epitope on keratocan Pre-treatments needed prior to usage: Endo- $\beta$ -galactosidase, Keratanase, Keratanase II, Chondroitinase ABC	(Gealy et al., 2007)

**Table 2.1** A table showing the specificities of antibodies used during the project.

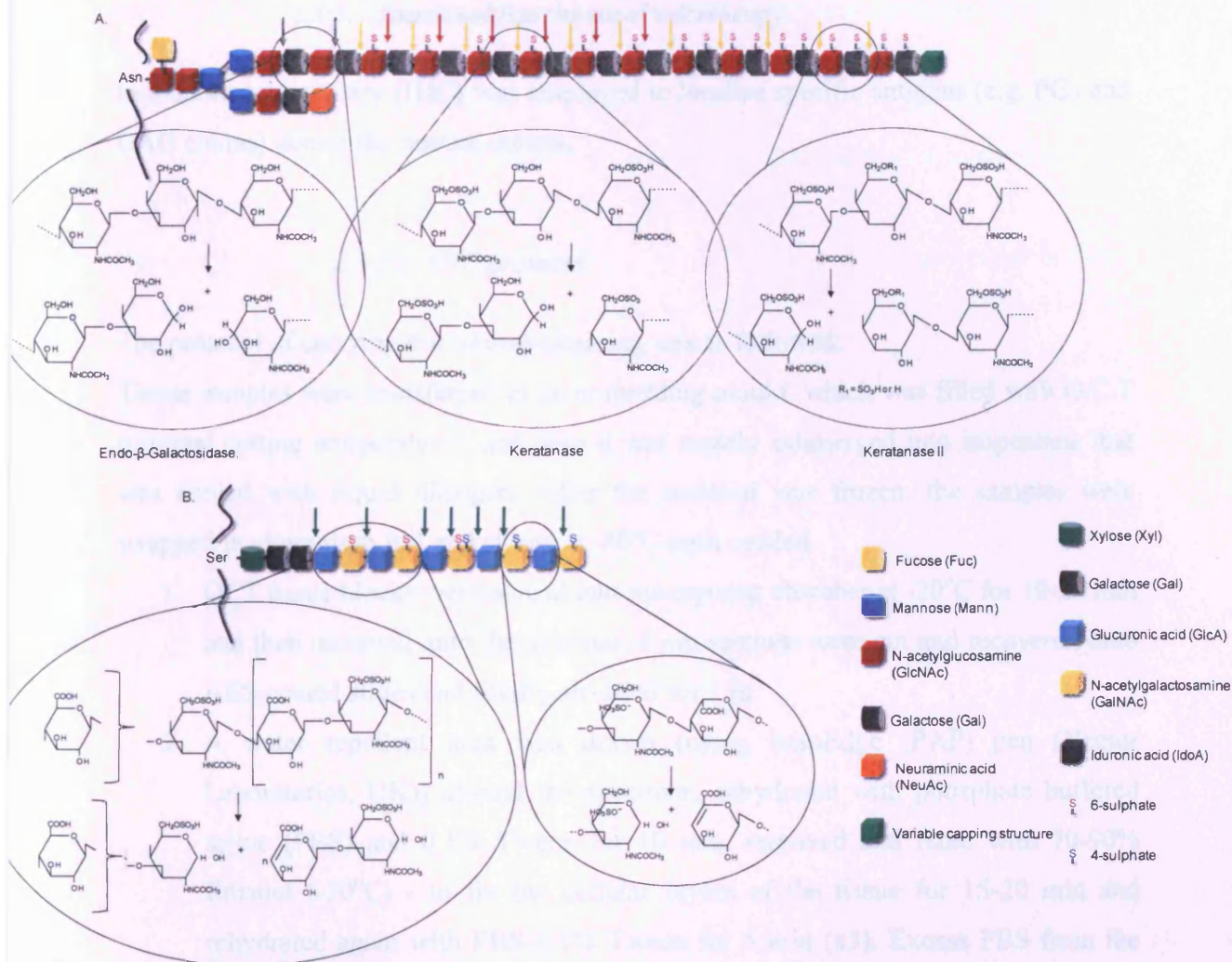


**Figure 2.5** A simple diagram illustrating the cleavage sites of the enzymes used in experiments. (A) KS-degrading enzymes: Endo- $\beta$ -galactosidase cleaves at  $\beta$ -1-4 galactosidic linkages where both the galactose and the GlcNAc residues are not sulphated galactosyl residues (grey arrows). Reaction products: oligosaccharides containing GlcNAc – Gal structure. It can also cleave at the same sites as Keratanase but at a much lower reaction. Keratanase cleaves at  $\beta$ -1-4-galactosidic linkages in which unsulphated galactose and sulphated N-acetyl glucosamine (GlcNAc) residues participate (red arrows). Reaction production: Gal, GlcNAc – Gal. Keratanase II cleaves at  $\beta$ -1-3-glucosaminidic linkages to galactose where the disaccharide structure can be either mono- or disulphated (yellow arrows). Reaction products: Gal – GlcNAc6S, Gal6S – GlcNAc6S. On cleavage, the enzyme requires the sulphate at 6-O-position of the participating glucosamine, but acts independently of the sulphate at 6-O-position of the galactose linked to the glucosamine. Diagram adapted from (Funderburgh, 2000). (B) CS/DS-degrading enzyme: Chondroitinase ABC cleaves N-acetylhexosaminide/N-acetylgalactosaminide linkages in chondroitin sulphate A, chondroitin sulphate C, chondroitin sulphate B (iduronic acid units in dermatan sulphate), chondroitin and hyaluronic acid, yielding mainly disaccharides with  $\delta$ -4-hexuronate at the non-reducing ends. Diagram adapted from (Esko et al., 2008).

Chemical structures adapted from (<http://www.seikagakubb.co.jp/bio/cgi-bin/search/edetail.php?code=100330>, 2007; <http://www.seikagakubb.co.jp/bio/cgi-bin/search/edetail.php?code=100455&PHPSESSID=be9a860cee56252ae8cf473a40d84b14>, 2007; <http://www.seikagakubb.co.jp/bio/cgi-bin/search/edetail.php?code=100810>, 2007; <http://www.seikagakubb.co.jp/bio/cgi-bin/search/edetail.php?code=100812>, 2007).

### 2.3.3. Immunohistochemical microscopy

Immunohistochemistry (IHC) was employed to localize specific antigens (e.g. PGs and GAG chains) across the bovine cornea.

#### 2.3.3.1. IHC protocol

The protocol of carrying out immunostaining was as followed:

Tissue samples were transferred to an embedding mould, which was filled with O.C.T (optimal cutting temperature), and then it was rapidly submerged into isopentane that was cooled with liquid nitrogen. After the material was frozen, the samples were wrapped in aluminium foil and stored at  $-80^{\circ}\text{C}$  until needed.

1. OCT tissue blocks were placed into the cryostat chamber at  $-20^{\circ}\text{C}$  for 10-20 min and then mounted onto the cryostat.  $8\ \mu\text{m}$  sections were cut and recovered onto AES-coated slides and finally air-dried for 1 hr.
2. A water repellent area was drawn (using ImmEdge (PAP) pen (Vector Laboratories, UK)) around the specimen, rehydrated with phosphate buffered saline (PBS) and 0.1% Tween for 10 min, removed and fixed with 70-90% Ethanol ( $-20^{\circ}\text{C}$ ) - to fix the cellular layers of the tissue for 15-20 min and rehydrated again with PBS-0.1% Tween for 5 min (x3). Excess PBS from the slides was removed before transferring to the humidity chamber.

Note: if using antibodies that needed pre-enzyme treatment (see Table 2.2 for enzyme preparation), the specific enzyme(s) were applied onto the tissue sections prior to the fixation. The pre-enzyme treated sections were incubated for 2 hr at  $37^{\circ}\text{C}$ . After incubation, tissue sections were washed with PBS-0.1% Tween (5 min/wash (x3)) and fixed as described as above.

1. Specimens were blocked in 5% goat serum (alternatively, IT Signal Enhancer can be used) (Invitrogen, UK) for 20 min, followed by the incubation of the primary antibody for 1 hr at room temperature (or overnight at  $4^{\circ}\text{C}$ ).

Note: blocking the tissue section prevents the nonspecific binding of the antibodies. Otherwise, the antibodies (primary or secondary) or other detection reagents may bind to any epitopes on the sample, independent of specificity. Excess blocking agent is usually added to saturate (block) any non specific binding sites that the antibodies may bind to. Then when the primary antibody is added, it only binds to its specific antigen.

Due to the fact that the blocking step is non-specific binding, separate blocking for primary or secondary antibodies is not needed.

2. Slides were then washed in PBS-0.1% Tween (5 min/wash (x3)) and then incubated with the secondary antibody (Alexa Fluor 488 goat anti-mouse IgG Fab fragments (Invitrogen, UK) for 1 hr.

Note: with storage, protein aggregates tend to form in the secondary antibody stock solution which can obscure fluorescence images and can cause high background. To avoid this problem, pellet any antibody aggregates by centrifugation of the working solution for 10 min at 7000 rpm.

3. Two negative controls were prepared, in replacement of the primary antibody: a) Negative Control Mouse IgG 1 (Dako Cytomation, Denmark); b) just PBS (as this would show the specificity of the primary antibody and the non specific binding of the secondary antibody, respectively).
4. Slides were washed thoroughly with PBS-0.1% Tween (5 min /wash (x3)) and finally mounted with Prolong Gold containing DAPI (Invitrogen, UK) to each specimen and covered with a cover slip. Slides were stored overnight at -20°C in slide tray and wrap in foil to prevent light exposure (fluorescent probes are light-sensitive).
5. Slides were thawed to room temperature before analyzed using an Olympus BX61 microscope and F-View digital camera.

Enzyme	Unit/ml	Buffer reconstitution
• Chondroitinase ABC – From <i>Proteus Vulgaris</i> (SIGMA-Aldrich, UK):	0.4	50 mM Tris (pH 8) and Sodium acetate
• Endo- $\beta$ -galactosidase – From <i>Bacteroides fragilis</i> (SIGMA-Aldrich, UK):	0.002	20 mM Tris-HCl (pH 7.5)
• Keratanase – From <i>Pseudomonas sp.</i> (Seikagaku, Japan)	0.4	10 mM Tris-HCl (pH 7.5) containing 0.1% bovine serum albumin (BSA)
• Keratanase II – From <i>Bacillus sp.</i> (Seikagaku, Japan)	0.004	10 mM Tris-HCl (pH 7.5) containing 0.1% BSA

**Table 2.2 Preparation of enzymes used for IHC.** Note: if using in combination of chondroitinase ABC with either/both end- $\beta$ -galactosidase and Keratanase enzymes, a 0.1 M Tris acetate (pH 6.8) buffer was used.

### 2.3.4. Enzyme-linked immunosorbent assay (ELISA)

Enzyme-linked immunosorbent assays (ELISAs) combines the specificity of antibodies with the sensitivity of simple enzyme assays, by using antibodies or antigens coupled to an easily-assayed enzyme, in which provides a useful measurement of antigen (e.g. the amount of KS) or antibody concentration. Unlike Western blots, which use precipitating substrates, ELISA procedures utilize substrates that produce soluble products.

There are two main variations on this method: the ELISA can be used to detect the presence of antigens that are recognized by an antibody or it can be used to test for antibodies that recognize an antigen. Either way, both methods require the preparation of a calibration curve during the assay. For this particular study, the competitive ELISA method was employed and a basic systematic illustration of this method is shown in Figure 2.6.

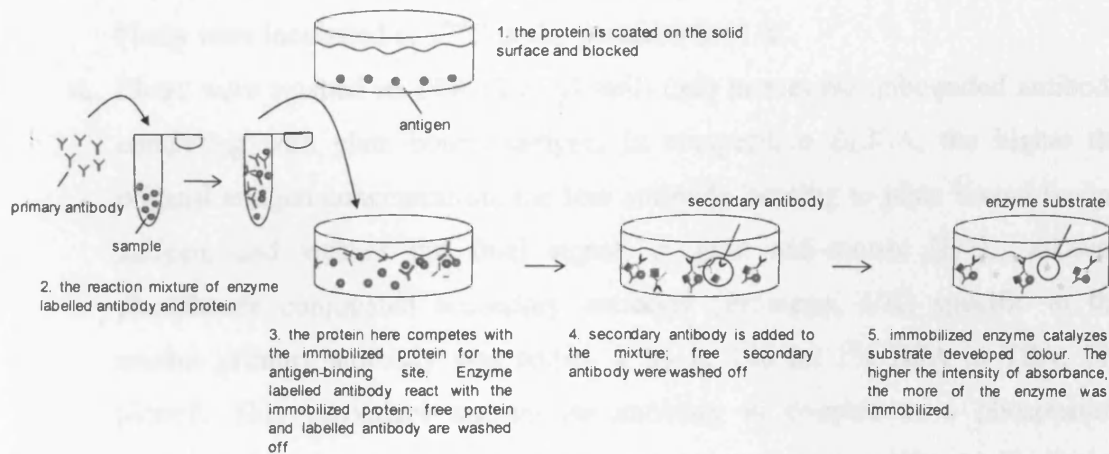


Figure 2.6 A simple diagram showing how competitive ELISAs work.

#### 2.3.4.1. ELISA protocol

The general outline of the protocol was as followed:

1. 96 well plates (Titretek, Alabama, US) were coated with bovine corneal stroma antigen (chondroitinase ABC treated) in 20 mM NaCO<sub>3</sub> buffer (pH 9.6) (100 µl/well) and incubated overnight at 37°C.
2. The coated microtiter plates were washed with 280 µl/well in Tris saline azide (TSA) (x3) and then blocked with the addition of 1% (wt/v) BSA in TSA, and

incubated for 1 hr at 37°C, as this prevented non specific binding. After incubation, the blocked microtiter plates were washed, air dried and then stored at 4°C until microplates were needed.

3. Known concentrations of bovine competing antigen were serially diluted to generate a standard curve. Bovine corneal biopsy digests were also serially diluted and both
4. Standards and samples were incubated with an equal volume of KSmAb, before adding them to the ELISA plate. Note: mAbs were initially prepared double the concentration. Both the known samples and samples were incubated for 1 hr at 37°C.
5. Plates were washed in TSA (280 µl/well) (x4) and banded antibody/antigen complexes (100 µl/well) added to the antigen coated wells. Bovine antigen competes with plate-bound bovine antigen for primary antibody binding, so that higher tissue levels of bovine KS result in less antibody binding to the plate bound antigen. Unused wells were then blocked using 100 µl 1% BSA in TSA. Plates were incubated at 37°C under parafilm for 1 hr.
6. Plates were washed in TSA (280 µl/well) (x6) to remove unbound antibody competing with plate bound antigen. In competitive ELISA, the higher the original antigen concentration, the less antibody binding to plate bound bovine antigen, and weaker the final signal. A goat anti-mouse (H+L) alkaline phosphatase conjugated secondary antibody (Promega, UK) specific to the murine primary antibody was added, 2 µg in 100 µl 1% BSA in TSA, 100 µl/well. This secondary anti-mouse antibody is coupled to a phosphatase enzyme, which is used to create a colour signal representing KSmAb binding to the ELISA plate-the inverse of competing antigen concentration plates were covered in parafilm and incubated for 1 hr at 37°C.
7. Plates were washed in TSA (280 µl/well) (x6) to remove unbound secondary antibody, before adding alkaline phosphatase substrate (p-nitrophenyl phosphate) tablets (x2) in DEA buffer (0.126 mM MgCl<sub>2</sub>, 1 M diethanolamine, pH 9.8) 100 µl/well. Plates were covered in parafilm and incubated for 1 hr at 37°C. Adding phosphatase substrate causes a metachromatic shift reaction, which is used to measure the amount of KS in this case in the sample with a spectrophotometer.

8. Colour development was quantified on a plate reader (Lab Systems, Multiscan MS plate reader) at 405 nm. From this read out, KS was quantified against a standard curve of known competing antigen.

#### 2.3.4.2. ELISA - Determining antibody concentration

The KS antibody concentrations were determined using a “shot gun titre” approach. The 96 well plates were prepared as described in section 2.2.4.4.1. A 1:3 serial dilution of antibodies were prepared, starting with a 1:50 dilution. No unknown samples were prepared at this point. Figure 2.7 shows how the KS antibodies, 5D4 and 1B4 concentrations were determined. The antibody dilutions were determined at a half way point of which the curve emerged to decrease exponentially. For this particular project, ~1:6000 (5D4) and ~1:150 (1B4) antibody dilution was deduced and used in subsequent inhibition ELISA assays.

Antibody dilution	5D4: Mean optical $A_{405}$	1B4: Mean optical $A_{405}$
1:50	3.587	3.219
1:150	3.480	1.494
1:450	3.587	0.524
1:1350	3.199	0.134
1:4050	1.781	0.054
1:12150	0.849	0.038
1:36450	0.320	0.010
1:109350	0.150	0.022
1:328050	0.141	0.024

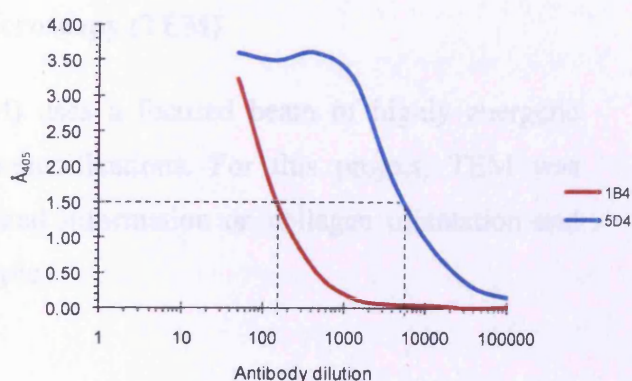


**Figure 2.7 Determining 5D4 and 1B4 antibody concentration used for quantifying the unknown amounts of KS content in the bovine corneal extracts.** The antibody dilutions were determined at a half way point of which the curve emerged to decrease exponentially.

#### 2.3.4.3. Keratan sulphate quantification

Standard curves were generated from the optical absorbance of known bovine KSPG extracts for each plate, and the bovine corneal extract were read from the standard curve as shown in Figure 2.8. The amount of KS was calculated from reading across from the % absorbance compared to ng/ml antigen on the standard curve and then

multiplied by the dilution factor and units were expressed in ng relative to per mg dry weight.

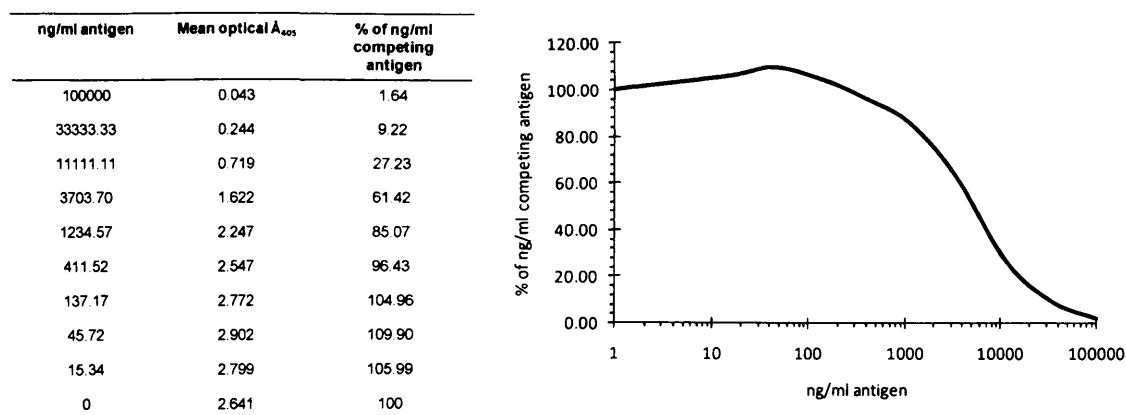


**Figure 2.8** An example of a 5D4 standard curve calculation from optical density. KS content of bovine corneal extracts was deduced by reading across from % absorbance compared to ng/ml antigen on the standard curve.

## 2.4. Transmission electron microscopy (TEM)

Transmission electron microscopy (TEM) uses a focused beam of highly energetic electrons to examine objects at high magnifications. For this project, TEM was employed, as this would give rise to visual information on collagen orientation and more importantly fibril diameter for example.

### 2.4.1. General preparation for TEM analysis

Prior to TEM analysis, fresh whole bovine eye globes (with small incisions at the sclera) were fixed in 4% paraformaldehyde in 0.1 M phosphate buffer overnight at 4°C. Corneas were dissected out with a 2-3 mm scleral rim attached and further fixed for 1 hr at room temperature. Fixed corneas were then cut in the same way as shown in Figure 2.2.

Biopsies of corneal tissue was post-fixed in 1% osmium tetroxide for 1 hr, then contrasted in 0.5% aqueous uranyl acetate (UA) for a further 1 hr. Sections were then dehydrated to remove all water from the sample through wash steps of increasing ethanol (70%, 90% and 100% (x2)) each for 15 min. Specimens were further immersed

in two changes of propylene oxide for 30 min and infiltrated with a 3:1 mix of propylene oxide and unpolymerized Araldite resin. Tops were left off specimen vials in a fume hood, so that the concentration of the resin increases. Following one more change in fresh resin, infiltrated specimens were placed in TEM embedding moulds filled with fresh resin. Polymerisation treatment was carried out at 60°C for 72 hr. After 72 hr, corneal resin blocks were left at room temperature, ready for ultra-thin sectioning.

#### *2.4.1.1. Positive and negative staining of collagen*

Although secondary fixation in osmium tetroxide provides some areas of electron density, this is usually not sufficient to provide high contrast, high definition images. A number of staining techniques are available to enhance the contrast of areas of interest. These fall into two major categories, positive staining and negative staining. Cationic and anionic stains the positive and negative amino acid, respectively. Positive staining is when the stain is washed off, leaving the bound stain, however if the stain is buffered to neutrality and not washed off, and settles in the gaps without binding, this is referred as negative staining.

In negative staining, only excess heavy metal staining solution is drained off, leaving a thin layer of stain around the specimen, outlining it and filling the internal voids with electron dense contrasting medium. The internal structure that can be seen is dependent on the size of the heavy metal staining molecule and the extent to which it can penetrate. In collagen fibril the interstices in the gap zones are large enough for penetration, giving the characteristic alternation of dark (gap) a light (overlap) zones along the negatively stained fibrils (Chapman and Hulmes, 1984). In negative stain microscopy, the electron beam primarily interacts with the stain. When the stain is added to the sample, the stain surrounds the sample and excludes the volume occupied by the sample; hence the use of the term 'negative staining' (i.e. the protein is not stained and appear white when scanned). When the electron beam passes through the specimen, the electrons are deflected upon interaction with the stain, yielding contrasted images. However, negative staining only shows surface detail and imposes a limit on the resolution. This is because of stain movement during imaging, variable

flattening of the 3D structure by dehydration, and artefacts may arise, if the stain is uneven; since the pattern of the stain deposition is dependent on the structure of the particle (Chen, Roseman and Saibil, 1998; Ruprecht and Nield, 2001). The advantages of negative staining methods are that they are rapid and provide high contrast images with data typically to  $\sim 20\text{\AA}$  resolution (Goodhew, 1975). Phosphotungstic acid (PTA) used at neutral pH is a common negative stain for collagen.

Positive staining is when a stain containing charged ions (positive or negative) interacts with the collagen and unbound stain is washed off. The banding pattern in positively stained collagen fibrils thus reflects the axial distribution of charged amino acid residues along a fibril. Collagen fibrils that are doubly stained with PTA and uranyl acetate (UA) allow anionic stain to bind onto the positively charged residues, and vice versa for the cationic stain. The uptake of phosphotungstate ions are thought to bind onto positively charged side chains of Arg, Lys, hydroxylysine, and His along the collagen molecule, whereas uranyl ions can bind to both charges, even though it is cationic ion. This result arises because UA is a weak electrolyte in aqueous solution, and acetate ions are for the most part associated with the uranyl ions, which interact with both carboxyl and amino groups. It is these charges that participate in binding reactions with all the charged residues on complexes such as collagen and the relative uptake on negatively charged and positively charged side chains are dependant on concentration and pH (Chapman and Hulmes, 1984).

The formulation of lead citrate, introduced by Reynolds (1963) is most widely used to increase contrast of membrane and other tissue components. It is at its most effective and stable at high pH (12-13) (Reynolds, 1963). Membrane staining results from lead interacting with previously bound acidic osmium molecules, which have an affinity for positive dye ions such as lead. Glycogen staining is a result from the attachment of lead to the hydroxyl groups of carbohydrates by chelation, and then additional lead accumulates around the primarily attached lead. Proteins with large numbers of sulfhydryl group are stained with lead complexes with negatively charged phosphate groups Lead is strongly chelated with citrate, reducing its tendency to form lead carbonate upon interaction with air. The basic mechanism of anionic staining sites have greater affinity for lead cations than does the citrate portion of the solution, while, at the same time,  $\text{CO}_2$  and  $\text{O}_2$  have less affinity for the lead (Dykstra and Reuss, 2003).

#### 2.4.1.2. Cupromeronic blue staining for GAG chains

Cupromeronic blue is an intense blue cationic dye developed specifically for electron microscopic localization and characterization of PGs and sulphated GAGs (keratan, dermatan, and chondroitin sulphates) and hyaluronan (hyaluronic acid). Hence this was approached in the project.

This cationic dye belongs to the group of reagents which includes; alcian blue and cetylphridinium, and can be used as a critical electrolyte concentration (CEC) method to differentiate between polyanions according to the type of anion (carboxylate, phosphate ester or sulphate ester) without the complication of non-ionic binding to nucleic acid bases. The isomeric cuprolinic blue was designed to have high affinity for nucleic acids, whereas the cupromeronic blue was designed to have no special affinity for nucleic acids, other than as polyphosphates. This cationic dye acts like intercalating dyes but its unique steric hindrance, due to methyl group placement, prevents the dye from intercalating into the stacked base pairs (Scott and Haigh, 1988a). Thus, this cationic dye can bind onto to GAG chains of PGs, as they are highly sulphated making them to have a negative net charge.

CEC is referred to the characteristic concentration of salt at which a given polyanion ceases to stain with a given dye. The higher the CEC, the fewer substrates are stained (i.e. the specificity of the reagent is increased). The structures that are strongly stained with this dye may represent binding to sulphated polyanions because they have a high CEC. The CEC method of cupromeronic blue staining of tissue polyanions require that staining be carried to an optical equilibrium. The specificity of cupromeronic blue for polyanions is primarily due to underlying specific ion effects. Thus staining with this dye is controlled by the ionic character of the predominant tissue polyanions e.g. KS, CS and DS in corneal matrix and phosphate DNA. At a critical concentration of an electrolyte, the dye is displaced from its complex by the substrate. This displacement is due to the cations of electrolyte compete with the cationic (isothiuronium) groups on cupromeronic blue for binding to the negative sites on the polyanions. The concentration of  $MgCl_2$  is essential to the stain for accomplishing this displacement. Such mechanism of  $MgCl_2$  is explained on the basis of  $Mg^{2+}$  competing with cupromeronic blue for binding sites on mucopolysaccharides (i.e. GAG chains). As the

concentration of  $Mg^{2+}$  increases, more binding sites are blocked from access to the cupromeronic blue. Thus, when using staining at a CEC would ensure that only the substrate (in this case GAG chains) are stained.

## 2.5. X-ray diffraction of collagen

X-ray diffraction allows structural, quantitative data to be gathered in a close to natural tissue state, without the need for lengthy tissue preparation, e.g. electron microscopy. X-ray diffraction patterns are obtained by focussing a monochromatic beam of x-rays through the specimen. Some x-ray passes straight through the specimen and is absorbed by a lead backstop behind the sample, whilst others are absorbed by the specimen itself. The remaining x-rays are scattered by the constituents of the sample and form a pattern on a detector placed behind the specimen.

A fibril placed vertically in an x-ray beam causes x-rays to be scattered both parallel to the fibril axis to form a meridional reflection and at right angles to the fibril axis to produce an equatorial reflection (Figure 2.9). In cornea, collagen fibrils within lamellae lie in all directions within the plane of the tissue causing both equatorial and meridional reflections to appear as a series of concentric circles. Due to the fact that equatorial reflections are broader than meridional reflections, the two can be easily distinguished and behave differently when tissue hydration increases (Meek and Quantock, 2001).

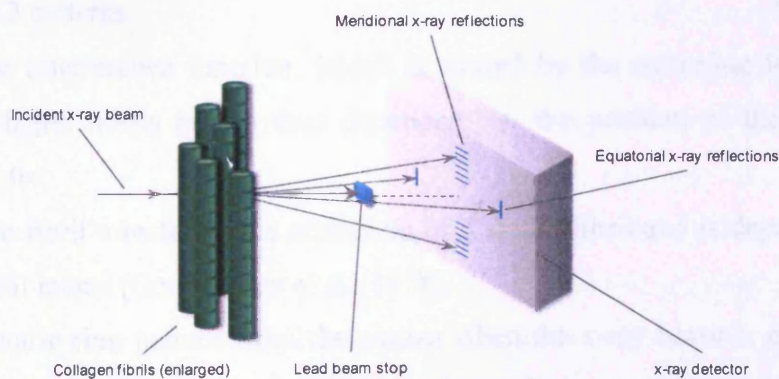


**Figure 2.9** A schematic diagram showing how an array of fibrils held vertically in an x-ray beam gives rise to meridional reflections in a direction parallel to the fibril axes equatorial reflections in a direction perpendicular to the fibril axes (Meek and Quantock, 2001).

The angle through which the x-rays are scattered is called scattering angle; the greater the scattering angle, the greater the radial distance of the reflection (R) from the centre of the pattern. When the x-rays are scattered at large angles ( $> 2$  degrees) high-angle patterns are recorded using a short specimen to detector distance ( $\sim 15$ - $20$  cm); when the x-rays are scattered through small angles ( $< 2$  degrees) low-angle patterns are recorded using a much larger specimen to detector distance of several metres (Meek and Quantock, 2001).

Small-angle meridional reflections produced by collagen are caused by the 65 *D*-periodicity along the fibril axis, whilst wide angle equatorial reflections arise from the lateral packing of the molecules within the stromal collagen fibrils. As collagen molecules are aligned roughly parallel to each other and scatter x-rays at right angles to the direction of their long axis, the orientation of the molecules can thus be said to represent the direction of the collagen fibrils at that position with the corneal stroma. The intensity of the reflection provides quantitative information regarding the number of molecules lying in a certain direction, thus regions of higher scattering intensity on the x-ray diffraction pattern indicate more collagen travelling in a particular direction. The cornea can produce a small-angle equatorial pattern and wide-angle equatorial pattern (from lateral packing of collagen molecules) and small-angle meridional pattern (from *D*-periodicity of collagen). The small-angle equatorial reflection is caused by the uniformity of fibril diameters and the regular spacing of collagen fibrils (over a short range), with each lamella of the corneal stroma. The small-angle equatorial reflection comprises 2 patterns:

- The interference function, which is caused by the scattering from an array of collagen fibrils and is thus dependent on the position of the collagen fibril centre.
- The fibril transform, the scattering of a single fibril and is dependent upon the fibril radius (Goodfellow et al., 1978).

The concentric ring pattern from the cornea when the x-ray beam is passed along the direction of the optical axis indicates the collagen fibrils are orientated in all directions equally in the plane of the cornea. The width of the ring is related to the range of interfibrillar spacing's present in the cornea. Quantitative data was calibrated using x-ray diffraction patterns from rat tail tendon, the known axial periodicity of 67 nm

means sample interfibrillar spacing and diameter may be calculated (Goodfellow et al., 1978; Sayers et al., 1982).

### **2.5.1. X-ray diffraction preparation**

Fresh whole bovine eye globes (with incisions made at the sclera) were fixed with 4% paraformaldehyde in 0.1 M phosphate buffer over night at 4°C. Whole corneas (with a 2-3 mm scleral rim attached) were removed and further fixed for 1 hr at room temperature. Fresh tissue samples were also prepared and both conditions were carefully and tightly wrapped in Clingfilm (Tesco, UK) (to minimize dehydration and associated structural changes), freeze-dried at -20°C and at -80°C and then transported on dry ice to SPring-8 (Super Photon Ring). Note: fresh and fixed bovine corneal tissues were prepared as this was due to cautions of corneal dehydration during preparations of the x-ray experiments.

### **2.5.2. Small angle X-ray scattering data collection**

All small angle x-ray experiments were carried out in beamline BL40XU at the SPring-8, a synchrotron radiation facility located in Japan. The facility consists of a storage ring containing an 8 GeV electron beam. The beam is extracted and run through undulators to produce synchrotron radiation with energies ranging from soft x-rays (300eV) to hard x-rays (300 KeV). At the beamline, the corneas were gently thawed and the tissue samples were further cut in strips (as shown in Figure 2.10) under a light microscope. Tissue samples were immediately placed between a single layer of Clingfilm to limit dehydration during exposure of the x-ray beam. Samples were then secured onto a Mylar (with a clear plastic cell window) sheet and mounted in the path of the beam that was focussed along the central anterior surface of the cornea (epithelium facing the x-ray beam) (Figure 2.10, Experiment 1). In another experiment the x-ray beam was focussed in a horizontal orientation with the cut edge perpendicular to the incident beam direction (Figure 2.10, Experiment 2). The plastic cell was placed in the x-ray beam ( $\lambda = 0.83\text{\AA}$ ) (measuring 25  $\mu\text{m}$  in diameter) so that the x-rays passed through the whole tissue. Diffraction patterns were recorded on 640 x 480 pixel detector, with a lead backstop between sample and detector to stop any undeviated rays.

Average x-ray intensity during data collection was recorded by an ion chamber between the incident beam and specimen. A series of sequential micrometer steps and sub second exposure time of x-ray was obtained along the corneal optical axis and vertically across the through the centre of the specimen, traversing its entire thickness.

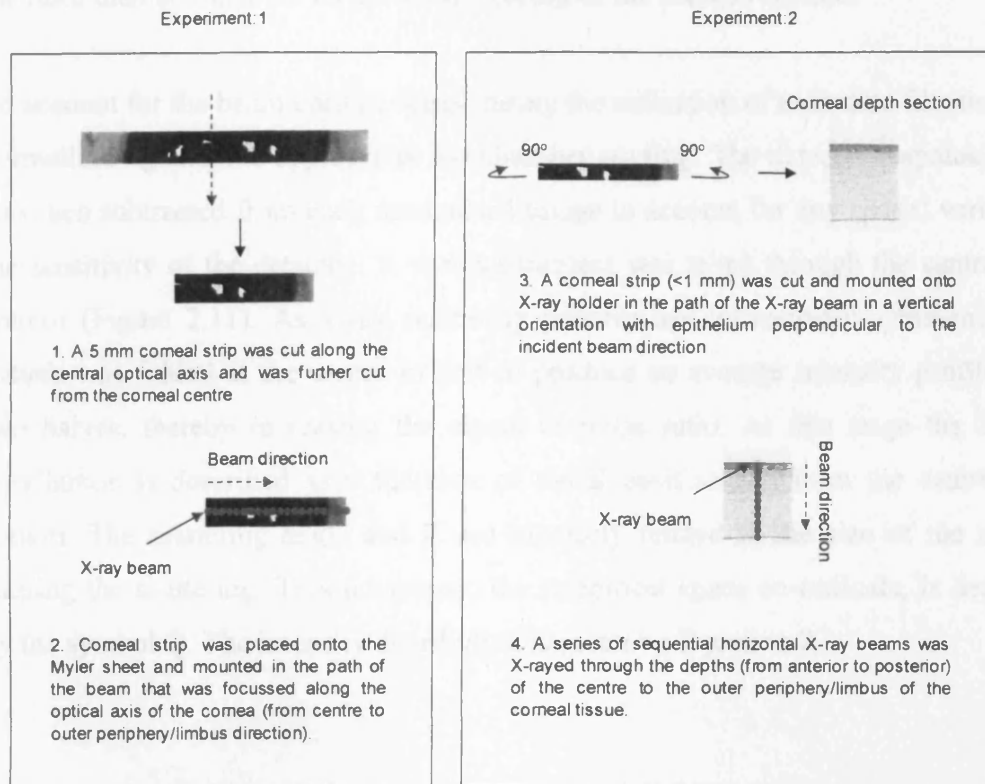


**Figure 2.10** A simplistic diagram showing how the corneas were prepared for x-ray analysis.

Details of the parameters topographically and across the depths of the cornea are shown in Chapter 4, Section 4.4.1, Table 4.1. X-ray patterns were recorded with sub-second exposure times on a cooled CCD camera (ORCAII-ER, Hamamatsu Photonics) - framing rate of 290/sec, coupled with an x-ray image intensifier (V5445P, Hamamatsu Photonics) 3 m behind the specimen. A fresh piece of rat tail tendon (vertically positioned) was used to calibrate (which has known 67 nm *D*-periodicity) against the tissue samples. To account for any spatial variation in the sensitivity of the detector a single detector response pattern from 420 mins exposure to the radioactive source ( $\text{Fe}^{55}$ ) was also recorded. Once the data was collected, the x-ray patterns were electronically analyzed in Cardiff.

### *2.5.2.1. Small angle x-ray scattering data analysis*

The x-ray patterns were analyzed using UNIX based image analysis software (Fit2d, produced by Dr A. Hamersley, ESRF, Grenoble, France) and a Windows based statistics (Microsoft Excel and Statsoft Statistica) package was used to obtain values for the fibril diameter and the interfibrillar spacing of the corneas studied.

To account for the beam current decay during the collection of each data file, they were normalized against the appropriate ion chamber reading. The detector response pattern was then subtracted from each normalised image to account for any spatial variation in the sensitivity of the detector. A vertical transect was taken through the centre of the pattern (Figure 2.11). As x-ray scattering patterns are intrinsically symmetrical, the pattern was folded at the centre in half to produce an average intensity profile of the two halves, thereby increasing the signal to noise ratio. At this stage the intensity distribution is described as a function of radial position (R) from the centre of the pattern. The scattering angle and R are inversely related to the size of the structure causing the scattering. This parameter, the reciprocal space co-ordinate, is designated by the symbol Q. The intensity distribution is given by Equation 2.

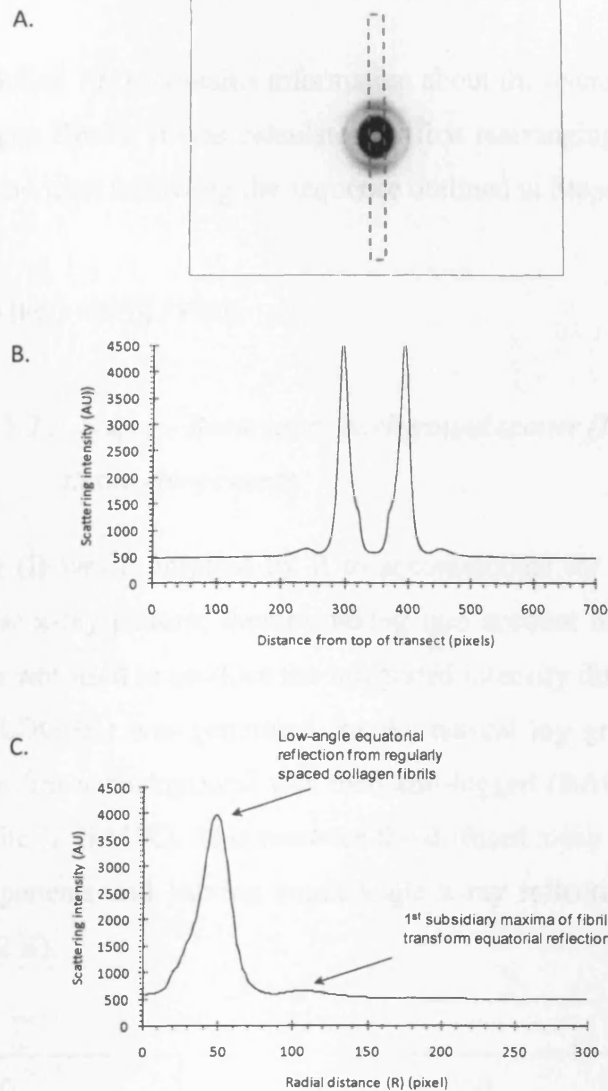


**Figure 2.11** Small angle x-ray scattering pattern from a mid central region of a bovine cornea (A). A vertical transect (dashed red line) was taken through the centre of the pattern to form an intensity profile of the x-ray pattern (B). The data was then folded about the centre to produce an average intensity profile of the two halves (C).

#### 2.5.2.2. Calculation of the intensity distribution from the equatorial scatter component:

$$\text{Equation 2: } I(Q) = F^2(Q) E(Q) + B(Q)$$

$I(Q)$  = the integrated intensity distribution

$F^2$  = the fibril transform (which takes the form of a first order Bessel function)

$E(Q)$  = the fibril interference function

B = the background scatter from other tissue components

The interference function  $E(Q)$  contains information about the average centre to centre spacing of the collagen fibrils. It was calculated by first rearranging Equation 2 in the form of Equation 3 and then following the sequence outlined in Steps 1-4.

**Equation 3:**  $E(Q) = (I(Q) - B(Q)) / F^2(Q)$

### 2.5.2.3. Step 1 - Removal of background scatter (B) caused by other tissue components

The scatter intensity (I) was multiplied by R to accommodate for the use of a linear scan across a circular x-ray pattern, thereby taking into account the fact that a small sample of the pattern was used to produce the integrated intensity distribution profile. A linear background (LOGBK) was generated for the natural log graph of I against R (Figure 2.12 A). The linear background was then anti-logged (BACK) and subtracted by the intensity profile (I\_BACK). This removes the diffused x-ray scattering from the stromal matrix components and leaving small angle x-ray reflections of the fibrillar collagen (Figure 2.12 B).

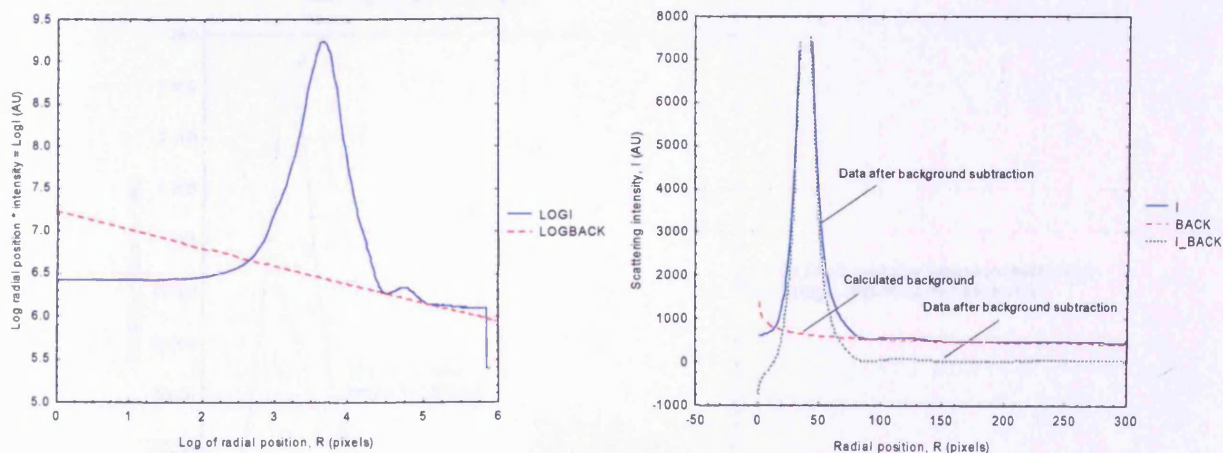


**Figure 2.12** Linear background generation (LOGBK) against radial position (LOGR) (A). The background scatter (BACK) was removed from the profile of scattering intensity against radial position (I) to leave the small angle reflections of the cornea (I\_Back) (B).

## 2.5.2.4. Step 2 – Removal of fibril transform (F2)

Since the collagen fibrils are cylinder shaped, small angle equatorial x-ray diffraction from a corneal lamella can be approximated as the fibril transform (scattering from a single fibril), multiplied by the interference function (derived from the ordered arrangement of the cylinders) (Worthington and Inouye, 1985). A theoretical fibril transform was fitted to the experimental data by varying two parameters: the fibril radius and an arbitrary scaling factor. The fibril transform, takes the form of a first order Bessel function (BESSEL). The transform has a maximum that produces a low, broad peak near the 3<sup>rd</sup> order of the collagen meridional reflection (i.e. the 1<sup>st</sup> subsidiary maximum of the experimental data). The Bessel function was fitted to this peak in the image profile (I\_BACK) (Figure 2.13), as this is because this peak is derived entirely from the fibril transform, with no significant contribution from the interference function (Worthington and Inouye, 1985). The interference function  $E(Q)$ , was obtained by dividing the image profile by the fibril transform. This interference function represents the probability of finding a fibril centre at a given distance from another fibril centre. This rises to a peak corresponding to the average nearest neighbour centre to centre spacing of the collagen fibril then oscillates at about the value of 1 (short range order). In order to determine the Bragg interfibrillar spacing, R must be calibrated.

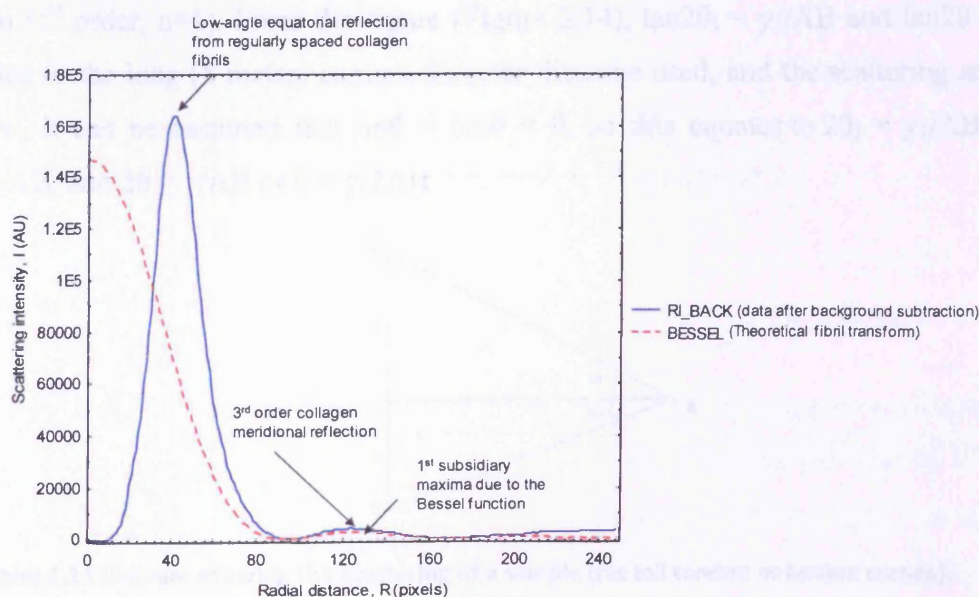


**Figure 2.13** The fibril transform (BESSEL) fitted to the profile of the scattering intensity (collagen) multiplied by radial position (RI\_BACK). The scattering intensity profile is then divided by the fibril transform to produce the interference function.

### 2.5.2.5. Step 3 - Calculating the interfibrillar Bragg spacing (IFBS) of corneal collagen

In rat tail tendon, collagen fibrils represent approximately 90% of the dry wt and are organized into three-dimensional quasi-crystals, parallel to the tendon axis (Hulmes et al., 1981), forming well-defined diffraction patterns that can be used for calibration. The meridional reflections obtained from the native collagen of the rat tail tendon exhibit an axial periodicity of 67 nm. When the x-ray diffraction pattern from cornea are calibrated against those meridional x-ray reflections from rat tail tendon collagen, the mean centre-to-centre collagen fibril Bragg spacing can be determined.

The interfibrillar Bragg spacing (IFBS) was deduced as shown in Figure 2.14. B, corresponds to the position of the sample and A of the detector.  $AC = y$  represents the distance from the centre to the peak corresponding to the Bragg spacing, on the linear scan of the rat tail tendon. Similarly,  $AC_1 = y_1$  is that distance on the linear scan of the bovine cornea.  $\theta$  is the half the scattering angle of the rat tail tendon and  $\theta_1$  half the scattering angle of the bovine cornea sample.

The wavelength used at the beamline is  $\lambda = 0.83$  nm and the order of the equatorial peak from cornea is  $n = 1$ . For rat tail tendon the interfibrillar Bragg spacing is  $d = 67$  nm (1<sup>st</sup> order,  $n=1$ ). From the figure (Figure 2.14),  $\tan 2\theta_1 = y_1/AB$  and  $\tan 2\theta = y/AB$ . Due to the long (8 metre) camera-detector distance used, and the scattering angle was low, it can be assumed that  $\sin\theta = \tan\theta = \theta$ , so this equates to  $2\theta_1 = y_1/AB$  or  $\theta_1 = y_1/2AB$ , and  $2\theta = y/AB$  or  $\theta = y/2AB$ .

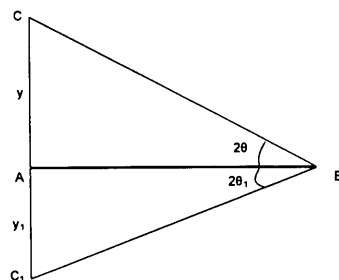


Figure 2.14 Diagram showing the scattering of a sample (rat tail tendon or bovine cornea).

For rat tail tendon, Bragg's law (Equation 4) can be arranged as:

$$\begin{aligned} \text{Equation 4:} \quad & n\lambda = 2d\sin\theta \\ \text{Rearrange equation:} \quad & \sin\theta = n\lambda/2d \\ \text{Since } n = 1 \quad & \Rightarrow \quad \sin\theta = \lambda/2d \\ \text{For small angles} \quad & \sin\theta = \theta \text{ (in radius)} \\ & \Rightarrow \quad \theta = \lambda/2d \end{aligned}$$

In rat tail tendon we showed that:

$$\begin{aligned} & \theta = \gamma/2AB \\ \text{Therefore} \quad & \lambda/2d = \gamma/2AB \\ \text{Rearrange equation:} \quad & AB = 2d\gamma/2\lambda \\ \text{Since } d = 67 \quad & \Rightarrow \quad AB = 67\gamma/\lambda \end{aligned}$$

For the cornea, Bragg's law may be written as follow:

$$\begin{aligned} & \theta_1 = n\lambda/2d_1 \\ d_1 = \text{corneal Bragg spacing to be determined, but from above:} \\ & \theta_1 = \gamma_1/2AB \\ \text{Therefore} \quad & n\lambda/2d_1 = \gamma_1/2AB \\ \text{Rearrange equation:} \quad & AB = 2d_1\gamma_1/2n\lambda \\ \text{Since } n = 1 \text{ for cornea} \\ & AB = d_1\gamma_1/\lambda \\ \text{Therefore} \quad & 67\gamma/\lambda = d_1\gamma_1/\lambda \\ \text{Or} \quad & d_1 = 67\gamma/\gamma_1 \end{aligned}$$

The IFBS of the bovine cornea can be defined as (Equation 5):

$$\text{Equation 5:} \quad \text{Interfibrillar Bragg spacing} = 67\gamma/\gamma_1$$

In relation to the software used for the analysis, the radial distance was calibrated using the position of the sharp meridional 1<sup>st</sup> order x-ray reflection and known 67 nm *D*-periodicity of rat tail tendon (Figure 2.15). The IFBS of corneal collagen was calculated by dividing the position of the 1<sup>st</sup> order reflection of rat tail tendon (Figure 2.15 B) by the position of the low-angle equatorial reflection of the corneal collagen (after the removal of background scatter and division by the fibril transform) and then multiplying the resulting number 67 (the *D*-period of rat tail tendon). Bragg spacing can

be converted to actual interfibrillar spacing using a multiplication factor of 1.12, based on the assumption that the cornea has a liquid-like packing arrangement (Worthington and Inouye, 1985).

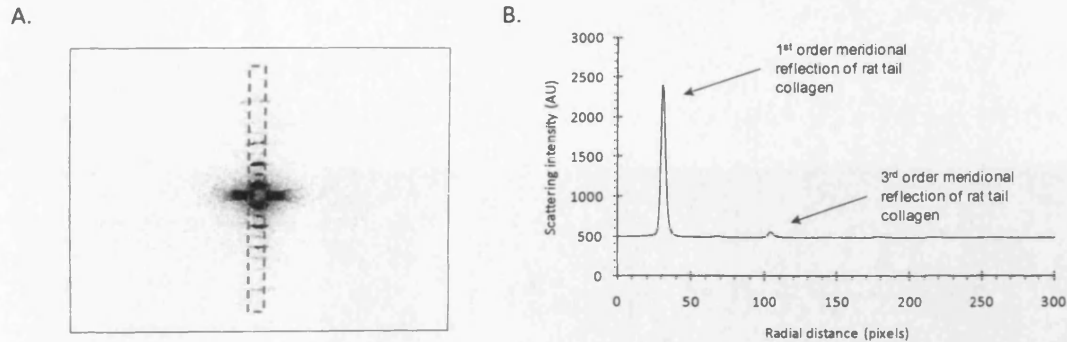


**Figure 2.15** Small angle x-ray intensity profile pattern of a rat tail tendon (A). The intensity profile was folded around the centre point to produce an average intensity profile (B).

#### 2.5.2.6. Step 4 – Calculating fibril diameter

Assuming that individual collagen approximated as infinitely long cylinders. Scattering from such cylinders takes the mathematical form of a 1<sup>st</sup> order Bessel function. The first subsidiary maximum of the fibril transform (BESSEL function) is related to the fibril diameter ( $2r$ ) as shown in Equation 6 (Worthington and Inouye, 1985) and 7:

**Equation 6:**  $2r = 5.14/\pi M$

$2r$  = fibril diameter

$M$  = Reciprocal space position of 1<sup>st</sup> subsidiary maximum ( $\text{nm}^{-1}$ )

$M$  can be calculated using a calibrant (in this case the rat tail tendon) via:

**Equation 7:** 
$$M = \frac{\text{1}^{\text{st}} \text{ subsidiary maximum position (i.e. "position" in Bessel file in pixels)}}{\text{1}^{\text{st}} \text{ order meridional idional peak position of calibrant (pixels)} \times D\text{-period of calibrant (nm)}}$$

---

### Chapter 3: Biochemical studies of the ECM across the bovine cornea

## 3.

### 3.1 Introduction

Corneal transparency is of fundamental importance of eyesight. Previous studies (Doutch et al., 2008; Doutch, 2009) have shown that corneal transmission (both in human and in bovine) gradually decreases from the central to the outer peripheral regions of the cornea. It was suggested that the reduction in transparency towards the periphery could be due to the increased corneal thickness, increased fibril diameters or an increased fibril disorder or an increase in the mismatch between the refractive indices of the fibrils and the ECM (Doutch et al., 2008). The increase in light scatter found towards the outer periphery is thought to be due to the larger fibrils and interfibrillar spacing found at this region, as previous studies have shown, using TEM (Borcherding et al., 1975) and x-ray analysis (Boote et al., 2003). Doutch and co-workers also acknowledge the refractive indices could also influence the ratio between fibrils and the interfibrillar substance. However, to date there has been limited studies as to whether the type of PG changes at the outer peripheral regions of the cornea. Early studies (Borcherding et al., 1975) have shown that the topographic distribution of GAG molecules from corneal centre to the outer periphery (in human) is more uniform, changing only at the outer periphery-limbus region, where KSPG is reduced relative to DSPG (Borcherding et al., 1975). However, these studies were based on hexosamine and uronic acid assays to quantify the content of KS (containing glucosamine and galactosamine) and CS/DS (containing glucuronic acid), respectively. The aim of this particular study was to extend these early finding by Borcherding *et al.* (1975) and Doutch *et al.* (2008, 2009) by investigating the sulphation patterns of GAGs across and tissue depths in defined regions of the cornea.

### 3.2 Methods

A summary plan is present in the figure below:

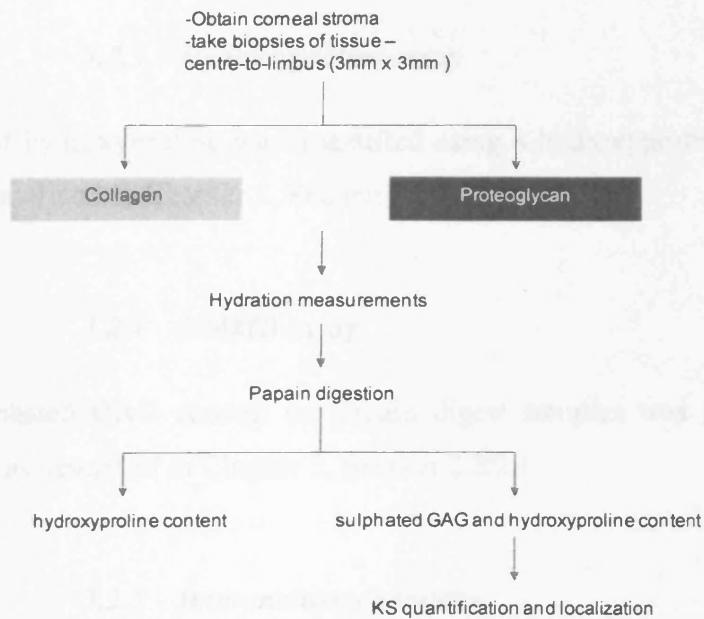


Figure 3.1 Summary plan of experiments.

#### 3.2.1 Corneal thickness measurements

Fresh bovine eyes with clear/transparent corneas ( $n = 10$ ) were selected and assessed by pachymetry for corneal thickness of each tissue region: centre (0-3 mm zone), periphery (3-6 mm zone), outer periphery (6-9 mm zone) and limbus (9-12 mm zone). Using a Ultrasonic Pachymeter (DGH Technology Inc, USA) each measurement was recorded as an average of 15 readings.

#### 3.2.2 Sample preparation for biochemical studies

Fresh bovine corneal stromas were excised as described in Chapter 2, section 2.1. The wet weights of the set of corneal biopsies were individually measured, the tissues were then freeze dried and finally stored until needed at  $-20^{\circ}\text{C}$ . Hydrations of the biopsies were calculated.

### 3.2.2.1 Papain digestion

Corneal biopsies (n = 10) were papain digested as described in Chapter 2, Section 2.1.1.1.

### 3.2.3 Hydroxyproline assay

The amount of hydroxyproline was quantified using a hydroxyproline assay (Blain et al., 2006) as described in Chapter 2, Section 2.2.1.1.

### 3.2.4 DMMB assay

The total sulphated GAG content on papain digest samples was measured using a DMMB assay as described in Chapter 2, Section 2.2.2.1.

### 3.2.5 Immunohistochemistry

Full thickness corneal biopsies (3 mm strips from corneoscleral rim to corneoscleral rim) were mounted for immunohistochemistry as described in Chapter 2, Section 2.3.1.1. Table 3.1 shows the primary antibodies used for this particular study.

Antibody	GAG chain detection	Pre-treatment	Dilution
5D4	Recognize linear penta-sulphated KS where both GlcNAc and Gal are sulphated	-	1:100
1B4	Recognize lesser sulphated KS sequences of N-acetyl lactosamine disaccharides	-	1:50
BKS-1	Keratanase generated KS neo-epitope	Keratanase II	1:20
3B3	Recognize chondroitin-6-sulphate	Chondroitinase ABC	1:20
2B6	Recognize chondroitin-4-sulphate	Chondroitinase ABC	1:20
1B5	Recognize chondroitin-0-sulphate	Chondroitinase ABC	1:20
<b>Collagen detection</b>			
Anti-collagen type I	Recognize the native (helical) form of collagen type I	-	1:100

Table 3.1 A summary of the antibodies used for this experiment.

### 3.2.6 KS quantification

Competitive ELISAs were used to quantify penta-sulphated hexasaccharides and tetra-sulphated hexasaccharides in small linear KS chains, which were recognized by the monoclonal antibodies 5D4 and 1B4, respectively (Caterson, Christner and Baker, 1983; Mehmet et al., 1986). 96 well EIA microtiter plates (MP Biomedicals, UK) were coated with 0.05  $\mu\text{g}$  chondroitinase ABC bovine corneal stroma antigen (kindly provided by Professor Bruce Caterson, Cardiff University) in 20 mM  $\text{NaCO}_3$  buffer (pH 9.6), and incubated for 2 hr at 37°C, followed by and overnight incubation at 4°C. The coated microtiter plates were washed with TSA buffer and the enacted sites were blocked with the addition of 1% (wt/v) BSA in TSA buffer, and incubated for 2 hr at 37°C. After incubation, the blocked microtiter plates were washed, air dried and then stored at 4°C until needed.

Papain digests of corneal tissue were serially diluted (1:3 serial dilution) and allowed to bind with an equal volume of 5D4 (1:6000 final dilution in 1% BSA/TSA) or 1B4 (1:150 final dilution in 1% BSA/TSA) and incubated to compete against the chondroitinase ABC treated bovine corneal antigen. A standard curve was generated from serial dilutions of chondroitinase ABC treated bovine corneal antigen/5D4 or 1B4, respectively. The plates were then washed with TSA before incubation with alkaline phosphatase – conjugated goat anti-mouse antibody (1:5000 dilution; Promega, Madison, WI). The plates were again washed before alkaline phosphatase substrate (p-nitrophenyl phosphate, 1 mg/ml) was applied in DEA buffer (pH 9.8). Colour development was quantified on a plate reader (Multiskan MS; Labsystems, Helsinki, Finland) at 405 nm, to determine the inhibition of binding.

Note: for all data analysis a statistical significance was ascertained by using statistical tests for the data groups: one-way ANOVA with post-hoc Tukey HSD.

### 3.3 Results – Biochemical studies

Figure 3.2 shows results for the changes across the bovine cornea in corneal thickness, hydration, hydroxyproline and sulphated GAG content. For all calculations see Appendix 1, Tables # 1-4. The corneal thickness increased from  $844.70 \pm 8.10 \mu\text{m}$

(central region) to  $1021.00 \pm 5.42 \mu\text{m}$  (limbus region) ( $P = \leq 0.01$ ). For such change in thickness across the cornea may be due to various factors, one being a minor change in hydration. For example hydration across the bovine cornea increased from  $3.67 \pm 0.50$  (central region) to  $4.28 \pm 0.71$  (outer periphery-limbus region), however this change was not significant ( $P = 0.171$ ). Furthermore, this increase in thickness in the outer periphery may also be explained by the changes in the amount of collagen; the amount of hydroxyproline present in the centre of the cornea (expressed as proportion/dry wt:  $0.06 \pm 0.01 \text{ mg/mg dry wt}$ ) increased to  $0.12 \pm 0.01 \text{ mg/mg dry wt}$  at the outer periphery. The data obtained from the DMMB analysis revealed no significant changes across the cornea, which may indicate that the sulphation of GAGs across the cornea remains relatively constant.

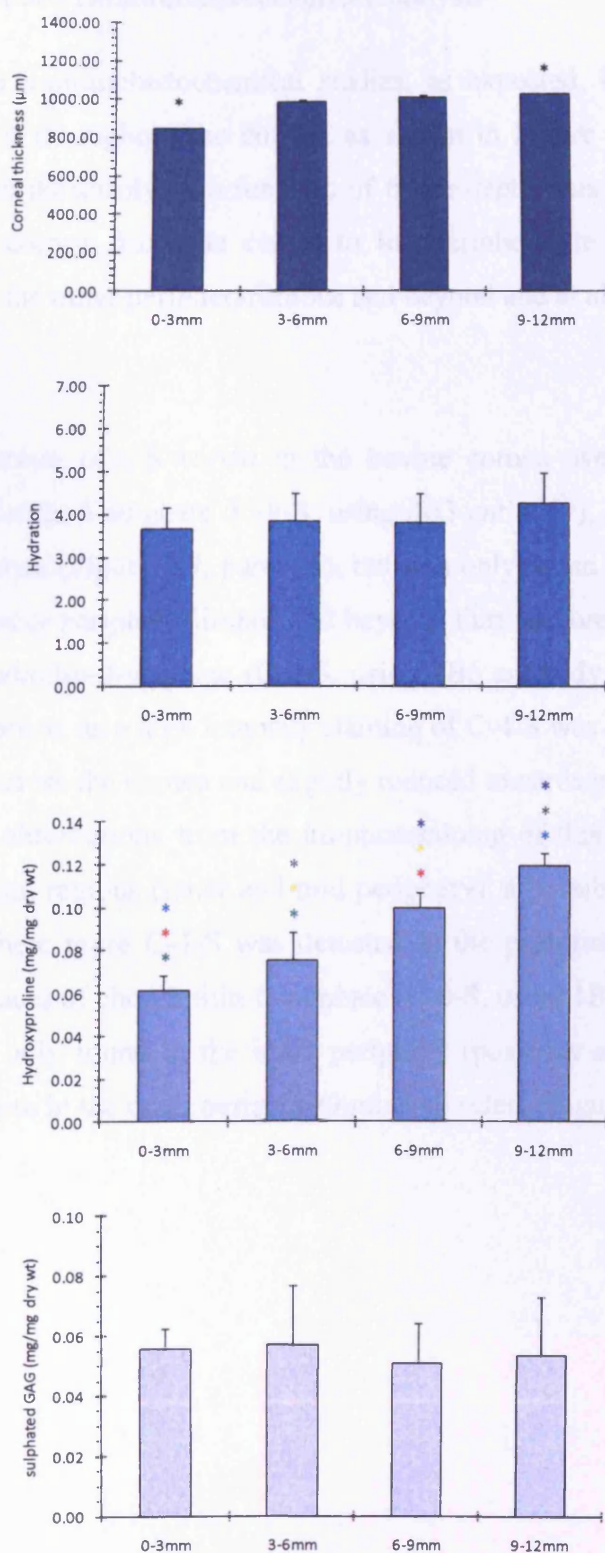


**Figure 3.2** Measurements of thickness, hydration, hydroxyproline and sulphated GAG content across the bovine cornea as a function of position. 0-3mm = centre, 3-6mm = inner periphery, 6-9mm mid periphery, 9-12mm outer periphery/limbus. One-way ANOVA and post-hoc Tukey HSD tests were employed to identify the significant differences between the groups. \*,\* P  $\leq$  0.01. \*,\*,\*,\* P  $\leq$  0.001. For all calculations, please see Appendix 1, Tables # 1-4.

### **3.4 Results – Immunohistochemical analysis**

Findings from the immunohistochemical studies, as expected, indicated that type I collagen was found throughout the cornea, as shown in Figure 3.3. The attempts to locate KS appeared uniformly as a function of tissue depth, this was seen throughout the depth of the cornea from the centre to the peripheral regions (Figure 3.4-6). However, towards the outer periphery/limbus and beyond and at all depths, less KS was detected.

The sulphation pattern of CS varied in the bovine cornea overall, such that when staining for chondroitin-6-sulphate (C-6-S, using 3B3 antibody), minimal staining was detected in the cornea (Figure 3.7, panel A), but was only found in the mid periphery, increasing in the outer periphery/limbus and beyond. Furthermore, the immunostaining revealed that chondroitin-4-sulphate (C-4-S, using 2B6 antibody) is the main form of CS found in the cornea, as a high intensity staining of C-4-S was detected (Figure 3.8). C-4-S was found across the cornea and slightly reduced towards outer periphery/limbus and sclera. Close observations from the immunostaining of this form of CS, showed that in the peripheral regions (inner and mid periphery), a possible gradient change of CS was found, where more C-4-S was detected in the posterior stroma (Figure 3.8, panel A). Minor traces of chondroitin-0-sulphate (C-0-S, using 1B5 antibody) were also detected, but was only found in the inner periphery (posterior stroma) and increased with increasing depth in the outer periphery/limbus to sclera (Figure 3.9).

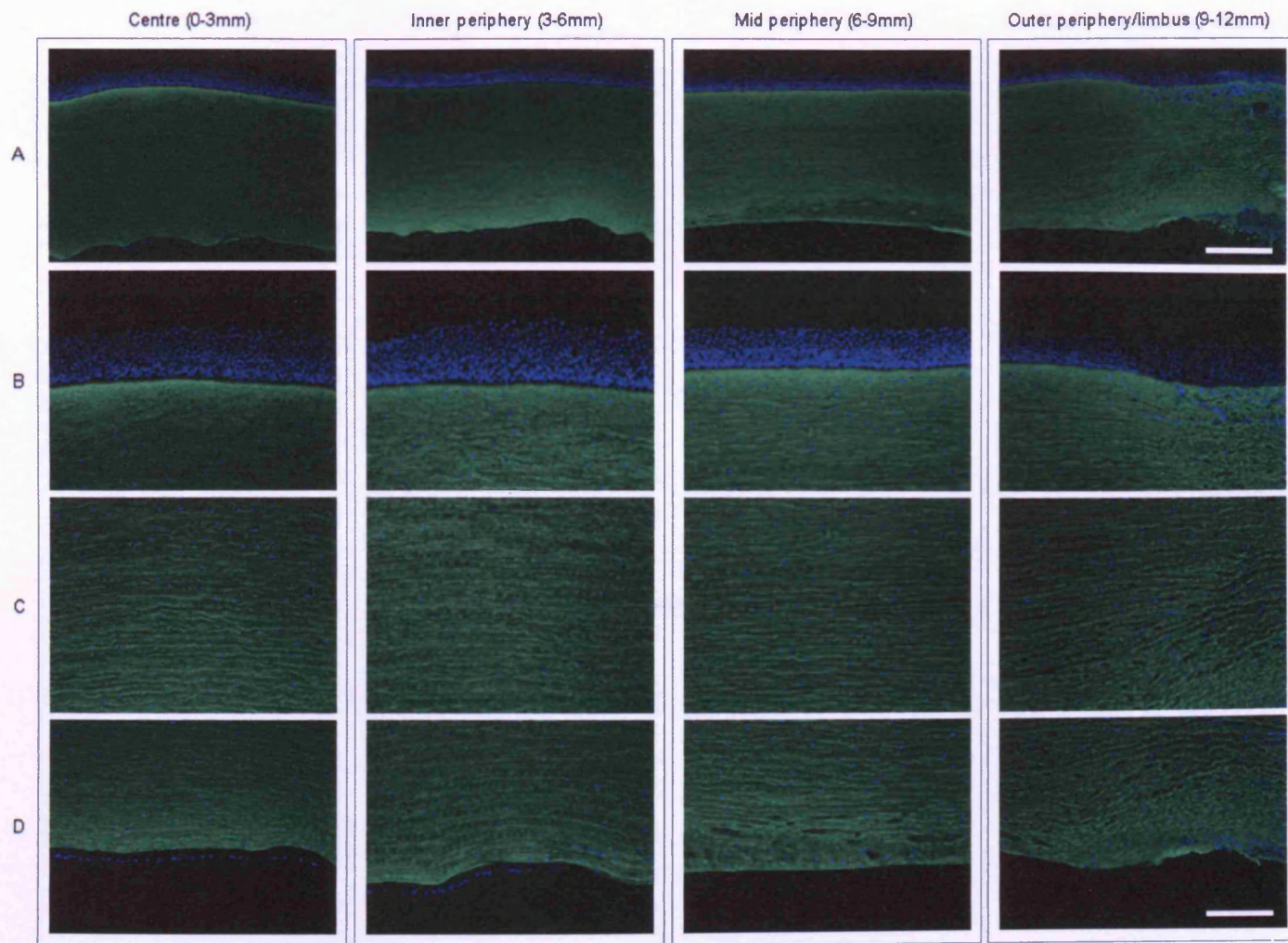


**Figure 3.3** Immunolocalization of type I collagen (green) and nuclear stained cells (blue), using anti-type I collagen and DAPI, respectively. Panel A, scale bar = 500 $\mu$ m. Panel B = anterior stroma, panel C = mid stroma and panel D = posterior. Panel B-D, scale bar = 200 $\mu$ m.

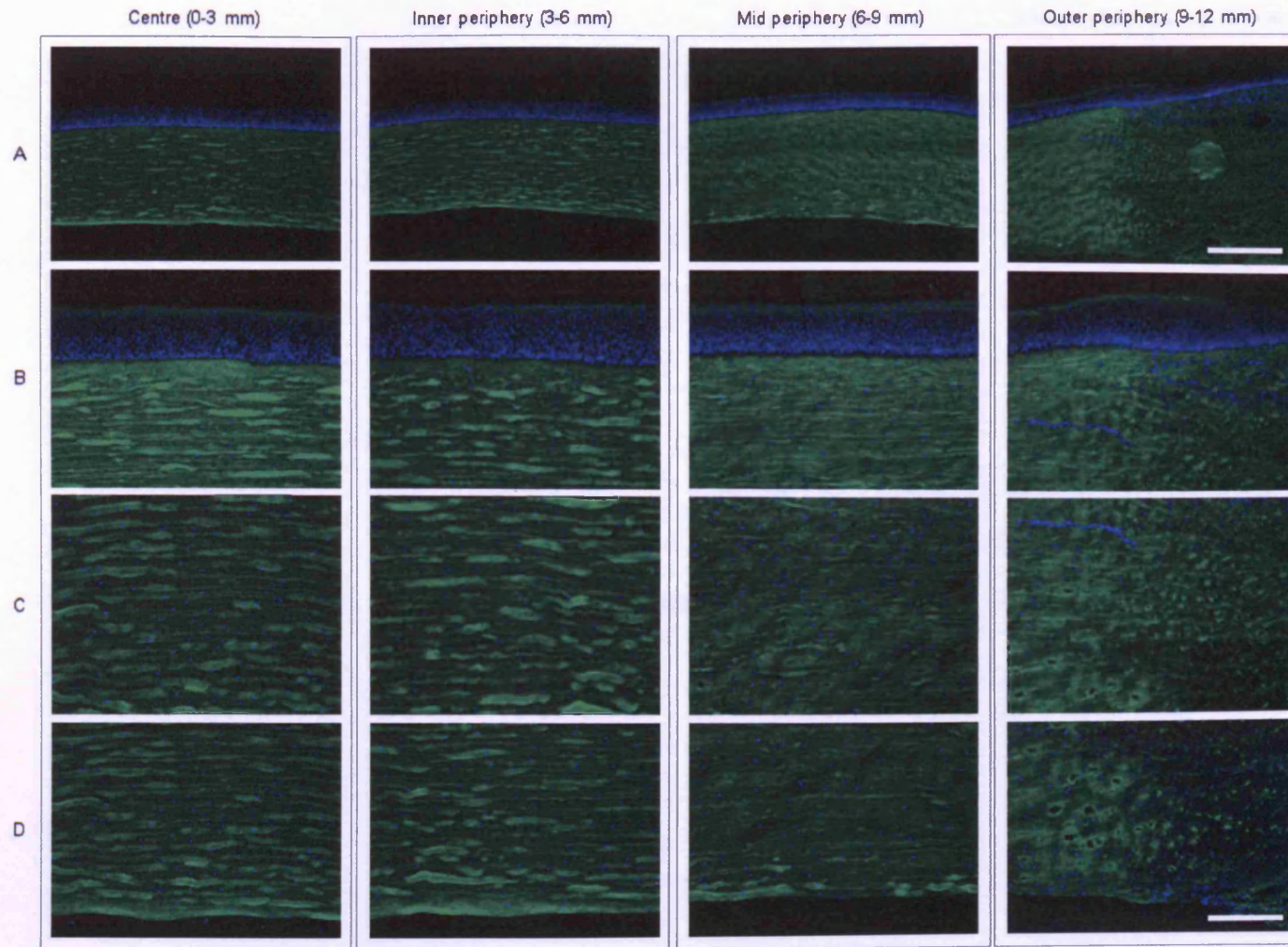


**Figure 3.4** Immunolocalization of over-sulphated KS (green) and nuclear stained cells (blue), using 5D4 antibody and DAPI, respectively. Panel A, scale bar = 500µm. Panel B = anterior stroma, panel C = mid stroma and panel D = posterior stroma. Panel B-D = 200µm.

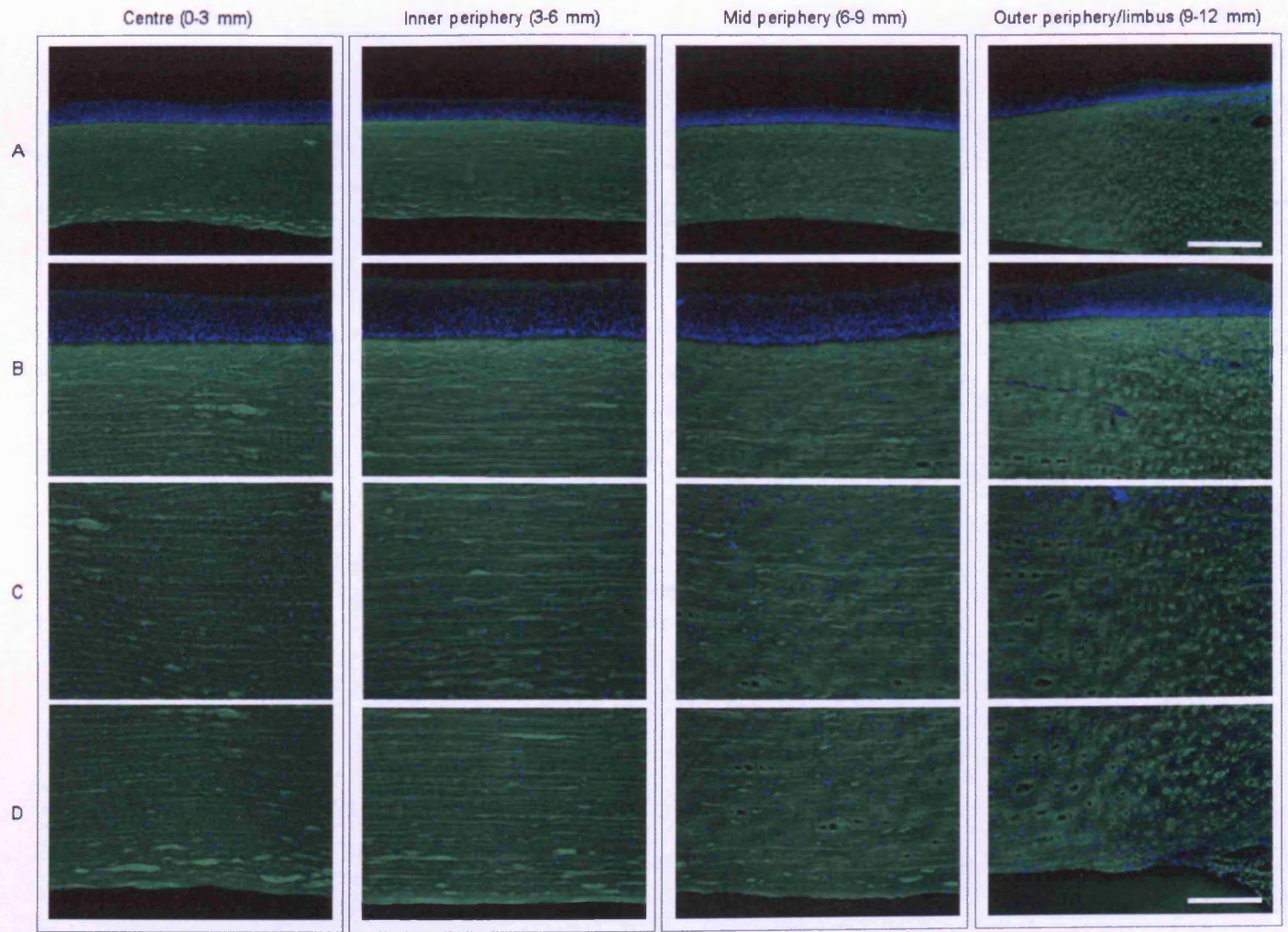


**Figure 3.5** Immunolocalization of lesser-sulphated KS (green) and nuclear stained cells (blue), using 1B4 antibody and DAPI, respectively. Panel A, scale bar = 500µm. Panel B = anterior stroma, panel C = mid stroma and panel D = posterior stroma. Panel B-D, scale bar = 200µm.

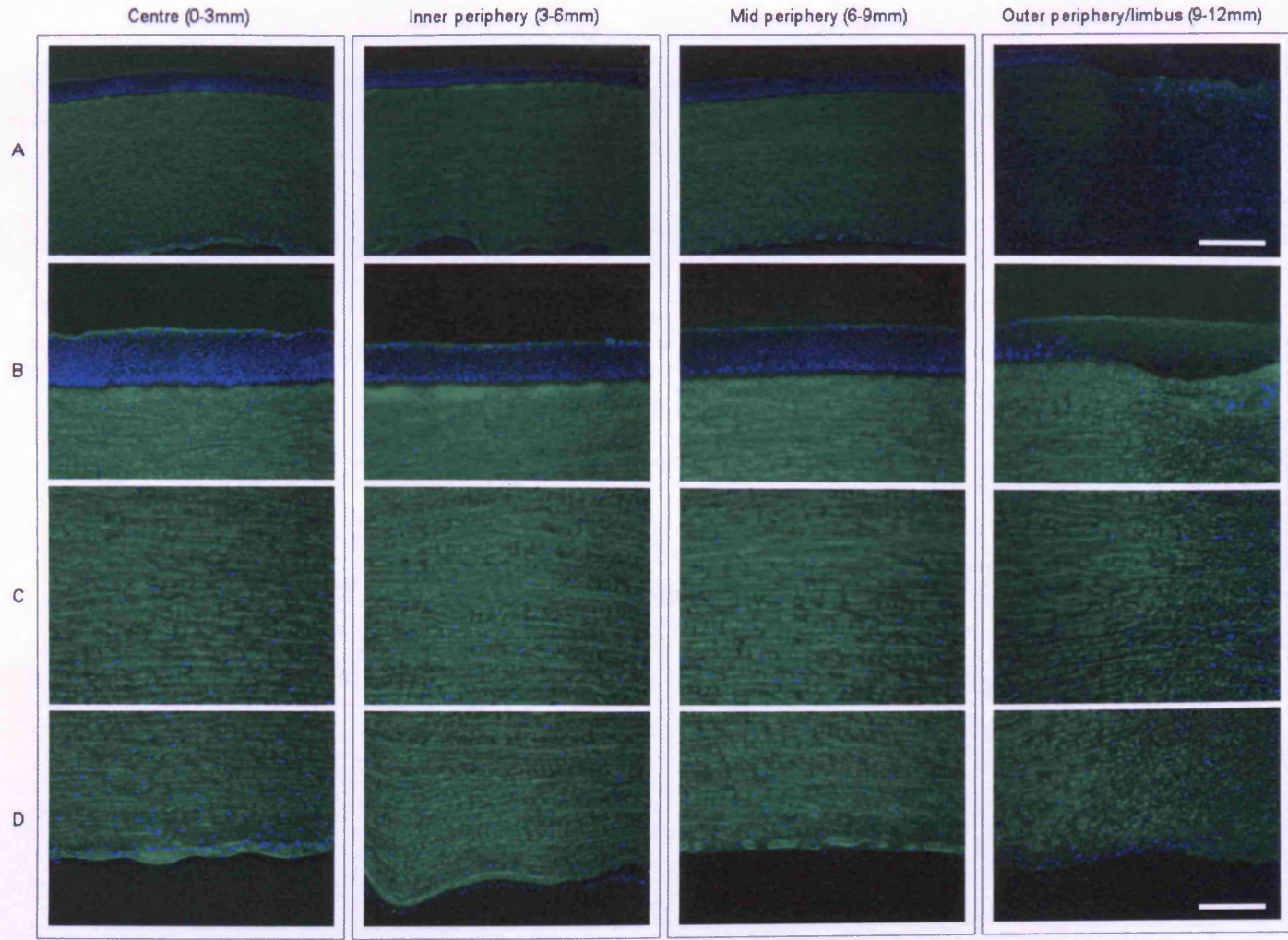


**Figure 3.6** Immunolocalization of neopeptide at the non-reducing terminal ends of KS (green) and nuclear stained cells (blue), using BKS-1 antibody and DAPI, respectively. Panel A, scale bar = 500µm. Panel B = anterior stroma, panel C = mid stroma and panel D = posterior stroma. Panel B-D, scale bar = 200µm.

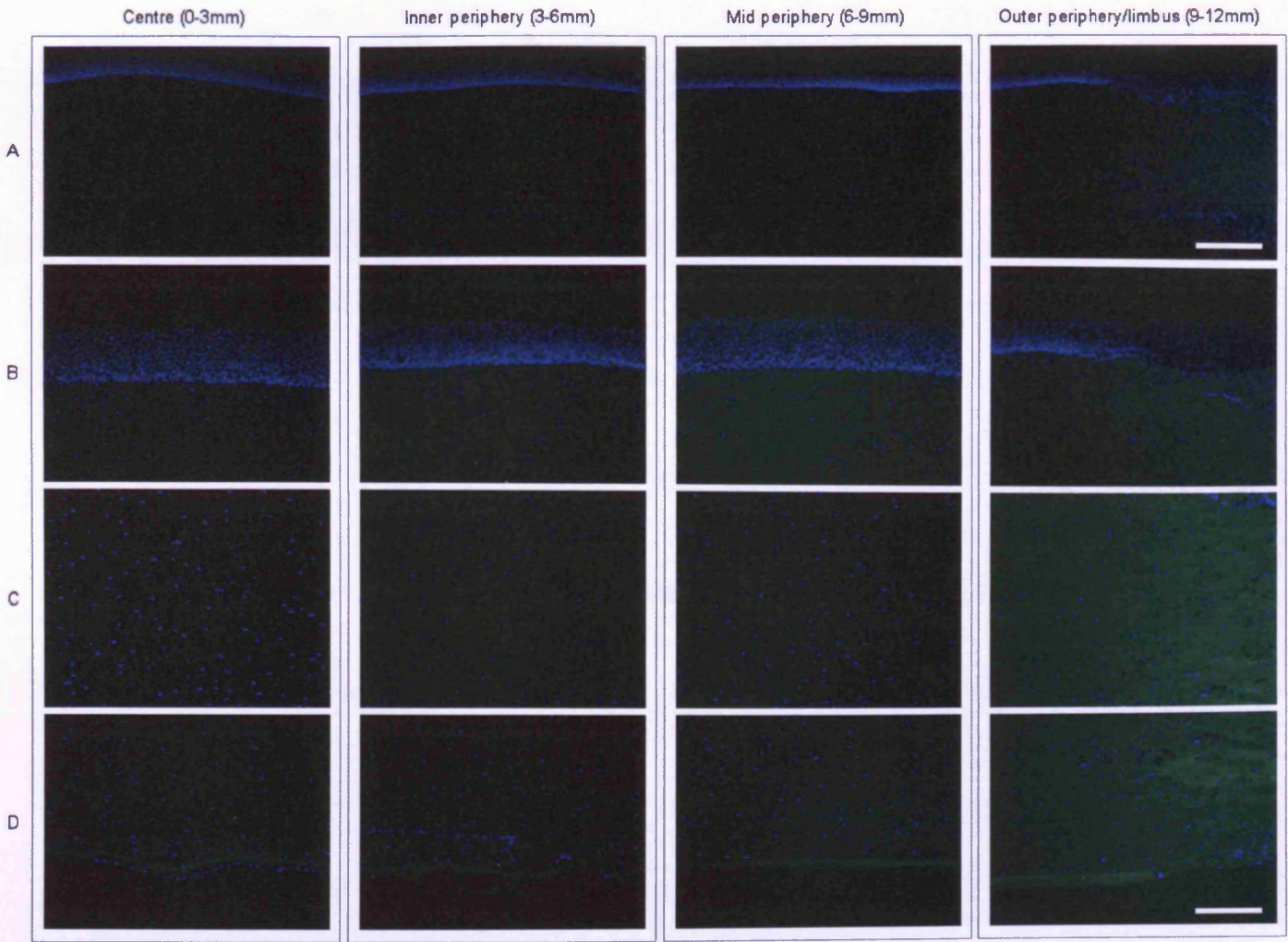


**Figure 3.7** Immunolocalization of chondroitin-6-sulphate (green) and nuclear stained cells (blue), using 3B3 antibody and DAPI, respectively. Panel A, scale bar = 500 $\mu$ m. Panel B = anterior stroma, panel C = mid stroma and panel D = posterior stroma. Panel B-D, scale bar = 200 $\mu$ m.

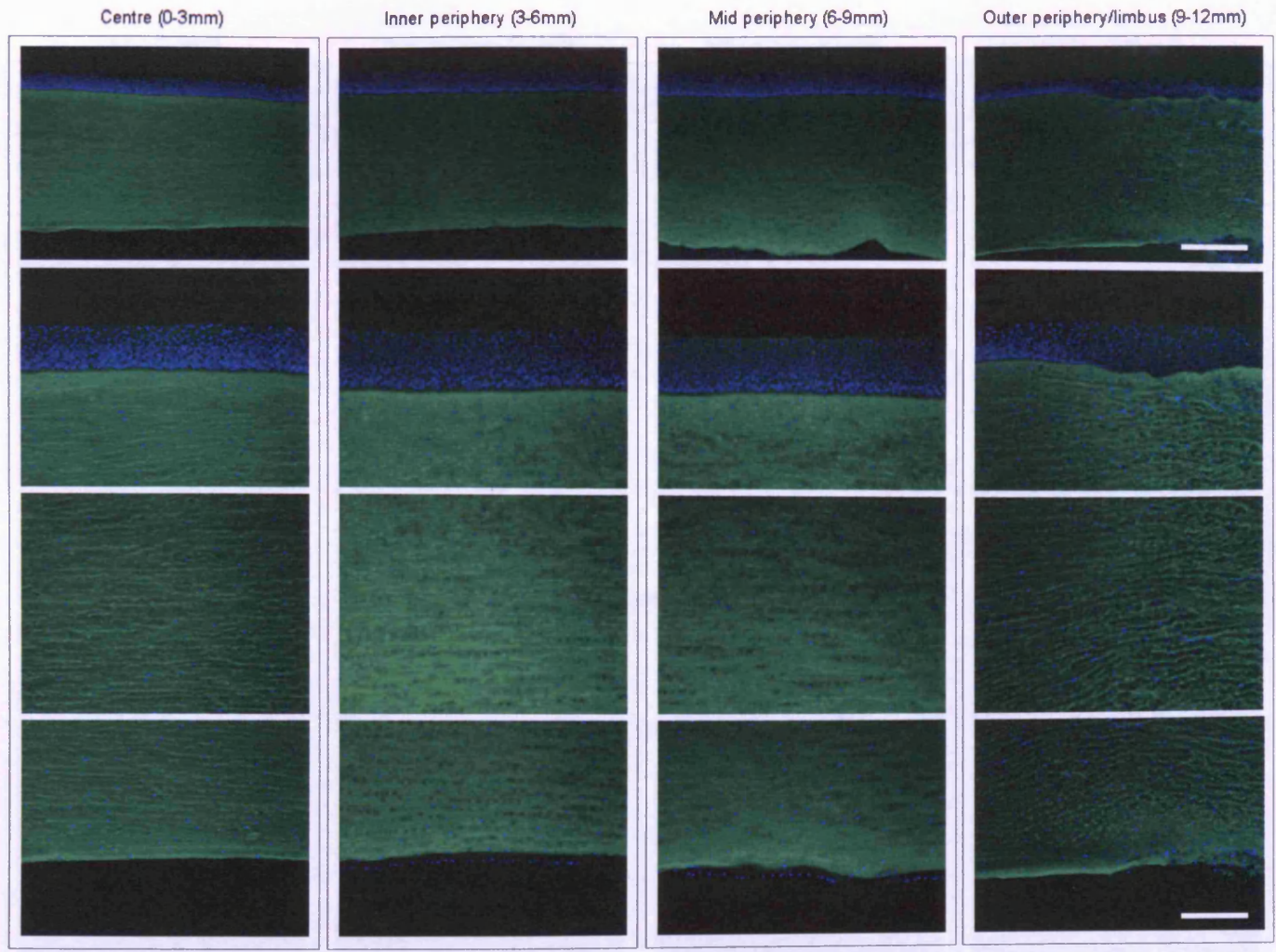


**Figure 3.8 Immunolocalization of chondroitin-4-sulphate (green) and nuclear stained cells (blue), using 2B6 antibody and DAPI, respectively. Panel A, scale bar = 200µm. Panel B = anterior stroma, panel C = mid stroma and panel D = posterior stroma. Panel B-D, scale bar = 200µm.**

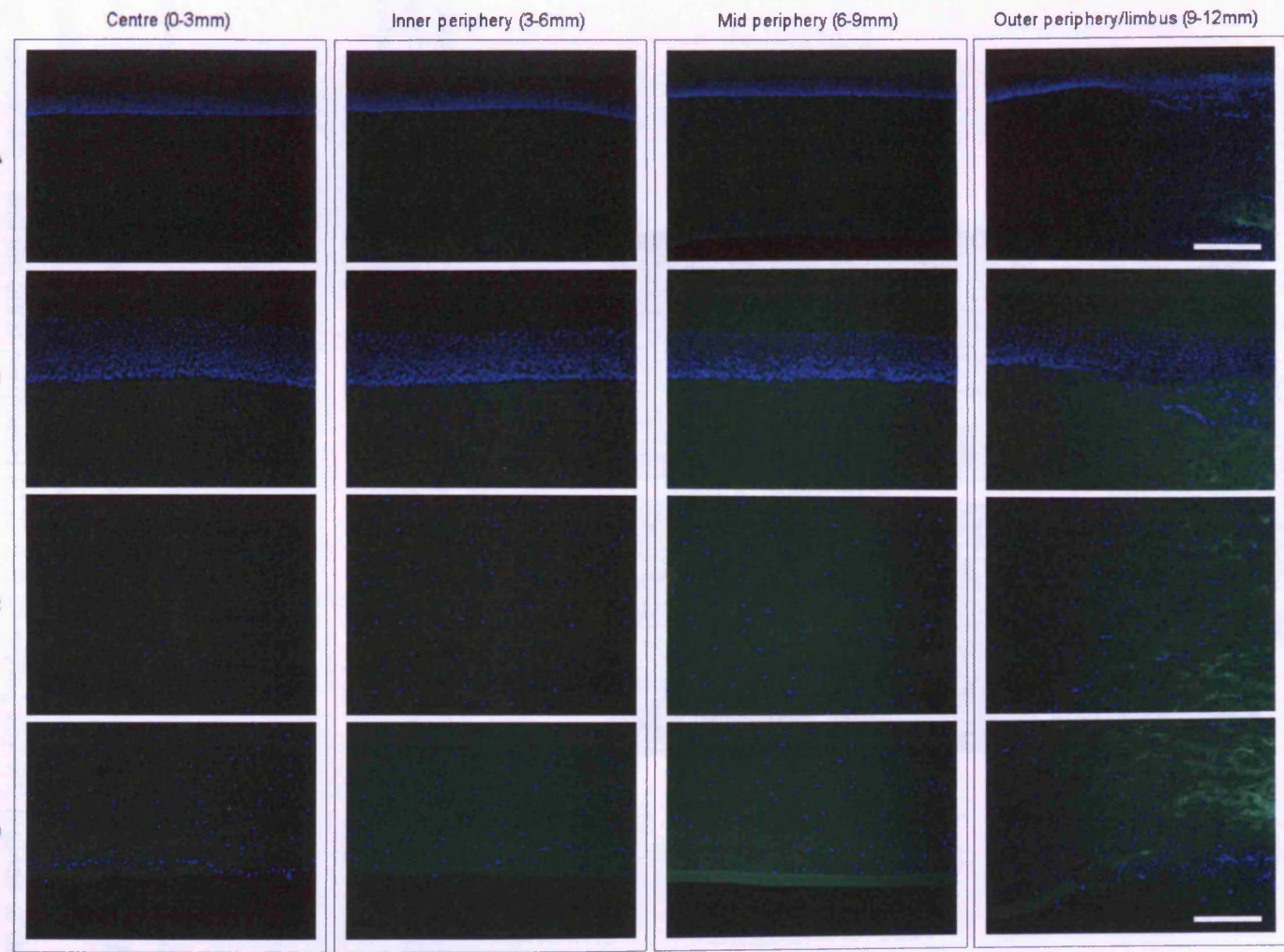


**Figure 3.9 Immunolocalization of chondroitin-0-sulphate and nuclear stained cells, using 1B5 antibody and DAPI, respectively.** Panel A, scale bar = 500µm. Panel B = anterior stroma, panel C = mid stroma and panel D = posterior stroma. Panel B-D, scale bar = 200µm.

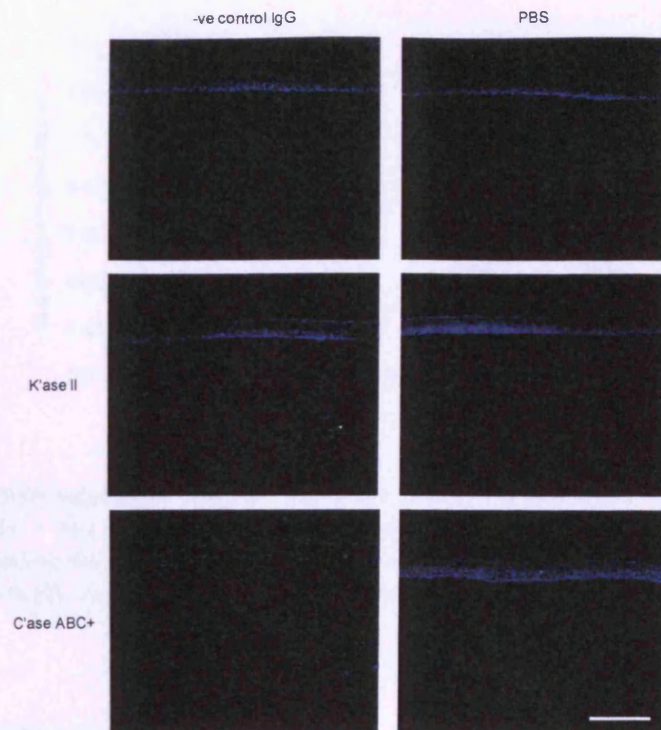


**Figure 3.10 Negative controls for immunolocalization of specific GAG types.** Controls showed negative staining to the specific primary antibodies and non random binding. K'ase II = keratanase II. C'ase ABC = chondroitinase ABC. Scale bar = 500  $\mu$ m

### 3.5 Results – KS quantifications

Sulphation patterns of KS GAGs were examined quantitatively across the cornea (Figure 3.11, see Appendix 1, Table # 5-6 for calculations). The amount of high-sulphated, 5D4-recognizable, KS GAG remained constant between the central ( $0.65 \pm 0.31$  ng/mg dry wt) and the outer peripheral ( $0.72 \pm 0.25$  ng/mg dry wt) regions of the cornea,  $P = 0.940$ . However, using 1B4 antibody, the amount of lesser sulphated KS GAG more than doubled in the outer peripheral-limbus region ( $0.80 \pm 0.30$  ng/mg dry wt) compared to the central region ( $0.20 \pm 0.05$  ng/mg dry wt),  $P = \leq 0.001$ . Furthermore, the data revealed that the high sulphated KS chains are relatively more abundant in central regions of the cornea when compared to lesser sulphated chains, with proportionally elevated levels of lesser sulphated KS found peripherally.

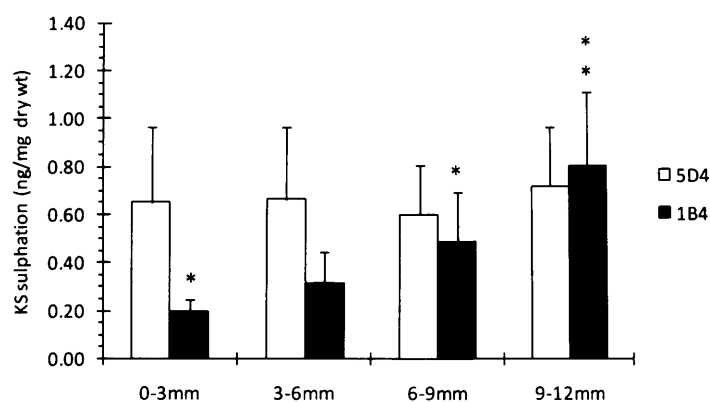


**Figure 3.11 KS GAG sulphation content across the bovine cornea.** 0-3mm = centre, 3-6mm = inner periphery, 6-9mm = mid periphery and 9-12mm outer periphery/limbus. 5D4 antibody was used to label higher sulphated KS GAG chains. 1B4 antibody was used to label lesser sulphated KS GAG chains. \*  $P \leq 0.001$ , \*  $P = 0.005$ . For all calculations, please see Appendix 1, Table 5-6.

### 3.6 Discussion

As previously mentioned, studies (Doutch et al., 2008; Doutch, 2009) have shown that corneal transparency (both in human and in bovine) decreases from the central to the outer peripheral regions of the cornea. This reduction in transparency towards the periphery could be due to many factors such as the increased corneal thickness, increased fibril diameters or an increased fibril disorder or an increase in the mismatch between the refractive indices of the fibrils and the matrix (Doutch et al., 2008). Previous studies (Borcherding et al., 1975; Boote et al., 2003) have found that there is an increase in fibril diameter and interfibrillar spacing, which could account for the decrease in transparency at the peripheral regions of the cornea. Doutch and co-workers (2008) have also suggested that the refractive indices could also change towards the periphery, if there was a change in the PG content; however the data obtained here on the total sulphated GAG content, showed no changes across the cornea (Figure 3.2). Thus, the refractive index ratio would be constant and PGs may not have a role in the reduced transparency at this region. The hydroxyproline content from our studies (Figure 3.2), revealed a significant increase towards the outer periphery/limbus regions, which may contribute the amount or volume and/or size of fibrils and therefore may cause the increase of light scatter found towards this region.

In the cornea, the collagen fibrils are arranged in a pseudo-hexagonal lattice form, and it is believed that this orderly arrangement of collagen fibrils gives rise to corneal transparency. It has been long believed that this lattice-like structure is sustained by the structural interactions between collagen fibrils and PGs (Bettelheim and Plessy, 1975; Borcharding et al., 1975). These PGs are glycosylated with KS or CS/DS and it is these GAGs that are thought to be responsible for the orderly interfibrillar spacing of the collagen fibrils.

Several studies (Bettelheim and Plessy, 1975; Bettelheim and Goetz, 1976) have shown that GAGs in the cornea are largely responsible for the water-binding capacity in this tissue. This is due to the sulphate groups on their PGs chains which are hydrophilic and can therefore interact with water molecules (Bettelheim and Plessy, 1975; Imberty et al., 2007). The negatively charged GAGs swell in solution to increase their conformational entropy. Repulsion of the GAG charges and Donnan osmotic pressure, consequently causes the positively charged ions to gravitate around the GAG chains and can cause the tissue to swell (Scott, 2003). In the case of GAG types, early studies by Bettelheim and collaborators indicated that the hydration behaviour of PGs differs from that of the corresponding GAGs. They showed that KS absorbed water two to three times more than PGs with CS/DS attached (Bettelheim and Plessy, 1975; Bettelheim and Goetz, 1976). This may be an indication as to why, in the present study, the hydration remained relatively constant across the cornea, as KS particularly highly sulphated KS (Figures 3.11) was relatively constant across the cornea.

It has been alleged (Heldblom, 1961; Bettelheim and Plessy, 1975; Bettelheim and Goetz, 1976) that although GAGs are largely responsible for the hydration of the cornea, KS plays a different role to CS in the hydration process. Corneal wound healing shows reduced KS and increased CS synthesis, and injury to Descemet's membrane and the endothelium transforms keratocytes to DS-producing cells (Anseth, 1961; Anseth and Fransson, 1969). Furthermore, it has been found that KS is more abundant than CS/DS (Bettelheim and Goetz, 1976), particularly in larger animals (Scott and Bosworth, 1990), and this may explain why KS was found more abundantly throughout the bovine corneas examined here.



The pattern of KS GAG distribution throughout the depths of the corneal stroma appears to alter distinctly during corneal development, whilst in adult corneas of different animal species, a KS gradient change is apparent (Scott, Haigh and Ali, 1988). During rabbit development, KS has been mainly found in the anterior two thirds of the stroma, whereas CS was found throughout the stroma (Cintron and Covington, 1990). Observations on chick cornea have showed that, during chick corneal morphogenesis, significant matrix deposition of high-sulphated KS epitopes occurred with an accumulation of KS proceeding in an anterior to posterior manner (Young et al., 2007b; Liles et al., 2010). These findings suggested that KS plays a vital part in the development and the maintenance of transparency.

Early studies by Scott and co-workers showed that in bovine corneas, the distribution of KS can be unique (Scott et al., 1988). When staining with alcian blue at a low MgCl concentration (0.2M), KS was present in the anterior stroma, and with high concentrations of MgCl (0.6 M and 0.8 M) in the alcian blue, at which only KS stains (Scott and Haigh, 1988a), more KS was found posteriorly. However, after chondroitinase ABC digestion and staining with alcian blue in 0.2 M MgCl, KS was present throughout the cornea. Scott and co-workers suggested that these differences in KS distribution are caused by the O<sub>2</sub> tension in the cornea, which play a crucial metabolic factor in GAG synthesis (Scott et al., 1988) (See Chapter 5 for more details).

Much of the early studies that have attempted to map the GAG distribution through the depths of the corneal stroma (in mature species) by quantifying the glucosamine:galactosamine ratio after chromatographic separation (Anseth, 1961; Bettelheim and Goetz, 1976), and a gradual increase in the ratio was seen when proceeding from the epithelium to the endothelium. The glucosamine:galactosamine ratio reflects the KS:CS ratio of GAGs, and it was suggested that a gradient of KS content in the cornea increased posteriorly and vice versa for CS (Bettelheim and Goetz, 1976). This follows the suggestion that the balance of the two kinds of PG is depended on the availability of O<sub>2</sub>, which must diffuse into the avascular tissue from the atmosphere (see Chapter 5 for more details). Furthermore, early studies (Scott and Haigh, 1988b; Balduini et al., 1992; Scott, 1992b) have shown that KS is produced more effectively than CS/DS during ambient O<sub>2</sub> pressures. Therefore, in this scenario in the deeper zones of the corneal stroma, where less O<sub>2</sub> is consumed by the cornea, one

would expect more KS. This would also make sense in that KS PGs not only absorb water molecules to a great extent in comparison to the CS/DS PGs but they can also transfer water molecules with ease since little is retained by them in the dehydration process (Bettelheim and Plessy, 1975). Thus, finding KS at the posterior region, near the endothelium, hence near the aqueous humor, may serve a purpose of facilitating the movement of water into the cornea via the endothelium ( $\text{Na}^+/\text{K}^+$  ATPase transporter and  $\text{NaHCO}_3$  transporter pump) (Maurice, 1972; Bettelheim and Plessy, 1975; Hodson and Miller, 1976). Other studies have shown that in macular corneal dystrophy type I corneas, in the posterior regions, the collagen fibril spacing is reduced, large-diameter collagen fibrils are found and it was suggested that this may be due to the influence of the abundance sulphated KS GAGs/PGs found at this region (Palka et al., 2010).

In the attempts to immunolocalize KS through the depths of the bovine cornea, it appeared to be evenly distributed as a function of tissue depth. This was seen throughout the depths of the central and the peripheral regions of the cornea. Although early studies focussed on the corneal centre, these findings fail to support Anseth *et al.* (1961) and Bettelheim and Goetz (1976) early work, where they quantitatively showed more KS was found posteriorly. Other studies involving antibodies, 5D4 and BKS-1, to histochemically locate KS in human cornea, also showed strong labelling in all depths of the cornea, however, when using immuno-TEM, 5D4 epitopes were found more abundant posteriorly (Akhtar et al., 2008b). Such differences found from Anseth *et al.* (1961) and Bettelheim and Goetz (1976) early work compared to our studies could be due to the fact IHC is based on qualitative observations. Although the aim of our studies was to show the location and distribution of the different KS sulphation patterns, IHC can face problems in IHC-staining, which may include strong background staining, weak target antigen staining and autofluorescence. The orientation of the KS associating onto the collagen fibril within lamellae may also be a problem, as this is because thin corneal sections were cut, and some KS epitopes may not be fully exposed for the specific antibody binding. Therefore, furthermore qualitative observation studies would be needed.

Nevertheless, the KS quantification studies (Figure 3.11) revealed that high sulphated KS chains were relatively more abundant in central regions of the cornea when compared to lesser sulphated chains. However, elevated levels of lesser sulphated KS

were found peripherally. This data concurs with early corneal studies (human) (Borcherding *et al.*, 1975), where the KS:CS ratio decreased towards the periphery, suggesting that the sulphation of KS may gradually decrease, and hence may explain why more lesser sulphated KS was found in the periphery (Figure 3.11). In addition, other studies using immunostaining have also shown high levels of KS are found in the human cornea and lower levels in the limbus and sclera (Akhtar *et al.*, 2008b). Furthermore, the change in sulphation status found in the cornea from our studies, may suggest the change in length of GAG chains, which could have possible implications for stromal water binding capacity, differential substitution either on KS PG core proteins and/or extracellular matrix architecture.

Early studies by Borcherding *et al.* (1975) showed that chondroitin was found throughout the cornea and becomes more sulphated towards the periphery and into the sclera. The data obtained here, indicated a slightly different pattern, such that very little chondroitin (C-0-S) itself was found in the central regions of the cornea, but it became more detectable in the outer peripheral and limbal regions (Figure 3.9). This would seem to indicate that chondroitin molecules become less sulphated in the peripheral regions of the cornea. The C-4-S epitope was found throughout the cornea, and gradually reducing towards the outer periphery/limbs regions (Figure 2.8). This correlates with early findings (Bettelheim and Goetz, 1976), that C-4-S was the main CS (40%) whereas only a small amount of DS and C-6-S was reported. Borcherding and co-workers also showed that, both CS and DS were found towards the peripheral and sclera regions, and as mentioned previously, both CS and DS contain 6-sulphated disaccharides. This may explain why C-6-S epitopes were detected towards the peripheral and limbal regions of the cornea. Nevertheless, CS/DS PGs can be structurally diverse, as this could be due to the chains having very low to moderate levels (15-64%) of sulphated disaccharides, and differing marked levels of 4- and 6-sulphate groups (Achur *et al.*, 2004). To confirm the differences in sulphation patterns of CS it would have been ideal to quantify the sulphation types of CS, by using ELISAs, but due to time constraints to the project this was not feasible.

The GAG components of PGs allow them to act as “spacers” between fibrils. The sulphation patterns of the GAG components on PGs contribute to this because the electrostatic fields they induce permit their aggregation and dissociation. Large CS/DS

PGs may control the spacing through stabilizing more than two adjacent fibrils, forming multimers and regulating the swelling pressure of the tissue through their sulphate residues (Lewis et al., 2010). CS contains more disaccharide motifs than KS (Plaas et al., 2001) and thus may have more sites for sulphation and a higher proportion of hydrophilic regions. This may explain why CS was found throughout the cornea, as it may act to control and stabilize the spacing of fibrils, whilst C-6-S detected more in the posterior regions of the stroma, where it may aid and regulate the swelling pressure of the tissue.

The sulphation status of corneal PGs is thought to be based on enzymatic activity (Akama et al., 2001 ; Hayashida et al., 2006), changes with development (Quantock and Young, 2008; Liles et al., 2010) and in corneal diseases such as macular corneal dystrophy (Quantock et al., 1990; Akama et al., 2000). Knockout mouse studies on the *Chst5* gene, which lacks the N-acetylglucosamine 6-O sulfotransferase enzyme, has shown no sulphated KS is detected but instead oversulphated CS/DS are found (Hayashida et al., 2006). A recent study (Parfitt et al., 2011 ) using 3D tomography electron microscopy have showed that in the *Chst5* knockout mice, greater lengths and thickness of CS/DS chains were seen compared to the null mice. Parfitt and co-workers have suggested that the overall balance of the electrostatic charges in the *Chst5*-null mouse cornea is maintained by the increased sulphation of the CS/DS chains in the absence of sulphated KS. It was also suggested that the high sulphation of CS/DS may facilitate further packing in order to maintain the corneal collagen fibril architecture.

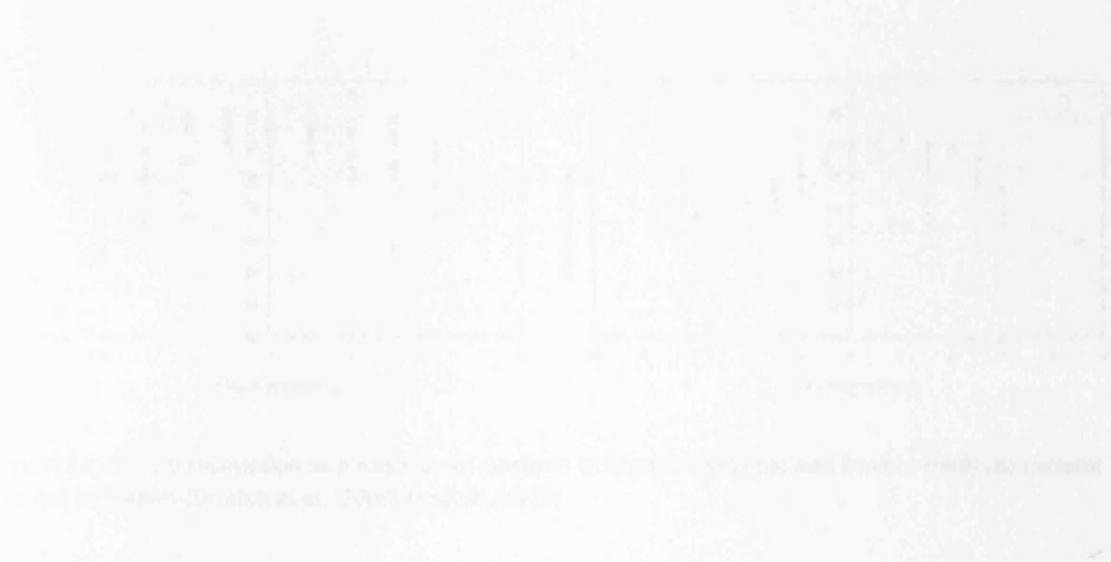
Close observations in the immuno study on KS GAGs, a detection of KS was found on the surface of the epithelium. This may be due to lubricin; a mucous glycoprotein that consists of KS and CS. Lubricin has been found in articular cartilage and has shown to be a boundary lubricant (Jay et al., 2001; Zappone et al., 2007). Therefore, KS found on the surface of the epithelium may contain a form of lubricin from the tear film, which may act as a lubrication of the surface of the cornea.

Type I collagen is the most predominant collagen type found in connective tissues and is the main collagen found in the cornea (Forrester et al., 2002), which we have confirmed from immunostaining (Figure 3.3). As stated, previous studies (Borcherding et al., 1975; Boote et al., 2003) have shown that the collagen fibril diameter increases

gradually towards the peripheral regions of the cornea. This may be associated with amount of type V collagen present in the collagen fibril. Studies have shown that a reduction in type V collagen result in large-diameter fibrils with a broad size distribution (Birk et al., 1988; Birk et al., 1990; Marchant et al., 1996b). This suggests that the interaction of type V with type I collagen is one mechanism modulating fibril diameter and is at least partially responsible for the regulation of collagen fibril formation. Thus, one might be expected to find more type V collagen molecules concentrated towards the centre of the cornea where collagen fibrils are narrower. However, staining for type V collagen is problematic because type I and type V collagen co-assemble into heterotypic fibrils. The entire triple-helical domain of the type V collagen molecules is buried within the fibril and type I molecules are present along the fibril surface. The retained N-terminal domains of the type V collagen are exposed at the surface, extending outwards through the gap zones (Birk, 2001). Nevertheless studies have overcome this problem, by extraction or enzyme or acid treatment on the tissue (Linsenmayer et al., 1983; Fitch et al., 1988; White et al., 1997; Bairati and Gioria, 2004). In the current study, attempts were made to use various anti-type V collagen antibodies to examine its distribution throughout the corneal stroma. However, the antibodies were found not to work satisfactory and, due to time constraints and lack of more purified antibodies, these experiments were curtailed.

---

## Chapter 4: Structural studies of collagen fibrils across the bovine cornea



## 4.

## 4.1 Introduction

Optical properties of the cornea can be influenced by the structural collagen changes and hence its biomechanical and optical functions. This particular study follows the previous chapter and in this present study, the collagen fibril diameter, fibril spacing in relation to the GAG chain distribution across the bovine cornea were examined. Previous studies (Borcherding et al., 1975; Boote et al., 2003) have investigated on human corneas, but there has been no data as to whether other species, such as cow, follow a similar fibril diameter and interfibrillar spacing trend across the cornea. As mentioned in the previous chapter, structural changes in the peripheral regions of the stroma (Borcherding et al., 1975; Boote et al., 2003) may explain the decrease in transparency at this region (Doutch et al., 2008). The % of light transmission in human corneas decreased approximately linearly up to 3 mm from the central axis and decreasing quadratically thereafter to the limbus (Figure 4.1 A). Similar results were also seen in bovine corneas (Figure 4.1 B) (Doutch, 2009).

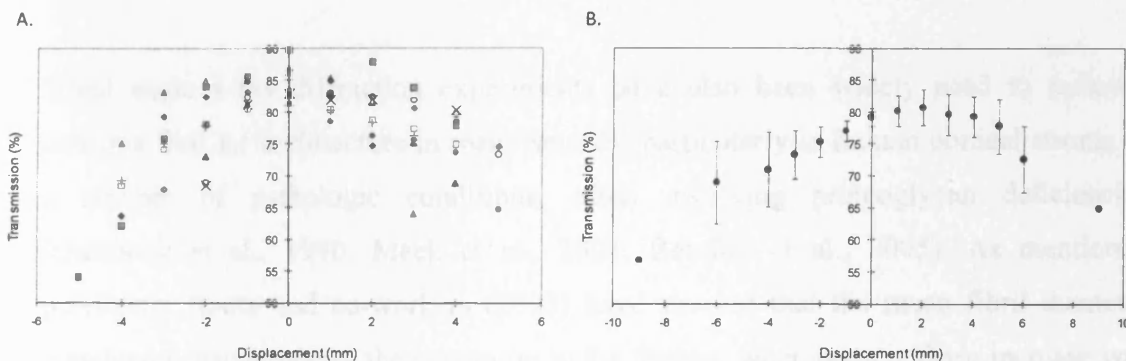


**Figure 4.1** Light transmission as a function of position in human (n=8) (A) and bovine (n=8) (B) corneal stroma at 550nm (Doutch et al., 2008; Doutch, 2009).

The cornea has high tissue strength in order to resist the force of intraocular pressure and maintain correct surface curvature for optimum light refraction. The tissue strength is determined by the diameter of the constituent collagen fibrils, their direction in relation to the applied force and the total collagen content (Hukins and Aspden, 1985).

TEM has been widely used to visualize collagen fibrils. Across a wide range of tissue types and species, it has been demonstrated that collagen fibrils have a range of diameters depending on the location and presumed function of the fibrils. In light of this, human TEM studies (Borcherding et al., 1975), have illustrated an increase in stromal fibril diameter (Figure 4.2). However measurements from electron micrographs have tended to show considerable variation among studies (Kanai and Kaufman, 1973; Borcherding et al., 1975; Craig and Parry, 1981; Freund et al., 1995), which has been related largely to tissue shrinkage during specimen preparation (Fullwood and Meek, 1993).

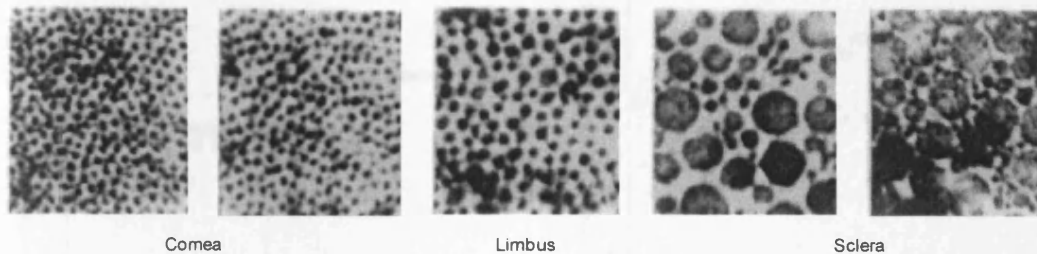


**Figure 4.2** Electron micrographs of collagen fibrils along the central vertical axis from human central cornea to sclera (Borcherding et al., 1975).

Small angle x-ray diffraction experiments have also been widely used to measure collagen fibrillar architecture in many species, particularly in human corneal stroma in a number of pathologic conditions, often involving proteoglycan deficiencies (Quantock et al., 1990; Meek et al., 2003; Beecher et al., 2005). As mentioned previously Boote and co-workers (2003) have showed that the mean fibril diameter remained constant across the cornea up to the limbus, whereupon a sharp increase was observed. In addition, it was found that the collagen fibrils in the prepupillary cornea were more closely packed than in the peripheral cornea, and there was a significant increase in spacing from the central cornea (approximately 57 nm) to the edge of the limbus (approximately 62 nm), followed by a much larger increase at the limbus itself (Boote et al., 2003).

Furthermore, the anterior and posterior stroma differ in specific ways, such that the collagen fibrils in the posterior stroma are more ordered (Komai and Ushiki, 1991; Freund et al., 1995), and the posterior cornea is more hydrated (Turss, Frient and

Dohlman, 1971), more easily swollen, and has a lower refractive index (Patel, Marshall and Fitzke, 1995) than the anterior stroma. The posterior lamellae are also wider and thicker (100-200  $\mu\text{m}$  wide and 1.0-2.5  $\mu\text{m}$  thick) than the anterior (0.5-30  $\mu\text{m}$  wide and 0.2-1.2  $\mu\text{m}$  thick) (Komai and Ushiki, 1991). In addition, a recent study on small-angle x-ray fibre diffraction on the depth of the human corneal matrix, reported that swollen human eye-bank corneas showed no significant change in collagen fibril diameter throughout the tissue, but a lower collagen interfibrillar spacing in the anterior-most stromal regions compared with the ultrastructure of the deeper cornea (Quantock et al., 2007) (Figure 4.3)

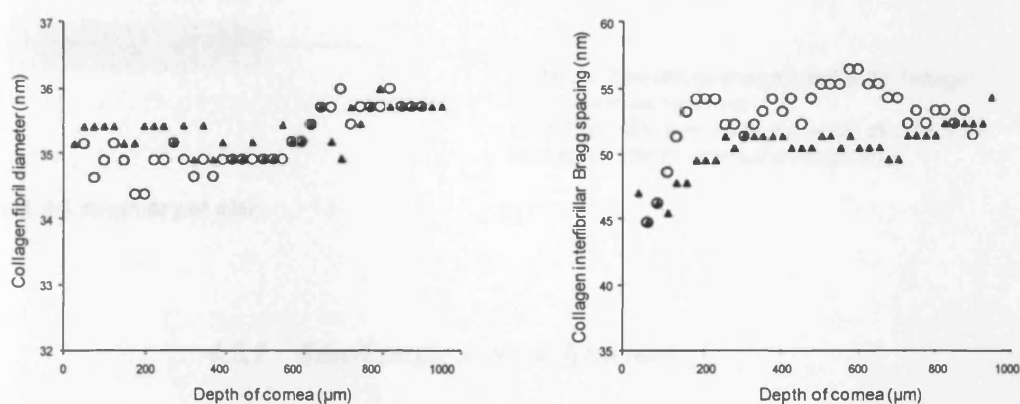


**Figure 4.3** Average collagen fibril diameter and mean centre-to-centre collagen fibril Bragg spacing in the left (solid triangles) and right (open circles) human eye-bank corneas. In the anterior regions of both corneas a lower fibril spacing is seen (Quantock et al., 2007).

Two structural techniques were applied; small angle x-ray diffraction and TEM. Small angle x-ray diffraction can give representative data on collagen fibrillar ultrastructure and orientation as an average throughout the whole stromal thickness or through the tissue thickness if a small x-ray beam is used. However, the data represents averages throughout the thickness of tissue sampled by the x-ray beam. Therefore, the x-ray diffraction analyses were supplemented with TEM studies to visualize the fibrils at different tissue depths.

## 4.2 Methods

A summary of the experiments carried out are shown in Figure 4.4.

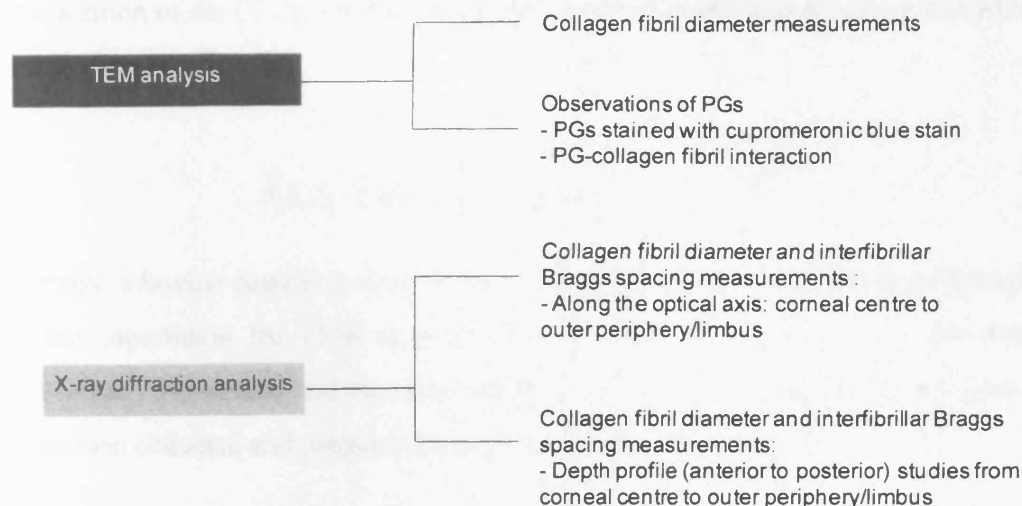


Figure 4.4 A summary of plan.

### 4.2.1 Small angle x-ray diffraction

Small angle x-ray diffraction was employed across the stroma (fresh ( $n = 3$ ) and fixed ( $n = 1$ ) tissue) and across the depth of the stroma ( $n = 3$ ) as a function of position on bovine corneas. Bovine corneal tissue was prepared as described in Chapter 2, Section 2.5.2 and details of the parameters topographically and across the depths of the cornea are shown in Table 4.1.

Corneal orientation: centre to outer periphery/limbus	Increment steps ( $\mu\text{m}$ )	Exposure time (ms)	No. of shots
Front: Experiment 1	100	500	480
Front: Experiment 2	100	500	600
Front: Experiment 3	100	100	200
Front: Experiment 4*	100	100	190
Depth: Experiment 1*	25	500	100
Depth: Experiment 2*	25	500	100
Depth: Experiment 3*	25	500	100

Table 4.1 Details of the x-ray parameters for the different tissue preparations. \* = corneal tissue was fixed prior to experiment.

Data analysis was carried out in accordance with protocols described in Chapter 2, Section 2.5.2.1. The IFBS and fibril radius was calculated from the interference function and the fibril transform, respectively. Both calculations were calibrated from the position of the 67 nm meridional reflection from a diffraction pattern of hydrated rat tail tendon.

#### **4.2.2 Electron microscopy**

Initially, a bovine corneal strip from the x-ray diffraction experiments was brought back to the department for TEM analysis. However, during processing of the tissue, the Descemet's membrane and the endothelium was detached. Fresh bovine corneas (n = 2) were then obtained and prepared as described in Chapter 2, Section 2.4.1.

For visualizing sulphated PGs, another fresh bovine cornea (n = 1) was fixed overnight in 2.5% glutaraldehyde in 25 mM sodium acetate buffer (pH 5.7) with 0.1 M MgCl<sub>2</sub> and 0.05% cuperomeric blue. The corneal tissue was then washed in buffer (x4) followed a wash in aqueous 0.5% sodium tungstate in 50% ethanol (15 min), to enhance the electron density of the PG-cuperomeric blue complex (Scott and Haigh, 1985; Scott and Bosworth, 1990). The tissue was then processed as described in Chapter 2, Section 2.4.1.

### **4.3 Results**

#### **4.3.1 Collagen fibril measurements - TEM analysis**

The data presented in Figure 4.5-7 illustrates micrographs from the central region of the cornea to the sclera, and within each region, the anterior to posterior zones. At low magnifications (x2000), the tissue appeared to consist of regularly arranged lamellae of collagen fibrils in the anterior of the cornea. The stromal lamellae in the mid and posterior regions appeared to be more layered and keratocytes were observed within the ECM. Furthermore, when moving towards the outer periphery/limbus and to the sclera, between the lamellae, fibroblasts are seen throughout the tissue and melanocytes (pigment cells – melanosomes) were found in the sclera adjacent to the ocular choroid.

At high magnifications (15K and 20K), as seen in Figure 4.5-7 and from the graph, presented in Figure 4.8, the fibril diameter at the anterior stroma from the centre to the mid periphery, the fibril diameter remained relatively uniform (centre =  $25.07 \pm 0.09$  (SEM) nm, mid periphery =  $22.35 \pm 0.08$  (SEM) nm). At the outer periphery/limbus regions of the anterior stroma, the fibrils appeared to vary in fibril diameter, but all over increased ( $27.28 \pm 0.19$  (SEM) nm). This was clearly evident in the anterior sclera, where larger fibrils were seen ( $73.20 \pm 0.96$  (SEM) nm). This increase in fibril diameter from the centre of the cornea to the sclera was also seen in the mid and posterior zones of the stroma.

At the centre of the cornea, the collagen fibrils appear to be uniform as a function of tissue depth (anterior =  $25.07 \pm 0.09$  (SEM) nm, posterior =  $22.99 \pm 0.08$  (SEM) nm). This regularity of fibril diameter was seen at the peripheral regions (inner periphery, mid periphery and outer periphery/limbus). Moving towards the sclera the fibril diameters were more uniform and smaller in the posterior zone of the tissue (anterior =  $73.20 \pm 0.96$  (SEM) nm, posterior =  $51.92 \pm 0.37$  (SEM) nm). This is clearly evident in Figure 4.5-7.

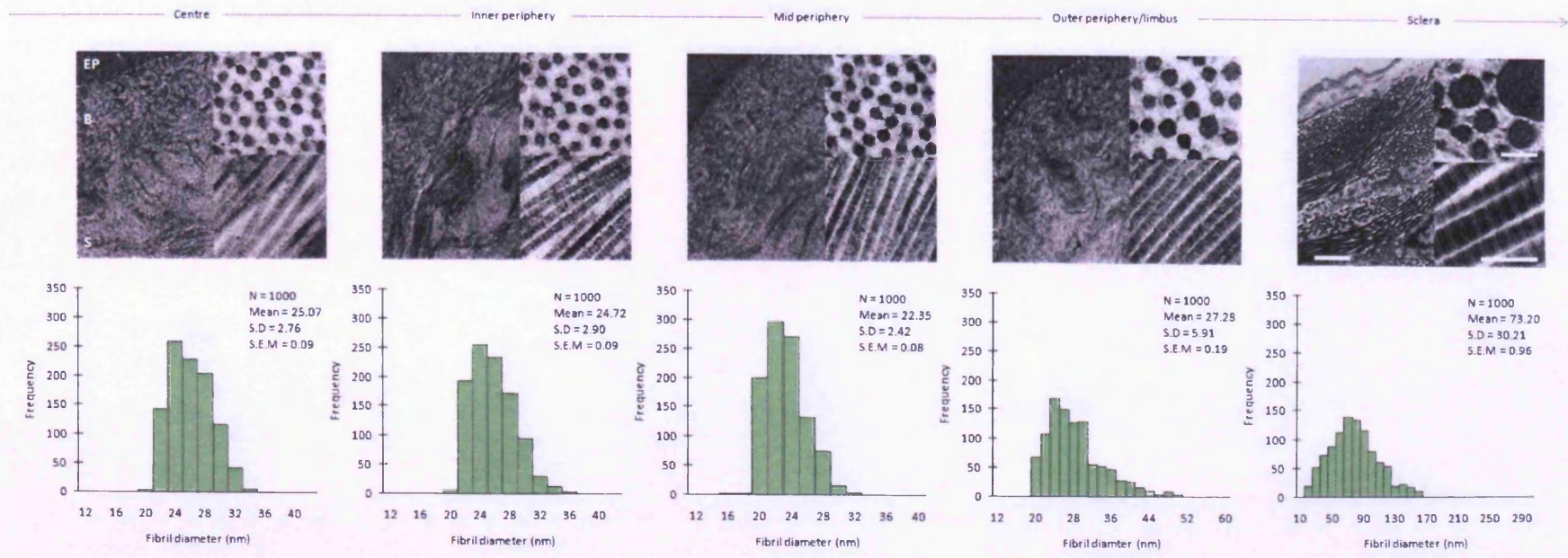


**Figure 4.5** Transmission electron micrographs across the bovine cornea (anterior stroma). Low magnification, scale bar = 2 μm. Longitudinal and cross sectional images of collagen fibrils, scale bar = 200 nm and 100 μm, respectively. EP = epithelium, B = Bowmans layer, S = stroma.

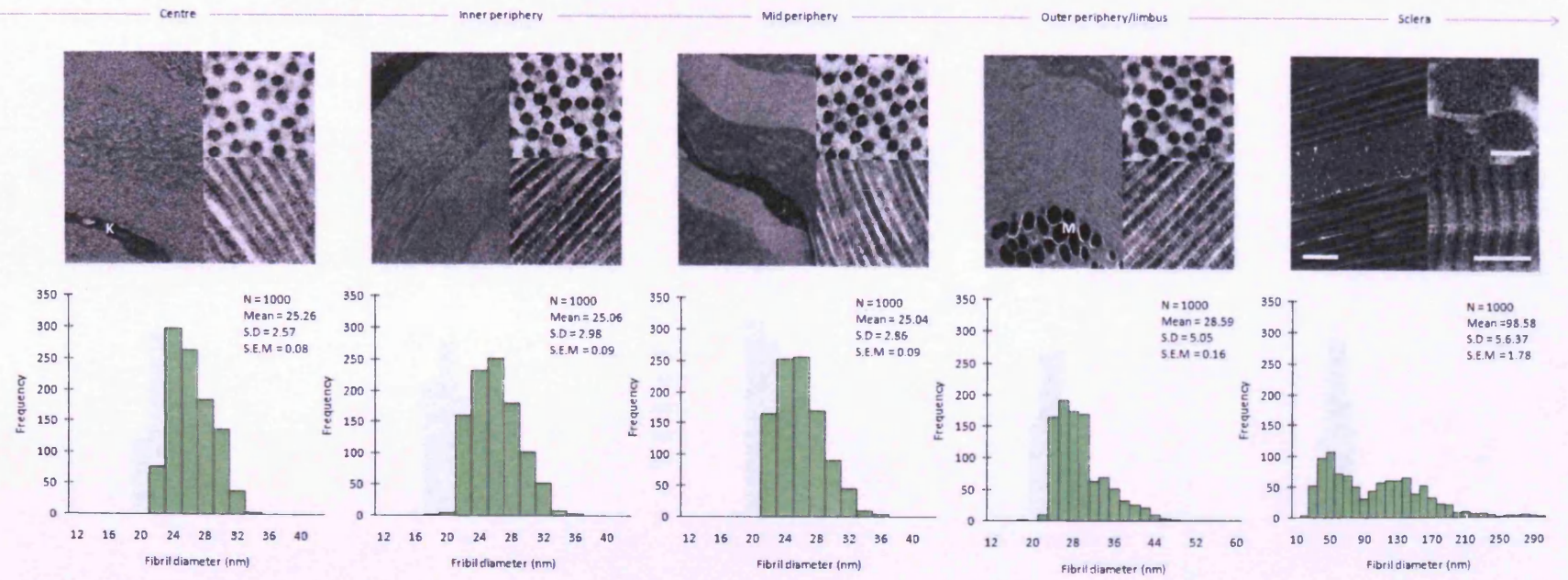


**Figure 4.6** Transmission electron micrographs across the bovine cornea (mid stroma). Low magnification, scale bar = 2  $\mu$ m. Longitudinal and cross sectional images of collagen fibrils, scale bar = 200 nm and 100 nm, respectively. K = keratocyte, M = melanocyte.

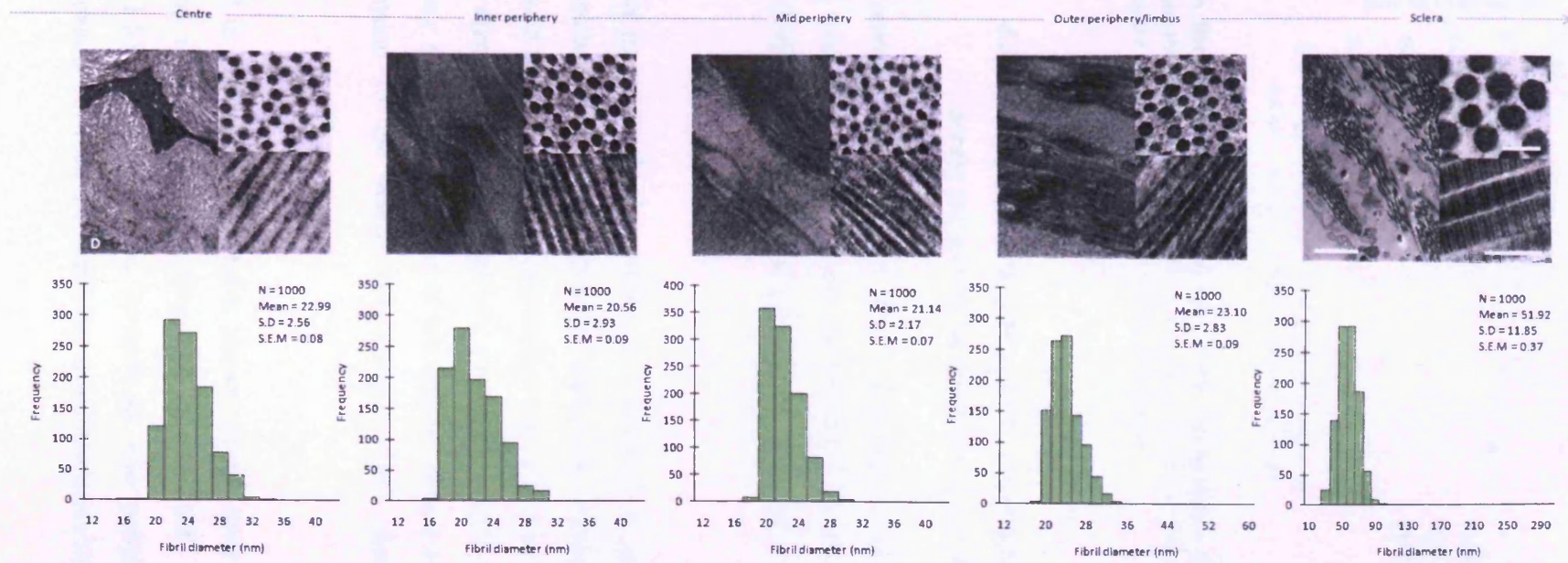


**Figure 4.7.** Transmission electron micrographs across the bovine cornea (posterior stroma). Low magnification, scale bar = 2  $\mu$ m. Longitudinal and cross sectional images of collagen fibrils, scale bar = 200 nm and 100 nm, respectively. D = Descemet's membrane.

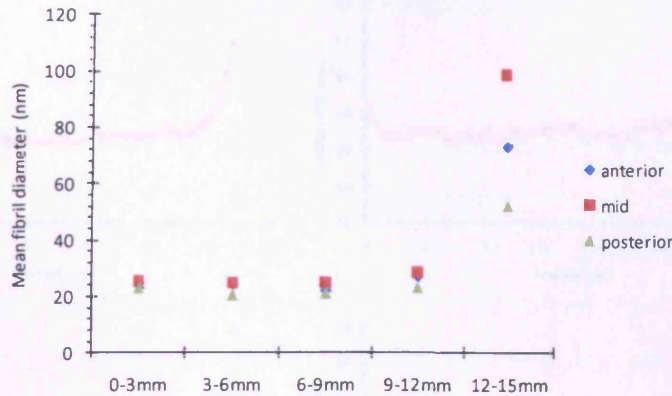


**Figure 4.8** The mean fibril diameter measurements from transmission electron micrographs at different depths across the bovine cornea. 0-3mm = centre, 3-6mm = inner periphery, 6-9mm mid periphery, 9-12mm = outer periphery/limbus and 12-15mm = sclera.

#### 4.3.2 X-ray diffraction analysis: Collagen fibril measurements across the cornea as a function of position

Fresh and fixed bovine corneal tissues were examined using small angle x-ray diffraction, as this was due to concerns of dehydration from the fresh tissue during processing. Both fibril diameter and collagen IFBS measurements showed similar trends overall.

The fibril diameters across the bovine cornea as a function of position are shown in Figure 4.9. The results, which are averages throughout the thickness of the cornea at each position, showed that in both fixed and fresh tissue, a similar trend was obtained, such that the fibril diameter remained relatively constant from the centre ( $35.74 \pm 0.44$  nm) to the periphery ( $35.81 \pm 0.50$  nm) of the cornea. However, towards the outer periphery and beyond to the sclera, the average fibril diameter increased to approximately 8%.

The data presented in Figure 4.9 also shows the centre-to-centre IFBS. The average fibril Bragg spacing remained constant from the centre ( $56.87 \pm 1.45$  nm) to the periphery ( $56.97 \pm 1.55$  nm) of the cornea. Towards the outer periphery and beyond the cornea, the Bragg spacing between the fibrils increased to approximately 4%.

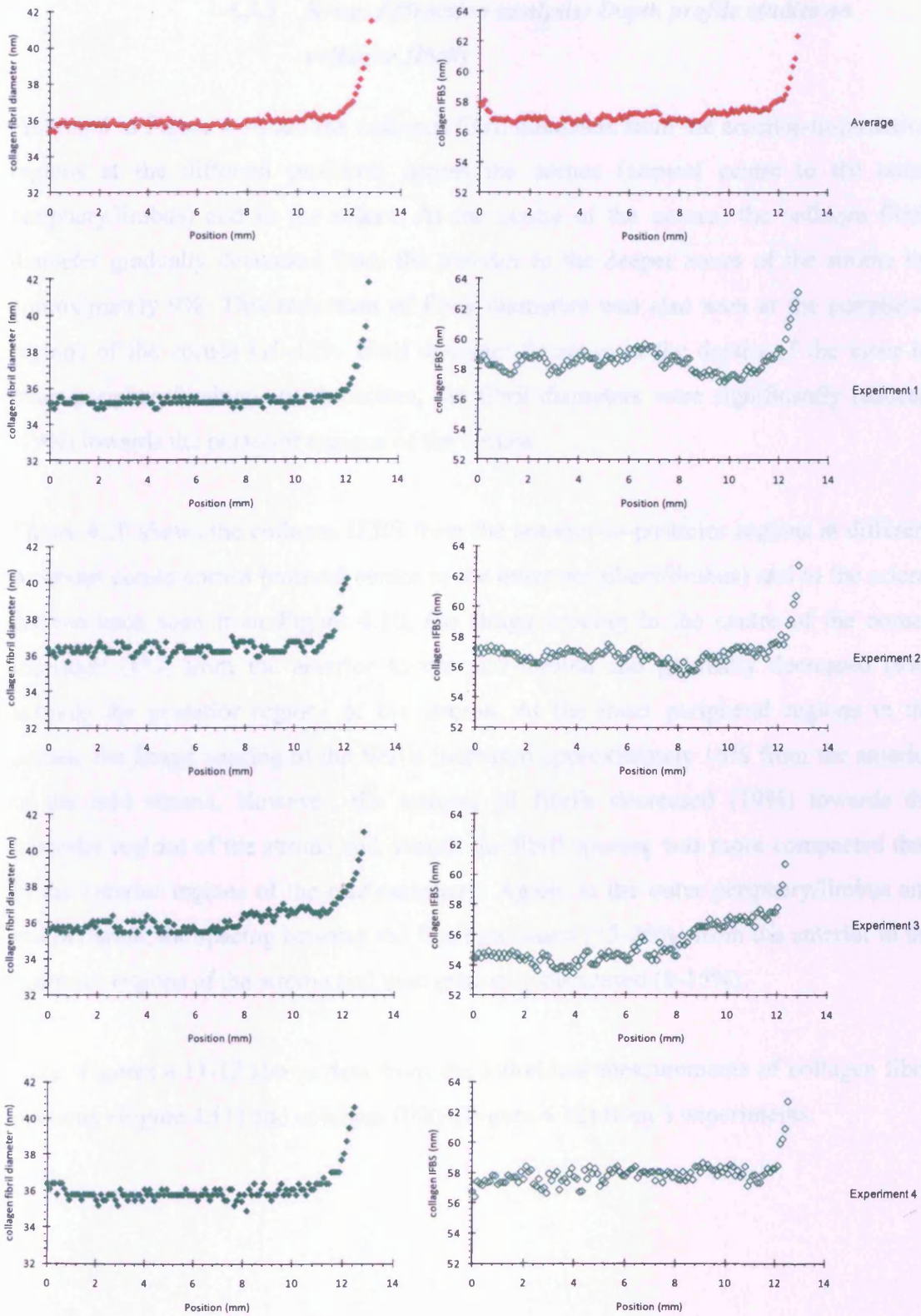


**Figure 4.9** Collagen fibril diameter (left) and IFBS (right) measurements across the bovine cornea. The average ( $n = 4$ ) fibril diameter and IFBS are shown in red and experiments 1-4 are shown in green. Experiments 1-3 = fresh bovine cornea. Experiment 4 = bovine was fixed (4% paraformaldehyde in 0.1 M phosphate buffer) prior to experiment.

### **4.3.3 X-ray diffraction analysis: Depth profile studies on collagen fibrils**

Presented in Figure 4.10 are the collagen fibril diameters from the anterior-to-posterior regions at the different positions across the cornea (corneal centre to the outer periphery/limbus) and to the sclera. At the centre of the cornea, the collagen fibril diameter gradually decreased from the anterior to the deeper zones of the stroma by approximately 9%. This reduction of fibril diameters was also seen at the peripheral regions of the cornea (10-12% fibril diameter decrease in the depths of the inner to outer periphery/limbus). At the sclera, the fibril diameters were significantly reduced (19%) towards the posterior regions of the cornea.

Figure 4.10 shows the collagen IFBS from the anterior-to-posterior regions at different positions across cornea (corneal centre to the outer periphery/limbus) and to the sclera. As can be seen from Figure 4.10, the Bragg spacing in the centre of the cornea increased (8%) from the anterior to the mid stroma and gradually decreased (9%) towards the posterior regions of the stroma. At the inner peripheral regions to the cornea, the Bragg spacing of the fibrils increased approximately 18% from the anterior to the mid stroma. However, the spacing of fibrils decreased (19%) towards the posterior regions of the stroma and overall the fibril spacing was more compacted than in the anterior regions of the mid periphery. Again, at the outer periphery/limbus and sclera region, the spacing between the fibril increased (15-20%) from the anterior to the posterior regions of the stroma and then gradually decreased (8-15%).

Note: Figures 4.11-12 shows data from the individual measurements of collagen fibril diameter (Figure 4.11) and collagen IFBS (Figure 4.12) from 3 experiments.

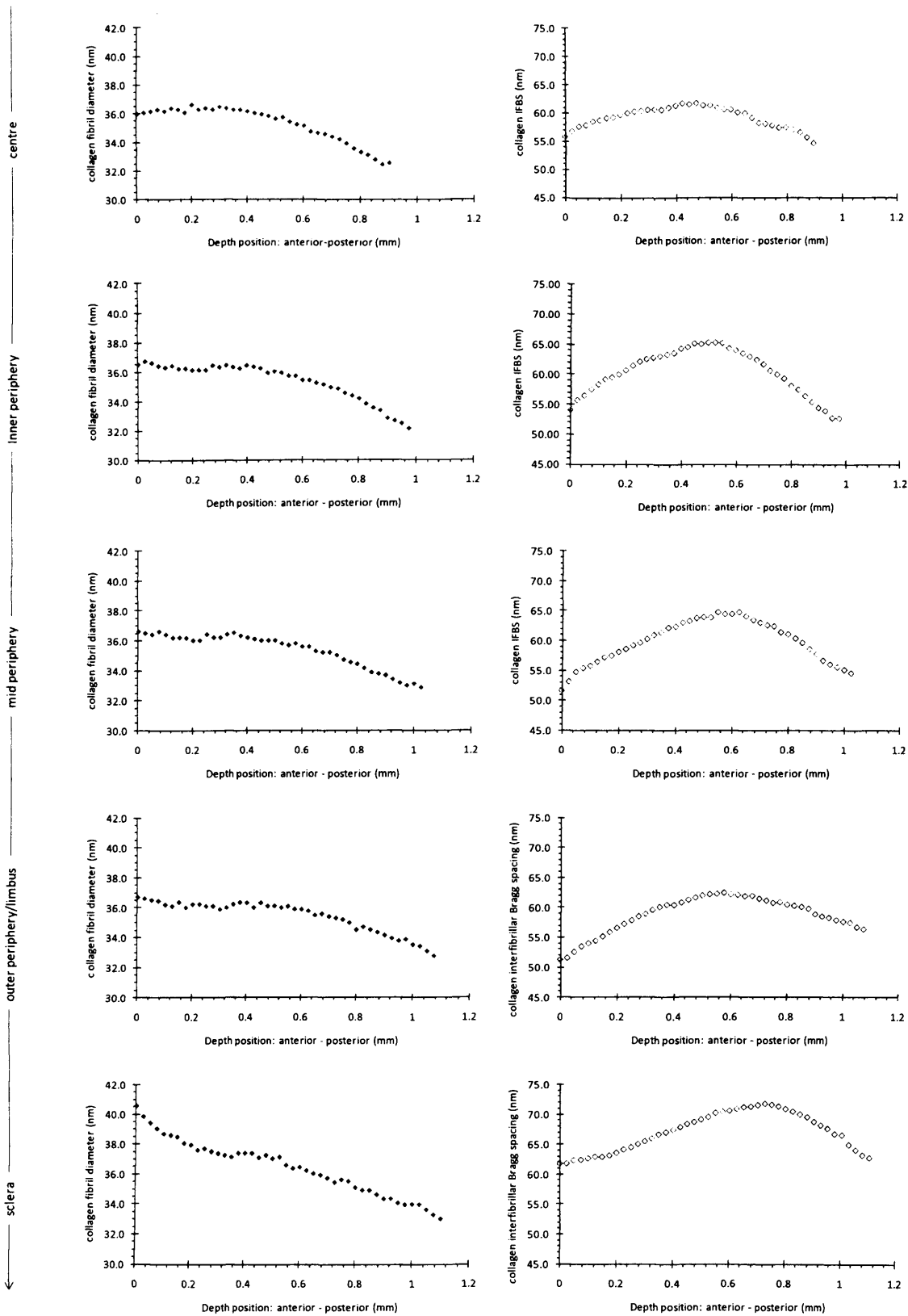
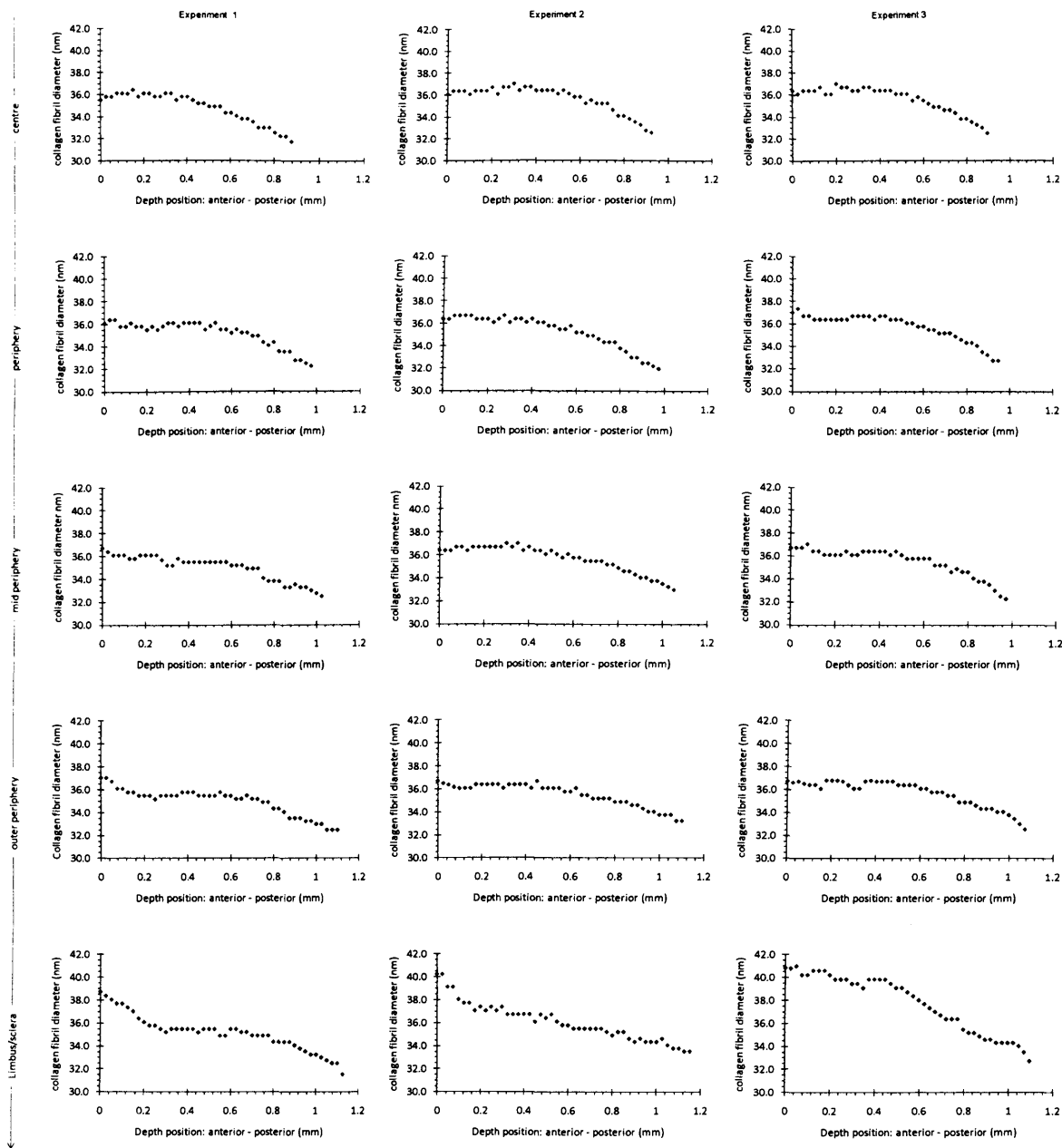
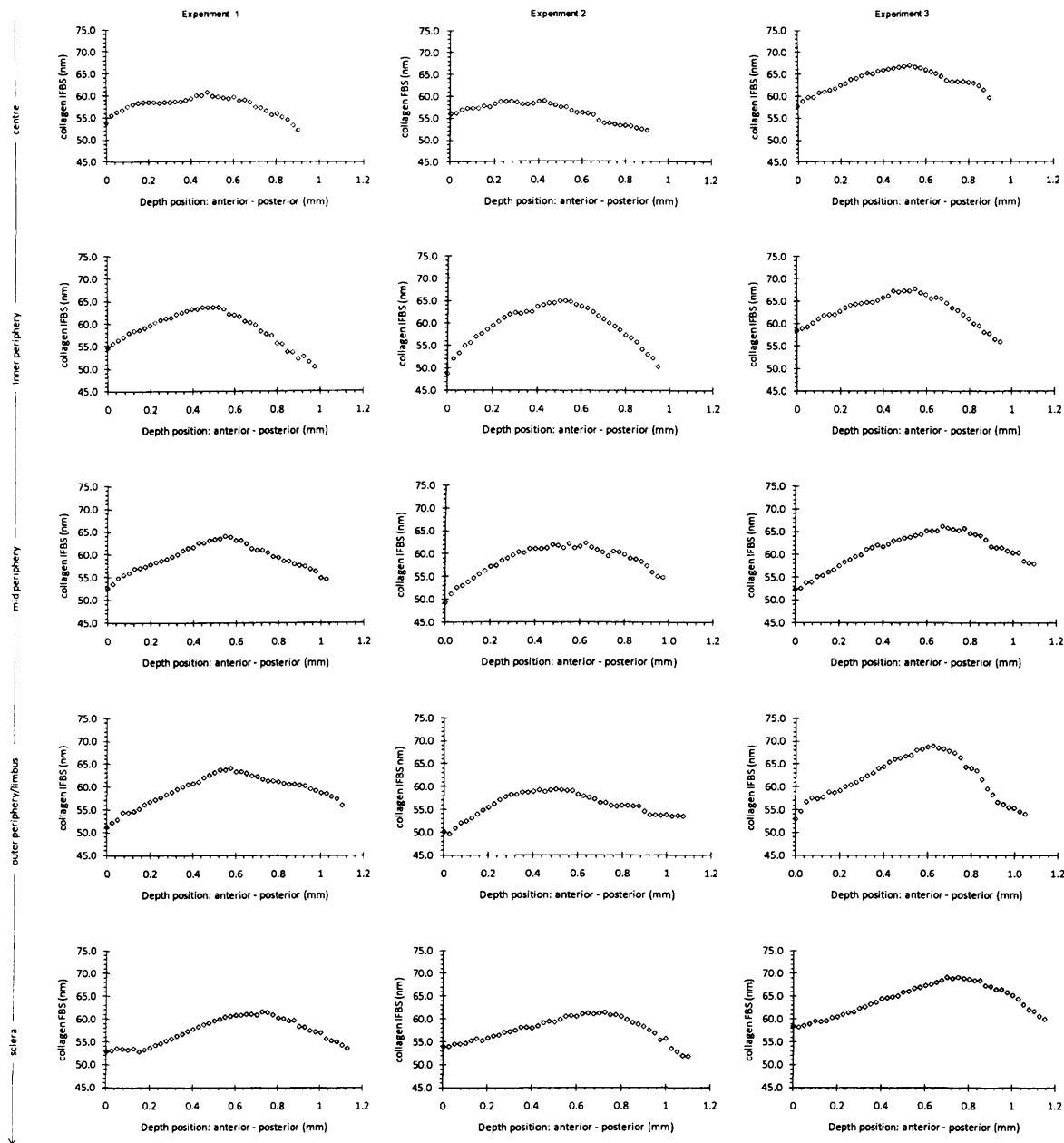


Figure 4.10 Collagen fibril diameter (left) and IFBS (right) measurements across and through the depth of the bovine cornea. All tissues were fixed (4% paraformaldehyde in 0.1 M phosphate buffer) prior for this particular experiment. 0 indicates starting point of the scan at the anterior surface of the cornea. N = 3.



**Figure 4.11** Data from experiments 1-3: collagen fibril diameters as a function of tissue depth in bovine cornea. All tissues were fixed (4% paraformaldehyde in 0.1 M phosphate buffer) prior for this particular experiment. 0 indicates starting point of the scan at the anterior surface of the cornea.



**Figure 4.12** Data from experiments 1-3: collagen IFBS as a function of tissue depth in bovine cornea. All tissues were fixed (4% paraformaldehyde in 0.1 M phosphate buffer) prior for this particular experiment. 0 indicates starting point of the scan at the anterior surface of the cornea.

#### 4.3.4 TEM analysis – PGs stained with cupromeronic blue

Presented in Figure 4.13 are panels of micrographs of bovine cornea prepared with cupromeronic blue stain to demonstrate PGs. Images from centre to sclera are shown (left to right) and PGs filaments of electron-dense material are shown both in transverse and longitudinal sections. Two prominent populations of cupromeronic blue stained

PGs (yellow and blue arrows) and similar collagen arrangements were seen as in previous data (Lewis et al., 2010). PG filaments were seen throughout the cornea, with some PGs extending between, or in contact with, two or more collagen fibrils. Long electron dense filaments (yellow arrow) were found throughout the corneal stroma, but were more apparent in the peripheral regions and in the deeper regions of the corneal stroma. Other PGs with shorter electron dense filaments (blue arrow) were also seen to occupy the space between adjacent fibrils and was found throughout cornea.

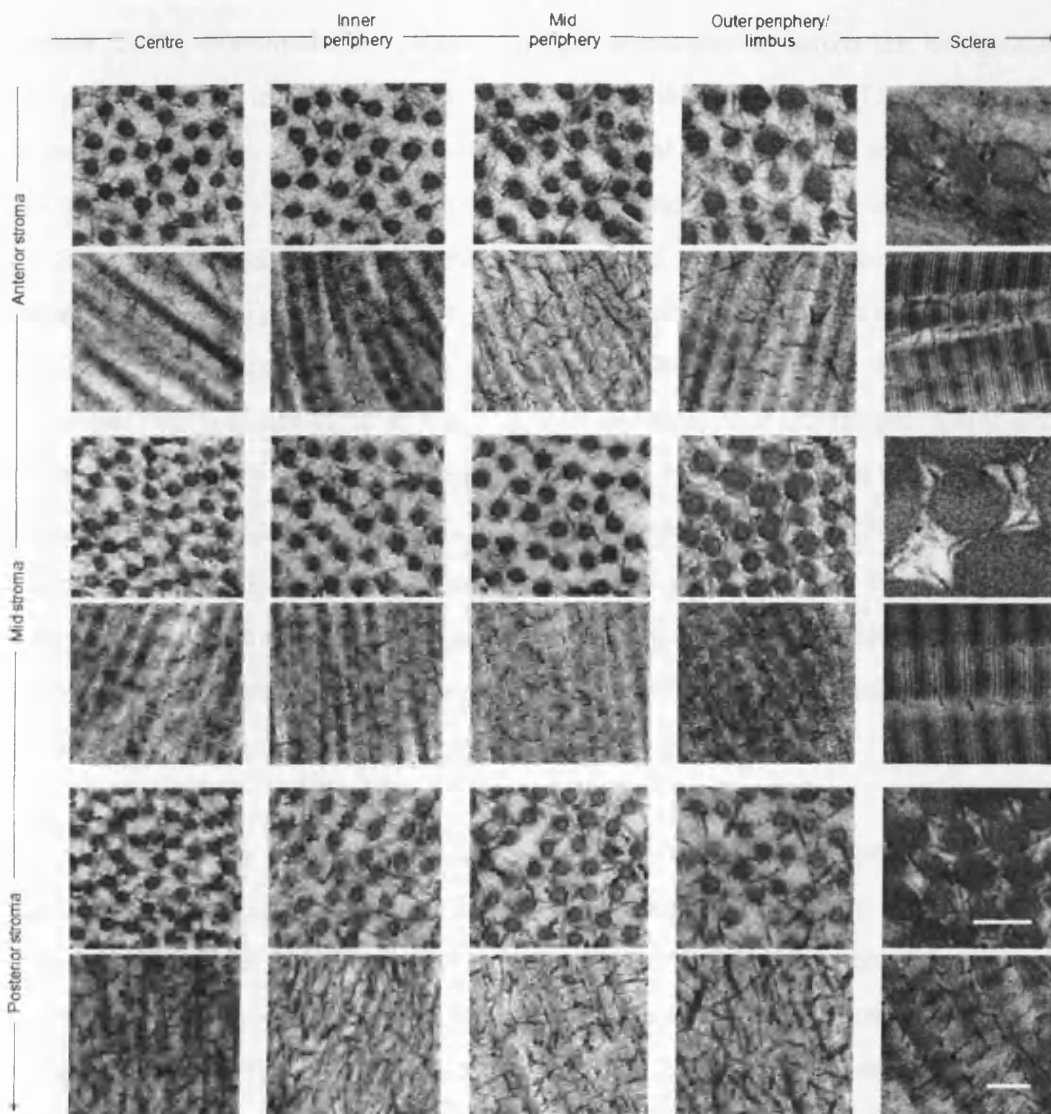


**Figure 4.13** Transmission electron micrographs from define regions of the bovine cornea, stained with cuperomeric blue. Micrograph images were taken from across (central regions of the cornea to the sclera) the depths (anterior to posterior regions) of the cornea. Two different populations of PGs: long electron dense filaments (yellow arrow) and short electron dense filaments (blue arrow) were seen. The scale bar for all longitudinal and cross sectional images of collagen fibrils = 200 nm and 100 nm, respectively.

#### 4.4 Discussion

The corneal matrix architecture is thought to be governed by the interactions between collagen fibrils and PG molecules modified with sulphated GAG side chains. The data presented here outline the contribution made by TEM and small angle x-ray scattering studies of the cornea to understanding the role of sulphated GAGs in the control of collagen architecture in cornea. In addition, we describe the first ever depth profiled data from bovine corneas.

Doutch (2009) examined the variation in light transmission across the bovine cornea. The pattern (shown in Figure 4.1 B), was similar to that in humans (Doutch et al., 2008) in that transmission decreased moving from central to peripheral cornea. In humans, Doutch *et al.* (2008) modeled this loss of transparency peripherally and explained it by the fact that collagen fibril diameters also increased moving from central to peripheral cornea (Boote et al., 2003). In the human, the corresponding peripheral increase of corneal thickness had only a minor effect on transmission. From the current work it seems that, using either TEM or x-ray diffraction, there is a similar peripheral increase in fibril diameters in the bovine cornea (Figure 4.8-9), However, in the bovine cornea, diameters only start to increase at about 10-12 mm from the centre (Figure 4.9) whereas transmission starts to decrease almost continuously away from the centre (Figure 4.1). It is possible that this thickness increase plays a more important role in the peripheral reduction in transmission than it does in humans, but further modeling studies on the bovine cornea would be required to test this hypothesis.

The average size of collagen fibril diameters in the anterior and posterior sclera was significantly different compared with those analyzed by x-ray diffraction. Such differences in fibril diameter could be due to the techniques employed. As previous mentioned, measurements from electron micrographs show considerable variation among studies which have been related largely to tissue shrinkage during tissue preparation (during aldehyde, osmium and ethanol treatment) (Fullwood and Meek, 1993). Thus we can use TEM to compare results from different samples or from different sites within a sample, where processing has been the same, but cannot compare absolute values with those from any other method of preparation or with those

from x-ray diffraction. In spite of this, both TEM and x-ray analysis confirmed an increase in fibril diameter from the central regions of the cornea to the sclera.

Collagen interfibrillar spacing is fairly constant across the bovine cornea until the last couple of millimeters before the sclera is reached. Again, this is in contrast to the human cornea where fibrils are clearly more closely spaced in the central compared to the peripheral cornea. The spacing of fibrils within the cornea is important to maintain a balance between transparency and biomechanical strength; more closely packed fibrils increase tissue strength but scatter more light. Cow corneas are larger than human corneas and are considerably less rigid. It is therefore possible that the size of the bovine eye limits the range of fibril diameters and fibril spacings required to maintain both tissue rigidity and an acceptable level of tissue transparency, and that the former is sacrificed in the cow in order to maintain the latter.

Depth profile studies from the bovine cornea (Figure 4.10) showed that fibril diameters fell off, particularly in the posterior layers of the cornea. Small compact collagen fibrils were also visualized in the deeper zones using TEM (Figures 4.7). Interfibrillar Bragg spacings through the depth of the cornea showed the same trend at all positions across the tissue, initially increasing to a depth of about 61-65 microns then falling off in the posterior 52-57 microns of the cornea (Figure 4.10). The anterior and posterior differences in the interfibrillar spacing are probably due to the differences in the lamellar organization in different depths of the cornea. Early studies (Komai and Ushiki, 1991; Freund et al., 1995) and in Figure 4.5, show that the lamellae are highly interwoven in the anterior stroma and become thicker, more stacked and distinct in the deeper regions of the stroma. Swelling properties in the different depths of the cornea may also be a cause in the differences between the anterior and posterior regions (Turss et al., 1971) One might expect the difference to be related to the GAG composition, however our IHC presented in Chapter 3 did not show any obvious correlations with respect to the distribution of sulphated GAGs. However, based on Anseth (1961) and Bettelheim and co-workers (1975) early work, the GAG distribution may also contribute the differences between the depths of the cornea (see Chapter 3 for more details), but further studies would be needed to test this hypothesis.

Other TEM studies have also showed that in the posterior stroma of human and rabbit corneas, the fibril diameters were approximately 4% and 15% smaller than in the anterior stroma (central region), respectively (Freund et al., 1995). However other human corneal studies have reported that the mean fibril diameters were relatively similar in all depths of the cornea (central region of cornea) (Akhtar et al., 2008a). Interestingly, Akhtar and co-workers (2008a) found that in keratoconus corneas, the mean fibril diameters and interfibrillar spacing were significantly smaller than in normal human corneas. They also found that the mean fibril diameters in the mid stroma were significantly larger than in the anterior and posterior stroma. In the normal human corneas, the mean interfibrillar spacing in the anterior stroma was lower than that in the middle and posterior stroma. However, compared with the normal corneas, in keratoconus, depending on the severity, the interfibrillar spacing frequency increased in the lower ranges (< 35 nm) and this was particularly evident in the more affected corneas (Akhtar et al., 2008a). Furthermore, depth profile studies from human eye-bank corneas showed no significant change in collagen fibril diameter throughout the central region of the tissue, although a lower collagen interfibrillar spacing in the anterior-most stromal regions was found compared with the spacing in the deeper cornea. Such differences from the two studies may probably be due the fact that swollen human corneas were used in the study (Quantock et al., 2007) as it is known that fibril spacing in the cornea is relatively sensitive to the tissue's water content. Previous x-ray scattering studies on corneal stroma have shown that water exclusively deposits into or is removed from the interfibrillar spaces, rather than within the fibrils themselves (Meek et al., 1991; Fratzl and Daxer, 1993). Therefore, such subtle variations in tissue hydration could produce changes in the spacing of the fibrils, without affecting their diameter.

In all TEM sections, regular diameters of collagen fibrils were found throughout the cornea and uniform interfibrillar spacing was seen within each region. Ultrastructurally, the regular compact collagen fibrils found in the centre and the deeper zones of the cornea may be associated with amount of type V collagen present in the collagen fibril. As studies have shown that when a reduction in type V collagen, it can result in large-diameter fibrils with broad size distribution (Birk et al., 1988; Birk et al., 1990; Marchant et al., 1996b). This may suggest a possible indication that the interaction of

type V with type I collagen is one mechanism modulating fibril diameter and is at least partially responsible for the regulation of collagen fibril formation.

Interestingly, towards the outer peripheral-limbal and particularly at the scleral region, less uniform fibrils (fibril diameter and interfibrillar spacing) were found, particularly at the anterior regions, as this may explain the reduced transparency found at the outer peripheral regions of the cornea (Doutch et al., 2008). In the corneal centre, the average fibril diameter was approximately 17% (anterior), 74% (mid) and 56% (posterior) smaller, compared to the sclera. The sclera was also considerably more disorganised and showed a greater change in fibril diameter between the anterior and the posterior. These differences between the anterior and posterior sclera of bovine eyes may be a reflection of variation in collagen-to-GAG chain ratios in the anterior sclera compared with the posterior sclera and/or different PG contents found in the sclera.

Corneal transparency is directly related to the ordered collagen fibril architecture that the cornea maintains. The core protein and the highly anionic GAG side chains of PGs are thought to regulate the collagen organization in the corneal stroma. To understand the relationship between PGs and collagen fibrils in the cornea, bovine corneas were treated with and without cuperomeric blue and images were taken at the anterior, mid and posterior of the stroma from the corneal centre to the sclera. Both longitudinal and transverse sections of collagen were examined. Both longitudinal and transverse images displayed the PG organization clearly, yet no distinct regular pattern of PG orientation was observed. With close observations, large, electron dense GAG chains were seen interconnecting collagen fibrils, and were found throughout the corneal stroma, but were more apparent in the peripheral regions and in the deeper regions of the corneal stroma. However, these long GAG chain filaments were found to a lesser extent throughout the cornea compared to another sub-population of smaller GAG chains, which were seen to interconnect neighbouring fibrils. It has been suggested that the two PG populations correspond to the different GAG chain types, CS/DS and KS (Anseth, 1961). Studies have suggested that small chains connecting adjacent fibrils are KS (Scott, 1992a), whereas the CS/DS form longer multimeric chains that extend among several collagen fibrils (Lewis et al., 2010). Furthermore, more studies would be needed to confirm CS/DS and KS and differentiate the two. This could be achieved by

using selective enzyme treatments, such as keratanase and chondroitinase ABC, prior to cuperomeric blue staining to identify the CS/DS and KS, respectively.

## Chapter 5: The effects of keratan sulphate in organ cultured corneas under normal and hypoxic O<sub>2</sub> conditions

## 5.

### 5.1 Introduction

The cornea is avascular in nature and is primarily dependent upon the atmosphere for its O<sub>2</sub> supply, particularly when the eye is opened. Contact lens wear impedes the flow of oxygen to the cornea (Fatt and St Helen, 1971); this is particularly important in soft lens wear as these lens types are relatively immobile on the ocular surface meaning that there is essentially no tear exchange behind the lens (Polse, 1979) which could potentially act as a secondary source of oxygenation.

Reduced oxygenation (hypoxia) of the cornea during contact lens wear is known to produce corneal swelling and consequently result in corneal edema. This is caused by an increase of lactate from anaerobic respiration created by an osmotic load that is balanced by an increased movement of water into the corneal stroma from the anterior chamber of the eye (Klyce, 1981). Other deleterious consequences of corneal hypoxia include:

- Neovascularisation in the peripheral areas of the cornea (Dixon and Bron, 1973), which can ultimately cause serious and permanent visual impairment if the new vasculature encroaches the pupil region.
- Engorgement of the limbal vasculature (Maldonado-Codina et al., 2004), which is cosmetically undesirable; the presence of trapped apoptotic corneal epithelial cells (microcysts) potentially leading to reduced vision in extreme cases; the development of striae and folds (Sarver, 1971) in the corneal stroma, potentially leading to reduced corneal transparency and reduced vision.
- Changes to corneal endothelial histology that can lead to intolerance of contact lens wear (Sweeney, 1992).
- An increase in the clinical severity of corneal infection and inflammation.

Contact lenses are held in place by the tears in the eye between the lens and the front of the eye. Changes in the cornea caused by contact lenses can be divided according to the structures affected (tear film, epithelium, stroma and endothelium) or according to the causes (Liesegana, 2002). The major consequence of contact lens wear is chronic hypoxia and others include tear film instability, allergy, toxicity, mechanical effects, inflammation and infection (Liesegana, 2002). The physiological changes differ among

the various contact lens materials (polymethylmethacrylate [PMMA], rigid gas permeable - RGP, soft hydrogel, silicone, and silicone hydrogel) and among various patterns of wear (daily, conventional, extended and overnight).

### 5.5.1 Low $O_2$ and its biochemical affects

If the  $O_2$  decreases below a critical level, the cornea shifts to anaerobic glycolysis using the Embden-Meyerhof pathway (Figure 5.1), in which glucose is broken down to pyruvate and then to lactate. Lactate does not diffuse rapidly out of the cornea, and can cause a decrease in aerobic metabolism and an accumulation of lactate in the stroma. Hypoxia thus creates a lower epithelial metabolic rate, an increase in epithelial lactate production, and an acidic shift in stromal pH. The degree of stromal acidosis varies, depending on the  $O_2$  transmissibility of the lens and the build up of  $CO_2$  under the lens.

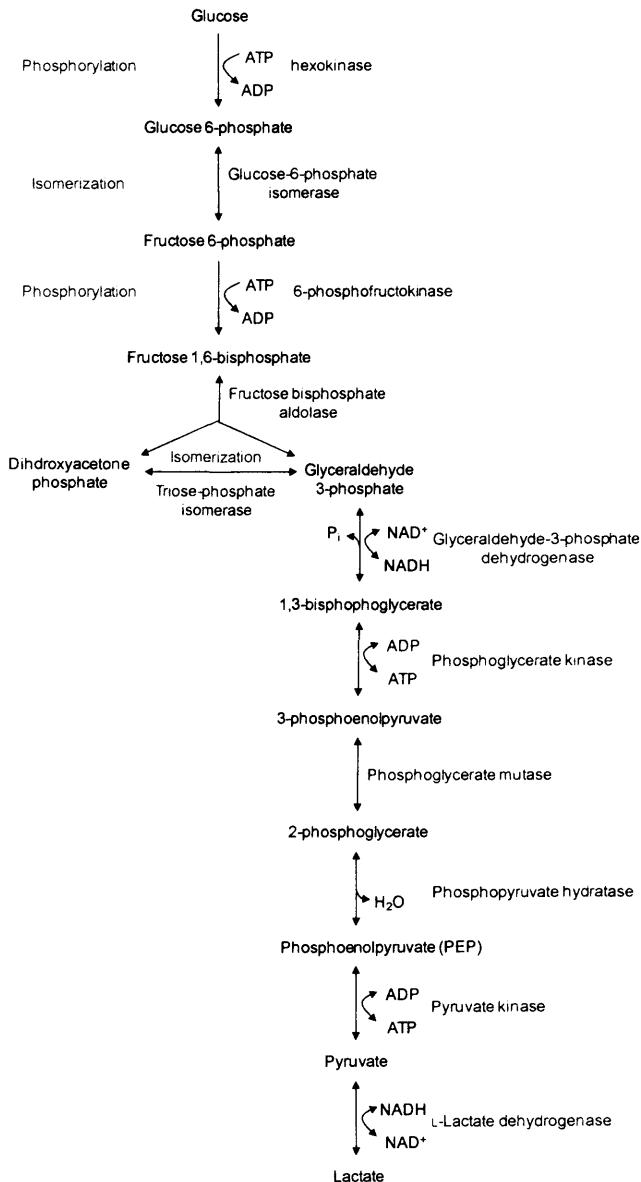


**Figure 5.1 Embden-Meyerhof pathway (EMP) – glucose degradation.** The pathway operates both under aerobic and anaerobic conditions. Under aerobic conditions, this pathway functions in conjunction with the TCA cycle in which the pyruvate generated through the EMP is oxidised to  $CO_2$  and  $H_2O$ . Under anaerobic conditions, pyruvate is reduced to lactate or ethanol. The pathway yields 2 moles of pyruvate and 4 ATP/mole of fructose diphosphate fermented. Of these 1 mole of ATP is used in the phosphorylation of glucose and the second is utilized for the phosphorylation of fructose-6-phosphate, the net yield is therefore only 2 moles of ATP/mole of glucose fermented.

Contact lens wear therefore can produce corneal hypoxia and an accumulation of CO<sub>2</sub>, both of which can cause acidosis (Bonanno, 1996). The pH of the epithelium, stroma, and the aqueous humor decreases significantly with contact lens wear when the O<sub>2</sub> permeability/transmissibility (Dk/L) is <100. CO<sub>2</sub> accumulation can result in acidosis, particularly in anterior layers of the cornea and can cause retardation of the normal CO<sub>2</sub> efflux (Figure 5.2). Corneal acidosis promotes endothelial polymegethism, epithelial microcysts, corneal edema, striate lines, infiltrative keratitis, and microbial keratitis. After prolonged corneal hypoxia, there is a depletion of the glycogen reserves of the cornea, diminished ATP, and ultimately a slowing of the water transport system in the endothelium. The combined effect of an accumulation of lactic acid in the stroma and a decrease in the pumping action of the endothelium can result in corneal edema.

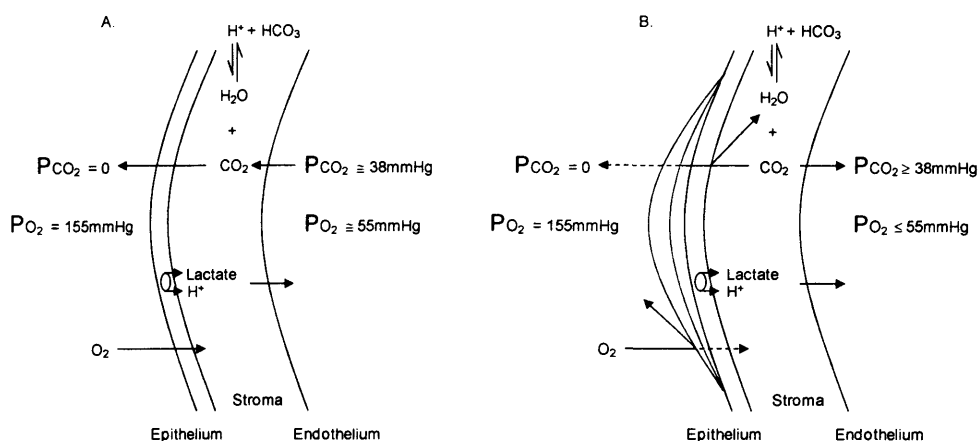


**Figure 5.2 Biochemical effects during contact lens wear.** (A) Normal eye. Metabolic production of lactate and H<sup>+</sup> by the epithelium is at its basal rate because O<sub>2</sub> is readily available. CO<sub>2</sub> rapidly diffuses down to a concentration gradient from aqueous to tears. (B) Open eye with contact lens. Epithelial oxygen and possibly aqueous PO<sub>2</sub> are reduced, which stimulates lactate production (osmotically causing corneal swelling) and H<sup>+</sup> production. Additionally, CO<sub>2</sub> efflux from the cornea is impeded, leading to higher stroma PO<sub>2</sub> which, when hydrated, produces a hydrogen and bicarbonate ion. Thus, the effects of hypoxia and hypercapnia on stromal pH are additive. In the closed lens-wearing eye, epithelial PO<sub>2</sub> is decreased and corneal PCO<sub>2</sub> is increased further because conjunctival PO<sub>2</sub> ≤ 55mmHg and PCO<sub>2</sub> ≥ 38mmHg (Bonanno, 1996).

### 5.5.2 Low O<sub>2</sub> and its affects on collagen

Reduced oxygen tension is observed in many physiological and pathological conditions, including high altitude residence, fetal development in the uterus, pulmonary fibrosis, wounded tissue, neoplasms (Helfman and Falanga, 1993), atherosclerosis (Bjornheden et al., 1999), and scleroderma (Silverstein et al., 1988). Under such hypoxic conditions, production and accumulation of collagen molecules are

active. Exposure of rats to hypoxia (10% oxygen) up-regulated collagen genes, causing increases in mRNA levels of procollagens  $\alpha 1(I)$ ,  $\alpha 1(III)$  and  $\alpha 2(IV)$  in peripheral lung parenchyma (Berg et al., 1998), in mRNA levels of procollagen  $\alpha 1(I)$  and in collagenous protein in heart tissue (Ostadal et al., 1995). In vitro hypoxic culture also elevated the mRNA level of procollagen  $\alpha 1(I)$  in dermal (Falanga et al., 1993), cardiac (Tamamori et al., 1997). The deposition of type IV collagen in mesangial cells (Kim et al., 1996) has also been found to increase.

In recent findings (Horino et al., 2002), low O<sub>2</sub> culture may cause an acceleration of hydroxylation in proline residues of procollagen during collagen synthesis in fetal rat lung fibroblasts. More interestingly, cultured human dermal fibroblasts (Falanga et al., 1991; Falanga, Zhou and Yufit, 2002) exposed to low oxygen (2% O<sub>2</sub>) for 24-72 hr, as compared to standard O<sub>2</sub> tension (20% O<sub>2</sub>) causes an increase of mRNA levels human  $\alpha 1(I)$  (COL1A1) procollagen gene and peptide synthesis of TGF- $\beta 1$ , an important regulator for fibrosis in the ECM. In addition, hypoxia itself can inhibit TGF- $\beta 1$ -induced corneal myofibroblast transformation,  $\alpha$ -SM actin expression and cause RhoA pathway activation.

### 5.5.3 Low O<sub>2</sub> and its affects on GAGs

KS and CS probably fulfil very similar roles in the cornea, keeping collagen fibrils apart at the right degree of swelling to permit passage of visible light through the cornea without excessive scattering; their functions are thus essential to corneal transparency and hence to sight. KS and CS are present in large quantities in connective tissues that have a shock-absorber function (e.g. cartilage and intervertebral disc), or a rigid shape maintained by turgidity due to GAG swelling pressure (cornea) (Scott, 1992b).

In the late 1980s the idea of KS biosynthesis was preeminent at tissue locations with low oxygen availability (Scott and Haigh, 1988b). The idea was that NAD-dependent oxidation of the glucose precursor, uridine diphosphate glucuronic acid, to galactose in KS was not oxygen dependent, unlike its conversion to glucuronic acid in the other main corneal GAGs; CS and DS (Stockwell and Scott, 1965). Thus, synthesis of CS/DS sulphate cannot proceed under hypoxic conditions. NAD; a key molecule for CS and

KS chain synthesis, is held to inhibit the oxidation step (i.e. NAD may inhibit UDPGlc dehydrogenase, resulting CS formation to decrease) (De Luca et al., 1976), and so the NAD:NADH ratio, as well as the pyruvate:lactate ratio, and cellular O<sub>2</sub> levels may therefore determine the relative rates of KS and CS/DS synthesized (Scott et al., 1989) (Figure 5.3). Thus, synthesis of CS/DS sulphate cannot proceed under hypoxic conditions. And it is this that has led to the “oxygen-lack” hypothesis of preferential KS production in the cornea as well as in articular cartilage.

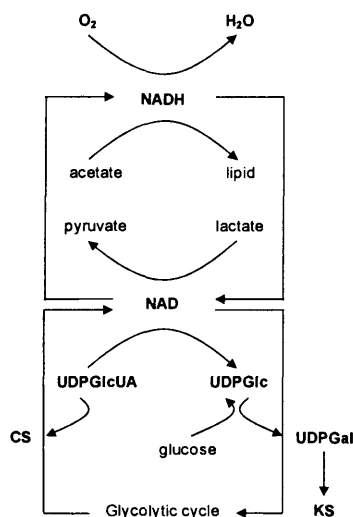


**Figure 5.3 Diagram of the O<sub>2</sub>-dependent pathway with NAD at the centre, leading to the synthesis of KS or CS.** The decision for making KS synthesis, depends the use of UDPGlc to make UDPGal, whereas UDP glucuronic acid (UDPGlcUA) for the use in CS synthesis. The NAD: NADH ratio is thought to determine whether CS or KS is made. NAD is oxidized to NADH via respiratory chain reactions or in lipid formation. Exchange of reducing power from NAD to lipid occurs via NADPH. NAD:NADH levels are reduced by adding lactate, acetaldehyde and other molecules that use NAD in a dehydrogenase reaction. The glycolytic cycle requires NAD, providing the basic energy requirement for the hypoxic cell (Scott, 1992b).

In the corneal stroma of large animals, O<sub>2</sub> utilization may be inefficient, in which O<sub>2</sub> diffuses over a long distance, and so it would be easier to make KS rather than CS/DS. Conversely, CS production in thin small corneas ought to proceed without difficulty, since O<sub>2</sub> would be easily available along a short diffusion path (Scott and Haigh, 1988b). For example in mature mice, shrew and frog corneas (70-100 µm thick) contained only CS/DS and minimal traces of KS, while bovine, human, porcine and other thick corneas contained over 60% KS (Scott and Bosworth, 1990).

The synthesis of GAG side chains is a post-translational event, but the rate of degradation or turnover of GAGs remain unclear, although, early studies have suggested that KS turn over is slow, in mature tissue (Davidson and Small, 1963). It has also been suggested that a lack of O<sub>2</sub> could affect many stages during GAG synthesis. The protein cores of corneal and cartilage CS-DS PGs are quite different, as are the linkage regions between the protein cores and the GAG side chains. Only the CS chains themselves are the same in the relevant cartilage, disc and corneal PGs (Scott, 1989). Thus assuming all three tissues operate on the same mechanism, chain elongation and completion could be a target of O<sub>2</sub> lack. Similarly, KS chain elongation could be a target for control by O<sub>2</sub> tension.

## **5.6 Aims**

To investigate the effects of KS under normal and low O<sub>2</sub> tension in organ cultured rabbit corneas. More specifically the goal was to gain a better understanding of the role of oxygen tension on the sulphation level of KS produced by rabbit cornea.

## **5.7 Methods**

Figure 5.4 presents an experimental plan that was employed for this particular chapter. Note that for this Chapter, all experiments were carried out during a 5 month placement at Doshisha University and Kyoto Prefectural University of Medicine, Japan. Note: white New Zealand rabbits were used for this particular study, this was because the animals were easier to access than fresh bovine eyes and due to animal regulations. The different regions across the rabbit cornea were also categorized with the same terminology as to the previous bovine studies (Chapter 3, Figure 2.1). However because the rabbit eyes itself are a lot smaller than bovine eyes, the rabbit cornea was categorized as the following: centre (0-3 mm), periphery (3-6 mm), outer periphery/limbus (6-9 mm) and sclera (9-12 mm).

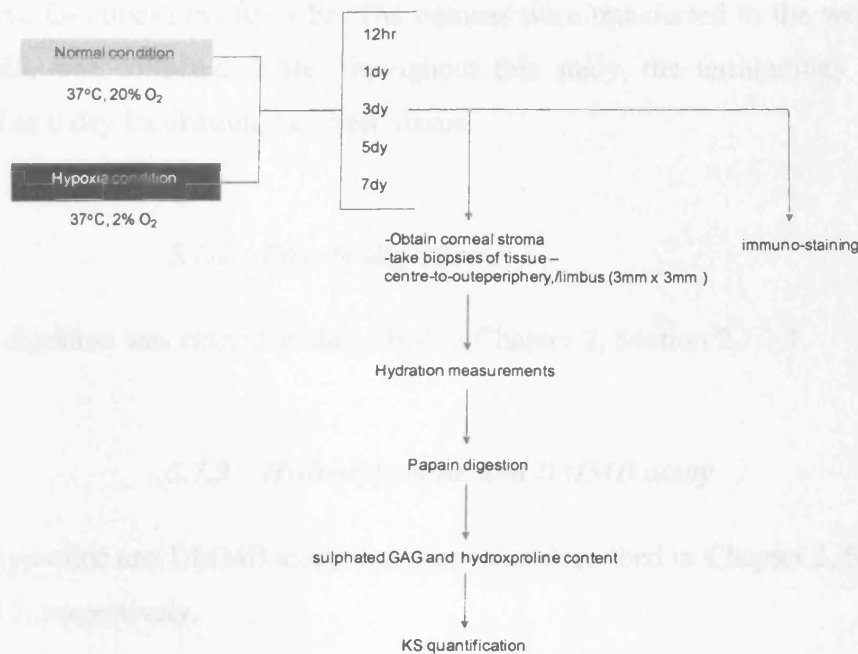


Figure 5.4 A summary of experiments that was employed.

### 5.7.1 Sample preparation

Whole rabbit eye globes were obtained from a local abattoir in Kyoto and transported on ice to the laboratory. 60 healthy eyes with clear/transparent corneas were selected for culturing as described by Crewe and Armitage (2001). Briefly, prior to culturing the corneas, 500 ml of culture medium (Eagle's MEM buffered with HEPES [4-(2-hydroxyethyl)-1-piperazineethanesulfonic acid] and containing 26 mM sodium  $\nu$ , 2% fetal bovine serum, 2 mM L-glutamine, penicillin, streptomycin and 5% dextran (wt/v)) (Crewe and Armitage, 2001) was prepared and 2.5 ml were transferred into each well of the 24 well plates (remaining medium was stored at 4°C). The plates were then incubated for 1 hr at their respective conditions; 37°C, 20% O<sub>2</sub> – normal atmospheric condition and 37°C, 2% O<sub>2</sub> – low oxygen condition. All 60 rabbit eyes dissected, corneas with corneoscleral rims (with intact epithelium and endothelium) were excised under aseptic conditions and transferred to their respective medium. Corneal samples were removed from the organ culture at various time points (½ day, 1 day, 3 day, 5 day and 7 day) and used for KS quantifications and immunohistochemistry. Media was changed every 2 days, and prior to changing the media, the media was thawed to room

temperature (20 min) and then 2.5 ml was aliquot into 24 well plates and incubated in respective O<sub>2</sub> conditions for 1 hr. The corneas were transferred to the well plates and the media was collected. Note: throughout this study, the terminology “control” is referred as 0 day incubation, i.e. fresh tissue.

### **5.7.2 Papain digestion**

Papain digestion was carried as described in Chapter 2, Section 2.1.1.1.

### **5.7.3 Hydroxyproline and DMMB assay**

Hydroxyproline and DMMB assay was carried as described in Chapter 2, Sections 2.4.1 and 2.4.2, respectively.

### **5.7.4 KS quantification**

Competitive ELISAs were employed to quantify KS as described in Chapter 2, Section 2.5.3 and ELISA preparations as described Chapter 3, Section 3.4.6. The colour development was quantified on a plate reader multi spectrophotometer; Viento XS, DS Pharma Biomedical at 405 nm, to determine the inhibition of binding.

### **5.7.5 Immunohistochemistry**

Immunostaining of corneal tissue was carried out as described in Chapter 2, Section 2.3.1.1. Immunostained tissue sections were analyzed using a Lecia MD6000B microscope and Lecia DFC500 View digital camera. Images were taken at 10x magnification. The antibody dilutions are shown in Table 5.1.

Antibody	Detection	Pre-treatment	Dilution
<b>5D4</b>	Recognises linear penta-sulphated KS where both GlcNAc and Gal are sulphated	-	1:100
<b>1B4</b>	Recognizes lesser sulphated KS sequences of N-acetyl lactosamine disaccharides	-	1:50
<b>BKS-1</b>	Keratanase generated KS neo-epitope	Keratanase II	1:100
<b>LUM-1</b>	Lumican core protein	Keratanase II, Chondroitinase ABC, Endo- $\beta$ -galactosidase	1:50
<b>KER-1</b>	Keratocan core protein	Keratanase II, Chondroitinase ABC, Endo- $\beta$ -galactosidase	1:50

Table 5.1 Antibody dilutions used.

## 5.8 Results

For this particular chapter, most of the work was focussed on the central regions of the rabbit cornea. For other regions of the cornea, hydration measurements, total sulphated GAG content and the immunolocalization were collected.

Note: for all data analysis a statistical significance was ascertained by using statistical tests for the data groups: one-way ANOVA with post-hoc Tukey HSD.

### 5.8.1 Corneal hydration

As previously mentioned, GAG chains are highly sulphated, and due to this hydrophilic property, they are thought to occupy the space between collagen fibrils where they aid to define the swelling properties of the stroma (Bettelheim and Plessy, 1975). The data presented here, illustrated that over the given time period, the whole cornea (centre, periphery, outer periphery and sclera) swelled, particularly by the 3<sup>rd</sup> day. For example in the central region, the hydration increased by 30% (normal conditions) to 36% (hypoxic conditions). However, when comparing between the conditions for a particular day, minor differences was found (Figure 5.5).

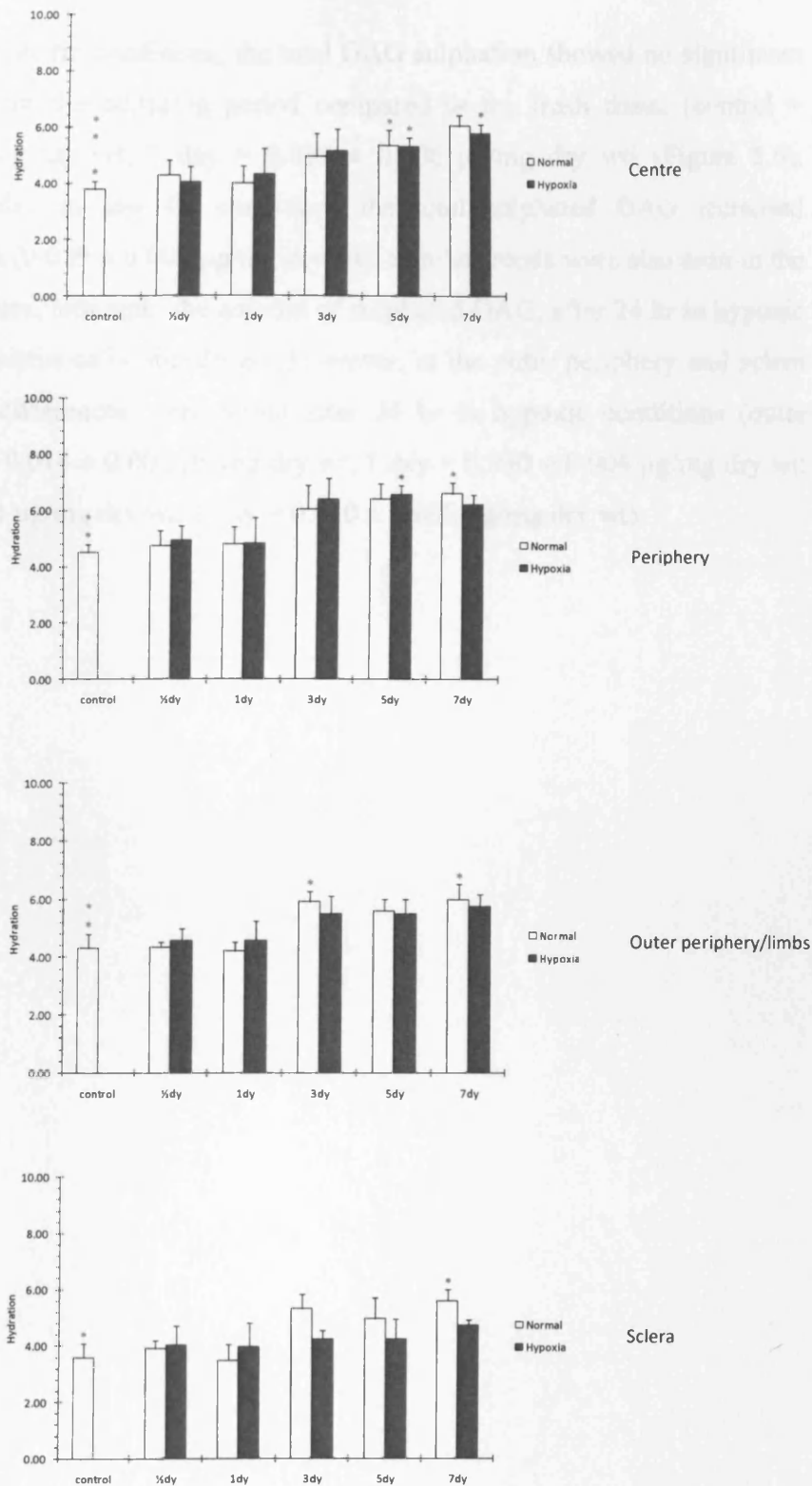


**Figure 5.5 Hydration differences between normal and hypoxic organ cultured corneas from centre to sclera.** One-way ANOVA and post-hoc Tukey HSD tests were employed to identify the significant differences between the groups. \*, \*\*, \*\*\* P = ≤0.01. For all calculations, please see Appendix 2, Tables ## 1-4.

### 5.8.2 Results: Sulphated GAG pattern

Under normal atmospheric conditions, the total GAG sulphation showed no significant differences throughout the culturing period compared to the fresh tissue (control =  $0.017 \pm 0.003$   $\mu\text{g}/\text{mg}$  dry wt, 7 day =  $0.019 \pm 0.006$   $\mu\text{g}/\text{mg}$  dry wt) (Figure 5.6). However, after 1 day in low O<sub>2</sub> conditions the total sulphated GAG increased significantly by 71% ( $0.029 \pm 0.007$   $\mu\text{g}/\text{mg}$  dry wt). Similar trends were also seen in the periphery of the cornea, although, the amount of sulphated GAG, after 24 hr in hypoxic conditions was not statistically significant. However, at the outer periphery and sclera regions significant differences were found after 24 hr in hypoxic conditions (outer periphery: control =  $0.014 \pm 0.001$   $\mu\text{g}/\text{mg}$  dry wt, 1 day =  $0.030 \pm 0.004$   $\mu\text{g}/\text{mg}$  dry wt: sclera:  $0.002 \pm 0.001$   $\mu\text{g}/\text{mg}$  dry wt, 1 day =  $0.010 \pm 0.002$   $\mu\text{g}/\text{mg}$  dry wt).

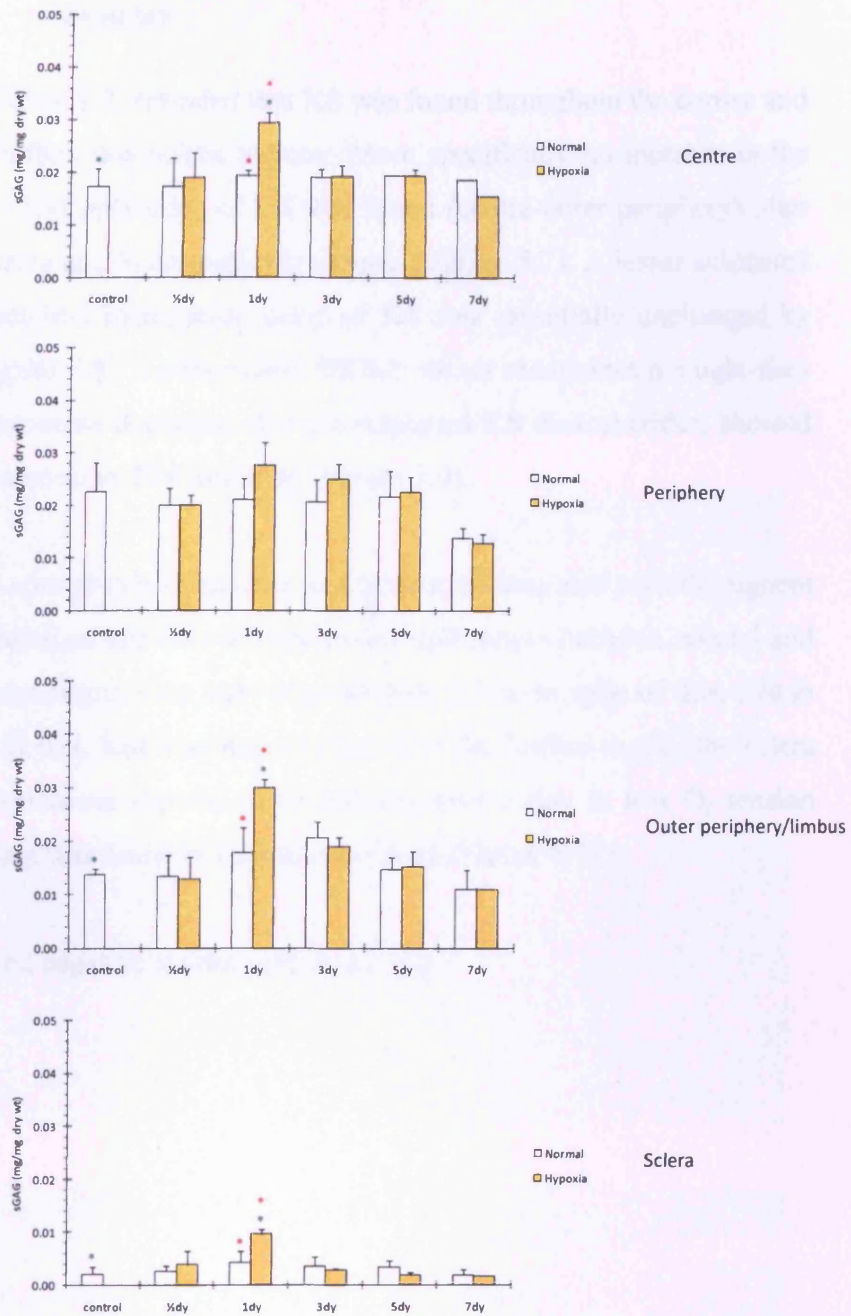


**Figure 5.6 Total sulphated GAG differences between normal and hypoxic organ cultured corneas from centre to sclera.** One-way ANOVA and post-hoc Tukey HSD tests were employed to identify the significant differences between the groups. \*,\* P = ≤0.01. For all calculations, please see Appendix 2, Tables ## 5-8.

### **5.8.3 Results: Immunolocalization of KS patterns and its core proteins**

The data presented in Figure 5.7, revealed that KS was found throughout the cornea and reducing towards the limbus and sclera regions. More specifically an increase in the over-sulphated epitope (5D4 antibody) of KS was found (centre-outer periphery) after only 1 day in organ culture at 2% atmospheric oxygen (Figure 5.7). A lesser sulphated (1B4 antibody), and thus less hydrophilic, form of KS was essentially unchanged by oxygen deprivation (Figure 5.8). Furthermore, BKS-1 which recognizes a single neo-epitope on KS after keratanase digestion of monosulphated KS disaccharides, showed similar staining distribution as to 5D4 antibody (Figure 5.9).

The detection of KSPG core proteins (lumican and keratocan) was also seen throughout the cornea. The localization of lumican showed minor differences between normal and low O<sub>2</sub> organ cultured conditions over the period (Figure 5.10). In spite of this, like in the localization of KS GAGs, less staining was found in the limbus and in the sclera regions. Interestingly, keratocan showed more staining after 1 day in low O<sub>2</sub> tension and detection of keratocan was found in limbus and sclera (Figure 5.11).

Negative controls showed negative staining (Figure 5.12).

Immunolocalization on oversulphated N-acetyl lactosamine disaccharides of KS

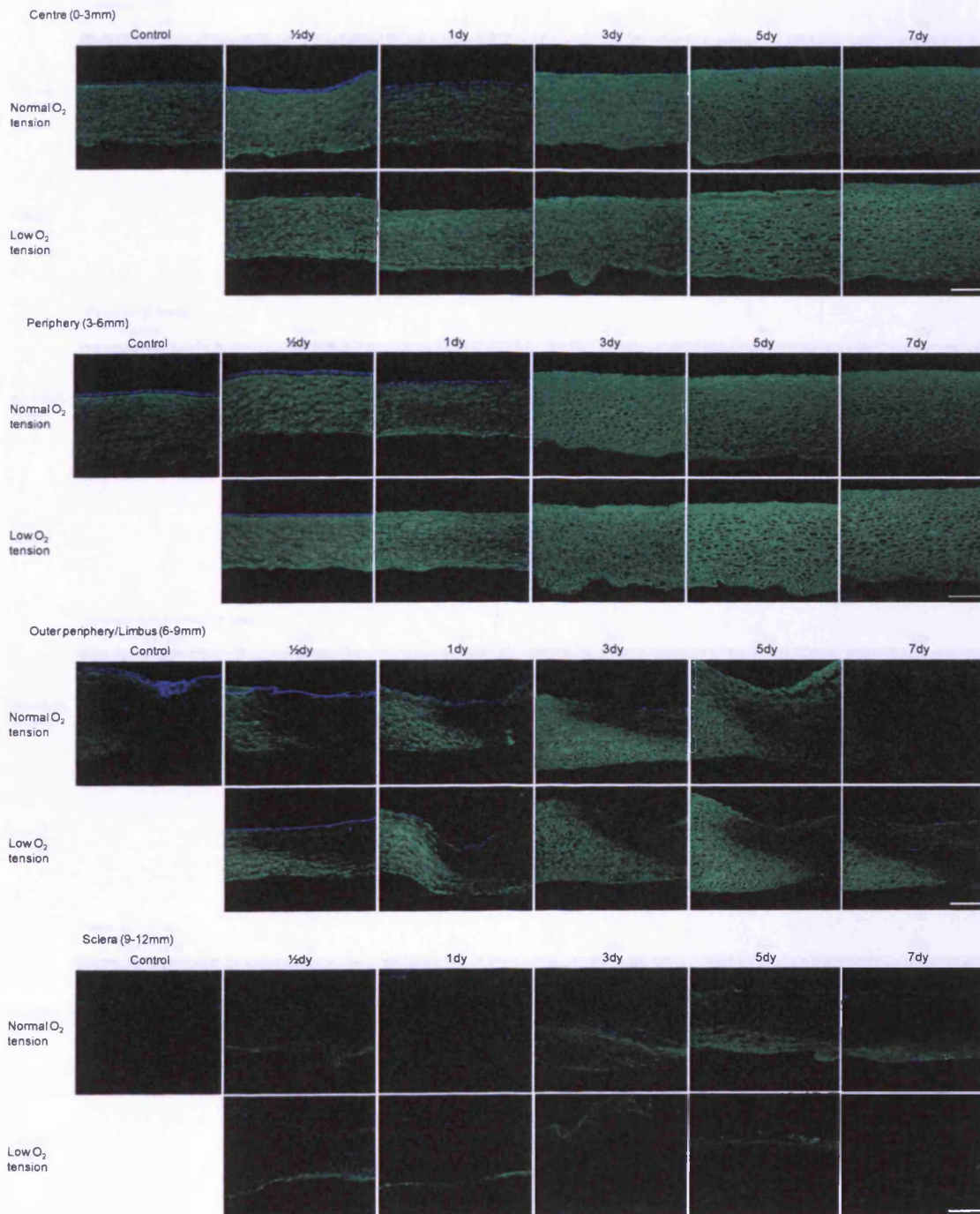


Figure 5.7 Immunolocalization of over-sulphated KS disaccharides (green), probed with 5D4 antibody and DAPI for cells (nucleus) (blue). Control = fresh tissue. Scale bar = 100  $\mu$ m.

Immunolocalization on lesser sulphated N-acetyl lacosamine disaccharides of KS

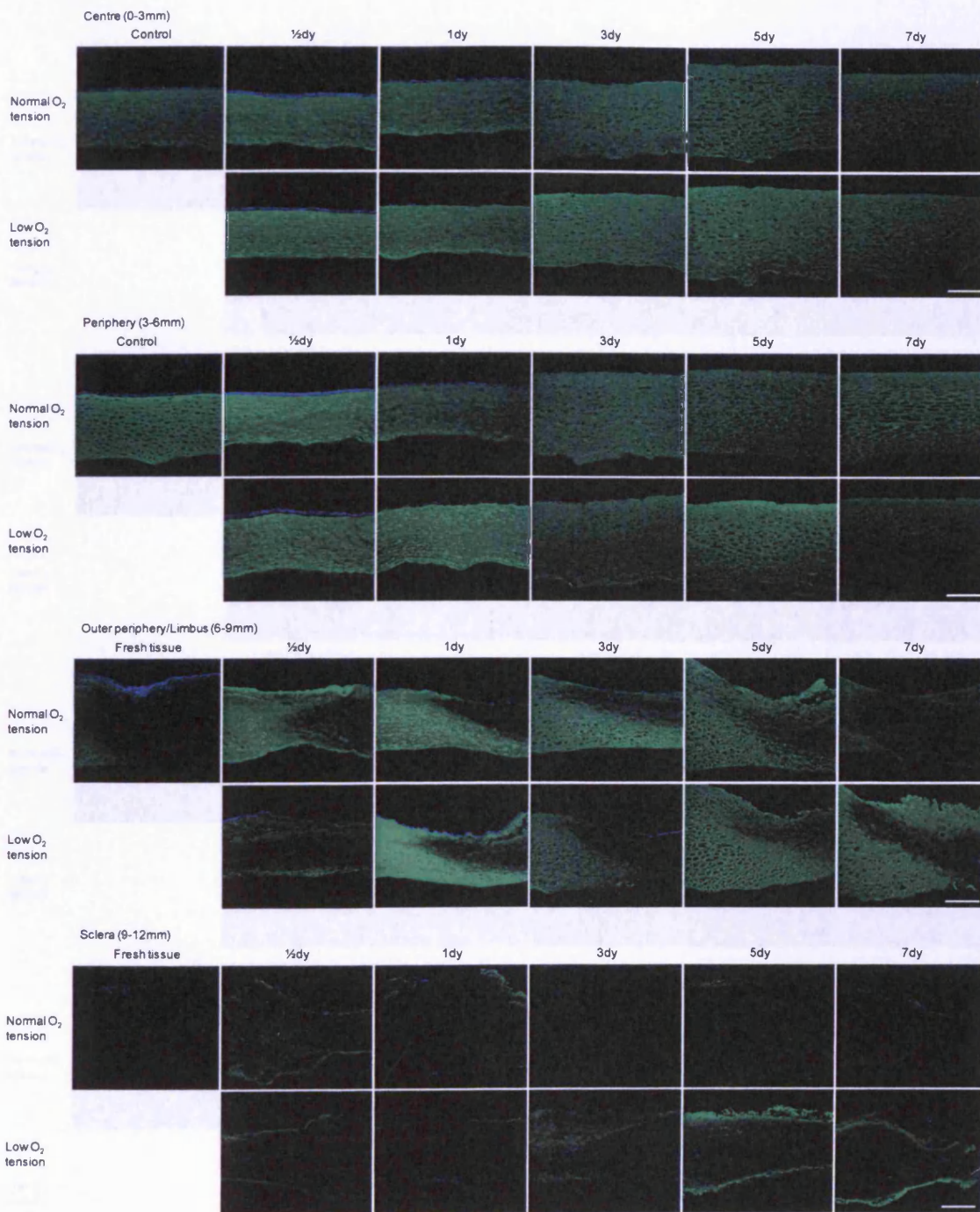
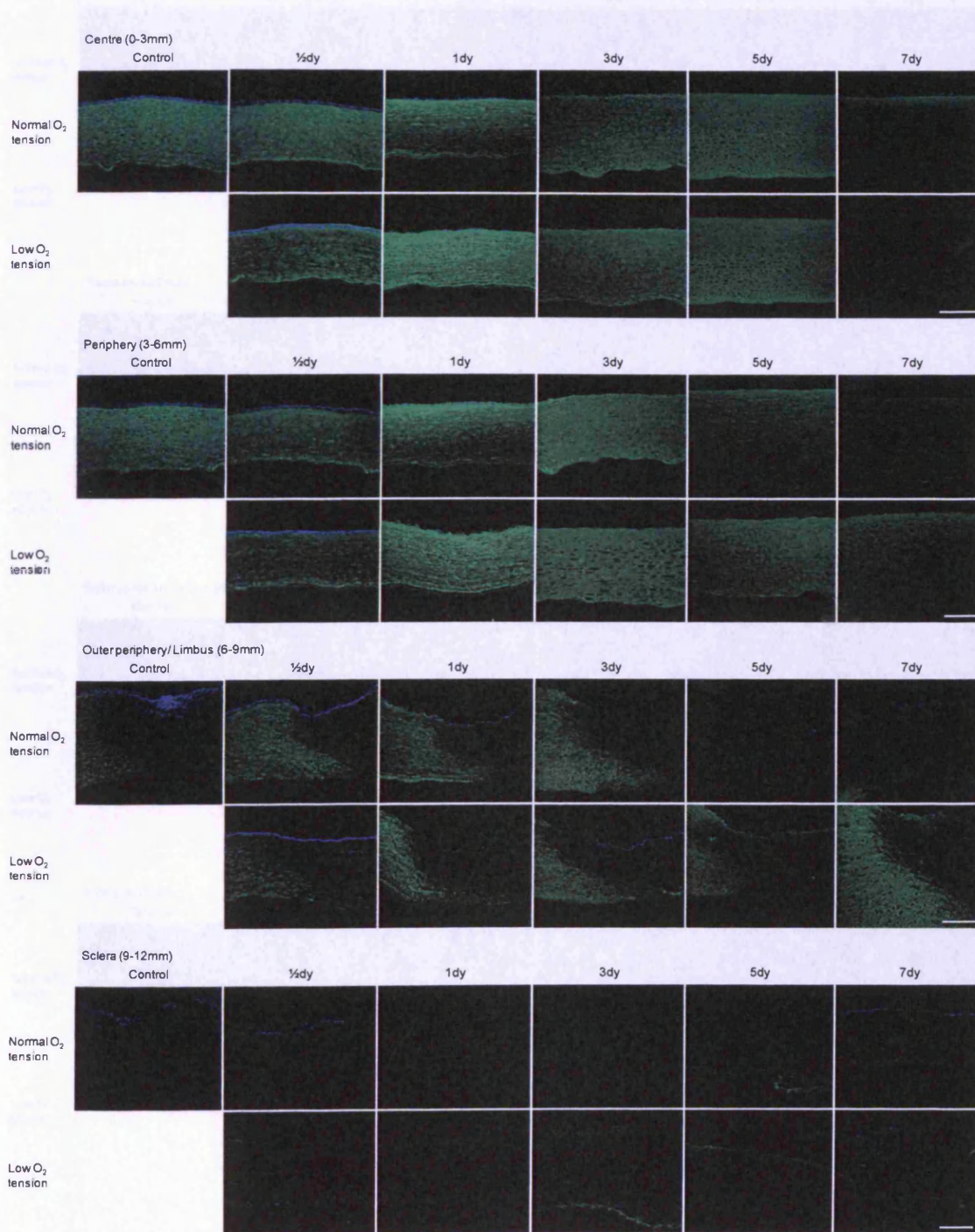


Figure 5.8 Immunolocalization of lesser-sulphated KS disaccharides (green), probed with 1B4 antibody and DAPI for cells (nucleus) (blue). Control = fresh tissue. Scale bar = 100  $\mu$ m.

*Immunolocalization of KS neoepitopes (N-acetyl-glucosamine-6-sulphate) at the non-reducing terminal of KS (BKS-1 antibody)*



**Figure 5.9** Immunolocalization of neoepitopes at the non-reducing terminal ends of KS (green), probed with BKS-1 antibody and DAPI for cells (nucleus) (blue). Control = fresh tissue. Scale bar = 100  $\mu$ m.

*Immunolocalization of KSPG: lumican*

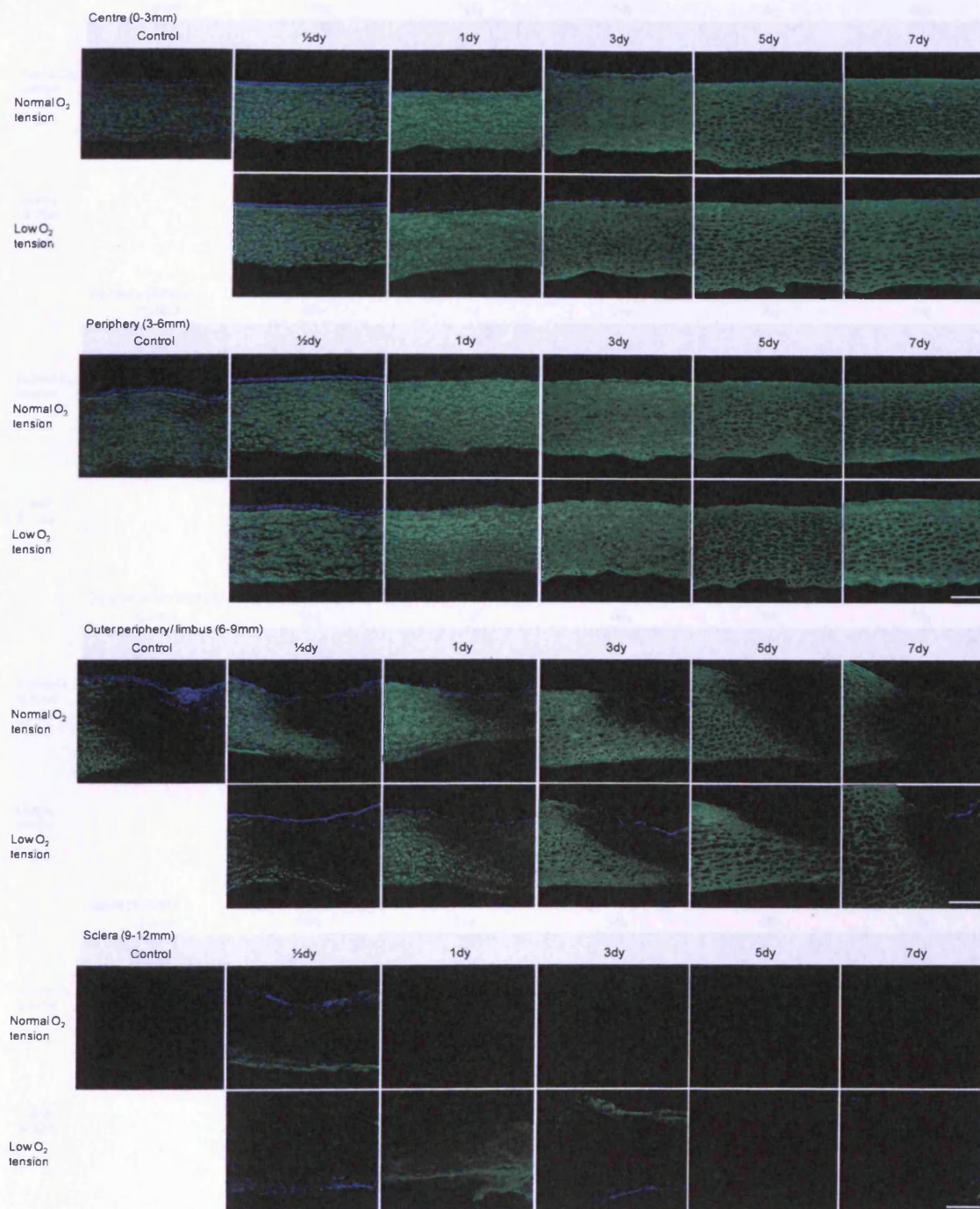


**Figure 5.10** Immunolocalization of lumican (green), probed with Lum-1 antibody and DAPI for cells (nucleus) (blue). Tissue sections were keratanase, keratanse II and chondroitinase ABC treated to remove the GAG chains. Control = fresh tissue. Scale bar = 100  $\mu$ m.

*Immunolocalization of KSPG: keratocan*

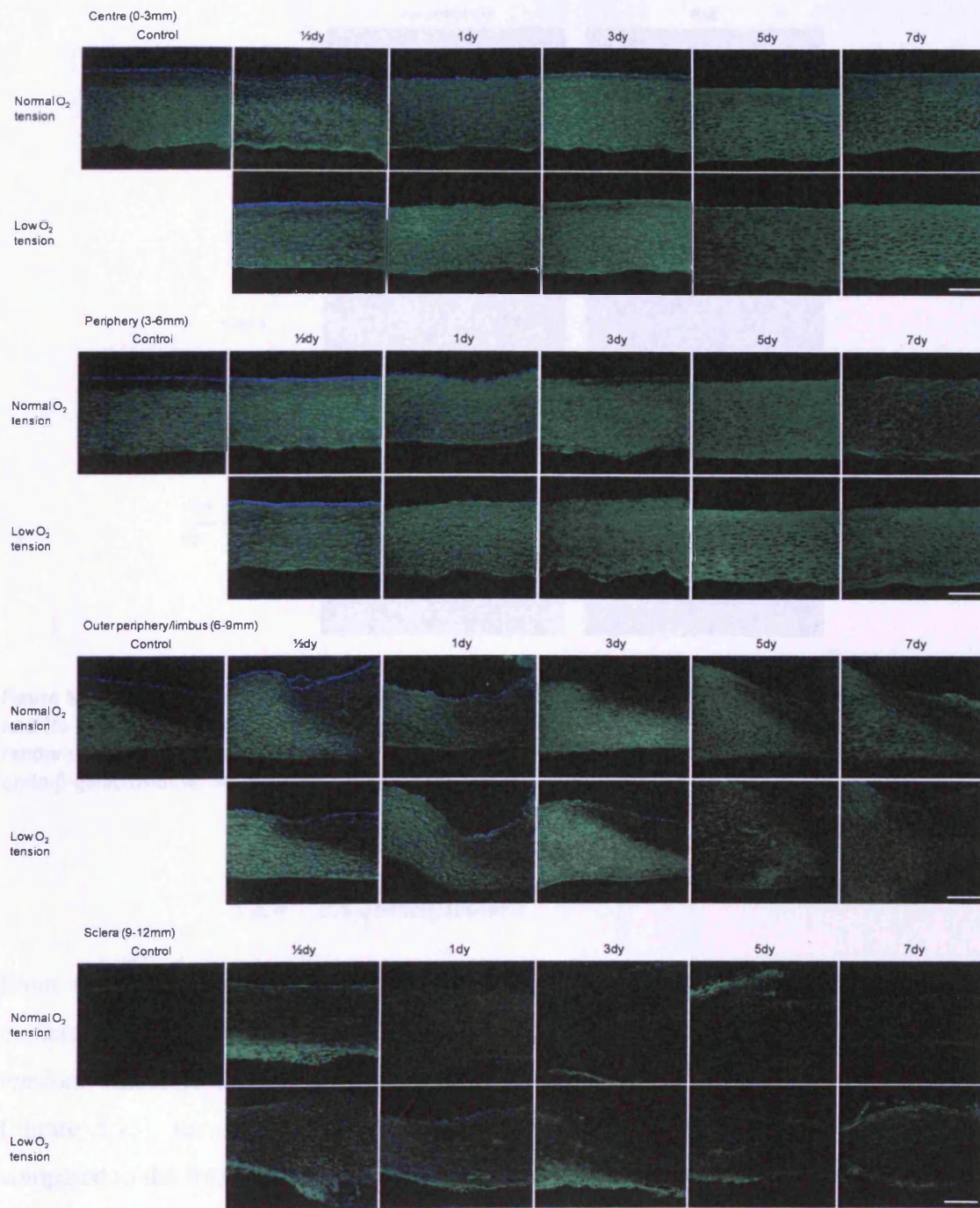


**Figure 5.11** Immunolocalization of keratocan (green), probed with Ker-1 antibody and DAPI for cells (nucleus) (blue). Tissue sections were keratanase, keratanse II and chondroitinase ABC treated to remove the GAG chains. Control = fresh tissue. Scale bar = 100  $\mu$ m.

*Negative control*

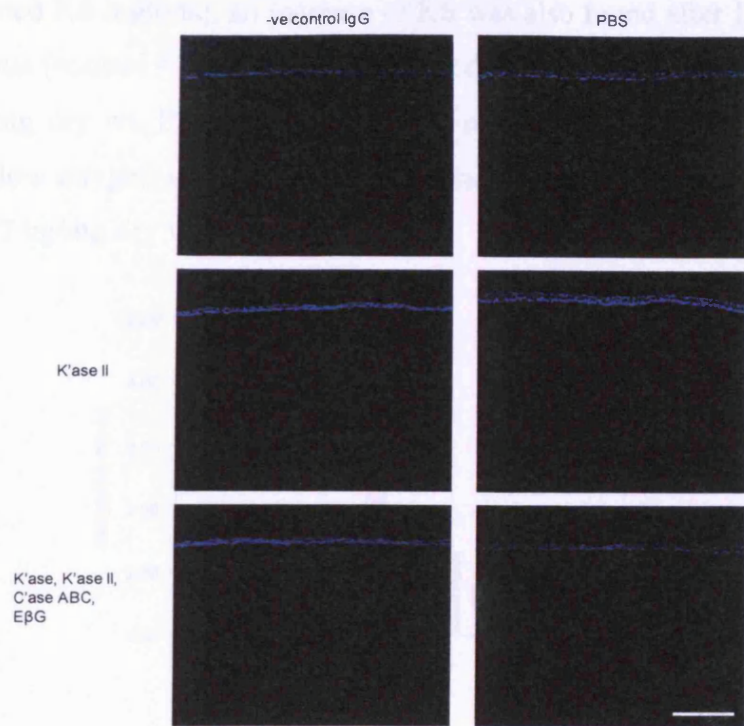


**Figure 5.12 Negative controls for immunolocalization of the different sulphation patterns of KS GAGs and its core proteins.** Controls showed negative staining to the specific primary antibodies and non random binding. K'ase and K'ase II = keratanase and keratanase II. C'ase ABC = chondroitinase ABC. EβG = endo-β-galactosidase. Scale bar = 100 μm.

#### 5.8.4 KS quantification

From the total sulphated GAG content and the immunohistochemistry data it was evident that the central regions of the cornea were greatly affected from the low O<sub>2</sub> tension. Therefore the KS content on the central regions of the cornea was quantified (Figure 5.13), the results showed an increase of over-sulphated KS within 12 hr compared to the fresh tissue (control =  $1.028 \pm 0.111$  ng/mg dry wt, low oxygen level =  $1.570 \pm 0.422$  ng/mg dry wt,  $P = 0.034$ ) and in 12 hr of normal atmospheric conditions (normal oxygen level =  $0.560 \pm 0.127$  ng/mg dry wt,  $P = \leq 0.001$ ). Most strikingly, a significant increase of over-sulphated KS was found after 1 day in low oxygen levels ( $4.009 \pm 0.279$  ng/mg dry wt) in comparisons to the fresh corneal tissue (control =  $1.028 \pm 0.111$  ng/mg dry wt,  $P = \leq 0.001$ ) and in 1 day normal atmospheric conditions ( $0.601 \pm 0.096$  ng/mg dry wt,  $P = \leq 0.001$ ). However, by the 3<sup>rd</sup> day of incubation, the amount of KS began to level off and minor differences were seen between the two

atmospheric conditions. As for lesser sulphated KS (using an epitope to recognize lesser sulphated KS regions), an increase of KS was also found after 1 day compared to the fresh tissue (control = 1.170 ± 0.204 ng/mg dry wt, 1 day low oxygen level = 1.912 ± 0.142 ng/mg dry wt, P = ≤0.01). However, minor differences were found between normal and low oxygen levels after 1 day of culturing (1 day normal oxygen level = 1.543 ± 0.277 ng/mg dry wt, P = 1.000).

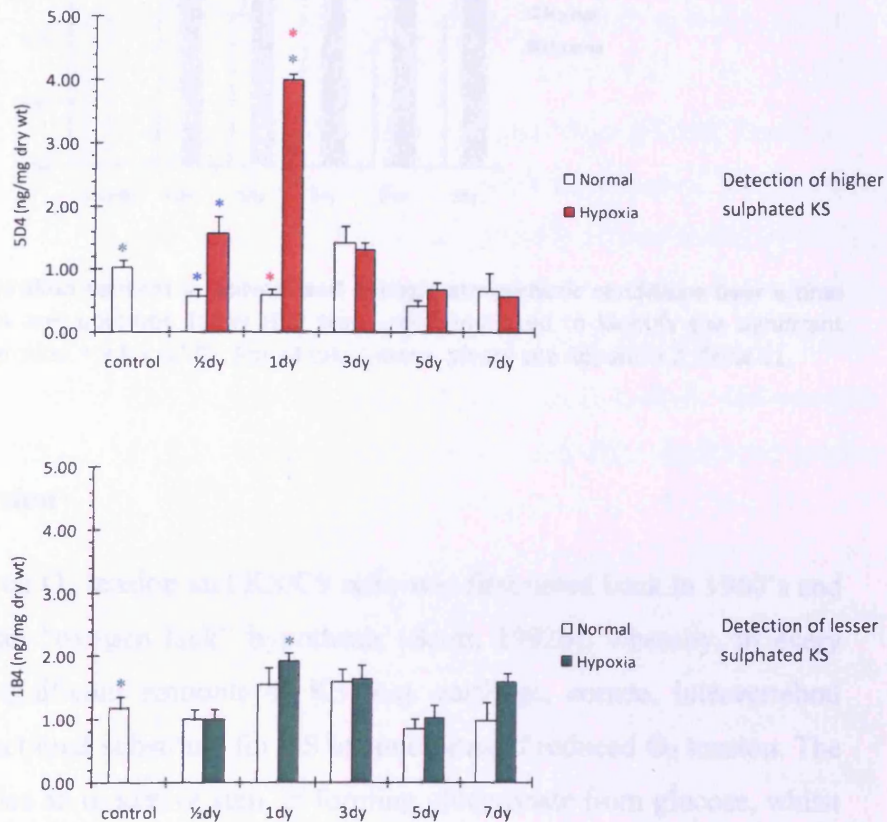


**Figure 5.13 Sulphation patterns of keratan sulphate in normal and hypoxic (2% O<sub>2</sub> level) organ cultured corneas at the central region.** 5D4 was used to probe higher/over sulphated KS. 1B4 was used to probe lesser sulphated KS. One-way ANOVA and post-hoc Tukey HSD tests were employed to identify the significant differences between the groups. \*,\*,\* P = ≤0.01. For all calculations, please see Appendix 2, Tables 9-10.

### 5.8.5 The effects of hydroxyproline content in low oxygen levels

The hydroxyproline data (Figure 5.14) also revealed after 1 day in O<sub>2</sub> deprivation, an increase of hydroxyproline content was found in comparison to the fresh tissue (control = 9 µg hydroxyproline/mg dry wt, 1 day low oxygen level = 10 µg hydroxyproline/mg dry wt, P = 0.010) and in 1 day normal atmospheric conditions (P = 0.052), suggesting

that low O<sub>2</sub> may play an important factor in collagen fibrogenesis as well as GAG synthesis. However, by the 3<sup>rd</sup> day of incubation in low O<sub>2</sub> minor significant changes were found between the two conditions.

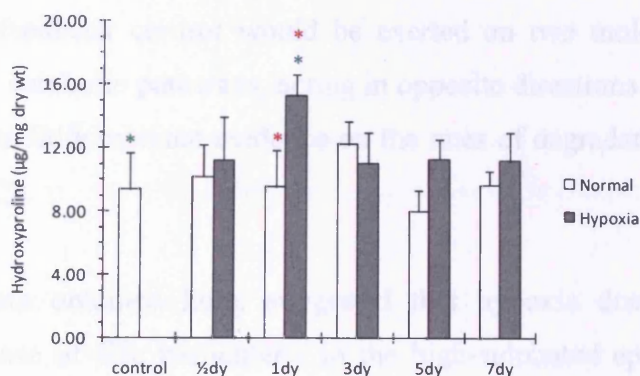


**Figure 5.14** The hydroxyproline content in normal and hypoxic atmospheric conditions over a time course. One-way ANOVA and post-hoc Tukey HSD tests were employed to identify the significant differences between the groups. \*,\* P = ≤0.01. For all calculations, please see Appendix 2, Table 11.

## 5.9 Discussion

The connection between O<sub>2</sub> tension and KS/CS ratio was first noted back in 1960's and later developed into an "oxygen lack" hypothesis (Scott, 1992b), whereby, in every ECM that contains significant amounts of KS (e.g. cartilage, cornea, intervertebral disc), KS can be a functional substitute for CS in conditions of reduced O<sub>2</sub> tension. The synthesis of CS includes an oxidative step, in forming glucuronate from glucose, whilst the sugars in KS (galactose and N-acetyl glucosamine) are not oxidized. Early studies hypothesized that CS synthesis has a net consumer of O<sub>2</sub> during the conversion of UDPGlc to UDPGlcUA, which is affected during low oxygen than that of KS, which does not consume O<sub>2</sub> at any stage of synthesis (Stockwell and Scott, 1965). The production of uridine diphosphate glucuronic acid is thought to be the key step, which is sensitive to hypoxia, lactate and NAD:NADH ratios.

Studies by Balduni *et al.* (1992), Stockwell and Scott (1965), Scott *et al.* (1987, 1992) have suggested the associations of O<sub>2</sub> tensions can influence the nature of the tissue, particularly during KS and CS/DS synthesis and breakdown. The tissue content of a given constituent is determined by the rates of biosynthesis and breakdown. In mature,

healthy tissue the two rates must balance. A change in circumstances leading to increased synthesis of KS, for example, must be followed by an increase in the rate of break down; otherwise the tissue content of KS would rise indefinitely. If there was a short lag before the rates balanced, KS content would increase to a new, stable level. This implies a feedback control would be exerted on two molecules, with different biosynthetic and catabolic pathways, acting in opposite directions as O<sub>2</sub> tension change. However, there is little relevant evidence on the rates of degradation or turnover of KS compared with CS.

The *in vitro* data obtained here, suggested that hypoxia does indeed result in a significant increase of KS, particularly in the high-sulphated epitope of KS in rabbit corneas after only 24 hr in organ culture at 2% atmospheric O<sub>2</sub> (Figure 5.13). Thus this may suggest that the turnover rate of KS is relatively rapid. However, a lesser sulphated KS, and therefore less hydrophilic, form of KS was essentially unchanged by O<sub>2</sub> deprivation. This probably due to the fact that rabbit corneas contain considerable quantities of oversulphated KS and very undersulphated CS-DS, similar to bovine cornea (Fransson and Anseth, 1967).

The mechanisms for making CS or KS are genetically defined. In the absence of the protein core there can be no PG, but conversely, it seems that many tissues contain protein cores that are not processed to (KS) PGs (Funderburgh, Caterson and Conrad, 1987), i.e. the GAG side chains do not grow, and thus it may suggest that the synthesis of GAG chains is a post-translational event.

Moreover, during KS synthesis, KS undergoes a series of steps, for example elongation and sulphation (Akama et al., 2002). In the absence of *Chst5* in KO mice (Hayashida et al., 2006) and sulfotransferase in human corneas with macular corneal dystrophy (Akama et al., 2000), an immature, truncated GAG and an atypical corneal phenotype are found. This may suggest that KS chain length and sulphation are governed by tissue-specific factors such as the presence of processing enzymes. The hydrophobicity provided by the sulphate may serve to prevent KS GAG chains collapsing during elongation and may explain the different sulphation between shorter and longer KS chains. The presence of increasing amounts of highly sulphated KS found after 1 day in low O<sub>2</sub> (Figure 5.13) may be due to the substrates for KS GAG production, such as 3

phosphoadenosine-5-phosphosulphate (PAPS) (Scott, 1992b), may facilitate the enhanced production of KS GAGs or KS chain length and/or greater sulphation. Coinciding with this, with greater sulphation could equate the allowance of more H<sub>2</sub>O molecules to bind along the chain, thus causing an increase of hydration in the cornea.

The cornea contains approximately 78% water and it can be thought as an elastic gel. Although the total concentration of the PGs in cornea is only 2%, there is increasing evidence that they are largely responsible for its swelling as well as water retention properties (Bettelheim and Plessy, 1975; Bettelheim and Goetz, 1976). The negative charge provided by the sulphation on the GAG chains is thought to bind onto water fluid, and exhibiting the hydration and swelling for the cornea. The hydration results obtained here (Section 5.5.1) showed that the corneas become hydrated over the culturing period, this may be due to the length of the KS chain being synthesised (as mentioned previously) or an increase production of KS GAGs and/or the depletion of ATP to function the water transport system in the endothelium, therefore causing the cornea to swell and become opaque.

Corneal swelling can be prevented by the continuous transport activity of the endothelial layer. The corneal endothelium governs the solutes (e.g. glucose) and nutrients from the aqueous humor to the superficial layers of the cornea, while at the same time, actively pumping water in the opposite direction from the stroma to the aqueous (known as the “pump-leak hypothesis”). This dual process is due to the Na<sup>+</sup>/K<sup>+</sup>ATPase and carbonic anhydrase located on the endothelium which they act as passive ion exchangers. The bicarbonate ions formed by the action of carbonic anhydrase are translocated across the cell membrane, allowing water to passively follow (Bonanno, 2003). Therefore, if the endothelium is damaged, the cells in the superficial layers of the cornea can become hypertonic with solutes and nutrients and as a consequence this can lead to cell apoptosis. This may explain by the 3<sup>rd</sup> to the 7<sup>th</sup> day of culturing, a low staining of cells was detected from the immuno studies.

Previous culture procedures have resulted in significant corneal swelling, particularly at the endothelial layer, which was reduced when corneas were cultured in base medium Dulbecco Modified Eagle Media (DMEM) containing 4 mM L-Glutamine and 10% Fetal Bovine Serum (FBS). However more recently, a media refinement based on a

concentration of 5% dextran has been used as a de-swelling agent evaluated to limit corneal swelling during long term culture. The thickness of the corneas increased with the time in culture, regardless of the type of media used (with or without dextran). Nash *et al.* (2010) showed the ability to successfully culture corneas for 22 days with reduced swelling in DMEM media with 5% dextran (Nash *et al.*, 2010). However, Borderie *et al.* (1997) found that the preservation of corneal swelling was moderate at 1-2 day, however by the 3-4 day of incubation, swelling was more severe in media containing dextran (Borderie *et al.*, 1997). The data presented here, also show similar results to Borderie and co-workers. In spite of this, there was very little difference in tissue hydration between the two atmospheric conditions.

Cells that are exposed to physical and chemical stresses from their environment undergo changes in expression of ECM genes in order to acclimatise or adapt themselves to new situations, resulting in remodelling of the ECM (Horino *et al.*, 2002). O<sub>2</sub> is a fundamental chemical of the ambient atmosphere and is essential for animals. O<sub>2</sub> takes part in energy production via oxidative phosphorylation in mitochondria, oxygenation of biomaterials for production of physiologically important molecules such as steroid hormone, catecholamines, and hydroxyproline in collagenous proteins.

In the case of collagen, recent studies (Horino *et al.*, 2002), have demonstrated low oxygen culture may cause the acceleration the hydroxylation of proline residues in procollagen during collagen synthesis in fetal rat lung fibroblasts. The data presented here, showed an increase in hydroxyproline during low O<sub>2</sub> tension, after 1 day, this may be due to upregulation in the synthesis of TGF-β1. As studies have showed that the synthesis of TGF-β1 was upregulated and causing the increase secretion of peptide synthesis (Falanga *et al.*, 1991).

It has been speculated that the ratio between KS and CS/DS is determined by rate of turnover of these GAG chains. Early studies have investigated the rates of reaction of the galactosyl transferase → KS and glucuronosyl transferase → CS, which are important in determining the balance of the synthesis of KS and CS. The K<sub>m</sub> of galactosyl transferase → KS for UDPGal was considerably lower than those of glucuronosyl transferase. In other words, minor amounts of the galactosyl transferase is need to produce KS than glucuronosyl transferase to produce CS and therefore may

mean that during KS production, galactosyl transferase is able to work optimally than glucuronosyl transferase in conditions of restricted supply of O<sub>2</sub> for example. The data given here showed that turnover rate of KS occurs relatively quickly.

Although our studies here focussed on KS, it would have been an interest in looking at the effects of CS in low O<sub>2</sub> condition and raise questions as to the whether if KS increases, does CS decrease in low O<sub>2</sub> and vice versa? Does the KS chain length just increase, meaning more sulphate groups on the chain during low O<sub>2</sub> conditions while CS remain low? Nevertheless, the extracellular spacing with the stromal matrix is limited and therefore there may be a feedback mechanism which reduces GAG synthesis when interfibrillar pressures become critical.

In summary the data suggests possible structural importance of corneal PGs in maintaining the collagenous ultrastructure and hydration status of the corneal stroma. In terms of the public health, this may be of interest and clinical importance to contact lens wearers.

6.1. GAGs and collagen fibril organization across the cornea

The overall matrix architecture is thought to be governed by the interactions between collagen fibrils and PG molecules modified with sulphated GAG side chains. The data presented in Chapter 3 and 4 is hoped to contribute a greater understanding in the role of sulphated GAGs in the GAG network, specifically in the context of collagen fibril organization.

Certain interactions have been identified (Dougherty et al., 2005) that may be important in the regulation of collagen fibril organization.

The corresponding polyanionic charges on the collagen fibrils may only be fully revealed on transection. From the data obtained, it would appear that the difference in the refractive index between the peripheral and central regions of the bovine cornea (Figures 4.2 and 4.3). The refractive index of the bovine cornea, distributed away from the centre is about 1.373 (1.374) near the centre (Figure 4.9) with the transection started to decrease the refractive index from the centre (Figure 4.1). It is possible that this decrease in refractive index is due to a greater role in the peripheral reduction of lamellae than in the central region. Further modeling studies on the bovine cornea would be needed to test this hypothesis. In addition, my data revealed that the hydroxyproline content also increased significantly across the cornea, this increase may contribute to the overall matrix network of collagen fibrils found in the different regions of the cornea.

Furthermore, my studies indicated that the refractive index is unlikely to alter across the cornea, as my data revealed that the total sulphated GAG content remained constant across the cornea. There are other components of the interstitial matrix that could alter, as there may be changes in composition. For that could change the refractive index. Early studies (Chiriacopol et al., 1975) have shown the possible transition between of KSPGs and DSPGs found across the bovine cornea. The aim of the whole project was to further expand on this and see if similar trends were seen in bovine

## 6.

### 6.1. GAGs and collagen fibril organization across the cornea

The corneal matrix architecture is thought to be governed by the interactions between collagen fibrils and PG molecules modified with sulphated GAG side chains. The data presented in Chapters 3 and 4 is hoped to contribute a greater understanding in the role of sulphated GAGs in the control of the collagen architecture in cornea. In addition, for the first time ever, depth profiled data from bovine corneas has been examined.

Corneal transparency decreases when moving from the central to the peripheral cornea (Doutch et al., 2008; Doutch, 2009). Doutch *et al.* (2008) modeled this loss of transparency peripherally and explained it by the fact that collagen fibril diameters also increased moving from central to peripheral cornea (Boote et al., 2003). In the human, the corresponding peripheral increase of corneal thickness had only a minor effect on transmission. From the data obtained in chapter 4, using either TEM or x-ray diffraction, there was a similar peripheral increase in fibril diameters in the bovine cornea (Figures 4.8 and 4.9). However, in the bovine cornea, diameters only start to increase at about 10-12 mm from the centre (Figure 4.9) whereas transmission started to decrease almost continuously away from the centre (Figure 4.1). It is possible that this thickness increase plays a more important role in the peripheral reduction in transmission than it does in humans, however, further modeling studies on the bovine cornea would be needed to test this hypothesis. In addition, my data revealed that the hydroxyproline content also increased significantly across the cornea, this increase may contribute to the amount and/or volume of collagen fibrils found in the different regions of the cornea.

Furthermore, my studies indicated that the refractive index is unlikely to alter across the cornea, as my data revealed that the total sulphated GAG content remained constant across the cornea. There are other constituents of the interfibrillar matrix that could alter, or there may be changes in unsulphated PGs that could change the refractive index. Early studies (Borcherding et al., 1975) have showed the possible transition change of KSPGs and DSPGs found across the human cornea. The aim of the whole project was to further expand on this and see if similar trends were seen in bovine

tissue. The hypothesis of this research was to investigate whether the changes in the sulphation patterns of GAG's are directly related to changes in ultrastructure, and hence transparency of the cornea.

From the whole study, our data showed that there is a direct correlation between the type of PG GAG chain and the organization of collagen fibrils from the central regions of the cornea to the limbus/sclera regions. In the central region of the cornea, the data revealed a uniform distribution of fibril diameters, lamellar arrangement, and of the overall amount of sulphated GAG chains. In general, particularly in large animals, such as a cow, KS is found to be the predominant (60-70% of total GAG) GAG chain type found in the cornea (Anseth, 1961; Borcharding et al., 1975). These authors have also found that in calf and pig corneas, the degree of sulphation are dependant on the length of the GAG chain. From the data, it was also evident that KS is the major GAG chain component throughout the cornea, particularly oversulphated KS.

From our studies, several significant changes appeared to take place between the outer periphery/limbus and the sclera. The amount of hydroxyproline, mean fibril diameter and the range of diameters increased greatly. The lamellae throughout this region were no longer uniform in either size or orientation. Recent small angle x-ray scattering studies also indicated that in human corneas, towards the periphery, the fibril diameter increased and appeared to merge with scleral fibres (Boote et al., 2011). This may have been due to the change in GAG types and their sulphations. For example the KS content from the central to the peripheral regions of the cornea reported here illustrated similar trends to Borcharding and co-workers' early work on human cornea (Borcharding et al., 1975). Their studies revealed that KS is found throughout the cornea and reduced towards the corneolimbus and beyond. Our study expanded on this, and showed that over-sulphated KS was found throughout the cornea, and lesser-sulphated KS was found more abundantly in the peripheral regions of the cornea.

The cornea that was stained with cupromeronic blue for TEM, showed two populations of electron dense filaments across the cornea. Studies have suggested that small chains connecting adjacent fibrils are KS (Scott, 1992a), whereas the CS/DS form longer multimeric chains that extend among several collagen fibrils (Lewis et al., 2010). From the current studies, large, electron dense chains were seen interconnecting

collagen fibrils, and were found throughout the corneal stroma, but were more apparent in the peripheral regions and in the deeper regions of the corneal stroma. However, these long GAG chain filaments were found to a lesser extent throughout the cornea compared to another sub-population of smaller GAG chains, which were seen to interconnect neighbouring fibrils and was found throughout the depths of the cornea. Nevertheless, further studies would be needed to confirm the different types of GAG chains.

Interestingly the immunohistochemistry data revealed that C-4-S was mainly present in the corneal stroma, with traces of unsulphated chondroitin (C-0-S) from the outer periphery onwards. C-6-S first appears in the posterior zone of the inner peripheral cornea, but increases such that it is present throughout all depths of the tissue by the time the limbus/sclera is reached. Early studies (Scott and Haigh, 1988b) have also found different patterns of sulphation in CS/DS GAGs. For example in bovine and rabbit corneas very little CS/DS is present, which is the main GAG component in rat and mouse corneas. The CS sulphation pattern of both rabbit (Scott and Haigh, 1988b) and bovine (Fransson and Anseth, 1967) corneas, was of a highly sulphated KS and low or undersulphated CS/DS. A transitional change of GAG chain type was also observed in TEM, where long electron dense filaments appeared more towards the periphery and posteriorly. In the sclera, the range of fibril diameter extended over 50 nm, however from observations it was difficult to observe the GAG chains, such that the fibrils were so large that the GAG chains appeared to be buried or squashed between fibrils (Figure 4.5-7). However, the amount of GAG chains did appear less per unit area on the micrograph images.

Early studies have reported (Meier and Hay, 1973; Meier and Hay, 1974a; Meier and Hay, 1974b) that both CS PGs and collagen of the primary stroma are produced by the embryonic chick corneal epithelium under the inductive influence of collagen from the lens basement membrane. Fibroblasts of mesenchymal origin migrate along the planes of the orthogonally arranged stromal “scaffold” and produce the secondary stroma. The fibroblasts do not begin to produce KS PG until the formation of the secondary stromas is essentially complete. In the human cornea, KS is not produced until the third trimester of pregnancy (Breen et al., 1970a). In addition, KS is found during latter stages of chick development (E12 to E18) (Liles et al., 2010). The evidence above has

shown that the formation of collagen fibrils of uniform diameter in the cornea does not involve KS. Early *in vivo* and *in vitro* studies (Wood, 1960; Toole and Lowther, 1968) have suggested that the size and orthogonal array of the collagen fibrils may be controlled by CS PGs.

The precise regulation of fibril spacing has been shown to be a requirement for maintaining corneal transparency (Maurice, 1957). This regular spacing between fibrils was demonstrated ultrastructurally using small x-ray diffraction, rather than TEM, which involves dehydration and fixation, and can distort *in vivo* fibril arrangement. Thus, measurements of interfibrillar spacing from micrograph images were not feasible, and so small angle x-ray diffraction was employed to measure the interfibrillar spacing as well as the fibril diameter. Using this technique allowed the tissue hydration to be maintained during the x-ray exposure so that processing artifacts could be eliminated. Furthermore, x-rays, like visible light, can pass through the entire corneal thickness, and the results thus represent averages throughout the corneal tissue, unlike EM, which requires considerable selectivity.

Early evidence (Breen et al., 1970b) has indicated that the GAGs containing PG surrounding the collagen fibrils of the cornea are covalently bound to the collagen. Due to the mutual repulsion of the highly negatively charged KS molecules on the surface of the PG subunits, their protein cores would orient perpendicular to the longitudinal axis of the collagen fibril. Such an arrangement would create a negatively charged field around each collagen fibril which would dynamically maintain precise spatial relationships between individual fibrils. Thus KS may serve to fine tune the matrix collagen fibril spacing during corneal growth for example (Liles et al., 2010).

## **6.2. GAGs and collagen fibril organization across the depths of the cornea**

GAG type distribution across the cornea may influence the fibril orientation and organization, so their location at different depths within the cornea may also be an important factor. The distribution of KS within the corneal stromal layer remains unclear. Early studies on cartilage (Stockwell and Scott, 1965) and cornea (Scott and Haigh, 1988b) emphasise the inverse relationship between tissue thickness and KS

content, and have provided parallel examples of the effects of KS tissue on low nutrient supply (e.g. low O<sub>2</sub>) during normal development. Studies have shown a gradient of KS content in the cornea, with KS increasing posteriorly (Anseth, 1961; Bettelheim and Goetz, 1976) which follows the decline of O<sub>2</sub> tension across the depth of the cornea. This would make sense such that KS PGs not only absorb water molecules to a great extent in comparison the CS/DS PGs but also transfer water molecules with ease since little is retained by them in the dehydration process (Bettelheim and Plessy, 1975). Therefore, finding KS at the posterior region, near the endothelium, hence near the aqueous humor may serve a purpose of facilitating the movement of water into the cornea via the endothelium (Na<sup>+</sup>/K<sup>+</sup> ATPase transporter and NaHCO<sub>3</sub> transporter pump) (Maurice, 1972; Bettelheim and Plessy, 1975; Hodson and Miller, 1976). Our current IHC studies showed no obvious KS GAG differences in the different depths of the stroma, as this may come down to the technique and preparations employed.

### 6.3. The effects of the cornea in low O<sub>2</sub>

As mentioned previously fibril orientation and arrangement is thought to be tightly regulated by the different complements of PGs and their GAG chains. It has been hypothesized that the balance of the two kinds of PG is dependent on the availability of O<sub>2</sub>, which must diffuse into the avascular tissue from the atmosphere (Scott and Haigh, 1988b). Scott and co-workers used the thickness of the cornea as the example for this hypothesis, such that the thicker the cornea the lower the average tissue O<sub>2</sub> tension would be (Scott and Bosworth, 1990; Scott, 1991b). No O<sub>2</sub> would be consumed *en route* from glucose to the constituent galactose and glucosamine residues of KS, whereas DS requires O<sub>2</sub> in the oxidation of glucose to hexuronic acid. KS would thus be a functional substitute for CS/DS in tissues where O<sub>2</sub> supplies are low (Scott and Haigh, 1988b). Organ cultured experiments have confirmed that the ratio of KS to CS/DS increased markedly as ambient O<sub>2</sub> partial pressure decreased (Balduini et al., 1992). Our preliminary *in vitro* data has suggested that hypoxia does indeed result in a significant increase in the high-sulphated KS in rabbit corneas after only 24 hr in organ culture at 2% atmospheric O<sub>2</sub>. But a lesser sulphated and therefore less hydrophilic form of KS was essentially unchanged by O<sub>2</sub> deprivation. Such different sulphation patterns found in the KS chain may be due the gene expression pattern, which may be altered under low O<sub>2</sub> tensions and therefore, the production of KSPG would be affected.

Alternatively, the biosynthesis of KSPG (or KS-GAG) is more efficient under a low O<sub>2</sub> conditions than that under the normal conditions as mentioned previously; therefore the substrates for KSPG production such as UDP-GlcNAc and PAPs may be more abundant in the cells at the hypoxic condition, leading enhanced KS-GAG production.

#### **6.4. Summary and future work**

The techniques used to study GAG chains and the associations with collagen fibrils has allowed us for the first time to show the possible changes between the sulphation of GAG chains and collagen fibrils across the bovine cornea as a function of position. In addition we have also shown the changes in fibril diameter and fibril spacing as a function of tissue depth from the corneal centre to the outer periphery/limbus and sclera. One might expect these fibril changes would also be associated with the different GAG types, or changes in the GAG sulphations, or the different swelling properties or different O<sub>2</sub> consumption level found in the different depths of the corneal stroma. The O<sub>2</sub> consumption level by the cornea can affect the type of GAG chain, particularly the KS sulphation level. Effectively the PG type and length of KS chain produced depend on the corneal thickness (Scott and Haigh, 1988b) and in our case, from our current studies, the cornea being deprived of O<sub>2</sub>. This O<sub>2</sub> consumption level by the cornea may be of interest to the biotech industry that produce and manufacture contact lenses to contact lens wearers.

A number of challenges lie ahead in the investigation of the interactions of GAG chains and their interactions with collagen fibrils from a structural and functional point of view. The results of our study have opened other possibilities, for example making comparisons with other species or investigating the role of GAGs in pathological corneas. One of the aims at the outset of this study was to investigate the collagen types that may contribute to the fibril diameter changes that were found in the outer periphery regions of the cornea. One would predict more type V collagen molecules found in small fibrils than large fibrils, as studies have suggested that the interaction of type I and type V collagen may contribute in regulating the diameter of fibrils (Marchant et al., 1996a) by limiting the lateral accretion of the heterotypic type I/V fibrils (Birk et al., 1988; Birk et al., 1990; Birk, 2001). However, due to the lack of antibodies available for type V collagen and the time constraints, it was difficult to carry out this

study. Furthermore, Fourier transform infrared spectroscopy (FTIR) (Ozaki, Mizuno and Kaneuchi, 1992; Belbachir et al., 2009) and liquid chromatography/electrospray ionization mass spectrometry (LC/ESI-MS) (Zhang et al., 2006) could be employed to investigate the collagen type changes qualitatively and/or quantitatively at their chemical composition level, as these techniques have shown specific fingerprint profile spectra corresponding to the different collagen types. In addition, these spectroscopy techniques could also show the possible changes in chemical composition levels of the different GAG types, for example the level of sulphate on the GAG chains may be altered as our KS quantification studies have showed.

From our preliminary studies on the effects of KS in low O<sub>2</sub> tension, further understanding is needed as to how and why the synthesis of KS, particularly highly sulphated KS, is influenced by O<sub>2</sub> level consumed by the cornea. If the gene expression patterns or the substrates for KSPG production are involved, effectively the types KSPG or KS-GAG chain length are affected. Therefore further studies involving in investigating the mRNA levels expressed of the respective KSPG and assays would be needed. Other studies involving corneas cultured in high levels of O<sub>2</sub> could also be carried out. For example, CS/DS synthesis is dependent on O<sub>2</sub>; therefore if high levels of O<sub>2</sub> are consumed by the cornea, would the levels of CS/DS increase and KS level remain constant or decrease in order to balance the total amount of GAGs present in the cornea? Early studies by Anseth (1969) showed that there was a decrease content of KS and CS GAGs in the rabbit stromal matrix after reversible edema was induced by endothelial cell wounding. Anseth also noted that after recovery from corneal edema, there was an increase in GAG content in the corneas (Anseth and Fransson, 1969). From our current studies the turnover rate of KS production occurred within 24 hr in low O<sub>2</sub> conditions, however if the cornea was resorted back to the normal atmospheric condition, would the KSPG (or KS-GAG) production resorted back to its original levels found in the cornea?

Kawachi S, Saito T, and Tanaka Y (1982) Subcellular localization characteristics of cathepsin B in cultured rat hepatoma cells. *Journal of Cell Biochemistry*, **18**, 1-10.

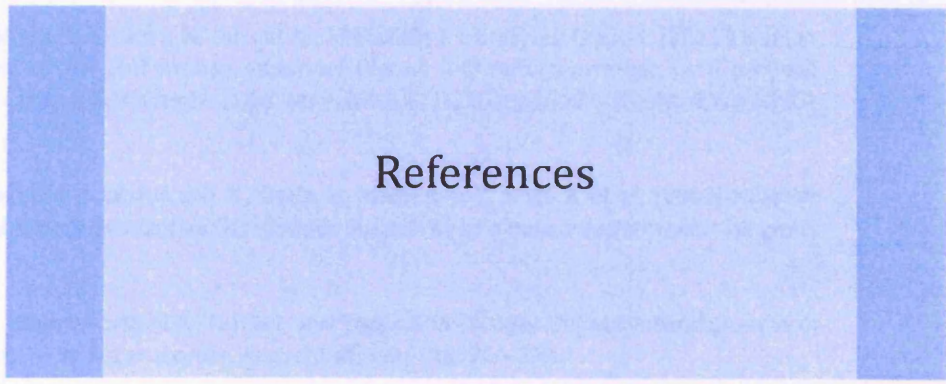
Marin G, Gherghel R, Gherghel S, V. Gherghel, V. P. Gherghel, C. and Gherghel S (2005) The effect of the presence of honey bees (*Apis mellifera*) on the development of *Trachea* in the presence of honey bees. *Journal of Cell Biochemistry*, **96**, 1-10.

Marin G, Gherghel R, Gherghel S, and Gherghel V (2005) The effect of the presence of honey bees (*Apis mellifera*) on the development of *Trachea* in the presence of honey bees. *Journal of Cell Biochemistry*, **96**, 1-10.

Marin G, Gherghel R, Gherghel S, and Gherghel V (2005) The effect of the presence of honey bees (*Apis mellifera*) on the development of *Trachea* in the presence of honey bees. *Journal of Cell Biochemistry*, **96**, 1-10.

Marin G, Gherghel R, Gherghel S, and Gherghel V (2005) The effect of the presence of honey bees (*Apis mellifera*) on the development of *Trachea* in the presence of honey bees. *Journal of Cell Biochemistry*, **96**, 1-10.

Marin G, Gherghel R, Gherghel S, and Gherghel V (2005) The effect of the presence of honey bees (*Apis mellifera*) on the development of *Trachea* in the presence of honey bees. *Journal of Cell Biochemistry*, **96**, 1-10.



References

Marin G, Gherghel R, Gherghel S, and Gherghel V (2005) The effect of the presence of honey bees (*Apis mellifera*) on the development of *Trachea* in the presence of honey bees. *Journal of Cell Biochemistry*, **96**, 1-10.

Marin G, Gherghel R, Gherghel S, and Gherghel V (2005) The effect of the presence of honey bees (*Apis mellifera*) on the development of *Trachea* in the presence of honey bees. *Journal of Cell Biochemistry*, **96**, 1-10.

Marin G, Gherghel R, Gherghel S, and Gherghel V (2005) The effect of the presence of honey bees (*Apis mellifera*) on the development of *Trachea* in the presence of honey bees. *Journal of Cell Biochemistry*, **96**, 1-10.

Marin G, Gherghel R, Gherghel S, and Gherghel V (2005) The effect of the presence of honey bees (*Apis mellifera*) on the development of *Trachea* in the presence of honey bees. *Journal of Cell Biochemistry*, **96**, 1-10.

Marin G, Gherghel R, Gherghel S, and Gherghel V (2005) The effect of the presence of honey bees (*Apis mellifera*) on the development of *Trachea* in the presence of honey bees. *Journal of Cell Biochemistry*, **96**, 1-10.

Marin G, Gherghel R, Gherghel S, and Gherghel V (2005) The effect of the presence of honey bees (*Apis mellifera*) on the development of *Trachea* in the presence of honey bees. *Journal of Cell Biochemistry*, **96**, 1-10.

Marin G, Gherghel R, Gherghel S, and Gherghel V (2005) The effect of the presence of honey bees (*Apis mellifera*) on the development of *Trachea* in the presence of honey bees. *Journal of Cell Biochemistry*, **96**, 1-10.

Marin G, Gherghel R, Gherghel S, and Gherghel V (2005) The effect of the presence of honey bees (*Apis mellifera*) on the development of *Trachea* in the presence of honey bees. *Journal of Cell Biochemistry*, **96**, 1-10.

Marin G, Gherghel R, Gherghel S, and Gherghel V (2005) The effect of the presence of honey bees (*Apis mellifera*) on the development of *Trachea* in the presence of honey bees. *Journal of Cell Biochemistry*, **96**, 1-10.

Marin G, Gherghel R, Gherghel S, and Gherghel V (2005) The effect of the presence of honey bees (*Apis mellifera*) on the development of *Trachea* in the presence of honey bees. *Journal of Cell Biochemistry*, **96**, 1-10.

- Abedin M Z, Ayad S, and Weiss J B (1982) Isolation and native characterization of cysteine-rich collagens from bovine placental tissues and uterus and their relationship to types IV and V collagens. *Biosci Rep* 2: 493-502.
- Achur R N, Muthusamy A, Madhunapantula S V, Bhavanandan V P, Seudieu C, and Channe Gowda D (2004) Chondroitin sulfate proteoglycans of bovine cornea: structural characterization and assessment for the adherence of Plasmodium falciparum-infected erythrocytes. *Biochim Biophys Acta* 1701: 109-119.
- Akama T O, Misra A K, Hindsgaul O, and Fukuda M N (2002) Enzymatic synthesis in vitro of the disulfated disaccharide unit of corneal keratan sulfate. *J Biol Chem* 277: 42505-42513.
- Akama T O, Nakayama J, Nishida K, Hiraoka N, Suzuki M, McAuliffe J, Hindsgaul O et al. (2001) Human corneal GlcNac 6-O-sulfotransferase and mouse intestinal GlcNac 6-O-sulfotransferase both produce keratan sulfate. *J Biol Chem* 276: J Biol Chem. 2001 May 2011;2276(2019):16271-16278. Epub 12001 Feb 16215.
- Akama T O, Nishida K, Nakayama J, Watanabe H, Ozaki K, Nakamura T, Dota A et al. (2000) Macular corneal dystrophy type I and type II are caused by distinct mutations in a new sulphotransferase gene. *Nat Genet* 26: 237-241.
- Akhtar S, Bron A J, Salvi S M, Hawksworth N R, Tuft S J, and Meek K M (2008a) Ultrastructural analysis of collagen fibrils and proteoglycans in keratoconus. *Acta Ophthalmol* 86: 764-772.
- Akhtar S, Kerr B C, Hayes A J, Hughes C E, Meek K M, and Caterson B (2008b) Immunochemical localization of keratan sulfate proteoglycans in cornea, sclera, and limbus using a keratanase-generated neoepitope monoclonal antibody. *Invest Ophthalmol Vis Sci* 49: 2424-2431.
- Andrikopoulos K, Liu X, Keene D R, Jaenisch R, and Ramirez F (1995) Targeted mutation in the col5a2 gene reveals a regulatory role for type V collagen during matrix assembly. *Nat Genet* 9: 31-36.
- Anseth A (1961) Studies on corneal polysaccharides. III. Topographic and comparative biochemistry. *Exp Eye Res* 1: 106-115.
- Anseth A, and Fransson L A (1969) Studies on corneal polysaccharides. VI. Isolation of dermatan sulfate from corneal scar tissue. *Exp Eye Res* 8: 302-309.
- Bairati A, and Gioria M (2004) Collagen fibrils of an invertebrate (*Sepia officinalis*) are heterotypic: immunocytochemical demonstration. *J Struct Biol* 147: 159-165.
- Balduini C, De Luca G, Passi A, Rindi S, Salvini R, and Scott J E (1992) Effect of oxygen tension and lactate concentration on keratan sulphate and chondroitin sulphate biosynthesis in bovine cornea. *Biochim Biophys Acta* 1115: 187-191.
- Bartold P M (1992) Distribution of chondroitin sulfate and dermatan sulfate in normal and inflamed human gingivae. *J dent res* 71: 1587-1593.
- Baum J P, Maurice D M, and McCarey B E (1984) The active and passive transport of water across the corneal endothelium. *Exp Eye Res* 39: 335-342.
- Beecher N, Carlson C, Allen B R, Kipchumba R, Conrad G W, Meek K M, and Quantock A J (2005) An x-ray diffraction study of corneal structure in mimecan-deficient mice. *Invest Ophthalmol Vis Sci* 46: 4046-4049.
- Belbachir K, Noreen R, Gouspillou G, and Petibois C (2009) Collagen types analysis and differentiation by FTIR spectroscopy. *Anal Bioanal Chem* 395: 829-837.

- 
- Berman E R (1991) *Biochemistry of the eye. Cornea*. New York, London: Plenum Press, pp. 89-138.
- Bettelheim F A, and Goetz D (1976) Distribution of hexosamines in bovine cornea. *Invest Ophthalmol* 15: 301-304.
- Bettelheim F A, and Plessy B (1975) The hydration of proteoglycans of bovine cornea. *Biochim Biophys Acta* 381: 203-214.
- Birk D E (2001) Type V collagen: heterotypic type I/V collagen interactions in the regulation of fibril assembly. *Micron* 32: 223-237.
- Birk D E, Fitch J M, Babiarz J P, Doane K J, and Linsenmayer T F (1990) Collagen fibrillogenesis in vitro: interaction of types I and V collagen regulates fibril diameter. *J Cell Sci* 95 ( Pt 4): 649-657.
- Birk D E, Fitch J M, Babiarz J P, and Linsenmayer T F (1988) Collagen type I and type V are present in the same fibril in the avian corneal stroma. *J Cell Biol* 106: 999-1008.
- Birk D E, Fitch J M, and Linsenmayer T F (1986) Organization of collagen types I and V in the embryonic chicken cornea. *Invest Ophthalmol Vis Sci* 27: 1470-1477.
- Birk D E, Hahn R A, Linsenmayer C Y, and Zycband E I (1996) Characterization of collagen fibril segments from chicken embryo cornea, dermis and tendon. *Matrix Biol* 15: 111-118.
- Birk D E, Nurminskaya M V, and Zycband E I (1995) Collagen fibrillogenesis in situ: fibril segments undergo post-depositional modifications resulting in linear and lateral growth during matrix development. *Dev Dyn* 202: 229-243.
- Bishop P (1996) The biochemical structure of mammalian vitreous. *Eye (Lond)* 10 ( Pt 6): 664-670.
- Bishop P N (2000) Structural macromolecules and supramolecular organisation of the vitreous gel. *Prog Retin Eye Res* 19: 323-344.
- Bjornheden T, Levin M, Evaldsson M, and Wiklund O (1999) Evidence of hypoxic areas within the arterial wall in vivo. *Arterioscler Thromb Vasc Biol* 19: 870-876.
- Blain E J, Gilbert S J, Hayes A J, and Duance V C (2006) Disassembly of the vimentin cytoskeleton disrupts articular cartilage chondrocyte homeostasis. *Matrix Biol* 25: 398-408.
- Blochberger T C, Vergnes J P, Hempel J, and Hassell J R (1992) cDNA to chick lumican (corneal keratan sulfate proteoglycan) reveals homology to the small interstitial proteoglycan gene family and expression in muscle and intestine. *J Biol Chem* 267: 347-352.
- Bonanno J A (1996) Contact lens induced corneal acidosis. *CJAO J.* 22: 70-74.
- Bonanno J A (2003) Identity and regulation of ion transport mechanisms in the corneal endothelium. *Prog Retin Eye Res* 22: 69-94.
- Boot-Handford R P, Tuckwell D S, Plumb D A, Rock C F, and Poulson R (2003) A novel and highly conserved collagen (pro(alpha)1(XXVII)) with a unique expression pattern and unusual molecular characteristics establishes a new clade within the vertebrate fibrillar collagen family. *J Biol Chem* 278: 31067-31077.
- Boote C, Dennis S, Huang Y, Quantock A J, and Meek K M (2005) Lamellar orientation in human cornea in relation to mechanical properties. *J Struct Biol* 149: 1-6.

- Boote C, Dennis S, Newton R H, Puri H, and Meek K M (2003) Collagen fibrils appear more closely packed in the prepupillary cornea: optical and biomechanical implications. *Invest Ophthalmol Vis Sci* 44: 2941-2948.
- Boote C, Kamma-Lorger C S, Hayes S, Harris J, Burghammer M, Hiller J, Terrill N J et al. (2011) Quantification of Collagen Organization in the Peripheral Human Cornea at Micron-Scale Resolution. *Biophys J* 101: 33-42.
- Borcherding M S, Blacik L J, Sittig R A, Bizzell J W, Breen M, and Weinstein H G (1975) Proteoglycans and collagen fibre organization in human corneal scleral tissue. *Exp Eye Res* 21: 59-70.
- Borderie V M, Baudrimont M, Lopez M, Carvajal S, and Laroche L (1997) Evaluation of the deswelling period in dextran-containing medium after corneal organ culture. *Cornea* 16: 215-223.
- Bredrup C, Knappskog P M, Majewski J, Rodahl E, and Boman H (2005) Congenital stromal dystrophy of the cornea caused by a mutation in the decorin gene. *Invest Ophthalmol Vis Sci* 46: 420-426.
- Breen M, Weinstein H G, Andersen M, and Veis A (1970a) Microanalysis and characterization of acidic glycosaminoglycans in human tissues. *Anal Biochem.* 35: 146-159.
- Breen M, Weinstein H G, Johnson R L, Veis A, and Marshall R T (1970b) Acidic glycosaminoglycans in human skin during fetal development and adult life. *Biochim Biophys Acta* 201: 54-60.
- Brown J R, Crawford B E, and Esko J D (2007) Glycan antagonists and inhibitors: a fount for drug discovery. *Crit Rev Biochem Mol Biol* 42: 481-515.
- Burgeson R E (1988) New collagens, new concepts. *Annu Rev Cell Biol* 4: 551-577.
- Carlson E C, Mamiya K, Liu C Y, Gendron R L, Birk D E, Funderburgh J L, and Kao W W (2003) Role of Cys41 in the N-terminal domain of lumican in ex vivo collagen fibrillogenesis by cultured corneal stromal cells. *Biochem J* 369: 461-468.
- Caterson B, Christner J E, and Baker J R (1983) Identification of a monoclonal antibody that specifically recognizes corneal and skeletal keratan sulfate. Monoclonal antibodies to cartilage proteoglycan. *J Biol Chem* 14: 8848-8854.
- Caterson B, Christner J E, Baker J R, and Couchman J R (1985) Production and characterization of monoclonal antibodies directed against connective tissue proteoglycans. *Fed Proc* 44: 386-393.
- Chakravarti S (2006) Focus on molecules: keratocan (KERA). *Exp Eye Res* 82: 183-184.
- Chakravarti S, Magnuson T, Lass J H, Jepsen K J, LaMantia C, and Carroll H (1998) Lumican regulates collagen fibril assembly: skin fragility and corneal opacity in the absence of lumican. *J Cell Biol* 141: 1277-1286.
- Chakravarti S, Petroll W M, Hassell J R, Jester J V, Lass J H, Paul J, and Birk D E (2000) Corneal opacity in lumican-null mice: defects in collagen fibril structure and packing in the posterior stroma. *Invest Ophthalmol Vis Sci* 41: 3365-3373.
- Chakravarti S, Stallings R L, SundarRaj N, Cornuet P K, and Hassell J R (1995) Primary structure of human lumican (keratan sulfate proteoglycan) and localization of the gene (LUM) to chromosome 12q21.3-q22. *Genomics* 27: 481-488.
- Chapman J A (1974) The staining pattern of collagen fibrils. I. An analysis of electron micrographs. *Connect Tissue Res.* 2: 137-150.

- Chapman J A, and Hulmes D J (1984) Electron microscopy of collagen fibril. In: Ruggeri A, and Motta P M (eds.) *Ultrastructure of the connective tissue matrix*. Lancaster: Martinus Nijhoff Publishers, pp. 1-33.
- Chen S, Roseman A M, and Saibil H R (1998) Electron microscopy of chaperonins. *Methods Enzymol* 290: 242-253.
- Cintron C, and Covington H I (1990) Proteoglycan distribution in developing rabbit cornea. *J Histochem Cytochem* 38: 675-684.
- Cintron C, Hassinger L C, Kublin C L, and Cannon D J (1978) Biochemical and ultrastructural changes in collagen during corneal wound healing. *J Ultrastruct Res* 65: 13-22.
- Connon C J, Meek K M, Kinoshita S, and Quantock A J (2004) Spatial and temporal alterations in the collagen fibrillar array during the onset of transparency in the avian cornea. *Exp Eye Res* 78: 909-915.
- Connon C J, Meek K M, Newton R H, Kenney M C, Alba S A, and Karageozian H (2000) Hyaluronidase treatment, collagen fibril packing, and normal transparency in rabbit corneas. *J Refract Surg* 16: 448-455.
- Cornuet P K, Blochberger T C, and Hassell J R (1994) Molecular polymorphism of lumican during corneal development. *Invest Ophthalmol Vis Sci* 35: 870-877.
- Corpus L M, Funderburgh J L, Funderburgh M L, Bottomley G S, Prakash S, and Conrad G W (1996) Molecular cloning and tissue distribution of keratocan. Bovine corneal keratan sulfate proteoglycan 37A. *J Biol Chem* 271: 9759-9763.
- Craig A S, and Parry D A (1981) Collagen fibrils of the vertebrate corneal stroma. *J Ultrastruct Res* 74: 232-239.
- Craig A S, Robertson J G, and Parry D A (1996) Preservation of corneal collagen fibril structure using low-temperature procedures for electron microscopy. *J Ultrastruct Mol Struct Res*. 96: 172-175.
- Crewe J M, and Armitage W J (2001) Integrity of Epithelium and Endothelium in Organ-Cultured Human Corneas *Invest Ophthalmol Vis Sci* 42: 1757-1761.
- Davidson E A, and Small W (1963) Metabolism in vivo of connective-tissue mucopolysaccharides: III. Chondroitin sulfate and keratosulfate of cartilage *Biochim Biophys Acta* 69: 459-463.
- Davies Y, Lewis D, Fullwood N J, Nieduszynski I A, Marcyniuk B, Albon J, and Tullo A (1999) Proteoglycans on normal and migrating human corneal endothelium. *Exp Eye Res* 68: 303-311.
- Daxer A, Misof K, Grabner B, Ettl A, and Fratzl P (1998) Collagen fibrils in the human corneal stroma: structure and aging. *Invest Ophthalmol Vis Sci* 39: 644-648.
- de Jong J G, Wevers R A, Laarakkers C, and Poorthuis B J (1989) Dimethylmethylene blue-based spectrophotometry of glycosaminoglycans in untreated urine: a rapid screening procedure for mucopolysaccharidoses. *Clin Chem* 35: 1472-1477.
- De Luca G, Speziale P, Rindi S, Balduini C, and Castellani A A (1976) Effect of some nucleotides on the regulation of glycosaminoglycan biosynthesis. *Connect Tissue Res* 4: 247-254.
- Dixon W S, and Bron A J (1973) Fluorescein angiographic demonstration of corneal vascularization in contact lens wearers. *Am J Ophthalmol* 75: 1010-1015.
- Dolhnikoff M, Morin J, Roughley P J, and Ludwig M S (1998) Expression of lumican in human lungs. *Am J Respir Cell Mol Biol* 19: 582-587.

- Doutch J (2009) *Modelling corneal transparency with reference to stromal architecture*. Cardiff University.
- Doutch J, Quantock A J, Smith V A, and Meek K M (2008) Light transmission in the human cornea as a function of position across the ocular surface: theoretical and experimental aspects. *Biophys J* 95: 5092-5099.
- Dunlevy J R, Beales M P, Berryhill B L, Cornuet P K, and Hassell J R (2000) Expression of the keratan sulfate proteoglycans lumican, keratocan and osteoglycin/mimecan during chick corneal development. *Exp Eye Res* 70: 349-362.
- Dykstra M J, and Reuss L E (2003) Techniques - Ultrathin section staining. In: Dykstra M J, and Reuss L E [eds.] *Biological electron microscopy: Theory, techniques, and troubleshooting*. (2nd edn.) New York: Kluwer Academic/Plenum Publishers, pp. 179-189.
- Edward D P, Thonar E J, Srinivasan M, Yue B J, and Tso M O (1990) Macular dystrophy of the cornea. A systemic disorder of keratan sulfate metabolism. *Ophthalmology* 97: 1194-1200.
- Edwards C A, and O'Brien W D, Jr. (1980) Modified assay for determination of hydroxyproline in a tissue hydrolyzate. *Clin Chim Acta* 104: 161-167.
- El-Shabrawi Y, Kublin C L, and Cintron C (1998) mRNA levels of alpha1(VI) collagen, alpha1(XII) collagen, and beta ig in rabbit cornea during normal development and healing. *Invest Ophthalmol Vis Sci* 39: 36-44.
- Esko J D, Kimata K, and Lindahl U (2008) *Essentials of glycobiology*. Second ed. Cold Spring Harbor Laboratory Press, U.S.
- Falanga V, Martin T A, Takagi H, Kirsner R S, Helfman T, Pardes J, and Ochoa M S (1993) Low oxygen tension increases mRNA levels of alpha 1 (I) procollagen in human dermal fibroblasts. *J Cell Physiol* 157: 408-412.
- Falanga V, Quian S W, Danielpour D, Katz M H, Roberts A B, and Sporn M B (1991) Hypoxia upregulates the synthesis of TGF-beta 1 by human dermal fibroblasts. *J Invest Dermatol* 97: 634-637.
- Falanga V, Zhou L, and Yufit T (2002) Low oxygen tension stimulates collagen synthesis and COL1A1 transcription through the action of TGF-beta1. *J Cell Physiol* 191: 42-50.
- Farrell R A, and Hart R W (1969) On the theory of the spatial organization of macromolecules in connective tissue. *Bull Math Biophys* 31: 727-760.
- Farrell R A, and McCally R L (2000) Corneal Transparency. In: Albert D M, and JAKOBIEC F A [eds.] *Principles and Practice of Ophthalmology*. Philadelphia: W.B. Saunders Company., pp. 629-643.
- Fatt I, and St Helen R (1971) Oxygen tension under an oxygen-permeable contact lens. *Am J Optom Arch Am Acad Optom* 48: 545-555.
- Fitch J M, Birk D E, Mentzer A, Hasty K A, Mainardi C, and Linsenmayer T F (1988) Corneal collagen fibrils: dissection with specific collagenases and monoclonal antibodies. *Invest Ophthalmol Vis Sci* 29: 1125-1136.
- Fitzgerald J, and Bateman J F (2001) A new FACIT of the collagen family: COL21A1. *FEBS Lett* 505: 275-280.
- Fleischmajer R, MacDonald E D, Perlish J S, Burgeson R E, and Fisher L W (1990) Dermal collagen fibrils are hybrids of type I and type III collagen molecules. *J Struct Biol* 105: 162-169.

- Forrester J V, Dick A D, McMenemy P G, and Lee W R (2002) *The eye. Basic sciences in practice*. (2nd Edition edn.) Edinburgh, London, New York, Philadelphia, St. Louis, Sydney, Toronto.: Harcourt Publishers Limited, pp. ix-167.
- Fransson L A, and Anseth A (1967) Studies on corneal polysaccharides. IV. Chromatography of corneal glycosaminoglycans on ECTEOLA cellulose using formate buffers as eluting solvents. *Exp Eye Res* 6: 107-119.
- Fratzl P, and Daxer A (1993) Structural transformation of collagen fibrils in corneal stroma during drying. An x-ray scattering study. *Biophys J* 64: 1210-1214.
- Freund D E, McCally R L, Farrell R A, Cristol S M, L'Hernault N L, and Edelhauser H F (1995) Ultrastructure in anterior and posterior stroma of perfused human and rabbit corneas. Relation to transparency. *Invest Ophthalmol Vis Sci* 36: 1508-1523.
- Fullwood N J, and Meek K M (1993) A synchrotron X-ray study of the changes occurring in the corneal stroma during processing for electron microscopy. *J Microsc* 169: 53-60.
- Funderburgh J L (2000) Keratan sulfate: structure, biosynthesis, and function. *Glycobiology* 10: 951-958.
- Funderburgh J L (2002) Keratan sulfate biosynthesis. *IUBMB Life* 54: 187-194.
- Funderburgh J L, Caterson B, and Conrad G W (1987) Distribution of proteoglycans antigenically related to corneal keratan sulfate proteoglycan. *J Biol Chem* 1987: 11634-11640.
- Funderburgh J L, Corpuz L M, Roth M R, Funderburgh M L, Tasheva E S, and Conrad G W (1997) Mimecan, the 25-kDa corneal keratan sulfate proteoglycan, is a product of the gene producing osteoglycin. *J Biol Chem* 272: 28089-28095.
- Funderburgh J L, Funderburgh M L, Brown S J, Vergnes J P, Hassell J R, Mann M M, and Conrad G W (1993) Sequence and structural implications of a bovine corneal keratan sulfate proteoglycan core protein. Protein 37B represents bovine lumican and proteins 37A and 25 are unique. *J Biol Chem* 268: 11874-11880.
- Funderburgh J L, Funderburgh M L, Mann M M, and Conrad G W (1991a) Arterial lumican. Properties of a corneal-type keratan sulfate proteoglycan from bovine aorta. *J Biol Chem* 266: 24773-24777.
- Funderburgh J L, Funderburgh M L, Mann M M, and Conrad G W (1991b) Unique glycosylation of three keratan sulfate proteoglycan isoforms. *J Biol Chem* 266: 14226-14231.
- Gandhi N S, and Mancera R L (2008) The structure of glycosaminoglycans and their interactions with proteins. *Chem Biol Drug Des* 72: 455-482.
- Gealy E C, Kerr B C, Young R D, Tudor D, Hayes A J, Hughes C E, Caterson B et al. (2007) Differential expression of the keratan sulphate proteoglycan, keratocan, during chick corneal embryogenesis. *Histochem Cell Biol* 128: 551-555.
- Gelse K, Poschl E, and Aigner T (2003) Collagens--structure, function, and biosynthesis. *Adv Drug Deliv Rev* 55: 1531-1546.
- Giunta C, and Steinmann B (2000) Compound heterozygosity for a disease-causing G1489E [correction of G1489D] and disease-modifying G530S substitution in COL5A1 of a patient with the classical type of Ehlers-Danlos syndrome: an explanation of intrafamilial variability? *Am J Med Genet* 90: 72-79.
- Goldoni S, Owens R T, McQuillan D J, Shriver Z, Sasisekharan R, Birk D E, Campbell S et al. (2004) Biologically active decorin is a monomer in solution. *J Biol Chem* 279: 6606-6612.

- Goodfellow J M, Elliott G F, and Woolgar A E (1978) X-ray diffraction studies of the corneal stroma. *J Mol Biol* 119: 237-252.
- Goodhew P J [ed.] (1975) *Electron microscopy and analysis*. London: Wykeham publications.
- Gordon M K, and Hahn R A (2010) Collagens. *Cell Tissue Res* 339: 247-257.
- Gregory J D, Damle S P, Covington H I, and Cintron C (1988) Developmental changes in proteoglycans of rabbit corneal stroma. *Invest Ophthalmol Vis Sci* 29: 1413-1417.
- Grover J, Chen X N, Korenberg J R, and Roughley P J (1995) The human lumican gene. Organization, chromosomal location, and expression in articular cartilage. *J Biol Chem* 270: 21942-21949.
- Häkkinen L, Strassburger S, Kähäri V M, Scott P G, Eichstetter I, Lozzo R V, and Larjava H (2000) A role for decorin in the structural organization of periodontal ligament. *Lab Invest* 80: 1869-1880.
- Hascall V C, and Sajdera S W (1969) Proteinpolysaccharide complex from bovine nasal cartilage. The function of glycoprotein in the formation of aggregates. *J Biol Chem* 244: 2384-2396.
- Hasegawa N, Torii T, Kato T, Miyajima H, Furuhashi A, Nakayasu K, Kanai A et al. (2000) Decreased GlcNAc 6-O-sulfotransferase activity in the cornea with macular corneal dystrophy. *Invest Ophthalmol Vis Sci* 41: 3670-3677.
- Hassell J, Newsome D A, Krachmer J H, and Rodrigues M (1980) Macular corneal dystrophy: failure to synthesize a mature keratan sulfate proteoglycan. *Proc Natl Acad Sci U S A* 77: 3705-3709.
- Hassell J R, Kimura J H, and Hascall V C (1986) Proteoglycan core protein families. *Annu Rev Biochem* 55: 539-567.
- Hayashida Y, Akama T O, Beecher N, Lewis P, Young R D, Meek K M, Kerr B et al. (2006) Matrix morphogenesis in cornea is mediated by the modification of keratan sulfate by GlcNAc 6-O-sulfotransferase. *Proc Natl Acad Sci U S A* 103: 13333-13338.
- Hedbom E, and Heinegard D (1993) Binding of fibromodulin and decorin to separate sites on fibrillar collagens. *J Biol Chem* 268: 27307-27312.
- Heinegard D, and Sommarin Y (1987) Isolation and characterization of proteoglycans. *Methods Enzymol* 144: 319-372.
- Heldblom E E (1961) The role of polysaccharides in corneal swelling. *Exp Eye Res* 1: 81-91.
- Helfman T, and Falanga V (1993) Gene expression in low oxygen tension. *Am J Med Sci* 306: 37-41.
- Hirsch M, Prenant G, and Renard G (2001) Three-dimensional supramolecular organization of the extracellular matrix in human and rabbit corneal stroma, as revealed by ultrarapid-freezing and deep-etching methods. *Exp Eye Res* 72: 123-135.
- Hodge A J, and Schmitt F O (1960) The charge profile of the tropocollagen macromolecule and the packing arrangement in native-type collagen fibrils. *Proc Natl Acad Sci U S A* 46: 186-197.
- Hodson S, and Miller F (1976) The bicarbonate ion pump in the endothelium which regulates the hydration of rabbit cornea. *J Physiol* 263: 563-577.
- Holmes D F, Gilpin C J, Baldock C, Ziese U, Koster A J, and Kadler K E (2001) Corneal collagen fibril structure in three dimensions: Structural insights into fibril assembly, mechanical properties, and tissue organization. *Proc Natl Acad Sci U S A* 98: 7307-7312.

- 
- Horino Y, Takahashi S, Miura T, and Takahashi Y (2002) Prolonged hypoxia accelerates the posttranscriptional process of collagen synthesis in cultured fibroblasts. *Life Sci* 71: 3031-3045.
- Huang Y, and Meek K M (1999) Swelling studies on the cornea and sclera: the effects of pH and ionic strength. *Biophys J* 77: 1655-1665.
- Hukins D W L, and Aspden, R. M. (1985) Composition and properties of connective tissues. *Trends Biochem Sci* 10: 260-264.
- Hulmes D J, Jesior J C, Miller A, Berthet-Colominas C, and Wolff C (1981) Electron microscopy shows periodic structure in collagen fibril cross sections. *Proc Natl Acad Sci U S A* 78: 3567-3571.
- Hulmes D J, and Miller A (1981) Molecular Packing in Collagen. *Nature* 293: 234-239.
- Ihanamäki T, Pelliniemi L J, and Vuorio E (2004) Collagens and collagen-related matrix components in the human and mouse eye. *Prog Retin Eye Res* 23: 403-434.
- Imberty A, Lortat-Jacob H, and Perez S (2007) Structural view of glycosaminoglycan-protein interactions. *Carbohydr Res* 342: 430-439.
- Iozzo R V (1997) The family of the small leucine-rich proteoglycans: key regulators of matrix assembly and cellular growth. *Crit Rev Biochem Mol Biol* 32: 141-174.
- Iozzo R V (1998) Matrix proteoglycans: from molecular design to cellular function. *Annu Rev Biochem* 67: 609-652.
- Iozzo R V (1999) The biology of the small leucine-rich proteoglycans. Functional network of interactive proteins. *J Biol Chem* 274: 18843-18846.
- Iozzo R V, Moscatello D K, McQuillan D J, and Eichstetter I (1999) Decorin is a biological ligand for the epidermal growth factor receptor. *J Biol Chem* 274: 4489-4492.
- Iozzo R V, and Murdoch A D (1996) Proteoglycans of the extracellular environment: clues from the gene and protein side offer novel perspectives in molecular diversity and function. *Faseb J* 10: 598-614.
- Jaakkola P, and Jalkanen M (1999) Transcriptional regulation of Syndecan-1 expression by growth factors. *Prog Nucleic Acid Res Mol Biol* 63: 109-138.
- Jalbert I, and Stapleton F (2005) The corneal stroma during contact lens wear. *Cont Lens Anterior Eye* 28: 3-12.
- Jay G D, Tantravahi U, Britt D E, Barrach H J, and Cha C J (2001) Homology of lubricin and superficial zone protein (SZP): products of megakaryocyte stimulating factor (MSF) gene expression by human synovial fibroblasts and articular chondrocytes localized to chromosome 1q25. *J Orthop Res* 19: 677-687.
- Kadler K E, Baldock C, Bella J, and Boot-Handford R P (2007) Collagens at a glance. *J Cell Sci* 120: 1955-1958.
- Kadler K E, Holmes D F, Trotter J A, and Chapman J A (1996) Collagen fibril formation. *Biochem J* 316 ( Pt 1): 1-11.
- Kanai A, and Kaufman H E (1973) Electron microscopic studies of corneal stroma: aging changes of collagen fibers. *Ann Ophthalmol* 5: 285-287 passim.
- Kao W W, Funderburgh J L, Xia Y, Liu C Y, and Conrad G W (2006) Focus on molecules: lumican. *Exp Eye Res* 82: 3-4.

- Keene D R, Lunstrum G P, Morris N P, Stoddard D W, and Burgeson R E (1991) Two type XII-like collagens localize to the surface of banded collagen fibrils. *J Cell Biol* 113: 971-978.
- Kern P, Menasche M, and Robert L (1991) Relative rates of biosynthesis of collagen type I, type V and type VI in calf cornea. *Biochem J* 274: 615-617.
- Khoshnoodi J, Cartailier J P, Alvares K, Veis A, and Hudson B G (2006) Molecular recognition in the assembly of collagens: terminal noncollagenous domains are key recognition modules in the formation of triple helical protomers. *J Biol Chem* 281: 38117-38121.
- Kim S B, Kang S A, Park J S, Lee J S, and Hong C D (1996) Effects of hypoxia on the extracellular matrix production of cultured rat mesangial cells. *Nephron* 72: 275-280.
- Kitayama K, Hayashida Y, Nishida K, and Akama T O (2007) Enzymes responsible for synthesis of corneal keratan sulfate glycosaminoglycans. *J Biol Chem* 282: 30085-30096.
- Kjellen L, and Lindahl U (1991) Proteoglycans: structures and interactions. *Annu Rev Biochem* 60: 443-475.
- Klintworth G K (1976) Tissue culture in the inherited corneal dystrophies: possible applications and problems. *Birth Defects Orig Artic Ser* 12: 115-132.
- Klyce S D (1981) Stromal lactate accumulation can account for corneal oedema osmotically following epithelial hypoxia in the rabbit. *J Physiol* 321: 49-64.
- Knupp C, and Squire J M (2001) A new twist in the collagen story--the type VI segmented supercoil. *Embo J* 20: 372-376.
- Knupp C, and Squire J M (2005) Molecular packing in network-forming collagens. *Adv Protein Chem* 70: 375-403.
- Koch M, Bohrmann B, Matthison M, Hagios C, Trueb B, and Chiquet M (1995) Large and small splice variants of collagen XII: differential expression and ligand binding. *J Cell Biol* 130: 1005-1014.
- Koga T, Inatani M, Hirata A, Inomata Y, Zako M, Kimata K, Oohira A et al. (2005) Expression of a chondroitin sulfate proteoglycan, versican (PG-M), during development of rat cornea. *Curr Eye Res* 30: 455-463.
- Kokenyesi R, and Bernfield M (1994) Core protein structure and sequence determine the site and presence of heparan sulfate and chondroitin sulfate on syndecan-1. *J Biol Chem* 269: 12304-12309.
- Komai Y, and Ushiki T (1991) The three-dimensional organization of collagen fibrils in the human cornea and sclera. *Invest Ophthalmol Vis Sci* 32: 2244-2258.
- Kresse H, Hausser H, and Schonherr E (1993) Small proteoglycans. *Experientia* 49: 403-416.
- Lehmann O J, El-ashry M F, Ebenezer N D, Ocaka L, Francis P J, Wilkie S E, Patel R J et al. (2001) A novel keratocan mutation causing autosomal recessive cornea plana. *Invest Ophthalmol Vis Sci* 42: 3118-3122.
- Lewis P N, Pinali C, Young R D, Meek K M, Quantock A J, and Knupp C (2010) Structural interactions between collagen and proteoglycans are elucidated by three-dimensional electron tomography of bovine cornea. *Structure* 18: 239-245.
- Li W, Vergnes J P, Cornuet P K, and Hassell J R (1992) cDNA clone to chick corneal chondroitin/dermatan sulfate proteoglycan reveals identity to decorin. *Arch Biochem Biophys* 296: 190-197.

- Liesegang T J (2002) Physiologic changes of the cornea with contact lens wear. *CLAO J* 28: 12-27.
- Liles M, Palka B P, Harris A, Kerr B, Hughes C, Young R D, Meek K M et al. (2010) Differential relative sulfation of Keratan sulfate glycosaminoglycan in the chick cornea during embryonic development. *Invest Ophthalmol Vis Sci* 51: 1365-1372.
- Linsenmayer T F, Fitch J M, Schmid T M, Zak N B, Gibney E, Sanderson R D, and Mayne R (1983) Monoclonal antibodies against chicken type V collagen: production, specificity, and use for immunocytochemical localization in embryonic cornea and other organs. *J Cell Biol* 96: 124-132.
- Liu C Y, Birk D E, Hassell J R, Kane B, and Kao W W (2003) Keratan-deficient mice display alterations in corneal structure. *J Biol Chem* 278: 21672-21677.
- Lui N P, Baldwin J, Lennon F, Stajich J M, Thonar E J, Pericak-Vance M A, Klintworth G K et al. (1998) Coexistence of macular corneal dystrophy types I and II in a single sibship. *Br J Ophthalmol* 82: 241-244.
- Madri J A, Foellmer H G, and Furthmayr H (1982) Type V collagens of the human placenta: trimer alpha-chain composition, ultrastructural morphology and peptide analysis. *Coll Relat Res* 2: 19-29.
- Maldonado-Codina C, Morgan P B, Schnider C M, and Efron N (2004) Short-term physiologic response in neophyte subjects fitted with hydrogel and silicone hydrogel contact lenses. *Optom Vis Sci* 81: 911-921.
- Marchant J K, Hahn R A, Linsenmayer T F, and Birk D E (1996a) Reduction of type V collagen using a dominant-negative strategy alters the regulation of fibrillogenesis and results in the loss of corneal-specific fibril morphology. *J Cell Biol* 135: 1415-1426.
- Marchant J K, Hahn R A, Linsenmayer T F, and E. B D (1996b) Reduction of type V collagen using a dominant-negative strategy alters the regulation of fibrillogenesis and results in the loss of corneal-specific fibril morphology. *J Cell Biol* 135: 1415-1426.
- Marshall G E, Konstas A G, and Lee W R (1993) Collagens in ocular tissues. *Br J Ophthalmol* 77: 515-524.
- Maurice D M (1957) The structure and transparency of the cornea. *J Physiol* 136: 263-286.
- Maurice D M (1962) Clinical physiology of the cornea. *Int Ophthalmol Clin* 2: 561-572.
- Maurice D M (1972) The location of the fluid pump in the cornea. *J Physiol* 221: 43-54.
- Mayne R, Brewton R G, Mayne P M, and Baker J R (1993) Isolation and characterization of the chains of type V/type XI collagen present in bovine vitreous. *J Biol Chem* 268: 9381-9386.
- McEwan P A, Scott P G, Bishop P N, and Bella J (2006) Structural correlations in the family of small leucine-rich repeat proteins and proteoglycans. *J Struct Biol* 155: 294-305.
- McTigue J W (1967) The human cornea: a light and electron microscopic study of the normal cornea and its alterations in various dystrophies. *Trans Am Ophthalmol Soc* 65: 591-660.
- Meek K M, Blamires T, Elliott G F, Gyi T J, and Nave C (1987) The organisation of collagen fibrils in the human corneal stroma: a synchrotron X-ray diffraction study. *Curr Eye Res* 6: 841-846.
- Meek K M, and Boote C (2004) The organization of collagen in the corneal stroma. *Exp Eye Res* 78: 503-512.
- Meek K M, and Boote C (2009) The use of X-ray scattering techniques to quantify the orientation and distribution of collagen in the corneal stroma. *Prog Retin Eye Res* 28: 369-392.

- Meek K M, Chapman J A, and Hardcastle R A (1979) The staining pattern of collagen fibrils. Improved correlation with sequence data. *J Biol Chem* 254: 10710-10714.
- Meek K M, Elliott G F, and Nave C (1986) A synchrotron X-ray diffraction study of bovine cornea stained with cupromeronic blue. *Coll Relat Res* 6: 203-218.
- Meek K M, and Fullwood N J (2001) Corneal and scleral collagens--a microscopist's perspective. *Micron* 32: 261-272.
- Meek K M, Fullwood N J, Cooke P H, Elliott G F, Maurice D M, Quantock A J, Wall R S et al. (1991) Synchrotron x-ray diffraction studies of the cornea, with implications for stromal hydration. *Biophys J* 60: 467-474.
- Meek K M, and Leonard D W (1993) Ultrastructure of the corneal stroma: a comparative study. *Biophys J* 64: 273-280.
- Meek K M, and Quantock A J (2001) The use of X-ray scattering techniques to determine corneal ultrastructure. *Prog Retin Eye Res* 20: 95-137.
- Meek K M, Quantock A J, Boote C, Liu C Y, and Kao W W (2003) An X-ray scattering investigation of corneal structure in keratocan-deficient mice. *Matrix Biol* 22: 467-475.
- Meek K M, Quantock A J, Elliott G F, Ridgway A E, Tullo A B, Bron A J, and Thonar E J (1989) Macular corneal dystrophy: the macromolecular structure of the stroma observed using electron microscopy and synchrotron X-ray diffraction. *Exp Eye Res* 49: 941-958.
- Mehmet H, Scudder P, Tang P W, Hounsell E F, Caterson B, and Feizi T (1986) The antigenic determinants recognized by three monoclonal antibodies to keratan sulphate involve sulphated hepta- or larger oligosaccharides of the poly(N-acetyllactosamine) series. *Eur J Biochem* 157: 385-391.
- Meier S, and Hay E D (1973) Synthesis of sulfated glycosaminoglycans by embryonic corneal epithelium. *Dev Biol.* 35: 318-331.
- Meier S, and Hay E D (1974a) Control of corneal differentiation by extracellular materials. Collagen as a promoter and stabilizer of epithelial stroma production. *Dev Biol.* 38: 249-270.
- Meier S, and Hay E D (1974b) Stimulation of extracellular matrix synthesis in the developing cornea by glycosaminoglycans. *Proc Natl Acad Sci U S A* 71 2310-2313.
- Meyer K, Linker A, Davidson E A, and Weissmann B (1953) The mucopolysaccharides of bovine cornea. *J Biol Chem* 205: 611-616.
- Michelacci Y M (2003) Collagens and proteoglycans of the corneal extracellular matrix. *Braz J Med Biol Res* 36: 1037-1046.
- Moller-Pedersen T (2004) Keratocyte reflectivity and corneal haze. *Exp Eye Res* 78: 553-560.
- Müller L J, Pels E, Schurmans L R, and Vrensen G F (2004) A new three-dimensional model of the organization of proteoglycans and collagen fibrils in the human corneal stroma. *Exp Eye Res* 78: 493-501.
- Müller L J, Pels L, and Vrensen G F (1995) Novel aspects of the ultrastructural organization of human corneal keratocytes. *Invest Ophthalmol Vis Sci* 36: 2557-2567.
- Nakamura K (2003) Interaction between injured corneal epithelial cells and stromal cells. *Cornea* 22: S35-47.

- Nakazawa K, Hassell J R, Hascall V C, Lohmander L S, Newsome D A, and Krachmer J (1984) Defective processing of keratan sulfate in macular corneal dystrophy. *J Biol Chem* 259: 13751-13757.
- Nakazawa K, Suzuki S, Wada K, and Nakazawa K (1995) Proteoglycan synthesis by corneal explants from developing embryonic chicken. *J Biochem* 117: 707-718.
- Nash J R, Wilt N, Kong A, Raabe H, and Costin G (2010) Media refinement for a long term corneal culture model of eye irritation and post-treatment recovery. Gaithersburg: Institute for in vitro sciences.
- Neame P J, Kay C J, McQuillan D J, Beales M P, and Hassell J R (2000) Independent modulation of collagen fibrillogenesis by decorin and lumican. *Cell Mol Life Sci* 57: 859-863.
- Newton R H, and Meek K M (1998) Circumcorneal annulus of collagen fibrils in the human limbus. *Invest Ophthalmol Vis Sci* 39: 1125-1134.
- Nicholls A C, Oliver J E, McCarron S, Harrison J B, Greenspan D S, and Pope F M (1996) An exon skipping mutation of a type V collagen gene (COL5A1) in Ehlers-Danlos syndrome. *J Med Genet* 33: 940-946.
- Nieduszynski I A, Huckerby T N, Dickenson J M, Brown G M, Tai G H, Morris H G, and Eady S (1990) There are two major types of skeletal keratan sulphates. *Biochem J* 271: 243-245.
- Nilsson B, Nakazawa K, Hassell J R, Newsome D A, and Hascall V C (1983) Structure of oligosaccharides and the linkage region between keratan sulfate and the core protein on proteoglycans from monkey cornea. *J Biol Chem* 258: 6056-6063.
- Niyibizi C, and Eyre D R (1989a) Bone type V collagen: chain composition and location of a trypsin cleavage site. *Connect Tissue Res* 20: 247-250.
- Niyibizi C, and Eyre D R (1989b) Identification of the cartilage alpha 1(XI) chain in type V collagen from bovine bone. *FEBS Lett* 242: 314-318.
- Niyibizi C, Fietzek P P, and van der Rest M (1984) Human placenta type V collagens. Evidence for the existence of an alpha 1(V) alpha 2(V) alpha 3(V) collagen molecule. *J Biol Chem* 259: 14170-14174.
- Oldberg A, Antonsson P, Lindblom K, and Heinegard D (1989) A collagen-binding 59-kd protein (fibromodulin) is structurally related to the small interstitial proteoglycans PG-S1 and PG-S2 (decorin). *Embo J* 8: 2601-2604.
- Ostadal B, Kolar F, Pelouch V, and Widimsky J (1995) Ontogenetic differences in cardiopulmonary adaptation to chronic hypoxia. *Physiol Res* 44: 45-51.
- Ozaki Y, Mizuno A, and Kaneuchi F (1992) Structural Differences between Type I and Type IV Collagen in Biological Tissues Studied in Vivo by Attenuated Total Reflection/Fourier Transform Infrared Spectroscopy. *Applied Spectroscopy* 46: 626-630.
- Palka B P, Sotozono C, Tanioka H, Akama T O, Yagi N, Boote C, Young R D et al. (2010) Structural collagen alterations in macular corneal dystrophy occur mainly in the posterior stroma. *Curr Eye Res* 35: 580-586.
- Parfitt G J, Pinali C, Akama T O, Young R D, Nishida K, Quantock A J, and Knupp C (2011) Electron tomography reveals multiple self-association of chondroitin sulphate/dermatan sulphate proteoglycans in Chst5-null mouse corneas. *J Struct Biol* 174: 536-541.
- Parfitt G J, Pinali C, Young R D, Quantock A J, and Knupp C (2010) Three-dimensional reconstruction of collagen-proteoglycan interactions in the mouse corneal stroma by electron tomography. *J Struct Biol* 170: 392-397.

- Patel S, Marshall J, and Fitzke F W, 3rd (1995) Refractive index of the human corneal epithelium and stroma. *J Refract Surg* 11: 100-105.
- Pellegata N S, Dieguez-Lucena J L, Joensuu T, Lau S, Montgomery K T, Krahe R, Kivela T et al. (2000) Mutations in KERA, encoding keratocan, cause cornea plana. *Nat Genet* 25: 91-95.
- Plaas A H, West L A, Thonar E J, Karcioğlu Z A, Smith C J, Klintworth G K, and Hascall V C (2001) Altered fine structures of corneal and skeletal keratan sulfate and chondroitin/dermatan sulfate in macular corneal dystrophy. *J Biol Chem* 276: 39788-39796.
- Polse K A (1979) Tear flow under hydrogel contact lenses. *Invest Ophthalmol Vis Sci* 18: 409-413.
- Poole C A, Brookes N H, and Clover G M (1993) Keratocyte networks visualised in the living cornea using vital dyes. *J Cell Sci* 106 ( Pt 2): 685-691.
- Prockop D J, and Kivirikko K I (1995) Collagens: molecular biology, diseases, and potentials for therapy. *Annu Rev Biochem* 64: 403-434.
- Quantock A J, Boote C, Young R D, Hayes S, Tanioka H, Kawasaki S, Ohta N et al. (2007) Small-angle fibre diffraction studies of corneal matrix structure: a depth-profiled investigation of the human eye-bank cornea. *J Appl Crystallogr* 40: s335-s340.
- Quantock A J, Meek K M, Ridgway A E, Bron A J, and Thonar E J (1990) Macular corneal dystrophy: reduction in both corneal thickness and collagen interfibrillar spacing. *Curr Eye Res* 9: 393-398.
- Quantock A J, and Young R D (2008) Development of the corneal stroma, and the collagen-proteoglycan associations that help define its structure and function. *Dev Dyn* 237: 2607-2621.
- Quantock A J, Young R D, and Akama T O (2010) Structural and biochemical aspects of keratan sulphate in the cornea *Cell Mol Life Sci* 67: 891-906.
- Rada J A, Achen V R, Penugonda S, Schmidt R W, and Mount B A (2000) Proteoglycan composition in the human sclera during growth and aging. *Invest Ophthalmol Vis Sci* 41: 1639-1648.
- Rada J A, Cornuet P K, and Hassell J R (1993) Regulation of corneal collagen fibrillogenesis in vitro by corneal proteoglycan (lumican and decorin) core proteins. *Exp Eye Res* 56: 635-648.
- Reynolds E S (1963) The use of lead citrate at high pH as an electron-opaque stain in electron microscopy. *J Cell Biol* 17: 208-212.
- Rodahl E, Van Ginderdeuren R, Knappskog P M, Bredrup C, and Boman H (2006) A second decorin frame shift mutation in a family with congenital stromal corneal dystrophy. *Am J Ophthalmol* 142: 520-521.
- Ruprecht J, and Nield J (2001) Determining the structure of biological macromolecules by transmission electron microscopy, single particle analysis and 3D reconstruction. *Prog Biophys Mol Biol* 75: 121-164.
- Sage H, and Bornstein P (1979) Characterization of a novel collagen chain in human placenta and its relation to AB collagen. *Biochemistry* 18: 3815-3822.
- Saika S, Shiraishi A, Liu C Y, Funderburgh J L, Kao C W, Converse R L, and Kao W W (2000) Role of lumican in the corneal epithelium during wound healing. *J Biol Chem* 275: 2607-2612.
- Sajdera S W, and Hascall V C (1969) Proteinpolysaccharide complex from bovine nasal cartilage. A comparison of low and high shear extraction procedures. *J Biol Chem* 244: 77-87.

- Sandler S S (1974) Direct three-dimensional reconstruction of a corneal stromal lamella from electron micrographs. *J Theor Biol* 48: 207-213.
- Sarver M D (1971) Striate corneal lines among patients wearing hydrophilic contact lenses. *Am J Optom Arch Am Acad Optom* 48: 762-763.
- Sayers Z, Koch M H, Whitburn S B, Meek K M, Elliott G F, and Harmsen A (1982) Synchrotron x-ray diffraction study of corneal stroma. *J Mol Biol* 160: 593-607.
- Scott J E (1985) Proteoglycan histochemistry—a valuable tool for connective tissue biochemists. *Coll Relat Res* 5: 541-575.
- Scott J E (1988) How rational histochemistry produced order out of chaos in the "amorphous ground substance" (with a little help from biochemistry, biophysics etc.). *Eur J Histochem* 42: 29-34.
- Scott J E (1988) Proteoglycan-fibrillar collagen interactions. *Biochem J* 252: 313-323.
- Scott J E (1989) The chemical morphology of keratan sulphate proteoglycans. In: Greiling H, and Scott J E [eds.] *Keratan sulphate: chemistry, biology, chemical pathology*. London: The Biochemical Society, pp. 122-135.
- Scott J E (1991a) Proteoglycan: collagen interactions and corneal ultrastructure. *Biochem Soc Trans* 19: 877-881.
- Scott J E (1991b) Proteoglycan: collagen interactions in connective tissues. Ultrastructural, biochemical, functional and evolutionary aspects. *Int J Biol Macromol* 13: 157-161.
- Scott J E (1992a) Morphometry of cupromeronic blue-stained proteoglycan molecules in animal corneas, versus that of purified proteoglycans stained in vitro, implies that tertiary structures contribute to corneal ultrastructure. *J Anat* 180 ( Pt 1): 155-164.
- Scott J E (1992b) Oxygen and the connective tissues. *Trends Biochem Sci* 17: 340-343.
- Scott J E (1992c) Supramolecular organization of extracellular matrix glycosaminoglycans, in vitro and in the tissues. *Faseb J* 6: 2639-2645.
- Scott J E (2003) Elasticity in extracellular matrix 'shape modules' of tendon, cartilage, etc. A sliding proteoglycan-filament model. *J Physiol* 553: 335-343.
- Scott J E, and Bosworth T R (1990) A comparative biochemical and ultrastructural study of proteoglycan-collagen interactions in corneal stroma. Functional and metabolic implications. *Biochem J* 270: 491-497.
- Scott J E, and Haigh M (1985) 'Small'-proteoglycan:collagen interactions: keratan sulphate proteoglycan associates with rabbit corneal collagen fibrils at the 'a' and 'c' bands. *Biosci Rep* 5: 765-774.
- Scott J E, and Haigh M (1988a) Identification of specific binding sites for keratan sulphate proteoglycans and chondroitin-dermatan sulphate proteoglycans on collagen fibrils in cornea by the use of cupromeronic blue in 'critical-electrolyte-concentration' techniques. *Biochem J* 253: 607-610.
- Scott J E, and Haigh M (1988b) Keratan sulphate and the ultrastructure of cornea and cartilage: a 'stand-in' for chondroitin sulphate in conditions of oxygen lack? *J Anat* 158: 95-108.
- Scott J E, Haigh M, and Ali P (1988) Keratan sulphate is unevenly distributed from back to front of bovine cornea. *Biochem Soc Trans* 16: 333-334.
- Scott J E, Stockwell R A, Balduini C, and De Luca G (1989) Keratan sulphate: a functional substitute for chondroitin sulphate in O<sub>2</sub> deficient tissues? *Pathol Biol (Paris)* 37: 742-745.

- Scott P G, Grossmann J G, Dodd C M, Sheehan J K, and Bishop P N (2003) Light and X-ray scattering show decorin to be a dimer in solution. *J Biol Chem* 278: 18353-18359.
- Scott P G, McEwan P A, Dodd C M, Bergmann E M, Bishop P N, and Bella J (2004) Crystal structure of the dimeric protein core of decorin, the archetypal small leucine-rich repeat proteoglycan. *Proc Natl Acad Sci U S A* 101: 15633-15638.
- Silverstein J L, Steen V D, Medsger T A, Jr., and Falanga V (1988) Cutaneous hypoxia in patients with systemic sclerosis (scleroderma). *Arch Dermatol* 124: 1379-1382.
- Sini P, Denti A, Tira M E, and Balduini C (1997) Role of decorin on in vitro fibrillogenesis of type I collagen. *Glycoconj J* 14: 871-874.
- Smith J W, and Frame J (1969) Observations on the collagen and proteinopolysaccharide complex of rabbit cornea stroma. *J Cell Sci* 4: 421-436.
- Stadlmann J, Pabst M, Kolarich D, Kunert R, and Altmann F (2008) Analysis of immunoglobulin glycosylation by LC-ESI-MS of glycopeptides and oligosaccharides. *Proteomics* 8: 2858-2871.
- Stockwell R A, and Scott J E (1965) Observations on the acid glycosaminoglycan (mucopolysaccharide) content of the matrix of aging cartilage. *Ann Rheum Dis* 24: 341-350.
- Stone J E, Akhtar N, Botchway S, and Pennock C A (1994) Interaction of 1,9-dimethylmethylene blue with glycosaminoglycans. *Ann Clin Biochem* 31 ( Pt 2): 147-152.
- Suzuki M (1939) Prosthetic group of cornea mucoid. *J Biochem* 30: 185-191.
- Sweeney D F (1992) Corneal exhaustion syndrome with long-term wear of contact lenses. *Optom Vis Sci* 69: 601-608.
- Tai G H, Huckerby T N, and Nieduszynski I A (1996) Multiple non-reducing chain termini isolated from bovine corneal keratan sulfates. *J Biol Chem* 271: 23535-23546.
- Tai G H, Nieduszynski I A, Fullwood N J, and Huckerby T N (1997) Human corneal keratan sulfates. *J Biol Chem* 272: 28227-28231.
- Tamamori M, Ito H, Hiroe M, Marumo F, and Hata R I (1997) Stimulation of collagen synthesis in rat cardiac fibroblasts by exposure to hypoxic culture conditions and suppression of the effect by natriuretic peptides. *Cell Biol Int* 21: 175-180.
- Tasheva E S, Koester A, Paulsen A Q, Garrett A S, Boyle D L, Davidson H J, Song M et al. (2002) Mimecan/osteoglycin-deficient mice have collagen fibril abnormalities. *Mol Vis* 8: 407-415.
- Thomas J T, Ayad S, and Grant M E (1994) Cartilage collagens: strategies for the study of their organisation and expression in the extracellular matrix. *Ann Rheum Dis* 53: 488-496.
- Toole B P, and Lowther D A (1968) The effect of chondroitin sulphate-protein on the formation of collagen fibrils in vitro. *Biochem J* 109: 857-866.
- Trowbridge J M, and Gallo R L (2002) Dermatan sulfate: new functions from an old glycosaminoglycan. *Glycobiology* 12: 117R-125R.
- Tseng S C, Smuckler D, and Stern R (1982) Comparison of collagen types in adult and fetal bovine corneas. *J Biol Chem* 257: 2627-2633.

- Turss R, Frient M, and Dohlman C H (1971) Glucose concentration and hydration of the corneal stroma. *Ophthalm Res* 2: 253-260.
- Vogel K G, Paulsson M, and Heinegard D (1984) Specific inhibition of type I and type II collagen fibrillogenesis by the small proteoglycan of tendon. *Biochem J* 223: 587-597.
- Vogel K G, and Trotter J A (1987) The effect of proteoglycans on the morphology of collagen fibrils formed in vitro. *Coll Relat Res* 7: 105-114.
- von der Mark H, Aumailley M, Wick G, Fleischmajer R, and Timpl R (1984) Immunocytochemistry, genuine size and tissue localization of collagen VI. *Eur J Biochem* 142: 493-502.
- Waring G O, 3rd (1989) Making sense of keratospeak II: Proposed conventional terminology for corneal topography. *Refract Corneal Surg* 5: 362-367.
- Wessel H, Anderson S, Fite D, Halvas E, Hempel J, and SundarRaj N (1997) Type XII collagen contributes to diversities in human corneal and limbal extracellular matrices. *Invest Ophthalmol Vis Sci* 38: 2408-2422.
- Whitehart D R (1994) Biochemistry of the eye. In: C.M H [ed.] (2nd edition edn.) London: Butterworth-Heinemann, pp. 1-54.
- White J, Werkmeister J A, Ramshaw J A, and Birk D E (1997) Organization of fibrillar collagen in the human and bovine cornea: collagen types V and III. *Connect Tissue Res* 36: 165-174.
- Winnemöller M, Schön P, Vischer P, and Kresse H (1992) Interactions between thrombospondin and the small proteoglycan decorin: interference with cell attachment. *Eur J Cell Biol* 59: 47-55.
- Wirtz M K, Bradley J M, Xu H, Domreis J, Nobis C A, Truesdale A T, Samples J R et al. (1997) Proteoglycan expression by human trabecular meshworks. *Curr Eye Res* 16: 412-421.
- Woessner J F, Jr. (1961) The determination of hydroxyproline in tissue and protein samples containing small proportions of this imino acid. *Arch Biochem Biophys* 93: 440-447.
- Wood G C (1960) The formation of fibrils from collagen solutions. 3. Effect of chondroitin sulphate and some other naturally occurring polyanions on the rate of formation. *Biochem J* 75: 605-612.
- Worthington C R, and Inouye H (1985) X-ray diffraction study of the cornea. *Int J Biol Macromol* 7: 2-8.
- Yamabayashi S, Ohno S, Aguilar R N, Furuya T, Hosoda M, and Tsukahara S (1991) Ultrastructural studies of collagen fibers of the cornea and sclera by a quick-freezing and deep-etching method. *Ophthalmic Res* 23: 320-329.
- Ying S, Shiraishi A, Kao C W, Converse R L, Funderburgh J L, Swiergiel J, Roth M R et al. (1997) Characterization and expression of the mouse lumican gene. *J Biol Chem* 272: 30306-30313.
- Young R D, Akama T O, Liskova P, Ebenezer N D, Allan B, Kerr B, Caterson B et al. (2007a) Differential immunogold localisation of sulphated and unsulphated keratan sulphate proteoglycans in normal and macular dystrophy cornea using sulphation motif-specific antibodies. *Histochem Cell Biol* 127: 115-120.
- Young R D, Gealy E C, Liles M, Caterson B, Ralphs J R, and Quantock A J (2007b) Keratan sulfate glycosaminoglycan and the association with collagen fibrils in rudimentary lamellae in the developing avian cornea. *Invest Ophthalmol Vis Sci* 48: 3083-3088.
- Young R D, Tudor D, Hayes A J, Kerr B, Hayashida Y, Nishida K, Meek K M et al. (2005) Atypical composition and ultrastructure of proteoglycans in the mouse corneal stroma. *Invest Ophthalmol Vis Sci* 46: 1973-1978.

Zappone B, Ruths M, Greene G W, Jay G D, and Israelachvili J N (2007) Adsorption, lubrication, and wear of lubricin on model surfaces: polymer brush-like behavior of a glycoprotein. *Biophys J* 92: 1693-1708.

Zhan Q, Burrows R, and Cintron C (1995) Localization of type XII collagen in normal and healing rabbit cornea by in situ hybridization. *Exp Eye Res* 60: 551-561.

Zhang G, Sun A, Li W, Liu T, and Su Z (2006) Mass spectrometric analysis of enzymatic digestion of denatured collagen for identification of collagen type *J Chromatogr A* 1114: 274-277.

## Website references

<http://www.eyecare-for-you.com/anatomy-of-the-eye.php> (2009) *Anatomy of the Eye* [Online]. Available at: [Accessed:

[http://www.images.missionforvisionusa.org/anatomy/2005\\_10\\_01\\_archive.html](http://www.images.missionforvisionusa.org/anatomy/2005_10_01_archive.html) (2005) *Anatomy of the human eye* [Online]. Available at: [Accessed:

[http://www.nlm.nih.gov/medlineplus/ency/presentations/100206\\_2.htm](http://www.nlm.nih.gov/medlineplus/ency/presentations/100206_2.htm) (2010) *Lasik eye surgery - series* [Online]. Available at: [Accessed:

<http://www.seikagakubb.co.jp/bio/cgi-bin/search/edetail.php?code=100330> (2007) *Chondroitinase ABC(Proteus vulgaris)* [Online]. Available at: [Accessed:

<http://www.seikagakubb.co.jp/bio/cgi-bin/search/edetail.php?code=100455&PHPSESSID=be9a860cee56252ae8cf473a40d84b14> (2007) *Endo-beta-Galactosidase(Escherichia freundii)* [Online]. Available at: [Accessed:

<http://www.seikagakubb.co.jp/bio/cgi-bin/search/edetail.php?code=100810> (2007) *Keratanase(Pseudomonas sp.)* [Online]. Available at: [Accessed:

<http://www.seikagakubb.co.jp/bio/cgi-bin/search/edetail.php?code=100812> (2007) *Keratanase II (Bacillus sp.)* [Online]. Available at: [Accessed:

## Appendix 1

### Results: Corneal thickness

Sample	Centre (0-3mm) (mm)	Inner periphery (3-6mm) (mm)	Mid periphery (6-9mm) (mm)	Outer periphery/Limbus (9-12mm) (mm)
A	0.849	0.979	0.991	1.013
B	0.839	0.992	1.012	1.021
C	0.856	0.983	1.003	1.020
D	0.846	0.988	1.003	1.029
E	0.847	0.993	1.008	1.021
F	0.837	0.989	0.999	1.018
G	0.859	0.985	1.000	1.016
H	0.836	0.975	0.997	1.020
I	0.839	0.974	1.001	1.021
J	0.839	0.993	1.020	1.031
Average	0.845 ± 0.008	0.985 ± 0.007	1.003 ± 0.005	1.21 0.006

**Table # 1 Corneal thickness across the bovine cornea.**

### Results: Corneal hydration

Centre (0-3mm)	Wet wt (mg)	Dry wt (mg)	Hydration	Inner periphery (3-6mm)	Wet wt (mg)	Dry wt (mg)	Hydration
A	24.0	5.0	3.80	A	25.5	5.5	3.64
B	10.8	2.6	3.15	B	11.2	2.3	3.87
C	14.3	2.9	3.93	C	19.3	4.0	3.83
D	24.2	4.9	3.94	D	23.7	4.7	4.04
E	18.0	4.0	3.50	E	23.0	5.0	3.60
F	21.0	4.0	4.25	F	22.0	4.0	4.50
G	17.0	4.0	3.25	G	18.0	4.0	3.50
H	20.0	5.0	3.00	H	17.0	4.0	3.25
I	20.0	4.0	4.00	I	16.0	4.0	3.00
J	22.0	4.0	4.50	J	25.0	4.0	5.25
Average			3.732 ± 0.491	Average			3.847 ± 0.644

Mid periphery (6-9mm)	Wet wt (mg)	Dry wt (mg)	Hydration	Outer periphery/limbus (9-12mm)	Wet wt (mg)	Dry wt (mg)	Hydration
A	15.0	3.2	3.69	A	20.9	3.8	4.50
B	11.6	2.3	4.04	B	16.3	3.4	3.79
C	16.6	3.4	3.88	C	13.0	3.0	3.33
D	17.2	2.8	5.14	D	14.2	2.2	5.45
E	17.0	3.0	4.67	E	17.0	3.0	4.67
F	19.0	4.0	3.75	F	18.0	3.0	5.00
G	12.0	3.0	3.00	G	16.0	4.0	3.00
H	17.0	4.0	3.25	H	19.0	4.0	3.75
I	16.0	4.0	3.00	I	17.0	3.0	4.67
J	14.0	3.0	3.67	J	20.0	4.0	4.00
Average			3.809 ± 0.686	Average			4.217 0.770

**Table # 2 Corneal hydration across the bovine cornea.**

## Results: Hydroxyproline assay

Centre (0-3mm)	Average (mg/ml)	Hydroxyproline (mg)	Hydroxyproline/dry wt (mg/mg dry wt)
A	1.578	0.316	0.063
B	0.676	0.135	0.052
C	0.747	0.149	0.052
D	1.398	0.280	0.057
E	1.325	0.265	0.066
F	1.335	0.267	0.067
G	1.328	0.266	0.066
H	1.491	0.298	0.060
I	1.172	0.234	0.059
J	1.454	0.291	0.073
Average			0.061 ± 0.007

Inner periphery (3-6mm)	Average (mg/ml)	Hydroxyproline (mg)	Hydroxyproline/dry wt (mg/mg dry wt)
A	2.214	0.443	0.080
B	1.123	0.225	0.098
C	1.256	0.251	0.063
D	1.185	0.237	0.050
E	1.894	0.379	0.076
F	1.394	0.279	0.070
G	1.599	0.320	0.080
H	1.696	0.339	0.085
I	1.639	0.328	0.082
J	1.639	0.328	0.082
Average			0.075 ± 0.013

Mid periphery (6-9mm)	Average (mg/ml)	Hydroxyproline (mg)	Hydroxyproline/dry wt (mg/mg dry wt)
A	1.606	0.321	0.100
B	1.245	0.249	0.108
C	1.645	0.329	0.097
D	1.210	0.242	0.086
E	1.595	0.319	0.106
F	1.868	0.374	0.093
G	1.564	0.313	0.104
H	2.043	0.409	0.102
I	1.926	0.385	0.096
J	1.585	0.317	0.106
Average			0.100 ± 0.007

Outer periphery/limbus (9-12mm)	Average (mg/ml)	Hydroxyproline (mg)	Hydroxyproline/dry wt (mg/mg dry wt)
A	2.173	0.435	0.114
B	1.993	0.399	0.117
C	1.797	0.359	0.120
D	1.391	0.278	0.126
E	1.883	0.377	0.126
F	1.667	0.333	0.111
G	2.333	0.467	0.117
H	2.433	0.487	0.122
I	1.931	0.386	0.129
J	2.293	0.459	0.115
Average			0.120 ± 0.006

Table # 3 Hydroxyproline content across the bovine cornea.

## Results: Sulphated GAG

Centre (0-3mm)	Average sGAG (mg/ml)	sGAG (mg)	sGAG/dry wt (mg/mg)
A	1.053	0.253	0.051
B	1.301	0.140	0.054
C	1.069	0.153	0.053
D	0.936	0.227	0.046
E	0.891	0.178	0.059
F	1.165	0.245	0.061
G	1.413	0.240	0.060
H	1.217	0.243	0.049
I	1.367	0.273	0.068
J	0.997	0.219	0.055
Average		0.217 ± 0.045	0.056 ± 0.007

Inner periphery (3-6mm)	Average sGAG (mg/ml)	sGAG (mg)	sGAG/dry wt (mg/mg)
A	0.777	0.198	0.036
B	2.186	0.245	0.106
C	0.961	0.185	0.046
D	0.890	0.211	0.045
E	1.055	0.201	0.040
F	1.231	0.271	0.068
G	1.858	0.223	0.056
H	1.471	0.250	0.063
I	1.316	0.211	0.053
J	0.916	0.229	0.057
Average		0.220 ± 0.026	0.058 ± 0.019

Mid periphery (6-9mm)	Average sGAG (mg/ml)	sGAG (mg)	sGAG/dry wt (mg/mg)
A	0.834	0.125	0.039
B	1.171	0.136	0.059
C	1.057	0.175	0.052
D	1.007	0.173	0.062
E	1.178	0.200	0.067
F	1.107	0.310	0.039
G	1.658	0.199	0.066
H	1.246	0.212	0.053
I	0.672	0.108	0.027
J	0.946	0.133	0.044
Average		0.177 ± 0.059	0.051 ± 0.013

Outer periphery/limbus (9-12mm)	Average sGAG (mg/ml)	sGAG (mg)	sGAG/dry wt (mg/mg)
A	0.584	0.122	0.044
B	1.208	0.197	0.058
C	1.739	0.226	0.075
D	0.822	0.117	0.053
E	1.037	0.156	0.078
F	0.921	0.230	0.077
G	1.243	0.199	0.050
H	1.164	0.151	0.038
I	0.558	0.095	0.032
J	0.888	0.107	0.027
Average		0.160 ± 0.050	0.053 ± 0.019

Table # 4 Sulphated GAG content across the bovine cornea.

Results: ELISA - KS quantification

Centre (0-3mm)	Competing antigen (ng/ml)	1B4 (ng)	1B4/dry wt (ng/mg)
A	1956.301	1.235	0.247
B	2635.853	2.043	0.786
C	1518.361	0.628	0.216
D	5875.785	0.920	0.188
E	659.903	1.246	0.415
F	829.242	1.257	0.314
G	2553.915	0.951	0.238
H	2349.498	0.920	0.184
I	5005.085	1.235	0.309
J	4113.150	0.822	0.205
Average			0.195 ± 0.053

Centre (0-3mm)	Competing antigen (ng/ml)	5D4 (ng)	5D4/dry wt (ng/mg)
A	111.671	1.592	0.318
B	184.821	3.506	1.349
C	46.107	2.101	0.725
D	190.202	1.429	0.292
E	355.836	1.704	0.568
F	720.091	3.448	0.862
G	647.428	2.985	0.746
H	600.618	2.769	0.554
I	514.470	2.057	0.514
J	739.190	2.956	0.739
Average			0.651 ± 0.313

Inner periphery (3-6mm)	Competing antigen (ng/ml)	1B4 (ng)	1B4/dry wt (ng/mg)
A	1098.228	0.693	0.126
B	1290.217	0.590	0.256
C	1360.318	0.562	0.141
D	7651.965	1.198	0.255
E	1045.546	1.090	0.218
F	2289.604	1.105	0.276
G	3042.696	1.469	0.367
H	7924.603	1.269	0.317
I	4302.237	0.689	0.172
J	6903.992	1.196	0.299
Average			0.316 ± 0.126

Inner periphery (3-6mm)	Competing antigen (ng/ml)	5D4 (ng)	5D4/dry wt (ng/mg)
A	67.150	3.048	0.554
B	265.290	2.752	1.196
C	52.030	2.371	0.593
D	221.021	1.660	0.353
E	974.872	4.710	0.942
F	822.634	3.974	0.994
G	1431.272	2.926	0.732
H	902.285	1.845	0.461
I	384.936	3.646	0.911
J	318.713	3.019	0.755
Average			0.664 ± 0.303

Table # 5 KS content across the bovine cornea (centre and inner periphery). Note: 5D4 antibody specifically binds to linear penta-sulphated KS and 1B4 antibody specifically binds to lesser sulphated KS.

Results: ELISA - KS quantification

Mid periphery (6-9mm)	Competing antigen (ng/ml)	1B4 (ng)	1B4/dry wt (ng/mg)	Mid periphery (6-9mm)	Competing antigen (ng/ml)	5D4 (ng)	5D4/dry wt (ng/mg)
A	987.368	0.641	0.200	A	62.787	0.937	0.293
B	1469.692	2.208	0.960	B	87.564	1.190	0.518
C	2388.293	1.465	0.431	C	155.449	1.720	0.506
D	13799.925	1.074	0.384	D	257.370	1.611	0.575
E	5098.093	2.329	0.776	E	488.730	2.506	0.835
F	6122.919	2.797	0.350	F	477.720	2.450	0.306
G	5649.874	2.957	0.986	G	384.800	2.028	0.676
H	5955.896	3.117	0.779	H	458.150	2.415	0.604
I	8838.896	0.695	0.174	I	189.891	0.954	0.239
J	14508.549	1.140	0.380	J	473.547	2.380	0.793
Average		0.485 ± 0.210		Average		0.602 ± 0.209	

Outer periphery/limbus (9-12mm)	Competing antigen (ng/ml)	1B4 (ng)	1B4/dry wt (ng/mg)	Outer periphery/limbus (9-12mm)	Competing antigen (ng/ml)	5D4 (ng)	5D4/dry wt (ng/mg)
A	1379.053	0.895	0.320	A	126.747	1.892	0.676
B	1370.476	2.059	0.606	B	185.874	2.527	0.743
C	5031.193	3.087	1.029	C	291.110	3.221	1.074
D	14980.754	1.166	0.530	D	184.648	1.156	0.525
E	9819.479	2.188	1.094	E	276.379	2.268	1.134
F	7995.546	1.781	0.594	F	180.543	1.481	0.494
G	8891.169	5.101	1.275	G	398.416	2.355	0.589
H	6662.544	3.823	0.956	H	571.849	3.380	0.845
I	5676.496	1.525	0.508	I	70.911	1.074	0.358
J	11403.570	3.064	0.766	J	202.366	3.066	0.767
Average		0.805 ± 0.304		Average		0.720 ± 0.248	

**Table # 6 KS content across the bovine cornea (mid periphery and outer periphery/limbs).** Note: 5D4 antibody specifically binds to linear penta-sulphated KS and 1B4 antibody specifically binds to lesser sulphated KS.

## Appendix 2

### Results: Hydration results: Centre (0-3mm)

Control	Wet wt (mg)	Dry wt (mg)	Hydration
A	22.00	5.00	3.40
B	24.00	5.00	3.80
C	26.00	6.00	3.33
D	28.00	5.00	4.60
Average			3.783 ± 0.582

Normal			
½ dy	Wet wt (mg)	Dry wt (mg)	Hydration
A	26.00	5.00	4.20
B	28.00	5.00	4.60
C	30.00	6.00	4.00
D	32.00	6.00	4.33
Average			4.283 ± 0.252

1 dy			
Wet wt (mg)	Dry wt (mg)	Hydration	
A	28.00	5.00	4.60
B	24.00	5.00	3.80
C	24.00	5.00	3.80
D	24.00	5.00	3.80
Average			4.000 ± 0.400

3 dy			
Wet wt (mg)	Dry wt (mg)	Hydration	
A	26.00	5.00	4.20
B	26.00	4.00	5.50
C	30.00	5.00	5.00
D	30.00	5.00	5.00
Average			4.925 ± 0.538

5 dy			
Wet wt (mg)	Dry wt (mg)	Hydration	
A	32.00	5.00	5.40
B	36.00	6.00	5.00
C	32.00	5.00	5.40
D	39.00	6.00	5.50
Average			5.325 ± 0.222

7 dy			
Wet wt (mg)	Dry wt (mg)	Hydration	
A	30.000	4.000	6.50
B	34.000	5.000	5.80
C	44.000	6.000	6.33
D	32.000	5.000	5.40
Average			6.008 ± 0.504

Hypoxia			
½ dy	Wet wt (mg)	Dry wt (mg)	Hydration
A	26.00	5.00	4.20
B	24.00	5.00	3.80
C	26.00	5.00	4.20
D	20.00	4.00	4.00
Average			4.050 ± 0.191

1 dy			
Wet wt (mg)	Dry wt (mg)	Hydration	
A	24.00	5.00	3.80
B	26.00	5.00	4.20
C	28.00	5.00	4.60
D	28.00	5.00	4.60
Average			4.300 ± 0.383

3 dy			
Wet wt (mg)	Dry wt (mg)	Hydration	
A	30.00	5.00	5.00
B	32.00	6.00	4.33
C	32.00	5.00	5.40
D	34.00	5.00	5.80
Average			5.133 ± 0.625

5 dy			
Wet wt (mg)	Dry wt (mg)	Hydration	
A	36.00	6.00	5.00
B	38.00	6.00	5.33
C	34.00	5.00	5.80
D	36.00	6.00	5.00
Average			5.283 ± 0.379

7 dy			
Wet wt (mg)	Dry wt (mg)	Hydration	
A	40.00	6.00	5.67
B	38.00	6.00	5.33
C	36.00	5.00	6.20
D	34.00	5.00	5.80
Average			5.750 ± 0.358

Table ## 1 Corneal hydration at the central regions of the rabbit cornea that was cultured in normal and low O<sub>2</sub> level.

Results: Hydration results: Periphery (3-6mm)

Control	Wet wt (mg)	Dry wt (mg)	Hydration
A	24.00	5.00	3.80
B	26.00	5.00	4.20
C	30.00	5.00	5.00
D	24.00	4.00	5.00
Average			4.500 ± 0.600

Normal			
½ dy	Wet wt (mg)	Dry wt (mg)	Hydration
A	22.00	4.00	4.50
B	24.00	4.00	5.00
C	22.00	4.00	4.50
D	30.00	5.00	5.00
Average			4.750 ± 0.289

1 dy	Wet wt (mg)	Dry wt (mg)	Hydration
A	34.00	5.00	5.80
B	28.00	5.00	4.60
C	24.00	5.00	3.80
D	30.00	5.00	5.00
Average			4.800 ± 0.833

3 dy	Wet wt (mg)	Dry wt (mg)	Hydration
A	30.00	4.00	6.50
B	34.00	5.00	5.80
C	30.00	4.00	6.50
D	32.00	5.00	5.40
Average			6.050 ± 0.545

5 dy	Wet wt (mg)	Dry wt (mg)	Hydration
A	32.00	4.00	7.00
B	36.00	5.00	6.20
C	36.00	5.00	6.20
D	36.00	5.00	6.20
Average			6.400 ± 0.400

7 dy	Wet wt (mg)	Dry wt (mg)	Hydration
A	32.000	4.000	7.00
B	36.000	5.000	6.20
C	42.000	5.000	7.40
D	34.000	5.000	5.80
Average			6.600 ± 0.730

Hypoxia			
½ dy	Wet wt (mg)	Dry wt (mg)	Hydration
A	36.00	6.00	5.00
B	26.00	5.00	4.20
C	24.00	4.00	5.00
D	26.00	4.00	5.50
Average			4.925 ± 0.538

1 dy	Wet wt (mg)	Dry wt (mg)	Hydration
A	22.00	4.00	4.50
B	30.00	5.00	5.00
C	28.00	4.00	6.00
D	24.00	5.00	3.80
Average			4.825 ± 0.925

3 dy	Wet wt (mg)	Dry wt (mg)	Hydration
A	32.00	5.00	5.40
B	32.00	4.00	7.00
C	32.00	4.00	7.00
D	36.00	5.00	6.20
Average			6.400 ± 0.766

5 dy	Wet wt (mg)	Dry wt (mg)	Hydration
A	30.00	4.00	6.50
B	32.00	4.00	7.00
C	36.00	5.00	6.20
D	38.00	5.00	6.60
Average			6.575 ± 0.330

7 dy	Wet wt (mg)	Dry wt (mg)	Hydration
A	36.00	5.00	6.20
B	38.00	5.00	6.60
C	44.00	6.00	6.33
D	34.00	5.00	5.80
Average			6.233 ± 0.333

Table ## 2 Corneal hydration at the peripheral regions of the rabbit cornea that was cultured in normal and low O<sub>2</sub> level.

Results: Hydration – Outer periphery/limbus (6-9mm)

Control	Wet wt (mg)	Dry wt (mg)	Hydration
A	20.00	4.00	4.00
B	20.00	4.00	4.00
C	24.00	4.00	5.00
D	26.00	5.00	4.20
Average			4.300 ± 0.476

Normal			
½ dy	Wet wt (mg)	Dry wt (mg)	Hydration
A	26.00	5.00	4.20
B	26.00	5.00	4.20
C	32.00	6.00	4.33
D	28.00	5.00	4.60
Average			4.333 ± 0.189

1 dy	Wet wt (mg)	Dry wt (mg)	Hydration
A	28.00	5.00	4.60
B	26.00	5.00	4.20
C	24.00	5.00	3.80
D	26.00	5.00	4.20
Average			4.200 ± 0.327

3 dy	Wet wt (mg)	Dry wt (mg)	Hydration
A	22.00	3.00	6.33
B	26.00	4.00	5.50
C	28.00	4.00	6.00
D	34.00	5.00	5.80
Average			5.908 ± 0.350

5 dy	Wet wt (mg)	Dry wt (mg)	Hydration
A	34.00	5.00	5.80
B	36.00	6.00	5.00
C	34.00	5.00	5.80
D	34.00	5.00	5.80
Average			5.600 ± 0.400

7 dy	Wet wt (mg)	Dry wt (mg)	Hydration
A	38.000	5.000	6.60
B	32.000	5.000	5.40
C	34.000	5.000	5.80
D	36.000	5.000	6.20
Average			6.000 ± 0.516

Hypoxia			
½ dy	Wet wt (mg)	Dry wt (mg)	Hydration
A	34.00	6.00	4.67
B	30.00	6.00	4.00
C	28.00	5.00	4.60
D	30.00	5.00	5.00
Average			4.567 ± 0.416

1 dy	Wet wt (mg)	Dry wt (mg)	Hydration
A	30.00	6.00	4.00
B	28.00	5.00	4.60
C	26.00	4.00	5.50
D	26.00	5.00	4.20
Average			4.575 ± 0.665

3 dy	Wet wt (mg)	Dry wt (mg)	Hydration
A	34.00	5.00	5.80
B	24.00	4.00	5.00
C	36.00	5.00	6.20
D	30.00	5.00	5.00
Average			5.500 ± 0.600

5 dy	Wet wt (mg)	Dry wt (mg)	Hydration
A	30.00	5.00	5.00
B	32.00	5.00	5.40
C	32.00	5.00	5.40
D	36.00	5.00	6.20
Average			5.500 ± 0.503

7 dy	Wet wt (mg)	Dry wt (mg)	Hydration
A	32.00	5.00	5.40
B	28.00	4.00	6.00
C	36.00	5.00	6.20
D	32.00	5.00	5.40
Average			5.750 ± 0.412

Table ## 3 Corneal hydration at the outer periphery/limbus regions of the rabbit cornea that was cultured in normal and low O<sub>2</sub> level.

Results: Hydration – Sclera (9-12mm)

Control	Wet wt (mg)	Dry wt (mg)	Hydration
A	20.00	4.00	4.00
B	20.00	5.00	3.00
C	20.00	4.00	4.00
D	22.00	5.00	3.40
Average			3.600 ± 0.490

Normal			
½ dy	Wet wt (mg)	Dry wt (mg)	Hydration
A	32.00	6.00	4.33
B	28.00	6.00	3.67
C	24.00	5.00	3.80
D	24.00	5.00	3.80
Average			3.900 ± 0.296

1 dy	Wet wt (mg)	Dry wt (mg)	Hydration
A	30.00	6.00	4.00
B	30.00	6.00	4.00
C	24.00	6.00	3.00
D	24.00	6.00	3.00
Average			3.500 ± 0.577

3 dy	Wet wt (mg)	Dry wt (mg)	Hydration
A	26.00	4.00	5.50
B	28.00	5.00	4.60
C	34.00	5.00	5.80
D	32.00	5.00	5.40
Average			5.325 ± 0.512

5 dy	Wet wt (mg)	Dry wt (mg)	Hydration
A	32.00	6.00	4.33
B	32.00	5.00	5.40
C	32.00	6.00	4.33
D	34.00	5.00	5.80
Average			4.967 ± 0.749

7 dy	Wet wt (mg)	Dry wt (mg)	Hydration
A	34.000	5.000	5.80
B	36.000	6.000	5.00
C	34.000	5.000	5.80
D	34.000	5.000	5.80
Average			5.600 ± 0.400

Hypoxia			
½ dy	Wet wt (mg)	Dry wt (mg)	Hydration
A	30.00	5.00	5.00
B	24.00	5.00	3.80
C	22.00	5.00	3.40
D	20.00	4.00	4.00
Average			4.050 ± 0.681

1 dy	Wet wt (mg)	Dry wt (mg)	Hydration
A	28.00	6.00	3.67
B	26.00	5.00	4.20
C	24.00	4.00	5.00
D	24.00	6.00	3.00
Average			3.967 ± 0.846

3 dy	Wet wt (mg)	Dry wt (mg)	Hydration
A	32.00	6.00	4.33
B	24.00	5.00	3.80
C	26.00	5.00	4.20
D	28.00	5.00	4.60
Average			4.233 ± 0.333

5 dy	Wet wt (mg)	Dry wt (mg)	Hydration
A	26.00	6.00	3.33
B	32.00	6.00	4.33
C	32.00	6.00	4.33
D	36.00	6.00	5.00
Average			4.250 ± 0.687

7 dy	Wet wt (mg)	Dry wt (mg)	Hydration
A	34.00	6.00	4.67
B	30.00	5.00	5.00
C	34.00	6.00	4.67
D	34.00	6.00	4.67
Average			4.750 ± 0.167

Table ## 4 Corneal hydration at the scleral regions of the rabbit cornea that was cultured in normal and low O<sub>2</sub> level.

Results: DMMB assay – Centre (0-3mm)

Control	Average sGAG (mg/ml)	sGAG (mg)	sGAG/dry wt (mg/mg)
A	0.763	0.084	0.017
B	0.727	0.087	0.017
C	0.994	0.129	0.022
D	0.423	0.068	0.014
Average		0.092 ± 0.023	0.017 ± 0.003

Normal			
½ dy	Average sGAG (mg/ml)	sGAG (mg)	sGAG/dry wt (mg/mg)
A	0.781	0.102	0.020
B	0.604	0.085	0.017
C	0.542	0.081	0.014
D	0.669	0.107	0.018
Average		0.094 ± 0.013	0.017 ± 0.003

1 dy	Average sGAG (mg/ml)	sGAG (mg)	sGAG/dry wt (mg/mg)
A	0.640	0.090	0.018
B	0.825	0.099	0.020
C	0.658	0.079	0.016
D	0.969	0.116	0.023
Average		0.096 ± 0.016	0.019 ± 0.003

3 dy	Average sGAG (mg/ml)	sGAG (mg)	sGAG/dry wt (mg/mg)
A	0.603	0.078	0.016
B	0.675	0.088	0.022
C	0.620	0.093	0.019
D	0.650	0.098	0.020
Average		0.089 ± 0.008	0.019 ± 0.003

5 dy	Average sGAG (mg/ml)	sGAG (mg)	sGAG/dry wt (mg/mg)
A	0.613	0.098	0.020
B	0.727	0.131	0.022
C	0.527	0.084	0.017
D	0.593	0.113	0.019
Average		0.106 ± 0.020	0.019 ± 0.002

7 dy	Average sGAG (mg/ml)	sGAG (mg)	sGAG/dry wt (mg/mg)
A	0.888	0.133	0.027
B	0.517	0.088	0.018
C	0.442	0.097	0.016
D	0.438	0.070	0.014
Average		0.097 ± 0.027	0.019 ± 0.006

Hypoxia			
½ dy	Average sGAG (mg/ml)	sGAG (mg)	sGAG/dry wt (mg/mg)
A	0.560	0.073	0.015
B	0.810	0.097	0.019
C	0.615	0.080	0.016
D	1.013	0.101	0.025
Average		0.088 ± 0.014	0.019 ± 0.005

1 dy	Average sGAG (mg/ml)	sGAG (mg)	sGAG/dry wt (mg/mg)
A	0.954	0.115	0.023
B	0.933	0.121	0.024
C	1.315	0.184	0.037
D	1.179	0.165	0.033
Average		0.146 ± 0.034	0.029 ± 0.007

3 dy	Average sGAG (mg/ml)	sGAG (mg)	sGAG/dry wt (mg/mg)
A	0.571	0.086	0.017
B	0.605	0.097	0.016
C	0.647	0.103	0.021
D	0.652	0.111	0.022
Average		0.099 ± 0.011	0.019 ± 0.003

5 dy	Average sGAG (mg/ml)	sGAG (mg)	sGAG/dry wt (mg/mg)
A	0.588	0.106	0.018
B	0.532	0.101	0.017
C	0.595	0.101	0.020
D	0.742	0.134	0.022
Average		0.110 ± 0.016	0.019 ± 0.002

7 dy	Average sGAG (mg/ml)	sGAG (mg)	sGAG/dry wt (mg/mg)
A	0.358	0.079	0.013
B	0.452	0.086	0.014
C	0.442	0.080	0.016
D	0.525	0.089	0.018
Average		0.083 ± 0.005	0.015 ± 0.002

Table ## 5 Total sulphated GAG at the central regions of the rabbit cornea that were cultured in normal and low O<sub>2</sub> level.

Results DMMB assay – Periphery (3-6mm)

Control	Average sGAG (mg/ml)	sGAG (mg)	sGAG/dry wt (mg/mg)
A	1.129	0.136	0.027
B	0.604	0.079	0.016
C	0.590	0.100	0.020
D	0.775	0.109	0.027
Average		0.106 ± 0.024	0.022 ± 0.006

Normal			
½ dy	Average sGAG (mg/ml)	sGAG (mg)	sGAG/dry wt (mg/mg)
A	0.815	0.090	0.022
B	0.769	0.092	0.023
C	0.675	0.074	0.019
D	0.538	0.081	0.016
Average		0.084 ± 0.008	0.020 ± 0.003

1 dy	Average sGAG (mg/ml)	sGAG (mg)	sGAG/dry wt (mg/mg)
A	0.619	0.105	0.021
B	0.931	0.130	0.026
C	0.681	0.082	0.016
D	0.708	0.106	0.021
Average		0.106 ± 0.020	0.021 ± 0.004

3 dy	Average sGAG (mg/ml)	sGAG (mg)	sGAG/dry wt (mg/mg)
A	0.642	0.096	0.024
B	0.523	0.089	0.018
C	0.652	0.098	0.024
D	0.521	0.083	0.017
Average		0.092 ± 0.007	0.021 ± 0.004

5 dy	Average sGAG (mg/ml)	sGAG (mg)	sGAG/dry wt (mg/mg)
A	0.456	0.073	0.018
B	0.638	0.115	0.023
C	0.471	0.085	0.017
D	0.781	0.141	0.028
Average		0.103 ± 0.030	0.022 ± 0.005

7 dy	Average sGAG (mg/ml)	sGAG (mg)	sGAG/dry wt (mg/mg)
A	0.369	0.123	0.013
B	0.375	0.068	0.014
C	0.396	0.083	0.017
D	0.348	0.059	0.012
Average		0.083 ± 0.028	0.014 ± 0.002

Hypoxia			
½ dy	Average sGAG (mg/ml)	sGAG (mg)	sGAG/dry wt (mg/mg)
A	0.606	0.109	0.022
B	0.681	0.089	0.018
C	0.642	0.077	0.019
D	0.652	0.085	0.021
Average		0.090 ± 0.014	0.020 ± 0.002

1 dy	Average sGAG (mg/ml)	sGAG (mg)	sGAG/dry wt (mg/mg)
A	1.000	0.110	0.028
B	1.077	0.162	0.032
C	0.619	0.087	0.022
D	1.208	0.145	0.029
Average		0.126 ± 0.034	0.028 ± 0.004

3 dy	Average sGAG (mg/ml)	sGAG (mg)	sGAG/dry wt (mg/mg)
A	0.660	0.106	0.021
B	0.608	0.097	0.024
C	0.685	0.110	0.027
D	0.754	0.136	0.027
Average		0.112 ± 0.017	0.025 ± 0.003

5 dy	Average sGAG (mg/ml)	sGAG (mg)	sGAG/dry wt (mg/mg)
A	0.961	0.125	0.021
B	0.669	0.107	0.027
C	0.565	0.102	0.020
D	0.583	0.111	0.022
Average		0.111 ± 0.010	0.023 ± 0.003

7 dy	Average sGAG (mg/ml)	sGAG (mg)	sGAG/dry wt (mg/mg)
A	0.335	0.060	0.012
B	0.400	0.076	0.015
C	0.302	0.066	0.011
D	0.385	0.066	0.013
Average		0.067 ± 0.007	0.013 ± 0.002

Table ## 6 Total sulphated GAG at the peripheral regions of the rabbit cornea that were cultured in normal and low O<sub>2</sub> level.

Results: DMMB assay – Outer periphery (6-9mm)

Control	Average sGAG (mg/ml)	sGAG (mg)	sGAG/dry wt (mg/mg)
A	0.608	0.061	0.015
B	0.510	0.051	0.013
C	0.444	0.053	0.013
D	0.523	0.068	0.014
Average		0.058 ± 0.008	0.014 ± 0.001

Normal			
½ dy	Average sGAG (mg/ml)	sGAG (mg)	sGAG/dry wt (mg/mg)
A	0.563	0.073	0.015
B	0.629	0.082	0.016
C	0.283	0.045	0.008
D	0.540	0.076	0.015
Average		0.069 ± 0.016	0.013 ± 0.004

1 dy	Average sGAG (mg/ml)	sGAG (mg)	sGAG/dry wt (mg/mg)
A	0.477	0.067	0.013
B	0.742	0.104	0.021
C	0.558	0.073	0.015
D	0.877	0.114	0.023
Average		0.089 ± 0.023	0.018 ± 0.005

3 dy	Average sGAG (mg/ml)	sGAG (mg)	sGAG/dry wt (mg/mg)
A	0.600	0.066	0.022
B	0.692	0.090	0.022
C	0.615	0.086	0.022
D	0.473	0.080	0.016
Average		0.081 ± 0.010	0.021 ± 0.003

5 dy	Average sGAG (mg/ml)	sGAG (mg)	sGAG/dry wt (mg/mg)
A	0.410	0.070	0.014
B	0.588	0.106	0.018
C	0.440	0.075	0.015
D	0.365	0.062	0.012
Average		0.078 ± 0.019	0.015 ± 0.002

7 dy	Average sGAG (mg/ml)	sGAG (mg)	sGAG/dry wt (mg/mg)
A	0.410	0.078	0.016
B	0.263	0.042	0.008
C	0.350	0.060	0.012
D	0.217	0.039	0.008
Average		0.055 ± 0.018	0.011 ± 0.004

Hypoxia			
½ dy	Average sGAG (mg/ml)	sGAG (mg)	sGAG/dry wt (mg/mg)
A	0.342	0.058	0.010
B	0.598	0.090	0.015
C	0.494	0.069	0.014
D	0.429	0.064	0.013
Average		0.070 ± 0.014	0.013 ± 0.002

1 dy	Average sGAG (mg/ml)	sGAG (mg)	sGAG/dry wt (mg/mg)
A	1.042	0.156	0.026
B	1.231	0.172	0.034
C	0.996	0.129	0.032
D	1.044	0.136	0.027
Average		0.148 ± 0.020	0.030 ± 0.004

3 dy	Average sGAG (mg/ml)	sGAG (mg)	sGAG/dry wt (mg/mg)
A	0.581	0.099	0.020
B	0.652	0.078	0.020
C	0.535	0.096	0.019
D	0.552	0.083	0.017
Average		0.089 ± 0.010	0.019 ± 0.001

5 dy	Average sGAG (mg/ml)	sGAG (mg)	sGAG/dry wt (mg/mg)
A	0.421	0.063	0.013
B	0.538	0.086	0.017
C	0.492	0.079	0.016
D	0.427	0.077	0.015
Average		0.076 ± 0.010	0.015 ± 0.002

7 dy	Average sGAG (mg/ml)	sGAG (mg)	sGAG/dry wt (mg/mg)
A	0.277	0.044	0.009
B	0.417	0.058	0.015
C	0.331	0.060	0.012
D	0.260	0.042	0.008
Average		0.051 ± 0.009	0.011 ± 0.003

Table ## 7 Total sulphated GAG at the outer periphery regions of the rabbit cornea that were cultured in normal and low O<sub>2</sub> level.

Results: DMMB assay – Sclera (9-12mm)

Control	Average sGAG (mg/ml)	sGAG (mg)	sGAG/dry wt (mg/mg)
A	0.165	0.016	0.004
B	0.096	0.010	0.002
C	0.065	0.006	0.002
D	0.031	0.003	0.001
Average		0.009 ± 0.006	0.002 ± 0.001

Normal			
½ dy	Average sGAG (mg/ml)	sGAG (mg)	sGAG/dry wt (mg/mg)
A	0.083	0.013	0.002
B	0.177	0.025	0.004
C	0.100	0.012	0.002
D	0.079	0.009	0.002
Average		0.015 ± 0.007	0.003 ± 0.001

1 dy	Average sGAG (mg/ml)	sGAG (mg)	sGAG/dry wt (mg/mg)
A	0.104	0.016	0.003
B	0.256	0.038	0.006
C	0.129	0.016	0.003
D	0.290	0.035	0.006
Average		0.026 ± 0.012	0.004 ± 0.002

3 dy	Average sGAG (mg/ml)	sGAG (mg)	sGAG/dry wt (mg/mg)
A	0.092	0.012	0.003
B	0.098	0.014	0.003
C	0.075	0.013	0.003
D	0.190	0.030	0.006
Average		0.017 ± 0.009	0.004 ± 0.002

5 dy	Average sGAG (mg/ml)	sGAG (mg)	sGAG/dry wt (mg/mg)
A	0.159	0.025	0.004
B	0.113	0.020	0.004
C	0.128	0.022	0.004
D	0.054	0.009	0.002
Average		0.019 ± 0.007	0.003 ± 0.001

7dy	Average sGAG (mg/ml)	sGAG (mg)	sGAG/dry wt (mg/mg)
A	0.096	0.016	0.003
B	0.055	0.010	0.002
C	0.061	0.010	0.002
D	0.025	0.004	0.001
Average		0.010 ± 0.005	0.002 ± 0.001

Hypoxia			
½ dy	Average sGAG (mg/ml)	sGAG (mg)	sGAG/dry wt (mg/mg)
A	0.079	0.012	0.002
B	0.215	0.026	0.005
C	0.165	0.018	0.004
D	0.183	0.018	0.005
Average		0.019 ± 0.006	0.004 ± 0.001

1 dy	Average sGAG (mg/ml)	sGAG (mg)	sGAG/dry wt (mg/mg)
A	0.415	0.058	0.010
B	0.415	0.054	0.011
C	0.402	0.048	0.012
D	0.315	0.038	0.006
Average		0.049 ± 0.009	0.010 ± 0.002

3 dy	Average sGAG (mg/ml)	sGAG (mg)	sGAG/dry wt (mg/mg)
A	0.086	0.014	0.002
B	0.082	0.010	0.002
C	0.136	0.018	0.004
D	0.119	0.017	0.003
Average		0.014 ± 0.004	0.003 ± 0.001

5 dy	Average sGAG (mg/ml)	sGAG (mg)	sGAG/dry wt (mg/mg)
A	0.038	0.006	0.001
B	0.078	0.012	0.002
C	0.059	0.009	0.002
D	0.071	0.013	0.002
Average		0.010 ± 0.003	0.002 ± 0.000

7dy	Average sGAG (mg/ml)	sGAG (mg)	sGAG/dry wt (mg/mg)
A	0.055	0.009	0.002
B	0.053	0.008	0.002
C	0.090	0.015	0.003
D	0.036	0.006	0.001
Average		0.010 ± 0.004	0.002 ± 0.001

Table ## 8 Total sulphated GAG at the sclera regions of the rabbit cornea that were cultured in normal and low O<sub>2</sub> level.

Results: ELISA – 5D4: detecting higher sulphated KS

0 dy	Competing antigen (ng/ml)	5D4 (ng)	5D4/dry wt (ng/mg)
A	230.255	5.847	1.169
B	189.327	4.807	0.961
C	250.430	6.359	1.060
D	181.508	4.609	0.922
Average			1.028 ± 0.111

Normal			
½ dy	Competing antigen (ng/ml)	5D4 (ng)	5D4/dry wt (ng/mg)
A	185.927	3.405	0.681
B	140.672	2.576	0.515
C	131.597	2.410	0.402
D	210.151	3.849	0.642
Average			0.560 ± 0.127

Hypoxia			
½ dy	Competing antigen (ng/ml)	5D4 (ng)	5D4/dry wt (ng/mg)
A	295.532	8.777	1.755
B	239.430	7.111	1.422
C	178.916	5.313	1.063
D	274.619	8.156	2.039
Average			1.570 ± 0.422

1 dy	Competing antigen (ng/ml)	5D4 (ng)	5D4/dry wt (ng/mg)
A	169.168	2.487	0.497
B	248.505	3.653	0.731
C	201.165	2.957	0.591
D	198.633	2.920	0.584
Average			0.601 ± 0.096

1 dy	Competing antigen (ng/ml)	5D4 (ng)	5D4/dry wt (ng/mg)
A	407.862	17.963	3.593
B	473.967	20.874	4.175
C	467.125	20.573	4.115
D	471.738	20.776	4.155
Average			4.009 ± 0.279

3 dy	Competing antigen (ng/ml)	5D4 (ng)	5D4/dry wt (ng/mg)
A	309.453	6.977	1.395
B	317.266	7.154	1.788
C	293.029	6.607	1.321
D	261.842	5.904	1.181
Average			1.422 ± 0.260

3 dy	Competing antigen (ng/ml)	5D4 (ng)	5D4/dry wt (ng/mg)
A	245.347	6.299	1.260
B	336.510	8.639	1.440
C	236.398	6.069	1.214
D	250.588	6.433	1.287
Average			1.300 ± 0.098

5 dy	Competing antigen (ng/ml)	5D4 (ng)	5D4/dry wt (ng/mg)
A	234.891	2.188	0.438
B	240.602	2.241	0.374
C	282.164	2.628	0.526
D	186.937	1.741	0.290
Average			0.407 ± 0.100

5 dy	Competing antigen (ng/ml)	5D4 (ng)	5D4/dry wt (ng/mg)
A	166.027	3.500	0.583
B	233.946	4.932	0.822
C	178.916	3.772	0.754
D	160.280	3.379	0.563
Average			0.681 ± 0.127

7 dy	Competing antigen (ng/ml)	5D4 (ng)	5D4/dry wt (ng/mg)
A	133.777	2.568	0.514
B	223.053	4.281	0.856
C	102.714	1.971	0.329
D	250.717	4.812	0.962
Average			0.665 ± 0.295

7 dy	Competing antigen (ng/ml)	5D4 (ng)	5D4/dry wt (ng/mg)
A	172.562	2.783	0.464
B	265.696	4.285	0.714
C	158.798	2.561	0.512
D	180.563	2.912	0.582
Average			0.568 ± 0.109

Table ## 9 Over-sulphated KS quantifications at the central regions of the rabbit cornea that were cultured in normal and low O<sub>2</sub> level.

Results: ELISA – 1B4: detecting lesser sulphated KS

0 dy	Competing antigen (ng/ml)	1B4 (ng)	1B4/dry wt (ng/mg)
A	5894.755	5.821	1.164
B	5806.113	5.734	1.147
C	5681.088	5.610	0.935
D	7258.672	7.168	1.434
Average			1.170 ± 0.204

Normal			
½ dy	Competing antigen (ng/ml)	1B4 (ng)	1B4/dry wt (ng/mg)
A	2651.506	3.936	0.787
B	3368.896	5.000	1.000
C	4749.304	7.049	1.175
D	4183.247	6.209	1.035
Average			0.999 ± 0.160

Hypoxia			
½ dy	Competing antigen (ng/ml)	1B4 (ng)	1B4/dry wt (ng/mg)
A	5051.916	4.473	0.895
B	6993.095	6.192	1.238
C	5813.860	5.148	1.030
D	3995.897	3.538	0.885
Average			1.012 ± 0.165

1 dy	Competing antigen (ng/ml)	1B4 (ng)	1B4/dry wt (ng/mg)
A	5681.088	7.660	1.532
B	6795.625	9.163	1.833
C	4342.435	5.855	1.171
D	6066.435	8.180	1.636
Average			1.543 ± 0.277

1 dy	Competing antigen (ng/ml)	1B4 (ng)	1B4/dry wt (ng/mg)
A	4830.758	9.682	1.936
B	5169.893	10.362	2.072
C	4310.844	8.640	1.728
D	4830.758	9.682	1.936
Average			1.912 ± 0.142

3 dy	Competing antigen (ng/ml)	1B4 (ng)	1B4/dry wt (ng/mg)
A	5464.679	9.509	1.902
B	3588.056	6.244	1.561
C	4259.076	7.412	1.482
D	4097.703	7.131	1.426
Average			1.593 ± 0.213

3 dy	Competing antigen (ng/ml)	1B4 (ng)	1B4/dry wt (ng/mg)
A	4233.189	8.086	1.617
B	4342.435	8.294	1.382
C	4318.795	8.249	1.650
D	5049.129	9.644	1.929
Average			1.645 ± 0.224

5 dy	Competing antigen (ng/ml)	1B4 (ng)	1B4/dry wt (ng/mg)
A	11245.268	5.146	1.029
B	12270.896	5.616	0.936
C	8460.516	3.872	0.774
D	8785.541	4.021	0.670
Average			0.852 ± 0.161

5 dy	Competing antigen (ng/ml)	1B4 (ng)	1B4/dry wt (ng/mg)
A	2148.051	5.299	0.883
B	2594.928	6.401	1.067
C	2665.020	6.574	1.315
D	2110.560	5.206	0.868
Average			1.033 ± 0.208

7 dy	Competing antigen (ng/ml)	1B4 (ng)	1B4/dry wt (ng/mg)
A	2856.482	4.295	0.859
B	4651.448	6.993	1.399
C	3667.286	5.514	0.919
D	2592.389	3.897	0.779
Average			0.989 ± 0.279

7 dy	Competing antigen (ng/ml)	1B4 (ng)	1B4/dry wt (ng/mg)
A	2592.389	9.939	1.657
B	2639.131	10.119	1.686
C	1815.348	6.960	1.392
D	2131.766	8.173	1.635
Average			1.592 ± 0.135

Table ## 10 Lesser-sulphated KS quantifications at the central regions of the rabbit cornea that were cultured in normal and low O<sub>2</sub> level.

## Results: Hydroxyproline assay

0 dy	Average (mg/ml)	Hydroxyproline (mg)	Hydroxyproline/dry wt (mg/mg dry wt)
A	0.186	0.037	0.007
B	0.228	0.046	0.009
C	0.247	0.049	0.008
D	0.318	0.064	0.013

Average	0.049 ± 0.011	0.009 ± 0.002
---------	---------------	---------------

### Normal

½ dy	Average (mg/ml)	Hydroxyproline (mg)	Hydroxyproline/dry wt (mg/mg dry wt)
A	0.270	0.054	0.011
B	0.311	0.062	0.012
C	0.231	0.046	0.008
D	0.297	0.059	0.010

Average	0.055 ± 0.007	0.010 ± 0.002
---------	---------------	---------------

1 dy	Average (mg/ml)	Hydroxyproline (mg)	Hydroxyproline/dry wt (mg/mg dry wt)
A	0.179	0.036	0.007
B	0.272	0.054	0.011
C	0.202	0.040	0.008
D	0.302	0.060	0.012

Average	0.048 ± 0.012	0.010 ± 0.002
---------	---------------	---------------

3 dy	Average (mg/ml)	Hydroxyproline (mg)	Hydroxyproline/dry wt (mg/mg dry wt)
A	0.280	0.056	0.011
B	0.288	0.058	0.014
C	0.291	0.058	0.012
D	0.296	0.059	0.012

Average	0.058 ± 0.001	0.012 ± 0.001
---------	---------------	---------------

5 dy	Average (mg/ml)	Hydroxyproline (mg)	Hydroxyproline/dry wt (mg/mg dry wt)
A	0.177	0.035	0.007
B	0.247	0.049	0.008
C	0.245	0.049	0.010
D	0.211	0.042	0.007

Average	0.044 ± 0.007	0.008 ± 0.001
---------	---------------	---------------

7 dy	Average (mg/ml)	Hydroxyproline (mg)	Hydroxyproline/dry wt (mg/mg dry wt)
A	0.205	0.041	0.010
B	0.243	0.049	0.010
C	0.254	0.051	0.008
D	0.259	0.052	0.010

Average	0.048 ± 0.005	0.010 ± 0.001
---------	---------------	---------------

### Hypoxia

½ dy	Average (mg/ml)	Hydroxyproline (mg)	Hydroxyproline/dry wt (mg/mg dry wt)
A	0.240	0.048	0.010
B	0.295	0.059	0.012
C	0.223	0.045	0.009
D	0.377	0.075	0.019

Average	0.057 ± 0.012	0.014 ± 0.005
---------	---------------	---------------

1 dy	Average (mg/ml)	Hydroxyproline (mg)	Hydroxyproline/dry wt (mg/mg dry wt)
A	0.426	0.085	0.017
B	0.389	0.078	0.016
C	0.375	0.075	0.015
D	0.346	0.069	0.014

Average	0.077 ± 0.007	0.015 ± 0.001
---------	---------------	---------------

3 dy	Average (mg/ml)	Hydroxyproline (mg)	Hydroxyproline/dry wt (mg/mg dry wt)
A	0.328	0.066	0.013
B	0.255	0.051	0.008
C	0.266	0.053	0.011
D	0.296	0.059	0.012

Average	0.057 ± 0.007	0.011 ± 0.002
---------	---------------	---------------

5 dy	Average (mg/ml)	Hydroxyproline (mg)	Hydroxyproline/dry wt (mg/mg dry wt)
A	0.344	0.069	0.011
B	0.310	0.062	0.010
C	0.327	0.065	0.013
D	0.315	0.063	0.011

Average	0.065 ± 0.003	0.011 ± 0.001
---------	---------------	---------------

7 dy	Average (mg/ml)	Hydroxyproline (mg)	Hydroxyproline/dry wt (mg/mg dry wt)
A	0.274	0.055	0.009
B	0.319	0.064	0.011
C	0.335	0.067	0.013
D	0.293	0.059	0.012

Average	0.061 ± 0.005	0.011 ± 0.002
---------	---------------	---------------

Table ## 11 Hydroxyproline content in the central regions of the rabbit cornea that were cultured in normal and low O<sub>2</sub> level.

